REACTIONS OF DIOXYGEN AND NITRIC OXIDE WITH IRON(II) COMPOUNDS: MODELS FOR CHEMISTRY OCCURING IN THE ACTIVE SITES OF NON-HEME IRON ENZYMES

By Andrew L. Feig

B.S., Yale University, New Haven, CT (1990)

SUBMITTED IN PARTIAL FULFILLMENT
OF THE REQUIREMENTS FOR THE
DEGREE OF
DOCTOR OF PHILOSOPHY
at the
MASSACHUSETTS INSTITUTE OF TECHNOLOGY
September, 1995

Signature of Author_____
Department of Chemistry
August 15, 1995

Certified by_____
Stephen J. Lippard
Thesis Supervisor

Accepted by_____
Dietmar Seyferth
Chairman, Department Committee on Graduate Students

This doctoral thesis has been examined by a committee of the Department of Chemistry as follows:

Professor Alan Davison

Professor Stephen J. Lippard
Arthur Amos Noyes Professor of Chemistry

Professor Richard R. Schrock
Fredrick G. Keyes Professor of Chemistry

to Gran, ...

REACTIONS OF DIOXYGEN AND NITRIC OXIDE WITH IRON(II) COMPOUNDS: MODELS FOR CHEMISTRY OCCURING IN THE ACTIVE SITES OF NON-HEME IRON ENZYMES

By Andrew L. Feig

Submitted to the Department of Chemistry on August 15, 1995 in partial fulfillment of the requirements for the Degree of Doctor of Philosophy

ABSTRACT

Chapter I.

A comprehensive review (as of March 1994) of the literature pertaining to the reactions of dioxygen with non-heme iron centers in biology and chemistry is provided as background for the studies presented in Chapters 2 and 3. This survey pays particular attention to the role of iron and dioxygen reactions in the catalytic oxygenation mechanisms of mononuclear and dinuclear iron proteins. Other topics include the role of dioxygen in ferritin core formation, activated bleomycin and model compounds known to form stable dioxygen adducts from the reaction of dioxygen with a ferrous precursor.

Chapter II.

Stopped-flow kinetic studies on the reactions of $[Fe_2(OH)(Me_3TACN)_2(OAc)_2]^+$ and $[Fe_2(BIPhMe)_2(O_2CH)_4]$ with O_2 are presented. Mechanisms consistent with the kinetic data are proposed for the reactions. The main feature of the reactions is a bimolecular decay pathway

in which a tetranuclear μ^4-peroxide is proposed to be the transition state. Evidence for carboxylate shift involvement in the oxidation mechanisms is presented, providing a glimpse at how this class of structural equilibria can be used to control the chemistry at diiron centers in proteins.

Chapter III.

Mechanistic studies on the reactions of 3 analogous alkoxo-bridged diiron(II) complexes with O_2 have been performed. The primary difference across this series is one of ligand sterics. These complexes all exhibit a metastable μ-peroxo intermediate when studied at low temperature, but when studied at ambient temperatures, the decay of this intermediate was observed. The role of the ligand steric properties on O_2 reactivity was examined in this way. It was found that when access to the diiron center was unimpeded, the activation parameters for O_2 addition were similar to those for O_2 reacting with hemerythrin, but when the binding site was occluded, an internal rearrangement was necessary prior to O_2 binding. Like other diiron model compounds, the decay of the peroxide intermediate is proposed to involve a bimolecular event, and the formation of a tetranuclear transition state.

Chapter IV.

Reactions of non-heme iron centers with nitric oxide are reviewed in context with both biology and chemistry. Particular attention focuses on the use of nitric oxide as a spectroscopic probe for the active sites of non-heme iron enzymes. These studies have provided a framework from which theories about the nature of iron-nitrosyl bonds in the $\{FeNO\}^7$ systems have been elucidated. The potential role of NO in the inactivation of diiron

enzymes such as ribonucleotide reductase is also discussed. Finally, small molecule catalytic systems involveing iron nitrosyls are mentioned. This section deals primarily with a reaction involving the nitrate/nitrosyl couple and how this system effects oxo-transfer to olefinic substrates.

Chapter V.

A novel dinuclear iron dinitrosyl compound $[Fe_2(Et\text{-}HPTB)(OBz)\text{-}(NO)_2](BF_4)_2$ has been structurally and spectroscopically characterized. This compound is a potential model for the interaction of NO with ribonucleotide reductase and other dinuclear non-heme iron proteins in vivo. The complex has slightly bent nitrosyl ligands with FeNO angles of 167°. This angle is larger than expected for the $\{FeNO\}^7$ electronic configuration and a discussion of the bonding contrasts this complex with similar MNO complexes.

Chapter VI.

A new catalytic system for the nitration of olefins is presented. The nitroolefin products are useful intermediates in organic synthesis and can easily be reduced to form chiral centers adjacent to an amino groups which allows further functionalization. The reaction consumes NO and uses a dinuclear iron peroxide adduct as the precatalyst. A survey of potential substrates found that aryl olefins were the most reactive and a wide variety of substitution and functionality was acceptable.

Thesis Supervisor: Stephen J. Lippard

Title: Arthur Amos Noyes Professor of Chemistry

Table of Contents

List of Figures

List of Tables

List of Schemes

List of Equations

List of Abbreviations Used

1-MeIm	1-methylimidazole
2-KG	2-oxoglutarate, α-ketoglutarate
5-Me-HXTA	N,N′-(2-hydroxy-5-methyl-1,3-xylylene)bis(N-carboxymethylglycine)
ACV	δ-[5-amino-5-(hydroxycarbonyl)pentanoyl]-L-cysteinyl-D-valine
$AscH_2$	ascorbic acid
BF	benzoyl formate
BIPhMe	2,2′-bis(1-methylimidazolyl)phenylmethoxymethane
BLM	bleomycin
dAsc	dehydroascorbate
DMSO	dimethyl sulfoxide
DNA	deoxyribonucleic acid
DOPA	dihydroxyphenylalanine
DPA	dipicolinate
DPAH	dipicolinic acid
EDTA	ethylenediaminetetraacetate
ENDOR	electron nuclear double resonance
EPR	electron paramagnetic resonance
EtCN	propionitrile
Et-HPTB	N,N,N'N'-tetrakis(N-ethyl-2-benzimidazolylmethyl)-2-hydroxy-1,3-diaminopropane
EXAFS	extended X-ray absorption fine structure
FAD	flavin adenine dinucleotide
GC	gas chromatography
GC/MS	gas chromatography coupled to mass spectrometry
H	hydroxylase component of sMMO
h	Plank's constant
H_2BP	dihydrobiopterin
H_4BP	tetrahydrobiopterin
HB(3,5-iPr$_2$Pz)$_3$	hydrotris(3,5-diisopropylpyrazol-1-yl)borate
Hb	hemoglobin
HLF	human liver ferritin
HoSF	horse spleen ferritin
HPTB	N,N,N'N'-tetrakis(2-benzimidazolylmethyl)-2-hydroxy-1,3-diaminopropane

HPTMP	N,N,N'N'-tetrakis[(6-methylpyrid-2-yl)methyl]-hydroxy-1,3-diaminopropane
HPTP	N,N,N'N'-tetrakis(2-pyridylmethyl)-2-hydroxy-1,3-diaminopropane
HPTR	N,N,N′,N′-tetrakis(R-substituted)-2-hydroxy-1,3-diaminopropane
Hr	hemerythrin
IPNS	isopenicillin N synthase
k_b	Boltzman's constant
k_ψ	pseudo-order rate constant
KIE	kinetic isotope effect
Mb	myoglobin
MCD	magnetic circular dichroism
MeCN	acetonitrile
Me_3TACN	1,4,7-trimethyl-1,4,7-triazacyclononane
MPa	megapascals
MOPS	4-morpholinepropanesulfonic acid
NADH	nicotinamide adenine dinucleotide
NHE	normal hydrogen electrode
NMR	nuclear magnetic resonance
OAc	acetate
OBz	benzoate
OEP	octaethylporphyrin
PA	picolinate
PAH	phenalanine hydroxylase
4,5-PCD	protocatechuate 4,5-dioxygenase
PhIO	iodosylbenzene
py	pyridine
PMO	putidamonooxin (4-methoxybenzoate O-demethylase)
rHF	recombinant H chain ferritin
rLF	recombinant L chain ferritin
RMS	root mean squared
RNR	ribonucleotide reductase
RR	resonance Raman
sMMO	methane monooxygenase
SOD	superoxide dismutase
TACN	1,4,7-triazacyclononane
TH	thymine hydroxylase
THF	tetrahydrofuran
TRP	tryptophan hydroxylase
V_0	initial rate

Acknowledgements

There are so many people who helped me get through the last five years that I am afraid this section will sound like an acceptance speech from the Academy Awards Ceremony. No work comes out of a vacuum, however, and I must thank Steve first and foremost for gathering a group of scientists who are knowledgeable and with whom it has been fun to work. Steve, you have been the source of many good ideas over the years, but you gave me the freedom to walk down the paths I found most interesting. When I struggled with my science, your door was always open, but when I had a head of steam, you let me go my own way unimpeded. You have taught me a lot about good science and I will take these lessons with me forever. At this point, I should also thank Dave Sigman, my former research advisor at UCLA. You were instrumental in my choosing to do my Ph.D. with Steve. Your advice then, as always, was excellent.

Although I owe debts, large or small, to almost everyone who has come through the lab in the last few years, there are a few people who I wish to single out for special thanks. Axel, your work setting-up the stopped-flow facility got the lab started in this area. Together with Andreja and Sofi, you taught me kinetics. Without the patience all of you showed me, I could never have done this work. EPR Goddesses, you know who you are. You were life-savers and the cryostat is awed in your presence. Susanna, thanks for helping me collect the SQUID data. May the "cows" always come home and may the Susanna Radius be defined in the next edition of the CRC. Mike Scott, your help with the Siemens diffractometer made the transition to the new machine painless for me.

My subgroups have provided much support. As a member of iron, then MMO and then back to iron, I sometimes felt nobody really wanted to hear about my mechanisms or see another kinetic trace. Yet, you asked good questions and kept me on track both in the actual meetings and informally around the lab. Ann - I have to tell you one last time although I am sure you will remember forever - SCRIPT!!!! The stopped-flow is yours now. Take good care of the baby and keep it in line when it throws its temper tantrums. By the way - don't let Maria win too many of the bets. Speaking of which, Maria, I am expecting you to learn about wines - you are going to owe me a very nice bottle in 2010. Mike Keck and John Protasiewicz - the lab has never quite been the same since you two left. For one thing, the fishing and camping trips petered out, but the practical jokes will be remembered forever. May your students get even with you one day. Finally from lab, I need to thank my classmate and good friend Jackie Acho. We took separate roads out of graduate school, but our paths will cross again, probably on restaurant row. From fireworks on the 4th, to dinner parties, catered seminars and card games, your presence helped make life at MIT fun. Keep looking for the perfect spot for our restaurant.

Beyond the confines of the Lippard Lab some friends need to be thanked for helping me retain my sanity throughout this experience. Joanna and James - hiking, canoeing, skiing or show shoeing - you were always game for an excursion out of Boston or even just an evening around town. I have no idea how you manage the twins and graduate school. Hats off to you. It makes getting just a Ph.D. seem like a small feat in comparison. Graham and Liz - I am glad you have been in Boston these last few years. Dinner and bridge, bridge and dinner, occasionally just bridge and more bridge. You have helped me keep perspective on life and work. Rony - it took us awhile, but our bidding system finally got ironed out. You will be a difficult bridge partner to replace. Matt, Art and Dave, I have had many housemates since coming to Boston, but you are still my Roommates. We are spread across the country these days, but that has not changed our friendship.

Lastly, I need to thank my parents. They fostered in me the love of science and learning years ago and have encouraged me forward at every step. They have listened to my frustrations and shared my successes as if they were their own. Their constant support has made the hard times more manageable and the good times even better. Boulder is whole lot closer to Los Angeles than Boston was, so maybe I'll make it home a little more often - but then again, it might be fun to keep meeting in interesting parts of the world. Mom and Dad, I love you both.

CHAPTER I.

Reactions of Non-Heme Iron(II) Centers with Dioxygen in Biology and Chemistry[1,2]

Introduction

Reactions of dioxygen with ferrous ion and its complexes occur widely in nature. In biology, the best known and probably most studied systems are proteins that contain one or more iron-porphyrin units, examples being hemoglobin and cytochrome P-450. Another large and diverse category of proteins contains non-heme iron, especially the ubiquitous iron-sulfur clusters. Summaries of the chemistry of iron-porphyrin and iron-sulfur proteins are available elsewhere.[3-8] In the present review, we describe the chemistry of non-heme iron(II) centers with dioxygen.† Like their heme counterparts, proteins containing these units transport dioxygen and oxygenate a variety of substrates. Iron(II)-dioxygen reactions also mediate the controlled generation of protein and nucleic acid radicals as well as the assembly of the mineral core in the iron storage protein ferritin.

As information about biological non-heme iron systems has emerged, chemists have prepared models to mimic their structures and functions. These models have in turn enhanced our understanding of the physical properties and reactivities of the biological iron centers. Such knowledge has practical applications in chemical industry as well as the health sciences. One example of this applicability is methane monooxygenase (MMO), which has the unusual ability to oxidize hydrocarbons and halocarbons, among other substrates. Because of their broad range of substrates, methanotrophic bacteria have been used in bioremediation of the environment, for example, to remove chlorinated hydrocarbons from drinking water and oil from contaminated beaches.[9-12] Functional mimics of this chemistry could provide an economical source of methanol for use as an alternative fuel or

† Hereafter we exclude iron-sulfur complexes from this category.

as new catalysts for use in water purification and the cleanup of toxic waste. Important insights into developing such catalysts could arise from learning how dioxygen and methane are activated in the biological system. Apart from such practical applications, however, the selective oxidation of methane to methanol is fundamentally difficult to achieve under mild conditions. The desire to unravel how nature has solved this challenging problem in methane monooxygenase systems is in itself sufficient incentive for scientific investigation.

Most of the previous reviews of non-heme iron focused primarily on structural and physical properties, with less emphasis on dioxygen reactivity.[13-20] In the present article we approach the topic from a mechanistic point of view, paying special attention to the reactions of iron(II) centers with dioxygen. Structural properties are discussed and tabulated, but mainly to illustrate how they affect the reactivity of the iron center under consideration. Although often synthetically useful,[21-26] reactions of iron complexes with reduced forms of dioxygen (superoxide and peroxide) are treated only if generated in a reaction of ferrous precursors with dioxygen. A similar comment applies to the use of oxo-transfer reagents to mimic postulated high oxidation state intermediates in the reaction of iron(II) species with dioxygen. No effort is made to provide comprehensive coverage of small molecule catalysts. Instead, we present a few key systems that react by different mechanisms to illustrate the types of reactivity observed. The relevance of this chemistry to the biological systems will be noted.

The discussion begins with a summary of the redox properties of dioxygen and iron including autoxidation reactions of aquated ferrous iron and complexes with chelating ligands. Next we examine biological systems,

classifying them based upon their iron core structures. Three categories are delineated, mononuclear centers in 4-methoxybenzoate O-demethylase, extradiol catechol dioxygenases, isopenicillin N synthase, pteridine dependent enzymes, and α-keto acid dependent enzymes; dinuclear centers in hemerythrin, methane monooxygenase and ribonucleotide reductase; and polynuclear centers in ferritin. The antitumor antibiotic bleomycin is covered next and serves to bridge our discussions of proteins and model compounds. We treat model systems in the final section, beginning with the most stable dioxygen adducts formed in the reaction of ferrous compounds with dioxygen then moving to autoxidations and catalytic reactions that proceed through transient dioxygen intermediates. Wherever possible, we attempt to relate chemical reactivity to molecular structure.

Several enzymes that utilize the chemistry of non-heme iron, and for which redox chemistry has sometimes been invoked, have been explicitly excluded. Soybean lipoxygenase is not discussed because recent evidence indicates that the functional form of the enzyme is the ferric state.[27] The chemistry of intradiol catechol dioxygenases is also not treated because the predominant evidence favors substrate rather than dioxygen activation.[28-31] Iron-dependent superoxide dismutase has been omitted because it acts on a reduced form of dioxygen.[32] The recently discovered dinuclear iron protein Δ-9 desaturase is not discussed because at present there is insufficient knowledge of its mechanistic chemistry.[33] Finally, we do not cover non-enzymatic lipid peroxidation involving ferrous ions. The iron chemistry does not differ substantially from that involved in the oxidation of aqueous ferrous ions except that the radical generated is intercepted by an organic substrate.[34,35]

Redox Properties of Dioxygen and Iron

Kinetic, Thermodynamic, and Structural Properties

Life on earth depends upon the kinetic stability of the O_2 molecule with respect to its reactions with organic compounds, which are quite exothermic. The origin of this stability is the spin-triplet ground state of dioxygen.[36-38] Since organic and biological molecules usually have paired electrons and singlet ground states, their reactions with dioxygen are spin-forbidden. This kinetic barrier to reactivity can be surmounted by exciting the O_2 molecule to one of its singlet states, by a free radical pathway, or by complexation with a paramagnetic metal ion. The first process is endergonic, requiring 22.53 or 37.51 kcal/mol for excitation to the lowest ($^1\Delta_g$) or second lowest ($^1\Sigma_g^+$) lying singlet states, respectively.[37] It is usually accomplished photochemically.[39] Radical mechanisms circumvent the spin restrictions by producing two doublet molecules, but the processes by which radicals are generated are usually quite endothermic and inaccessible at ambient temperatures.[38] Metal ions can also overcome the spin barrier and provide a low-energy pathway for oxidation reactions. Thus metal ion cofactors are often used in biology for reactions involving dioxygen. When the dioxygen molecule binds to a metal ion, its 2p electrons interact with the d orbitals of the metal as shown, for example, for a hypothetical $Fe^{II}L_5$ species in Figure 1.1. Depending on the energy separation Δ, the adduct can have either a singlet or a triplet ground state. Regardless of the ground spin state of the adduct, its low-lying excited states can usually facilitate a spin-allowed reaction with singlet molecules. Although the beneficial use of such metal-dioxygen complexes in biology will dominate the ensuing discussion, the toxicity of the O_2 molecule can also be traced to the formation of highly reactive oxygen species that are similarly produced in reactions with metal ions.[40,41]

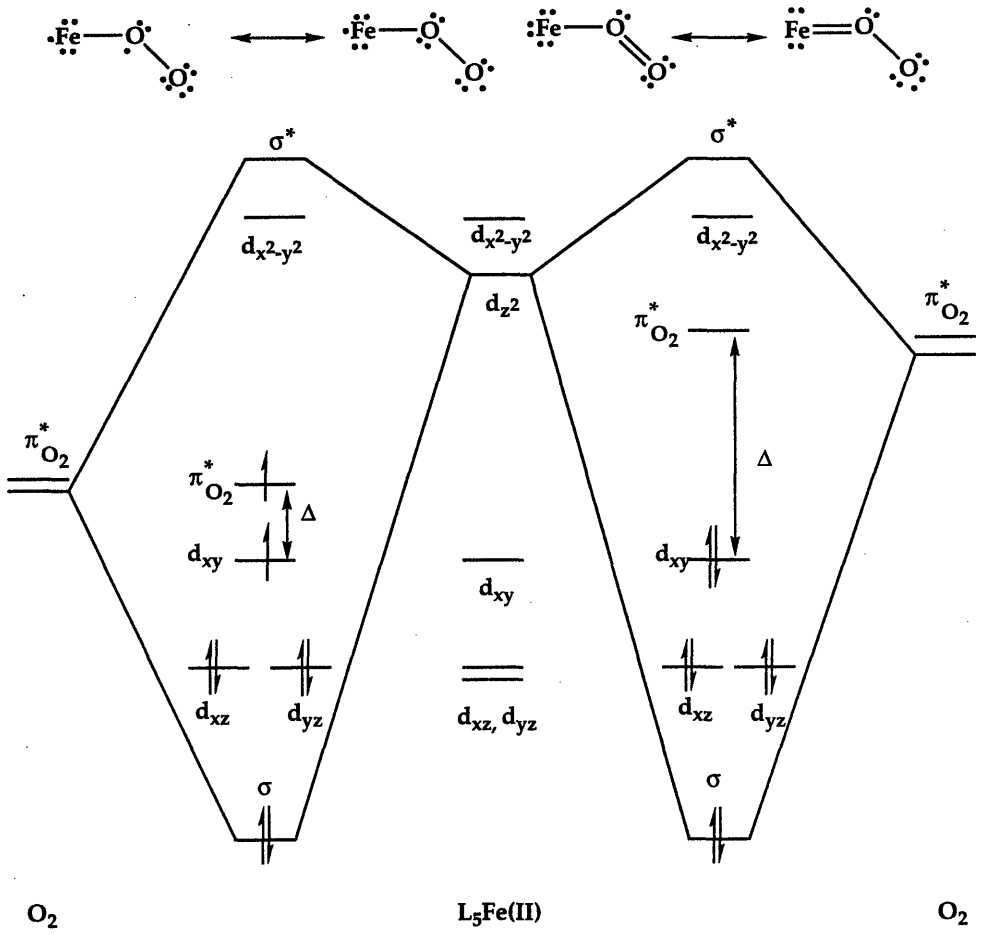

Figure 1.1. A qualitative MO scheme for the bonding in a hypothetical mononuclear iron-dioxygen complex, showing both σ and π interactions between iron and coordiated O_2. When Δ > pairing energy, this scheme is analogous to the $Fe^{II}(O_2)$-$Fe^{IV}(O_2^{2-})$ valence-bond resonance hybrids. (Adapted with permission from ref. 37.)

A second salient feature of metal ions with respect to their ability to mediate biological oxidations is the availability of multiple redox states. In the case of iron, the biologically relevant oxidation states are most often +2 and +3. That iron is required by an enzyme does not necessarily imply a redox role in dioxygen activation, however.[28] For example, some oxygenases, such as catechol 1,2-dioxygenase, use the Lewis acidity of iron(III) to induce substrate activation of dioxygen. In these cases, iron redox chemistry does not appear to be directly involved. The best way to establish a redox function is to observe oxidation state changes during enzyme turnover. Less direct evidence is the requirement of the reduced, ferrous state for activity. In addition to the common oxidation states, ferryl (Fe^{IV}=O) and perferryl (Fe^{V}=O) units have been invoked in several iron-dioxygen systems discussed below. Such species might arise from two-electron oxidation of iron(II) in a manner analogous to well precedented chemistry of iron(II) porphyrins.[42,43] In these systems, high oxidation state iron is stabilized by electron delocalization from the porphyrin ring, which forms a cation radical.[25,42-46] For non-heme iron, the ability of ligands to act in a similar manner is less obvious. In some of the model complexes, metal-bound pyridyl radicals could be invoked as a means of reducing the formal oxidation state of the iron center from +4 to +3. A second iron(II) center can also delocalize and stabilize the charge of the ferryl unit, as will be shown.

One important property of the dioxygen molecule is its propensity to accept electrons in pairs. Single electron transfer reactions, available at an energetic price, are less frequently encountered. This thermodynamic preference is manifest by electrochemical potentials of the dioxygen molecule in aqueous solution (Figure 1.2). An examination of the diagrams

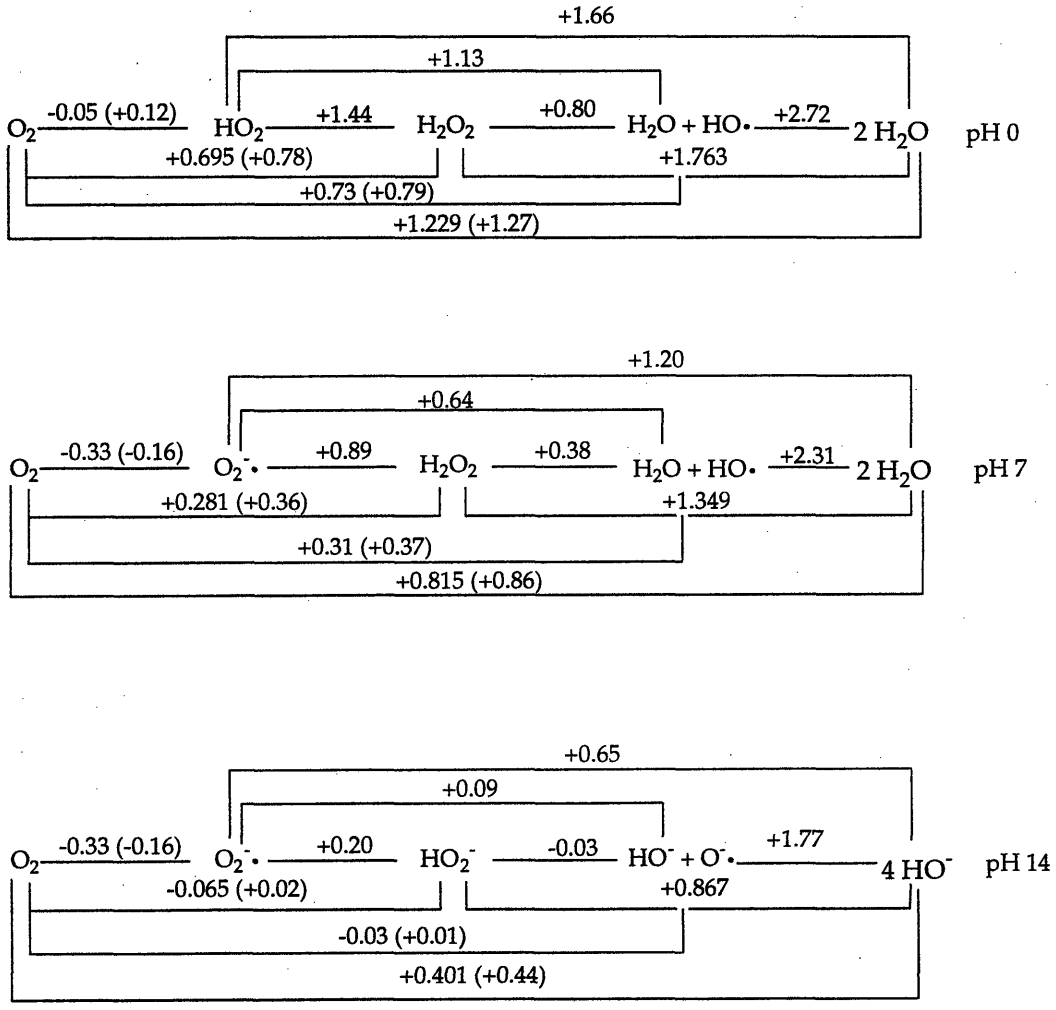

Figure 1.2. Standard reduction potentials (in volts) for dioxygen species in water. Formal potentials are given for O_2 at 1 atm or (in parentheses) at unit activity. (Reprinted from ref. 47. Copyright 1988 Plenum.)

in this figure shows that reduction of dioxygen to superoxide in a one-electron step occurs at a potential ≈ 0.5 V more negative than the two-electron reduction at the same pH. Even more negative electronic barriers are required for the one-electron reduction of hydrogen peroxide relative to its two-electron reduction. This property strongly influences the chemistry of iron(II) with dioxygen. Since the common redox step for Fe^{II} is oxidation to Fe^{III}, there is a natural mismatch between the electron-transfer preferences of the metal ion and dioxygen. One solution is to combine two ferrous ions into a single unit. Such species, formerly designated as diiron oxo units because of the occurrence of (μ-oxo)diiron(III) cores in several non-heme iron proteins,[13,17] are more appropriately referred to as diiron carboxylates based on recent structural revelations.[48,49] Reaction of such a diiron carboxylate center in its reduced form with dioxygen can generate a diiron(III) peroxide species. Alternatively, four-electron reduction of the O_2 molecule can yield two Fe^{IV} ions and two H_2O molecules. In mononuclear systems it is less certain how two-electron redox reactions are accommodated. Since an external reductant such as ascorbate, NADH, or [2Fe-2S] is usually required for both mono- and dinuclear iron systems, it is possible that the iron center cycles through two or more one-electron steps during each round of catalysis. Another possibility is that the ferrous ion is oxidized to an Fe^{IV} peroxide which then accepts electrons from an exogenous reductant. A third option is that, since many of the proteins are multimers, long-distance electron transfer pathways might supply electrons from remote iron centers to the mononuclear catalytic site. Finally, a protein side chain such as that of tyrosine or cysteine could provide the required electron.

Apart from these kinetic and thermodynamic properties, the chemistry of iron and dioxygen is characterized by the favored modes of coordination of the O_2 molecule to mono- and dinuclear centers. Figure 1.3 presents several known and postulated binding modes. Three of these geometries have been structurally characterized, the bent end-on coordination (**h**) found in hemoglobin,[6] the *syn*-terminal mode (**e**) of hemerythrin,[50] and the μ^4-mode (**j**) found in $[Fe_6(O_2)(O)_2(OBz)_{12}(H_2O)_2]$ (**1**), the only crystallographically characterized ferric peroxide model complex.[51] Which ones are likely to be found in metalloproteins? By comparison to copper-dioxygen systems, which have been more thoroughly investigated, binding modes **a-e** might be expected for dinuclear centers[52] whereas **g** and **h** are known for dioxygen complexes of other transition metals.[36,37] The 1,2-bridging peroxide model has been proposed for several iron systems to be discussed below.[53-55] Some of these coordination geometries can be experimentally distinguished by vibrational spectroscopy, especially with the aid of isotopically labeled dioxygen (^{16}O-^{18}O).[56,57]

Theoretical calculations favor end-on binding of dioxygen to an iron atom.[58] Experimental evidence on ferrous and ferric dioxygen adducts formed by matrix isolation techniques indicate predominance of the side-on geometry (**g**), for which ν(O-O) = 956 cm^{-1}.[59,60] These studies employ "naked" metal ions and are extremely crude models for biological or even small molecule analogs of non-heme iron. The steric and electronic effects of other ligands in the coordination sphere on the binding modes and reactivity of dioxygen are likely to be quite significant. This property is exemplified by the different chemical reactivities of hemerythrin, methane monooxygenase, and ribonucleotide reductase, all of which contain similar diiron carboxylate cores.

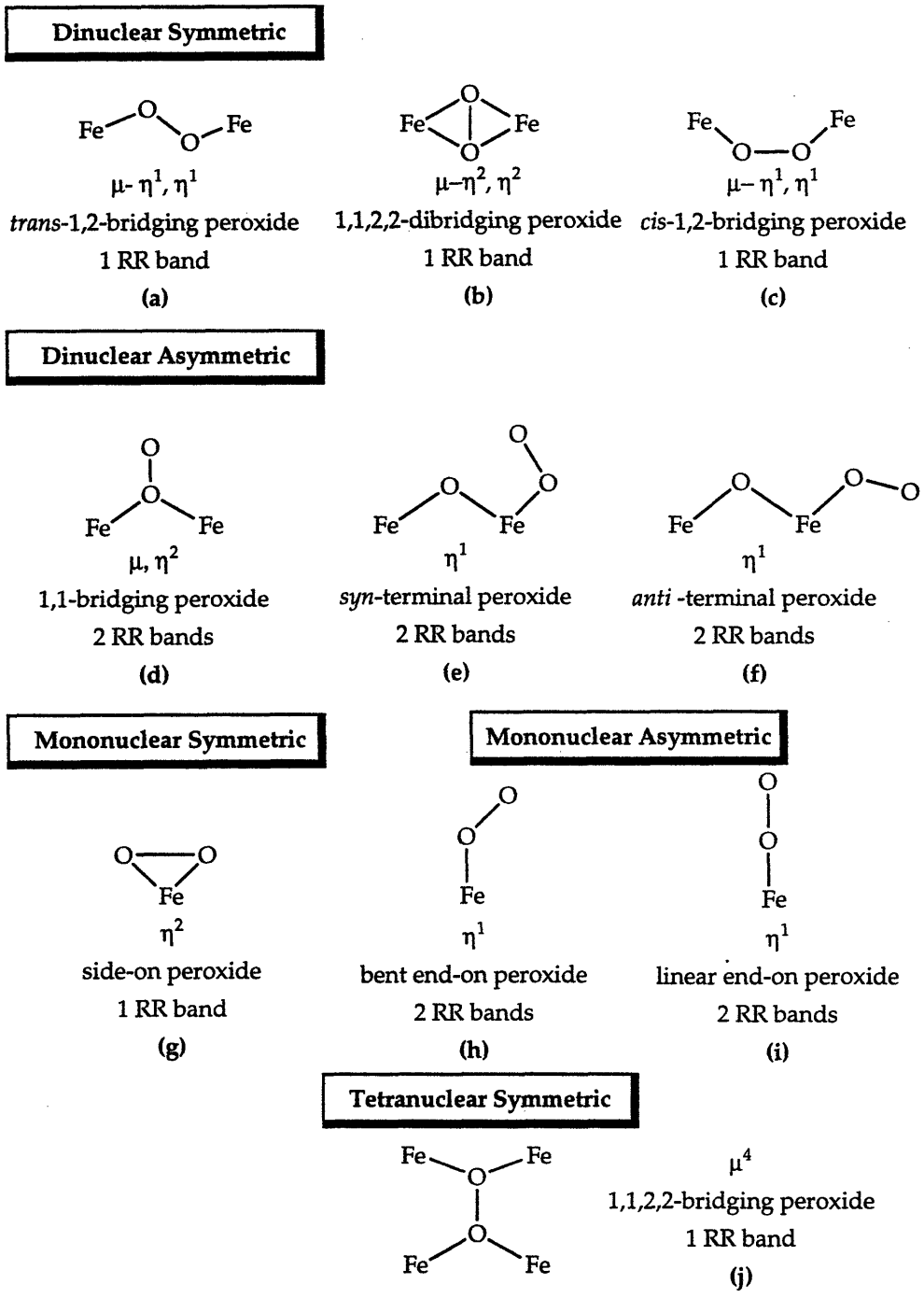

Figure 1.3. Potential dioxgyen binding modes for mono- and dinuclear iron compounds. The number of resonance Raman (RR) bands refers to the O-O or Fe-O stretching frequencies when using ^{16}O-^{18}O.

Autoxidation Reactions of Iron(II)

As an introduction to the reaction chemistry of dioxygen with iron(II), we first discuss the autoxidation of aqueous ferrous ion in the absence and presence of chelating ligands. These processes have been investigated for many years and, although they appear deceptively simple, the reactions are in fact extremely complex and difficult to define mechanistically. We begin with this discussion because it raises key issues that will appear later in the treatment of the chemistry of the biological and model systems. Formally, autoxidation has been defined as a spontaneous and self-catalyzed oxidation reaction.[61] In this review, we use the term specifically to denote reactions with dioxygen that result in its complete reduction to water without diverting oxidizing equivalents toward an external substrate. In the case of autoxidation involving Fe(II), the reaction is given in eq 1.1.

$$4Fe^{II} + O_2 + 4H^+ \longrightarrow 4Fe^{III} + 2H_2O \qquad (1.1)$$

When autoxidation occurs in biological systems or small molecule mimics, it is usually an undesired side reaction proceeding in parallel with the main oxidation process and resulting in the loss of catalytic activity. In biological systems, autoxidation often leads to inactive, or met, forms of a protein. In vivo there are usually specific reductases present to reduce the iron atoms to their functional oxidation states and restore activity. Formation of the met form of a purified protein in vitro, however, usually terminates the reaction. In a similar manner, catalytic systems that consume O_2 can also undergo autoxidation leading to loss of activity.

Several issues are important to raise at the beginning of our discussion of the reactions of non-heme iron(II) systems with dioxygen. One

is whether O_2 and O_2^- coordinate directly to iron during the reaction. The issue of inner- versus outer-sphere mechanisms attains special importance during our treatment of reactions involving coordinatively saturated species such as $[Fe^{II}(EDTA)]^{2-}$. Other points of general interest are the extent to which pH influences the course of the reaction and whether radicals derived from dioxygen are present as intermediates in the chemistry. These last two properties are controlled in non-heme iron proteins by the choice of ligands and the composition of the protein pocket surrounding the active site.

Reactions of Aquated Iron(II)

Iron(II) reacts with dioxygen in water by multiple pathways. Early workers assumed that the reaction occurs by a mechanism in which ferrous ion was first oxidized to the ferric state with concomitant reduction of dioxygen to superoxide ion (O_2^-), (eq 1.2).[62] The superoxide produced in this

$$Fe^{II} + O_2 \rightleftharpoons Fe^{III} + O_2^- \quad (1.2)$$

$$O_2^- + H^+ \rightleftharpoons HO_2 \quad (1.3)$$

$$Fe^{II} + HO_2 \longrightarrow Fe^{III} + HO_2^- \quad (1.4)$$

$$HO_2^- + H^+ \rightleftharpoons H_2O_2 \quad (1.5)$$

step was then postulated to react immediately with another equivalent of ferrous ion yielding, upon protonation, hydrogen peroxide and a second equivalent of ferric ion (eqs 1.3-1.5). Hydrogen peroxide reacts rapidly with iron(II) via the Haber-Weiss scheme (Fenton's reaction), ultimately yielding water and more ferric ion (eqs 1.6-1.8).[63] The stoichiometry of the net reaction is given in eq 1.1. The rate constant for the oxidation of $[Fe(H_2O)_6]^{2+}$

Fenton chemistry

$$Fe^{II} + H_2O_2 \longrightarrow Fe^{III} + OH^- + OH\bullet \quad (1.6)$$

$$Fe^{II} + OH\bullet \longrightarrow Fe^{III} + OH^- \quad (1.7)$$

$$OH^- + H^+ \rightleftharpoons H_2O \quad (1.8)$$

by dioxygen in the first step is several orders of magnitude less than the back reaction (eq 1.2).[64] From this observation and a theoretical analysis it was concluded that dioxygen must coordinate to the metal ion in order to be activated.[65] Interestingly, such a conclusion is similar to that reached in later work on inner- and outer-sphere electron-transfer pathways[66] and requires modification of the mechanism postulated in eqs 1.2-1.8.

Support for an inner-sphere electron-transfer pathway was provided by the effects of counterions and chelating agents on the rate law for the autoxidation reaction.[65] Depending upon the pH and the choice and concentration of counter ions, the reaction can be either first- or second-order with respect to the concentration of iron(II) (eqs 1.9, 1.10).[65,67-70] At

$$\frac{d[Fe^{III}]}{dt} = k'[Fe^{II}][O_2] \quad (1.9)$$

$$\frac{d[Fe^{III}]}{dt} = k''[Fe^{II}]^2[O_2] \quad (1.10)$$

constant pH, the rate of oxidation decreases in the series pyrophosphate[69] > phosphate[68] > chloride[71,72] > sulfate[72,73] > perchlorate.[67] Two parallel reactions occur, the relative importance of which depends on the binding constant of the anion for the aquated ferrous ion. The complete rate law (eq 1.11) could be accounted for by the mechanism depicted in eqs 1.12-1.20.

Anion binding favors the pathway that is first order in iron(II), depicted

$$\frac{d[Fe^{III}]}{dt} = k'[Fe^{II}(L)][O_2] + k''[Fe^{II}]^2[O_2] \text{ (L = bound anion)} \quad (1.11)$$

$$[Fe^{II}(H_2O)_6]^{2+} \rightleftharpoons [Fe^{II}(H_2O)_5(OH)]^{+} + H^{+} \quad (1.12)$$

$$[Fe^{II}(H_2O)_6]^{2+} + L^{-} \rightleftharpoons [Fe^{II}(H_2O)_5(L^{-})]^{+} + H_2O \quad (1.13)$$

$$[Fe^{II}(H_2O)_6]^{2+} + O_2 \rightleftharpoons [Fe^{II}(H_2O)_5(O_2)]^{2+} + H_2O \quad (1.14)$$

$$[Fe^{II}(H_2O)_5(O_2)]^{2+} \rightleftharpoons [Fe^{III}(H_2O)_5(O_2^{-})]^{2+} \quad (1.15)$$

$$[Fe^{III}(H_2O)_5(O_2^{-})]^{2+} + [Fe^{II}(H_2O)_6]^{2+} \longrightarrow [(H_2O)_5Fe^{III}(O_2^{2-})Fe^{III}(H_2O)_5]^{4+} + H_2O \quad (1.16)$$

$$[(H_2O)_5Fe^{III}(O_2^{2-})Fe^{III}(H_2O)_5]^{4+} + 2H^{+} + 2H_2O \longrightarrow 2\,[Fe^{III}(H_2O)_6]^{3+} + H_2O_2 \quad (1.17)$$

$$[Fe^{III}(H_2O)_5(O_2^{-})]^{+} + H^{+} + H_2O \rightleftharpoons [Fe^{III}(H_2O)_6]^{3+} + HO_2 \quad (1.18)$$

$$[Fe^{II}(H_2O)_6]^{2+} + HO_2 \xrightarrow{\text{fast}} [Fe^{III}(H_2O)_5(HO_2^{-})]^{2+} + H_2O \quad (1.19)$$

$$[Fe^{III}(H_2O)_5(HO_2^{-})]^{2+} + H^{+} + H_2O \longrightarrow [Fe^{III}(H_2O)_6]^{3+} + H_2O_2 \quad (1.20)$$

in eq 1.9, whereas the second order pathway (eq 1.10) dominates for species containing no bound anion.[65,68,69,74] The equilibrating species shown in eqs 1.12 and 1.13 should be considered to be present in each of the subsequent reactions even though they are not explicitly indicated. Hydrogen peroxide formed by eqs 1.17 and 1.20 will react rapidly with more Fe^{II} as indicated in eqs 1.6-1.8. These equations (1.12-1.20) differ from those previously proposed (eqs 1.2-1.8) owing to dioxygen coordination to iron(II). As indicated above, the result is electron transfer by an inner- rather than an outer-sphere mechanism. The anion-dependent rate acceleration arises from stabilization of ferric species, including those postulated in the transition state.[69]

The pH dependence is more complex than expected on the basis of a shift in the redox potentials and can be rationalized in a manner similar to the effects of anion binding. At higher pH values, one of the coordinated water molecules is deprotonated, again stabilizing iron(III). Because of the insolubility of ferric species with increasing pH, studies have been limited to pH values ≤ 2. Moreover, the reactions were usually followed for only a fraction of a half-life, with the analyses being based on initial rates. This limitation results from the relatively sluggish reaction velocities. For example, $k \approx 3.1 \times 10^{-5} - 1.4 \times 10^{-6}$ M^{-1} atm^{-1} s^{-1} for $Fe(SO_4)$ in water at 140-180° C, $[Fe]_0 = 1.0 - 30.0$ mM, 1 atm O_2,[69] corresponding to $t_{1/2} \approx 6600$-9000 h.

The high dielectric constant of water makes it an extremely good solvent for stabilizing the charge separation required by solvated ion pairs. By shifting from water to solvents with lower dielectric constants, the effects of anion binding to iron are enhanced. For example, the ability of chloride ion and solvent to affect the autoxidation of $FeCl_2$ in alcohols has been studied.[75,76] A large solvent-dependent rate enhancement and overall third-order kinetics were observed (eq 1.10), consistent with formation of a diferric peroxide intermediate and increased anion binding.[76]

Reactions of Chelated Iron(II) Complexes

Several workers have examined the effects of chelating ligands on the autoxidation of Fe^{II}.[64,77-81] In the presence of chelating agents such as EDTA, a two-term rate law was obtained (eq 1.21).[77] These results were interpreted as evidence for an equilibrium involving the parent chelate and its monoprotonated form (eq 1.22), the latter providing an open coordination site on iron. Both forms react with dioxygen, but at different rates. The fact

$$\frac{d[Fe^{III}]}{dt} = k_p[Fe^{II}(HZ)][O_2] + k_n[Fe^{II}(Z)][O_2] \quad (1.21)$$

$$[Fe^{II}(Z)]^{2-} + H^+ \rightleftharpoons [Fe^{II}(HZ)]^- \quad (1.22)$$

that the $k_p > k_n$ in every case suggested that a vacant coordination site on iron, provided by the dissociation of a single arm of the chelating ligand, accelerated the reaction rate by removing steric hindrance to the attacking O_2 molecule.[77] From an electronic point of view, this trend is counter-intuitive since protonation reduces the negative charge of the ligand and should stabilize the iron(II) form. It should also be noted that ferric ion can become 7-coordinate, as in the crystallographically characterized $[Fe^{III}(EDTA)(OH_2)]^-$ complex.[82] Thus, a site might be available for O_2 coordination regardless of the ligand protonation state. An alternative possibility is that the protonated arm of the ligand facilitates hydrogen ion transfer to bound superoxide, releasing HO_2.[77] Formation of free HO_2 was not definitively demonstrated, however. Analysis of the pH dependence of the reaction showed the maximal rate to occur at pH 3, with high and low pH limits determined by the values at which ligand dissociation occurred.[78]

The kinetics of this process were more recently examined in greater detail.[64] It was concluded that the mechanism involved only outer-sphere pathways (eqs 1.2-1.7). The pH-dependence of the reaction would then arise from protonation of free superoxide ion and attendant changes in its redox potential. In this scheme, reactions with hydrogen peroxide are rapid, so only eqs 1.2 and 1.4 affect the observed rate law and rate constant. Radical trapping studies of this autoxidation reaction revealed multiple species including superoxide ion, hydroxyl radical, and buffer based radicals.[81,83] The exact origin of their formation was not demonstrated experimentally,

although radical chain mechanisms initiated by OH• or O_2^- were proposed.[81] Unfortunately, the ability to trap radicals is consistent with either inner- or outer-sphere mechanisms. Other studies contradict these findings and support inner-sphere oxidation pathways.[78,80] Furthermore, a dioxygen adduct of Fe^{III}(EDTA) was prepared by addition of superoxide to the ferrous chelate complex at high pH[21] or of hydrogen peroxide to the ferric chelate.[84] The isolation of such an adduct provides strong evidence for binding, at least at high pH, but does not provide any insight into what might be happening under other conditions.

To summarize, the primary finding from these studies is that chelation significantly increases the rate of autoxidation. Autoxidation reactions have been studied for more than 40 years and are deceptively simple when written in the form of eq 1.1. The detailed mechanism is still being debated and, in view of the conflicting evidence, it is difficult to determine whether an inner- sphere or outer-sphere pathway predominates. Most likely, both pathways are available and, by varying reaction conditions, one may observe either mechanism. These considerations raise an important point regarding the interpretation of kinetic data. Although comparisons are frequently made among studies from different laboratories, unless the experimental conditions are identical it may be impossible to reconcile discrepancies.

Reactions of Biological Iron(II) Centers with Dioxygen

Protein systems that use the reaction of dioxygen with Fe^{II} are functionally quite diverse. They can be divided into general classes, mononuclear, dinuclear and polynuclear according to the number of iron atoms in the active site. The ferroxidase center in ferritin, which loads iron

into the mineral core of the protein, is classified here as polynuclear. On a functional level, however, it falls somewhere between the other two classes. As discussed below, its redox chemistry follows multiple pathways, one of which results in the formation of mononuclear and dinuclear intermediates. A non-protein system, iron-bleomycin, is presented at the end of this section because it is a natural product used in medicine as an antitumor agent. In our discussion of each system we focus on the reaction of iron(II) with dioxygen. Sufficient background will be presented to place the dioxygen reaction in context; for greater detail, however, the reviews cited should be consulted. As stated above, several non-heme-iron enzymes have been excluded from discussion. Reviews on these systems, which include iron-dependent superoxide dismutase,[32,85] lipoxygenases[86] and intradiol catechol dioxygenases,[28,29] are available elsewhere.

Mononculear Enzymes

4-Methyoxybenzoate O-Demethylase (Putidamonoxin)

In addition to methanotrophs which require methane, there are numerous other bacteria that consume aromatic hydrocarbons as their sole carbon and energy source.[87] Like MMO, the enzymes used by these organisms are of interest for their potential application in the bioremediation of chemical waste. One such enzyme, obtained from *Pseudomonas putida*, is 4-methoxybenzoate O-demethylase (putidamonooxin, PMO), which contains both a [2Fe-2S] cluster and a mononuclear non-heme iron site.[88-93] This enzyme catalyzes the conversion of 4-methoxybenzoic acid into 4-hydroxybenzoic acid and formaldehyde (eq 1.23). Many other substrates can bind to the enzyme,[94] however, some of which get hydroxylated and others of which do not. Substrates falling in the former category are termed "coupled," whereas

"uncoupled" substrates are competitive inhibitors that bind to the active site and allow enzyme turnover, but are not oxidized in the process. In the latter case, reductant is consumed and dioxygen is converted stoichiometrically to hydrogen peroxide.[91] When 3- or 4-hydroxybenzoate is used, the hydroxylation reaction affords the corresponding catechol (eq 1.24).[95] This chemistry is similar to the F208Y R2 mutant, described in detail below, which oxidizes a tyrosyl residue to dopamine on exposure of its ferrous form to dioxygen. In PMO, dioxygen reacts with the mononuclear ferrous center, and a ferric peroxide has been postulated as the active species.[96] NADH donates electrons by way of the iron sulfur cluster during turnover. It should be noted that, in certain cases, the observed product of the catalytic reaction is the result of further rearrangement after the hydroxylation step.[95]

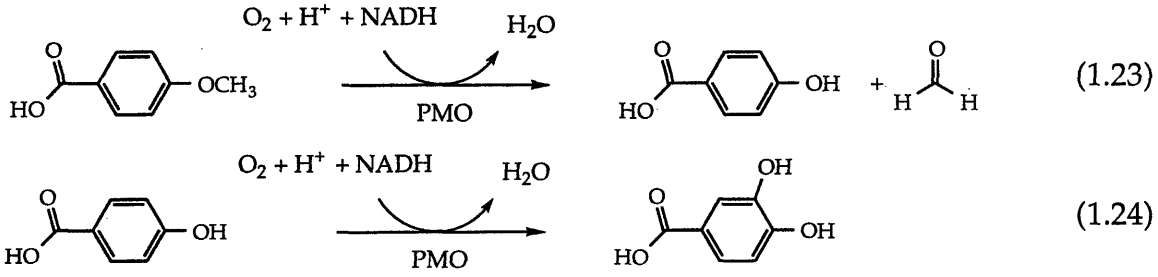

The structure of the non-heme iron center of PMO is less well defined than those of many other iron enzymes. Data obtained from EPR[96] and Mössbauer[97] spectroscopic studies, summarized in Table 1.1, are similar to those for the iron center in 3,4-protocatechuate dioxygenase discussed below,[97] but further work is required to establish the identity of the two enzyme active sites. The only certainty regarding the iron coordination sphere in PMO is the availability of exogenous ligand binding sites, which was demonstrated by the effect of ^{14}NO binding on the EPR spectrum. NO

Table 1.1. Spectroscopic Properties of Putidamonooxin and Protocatechuate Dioxygenase.

	Parameter	PMO + NO, no substrate	PMO + 4-NH_2-OBz + NO[a]	PMO + 4-4-OMe-OBz + NO[b]	oxidized PMO	3,4-PCD	reduced 4,5-PCD	reduced 4,5-PCD + substrate	reduced 4,5-PCD + substrate + NO	oxidized 4.5-PCD
Mössbauer	D, cm^{-1}			12	-1.8	-2			12	
	E/D			0.01	0.05	0.03			0.02	
	ΔE_Q, mm s^{-1}			-1.4	0.55	-0.5	2.22	2.33 2.80	-1.67	
	η			0.2	0.15				0.07	
	$A_0/g_N\beta_N$, T[c]			-23.5	-21.05				-32	
	Γ, mm s^{-1}			0.30	0.30					
	δ, mm s^{-1}			0.68	0.50	0.44	1.28	1.27 1.22	0.66	
	T, K				1.5 - 4.2	4.2 - 20	4.2	4.2	4.2	
EPR	g_1[d]	4.162	4.170	-						
	g_1[e]	4.093	4.08	4.101						
	g_2[e]	3.975	3.99	3.960						
	g_2[d]	3.892	3.882	-						
	g_3[d], g_3[e]	2.0	2.0	2.0						
	g						silent	4.35	4.21 3.77 1.99	6.4 5.5 4.3 2.0
ref.		97	97	97	97	99	98	99	98	98

[a]Uncoupling substrate. [b]Tight coupling substrate. [c] The parameter $A_0/g_N\beta_N$ is in units of internal field per spin 1, where $A_0 = A_x = A_y = A_z$, g_N is the nuclear g-factor, and β_N is the nuclear magneton. [d]Indicates spectral species with large tetragonal distortion. [e]Indicates spectral species with small tetragonal distortion.

mimicked the dioxygen binding step but did not turn over the enzyme.[96] Addition of coupled substrates to the NO-enzyme complex significantly altered the EPR spectrum, but uncoupled substrates caused no change. This result indicates that coupled substrates either bind directly to the metal center or induce structural rearrangements in the active site. The ferrous ion is bound quite loosely to the enzyme. In the absence of substrate, the equilibrium is such that 2/3 of the iron is free in solution.[96] The binding of both substrate and NO to the metalloenzyme stabilizes the iron center, preventing dissociation of ferrous ion.

Equation 1.25 sets forth a scheme for the dioxygen chemistry of PMO,[96] in which the iron-sulfur clusters feed electrons to the non-heme iron center one at a time. Species B-D are postulated to be EPR silent, and E and F never form in sufficient quantities to detect under turnover conditions.[96] With NO, D' (the NO analog of D) has been observed. Although D' should have a partially reduced [2Fe-2S] cluster, its EPR signal was unaffected by addition of NO.

$$\underset{A}{Fe^{III}} \xrightarrow{+e^-} \underset{B}{Fe^{II}} \xrightarrow{+O_2} \underset{C}{Fe^{II}{-}O_2} \rightarrow \underset{D}{Fe^{III}{-}O_2^-} \xrightarrow{+e^-} \underset{E}{Fe^{II}{-}O_2^-} \rightarrow \underset{F}{Fe^{III}{-}O_2^{2-}} \qquad (1.25)$$

On the basis of results obtained with 4-vinyl benzoate, a ferric peroxide intermediate was postulated as the active hydroxylating species.[100] By using $^{18}O_2$, it was found that both oxygen atoms in the product, 4-(1,2-dihydroxyethyl)benzoate, were derived from the dioxygen molecule. The ability of the enzyme to function as a dioxygenase rules out the possible involvement of a ferryl species, the formation of which would require one of the oxygen atoms to be lost to solvent.

Any complete mechanism for this enzyme must also account for the high proportion of NIH-shifted product observed during turnover.[101] This property is usually interpreted as evidence for opening of an epoxide intermediate at either of its two C-O bonds. It is unclear at present whether ferric peroxides are capable of catalyzing such reactions without first decomposing heterolytically into a perferryl species. The intermediate in such a non-ferryl mechanism might be a dioxetane, a four-membered cyclic peroxide, which could lead to significant NIH shifts by a ring-opening mechanism analogous to that of an oxirane.

Extradiol Catechol Dioxygenases

Catechol dioxygenases are important enzymes involved in the catabolism of aromatic compounds. They catalyze the cleavage of aromatic rings to form linear unsaturated diacids or acid-aldehydes (Figure 1.4). The extradiol catechol dioxygenases such as protocatechuate 4,5-dioxygenase, catechol 2,3-dioxygenase, and many others, are not nearly as well studied as their intradiol counterparts, catechol 1,2-dioxygenase and protocatechuate 3,4-dioxygenase.[28,29,38,102] The intradiol enzymes use a novel substrate activation mechanism in which catechol binds to a ferric site that does not undergo redox chemistry during turnover.[28,29,38,102-105] In these enzymes, dioxygen reacts directly with the substrate-bound ferric form of the enzyme rather than with the ferrous form. The extradiol catechol dioxygenases, on the other hand, require the ferrous form of the enzyme.[28,29] This finding was an initial indication that an iron-dioxygen intermediate was involved in the enzyme mechanism. For simplicity, we focus our discussion on the chemistry of protocatechuate 4,5-dioxygenase (4,5-PCD) from *Pseudomonas testosteroni*, the best studied of the extradiol enzymes.

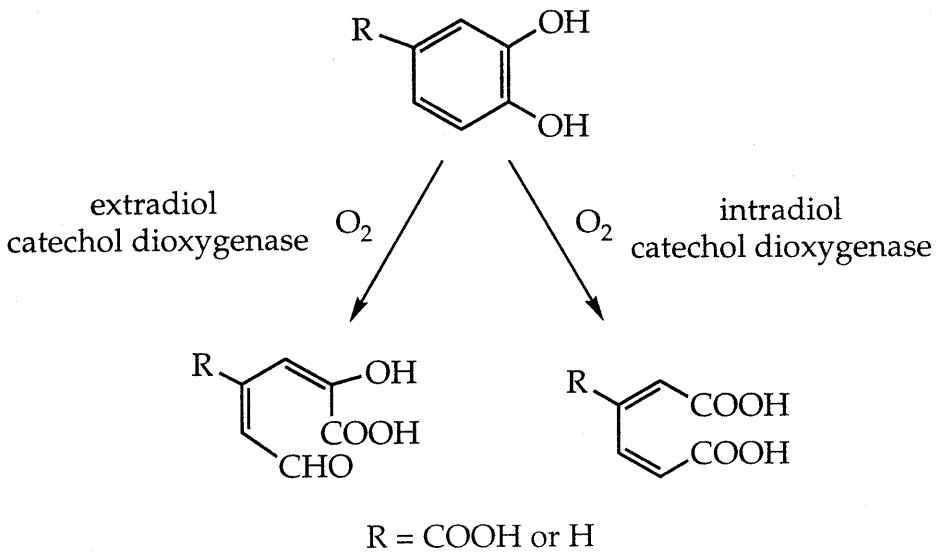

Figure 1.4. Reactions of extradiol and intradiol catechol dioxgyenases.

4,5-PCD contains a single ferrous site per $\alpha_2\beta_2$ tetramer (MW = 52.3 kDa),[98] the nature of which has been examined spectroscopically (Table 1.1). Mössbauer studies on the *Pseudomonas testosteroni* enzyme revealed a high spin octahedral ferrous ground state (δ = 1.28 mm s^{-1}, ΔE_Q = 2.22 mm s^{-1} at 4.2 K).[98] Mössbauer parameters for 4,5-PCD from other organisms are slightly different but still characteristic of a high spin ferrous center.[106] One of the most interesting findings is that the Mössbauer parameters shift upon addition of substrate, providing evidence, although not proof, for inner-sphere coordination. Longer range interactions due to side-chain reorganization upon substrate binding can also lead to spectral changes for the iron center. In the presence of catechol, the data revealed two quadrupole doublets assigned to substrate bound and free forms of the enzyme.[98] In both the presence and absence of substrate, NO binding also affected the iron Mössbauer spectrum.[98]

A series of EPR experiments has been carried out on this enzyme. The ferrous form was EPR silent, but after oxidation to Fe^{III} species several signals appeared (g=6.4, 5.5, 4.3) and were assigned to a heterogeneous mixture of products.[98] Once again, substrate and NO binding affected the spectra, further supporting the existence of a ternary (E-S-O_2) complex in which each component is bound to the iron center.[107] The use of isotopically labeled water ($^{17}OH_2$) indicated that at least two, and possibly a third, iron coordination sites contained bound water in the absence of substrate and dioxygen.[108] Detailed studies of the electronic structure of the iron center in catechol 2,3-dioxygenase using MCD were interpreted by a slightly different model having a 5-coordinate, square pyramidal active site geometry.[109]

A postulated mechanism for the reaction is shown in Figure 1.5.[107] Following enzyme-substrate complex formation, dioxygen binds to the ferrous form of the enzyme without oxidizing it to a ferric superoxide intermediate. This conclusion was based on the observation that autoxidation of the enzyme is slow. Whereas most ferrous enzymes must be kept strictly anaerobic to prevent such oxidative inactivation, 4,5-PCD must be oxidized with hydrogen peroxide or some other suitable oxidant to inactivate it completely.[98] This property indicates that, in the absence of substrate, the ferric-superoxide species is not thermodynamically favored in this system. A dioxygen adduct, although not detected in the absence of substrate, is inferred from the NO complex mentioned above. In addition, in the presence of substrate, the binding constants for NO and other exogenous ligands are significantly larger, an effect similar to the one discussed above for PMO.[108,109] The exact cause of such substrate effects is not known, but substrate binding may change the redox potential of the iron center, making it more susceptible to oxidation by dioxygen.[110,111] In the presence of substrate, the bound dioxygen molecule is postulated to attack the coordinated catecholate leading ultimately to ring opening, as indicated in Figure 1.5.[107] This reaction amounts to a nucleophilic attack on a benzene ring. If C-5 were to acquire semiquinone character during oxidation of iron(II) to iron(III), however, a radical attack of the coordinated dioxygen might be possible. More work is required to establish the mechanism.

Pteridine-Dependent Reactions

This class contains 3 known iron enzymes that utilize dioxygen, phenylalanine hydroxylase (PAH), tyrosine hydroxylase (TH) and tryptophan hydroxylase (TRH). The reactions catalyzed, shown in Figure 1.6, are all used

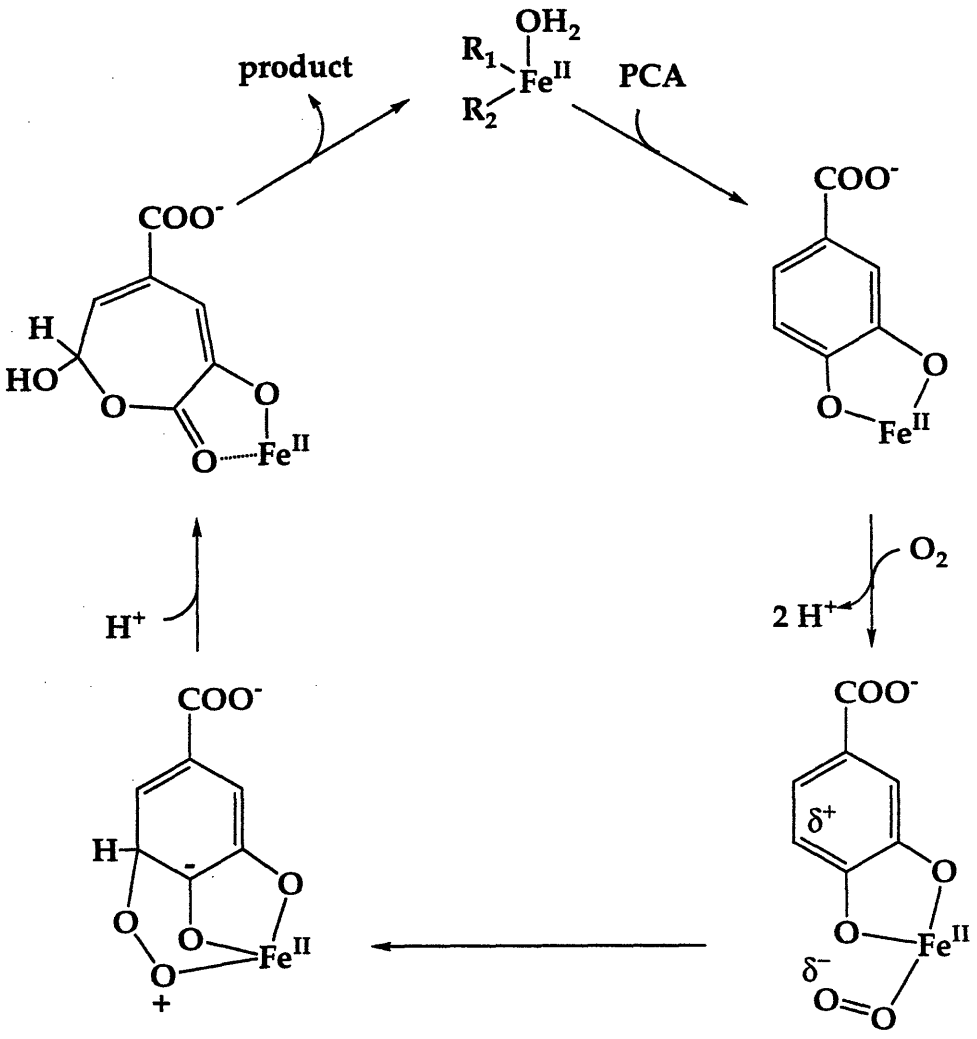

Figure 1.5. Proposed mechanism for the oxidation of 4,5-PCD. (Adapted with permission from ref. 107.)

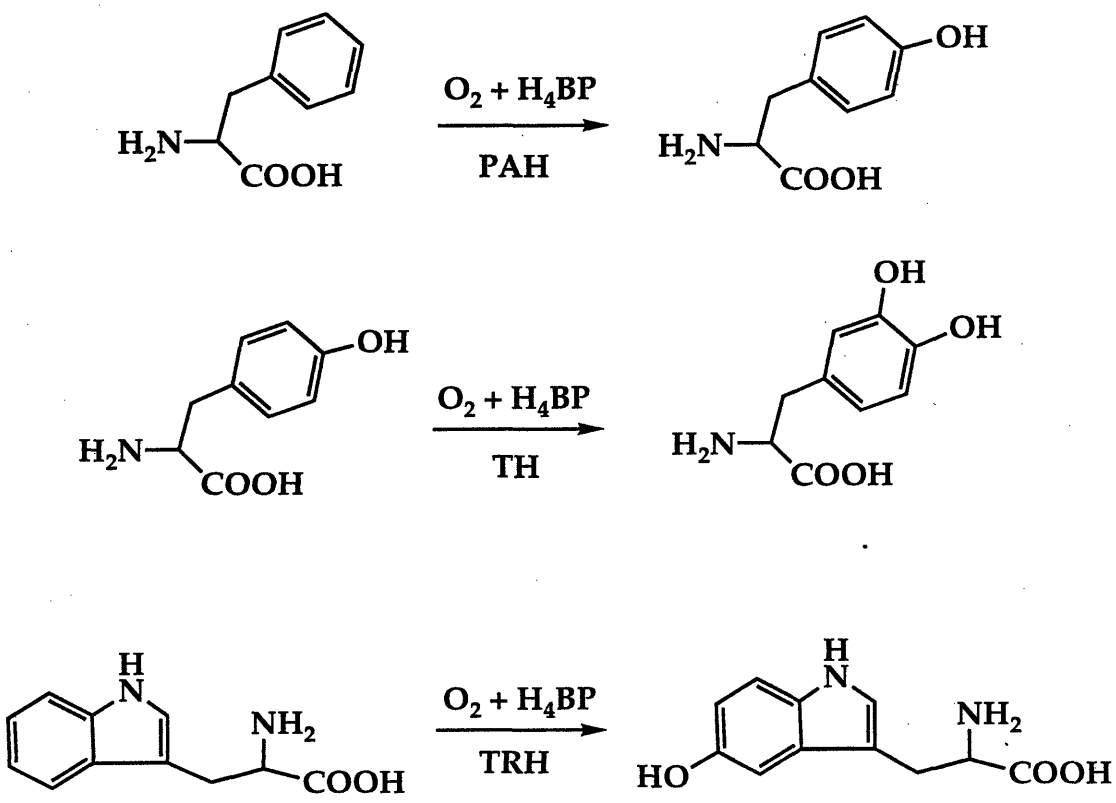

Figure 1.6. Reactions of the pteridine-dependent non-heme iron enzymes. PAH = phenylalanine hydroxylase; TH = tyrosine hydroxylase; TRH = tryptophan 5-hydroxylase; H_4BP = tetrahydrobiopterin.

in mammalian amino acid metabolism. The product of the TH-catalyzed reaction, the catecholamine L-DOPA, is especially important because it is the precursor of the neurotransmitters epinephrine and norepinephrine. Most work in this area has been carried out on PAH, primarily because of its ease of isolation. We therefore focus our discussion on this enzyme, since others in the class are likely to behave similarly.[112] The pteridine used naturally by these systems is tetrahydrobiopterin (H_4BP), which gets oxidized to quinonoid dihydrobiopterin (H_2BP) during turnover.[112] Many analogs of this reductant are active in the catalytic system and their use has been instrumental in determining the enzyme mechanism.[113] Complete reviews on all the pterine-dependent enzymes are available elsewhere.[113,114]

The nature and structure of the iron site in PAH have been somewhat neglected. Our ability to make reasonable interpretations regarding structure-function relationships in this system is therefore hampered. A discussion of the chemical properties of the system will allow comparisons to be made with other reactions of ferrous iron with dioxygen, however. When more structural information is available, a reanalysis will be necessary.

By analogy to flavin systems, it was originally proposed that dioxygen reacts directly with the organic cofactor to generate 4a-hydroperoxy-tetrahydrobiopterin (4a-OOH), which decays to form the active oxidant. Substantial evidence has been acquired in support of this hypothesis.[113,115,116] According to this mechanism, iron(II) would react with the peroxidated cofactor, rather than with dioxygen itself, forming an iron(II) peroxypterine (Fe-OO-4a) adduct. Heterolytic decomposition of this intermediate is proposed to yield 4aOH and a ferryl species that is the active oxidant. This theory appeared to be supported by the existence of what was

believed to be a PAH that contained no metal ion isolated from *Chromobacterium violaceum*,[117] since the heterolytic cleavage of hydroperoxides is known to occur under certain metal-free conditions. In such a case, OH· would be the active species. It was subsequently shown, however, that a Cu(I) cofactor had been overlooked.[118] Thus, all known enzymes of this class require reduced metal cofactors for activity.

This fact raises the possibility that a reaction between reduced metal and dioxygen precedes formation of the 4a-OOH intermediate. The strongest evidence for such a role for iron in PAH is the diminished oxidation rate of the cofactor in its absence. Were the synthesis of the 4a-OOH intermediate independent of protein-bound Fe^{II}, the unstable peroxide should still form rapidly, although its decomposition would be altered by the lack of functional protein. Based on chemistry observed in other enzymes and model systems, and the clear requirement for reduced iron, it may be that a ferric-superoxide/ferrous-dioxygen adduct forms initially which then peroxidizes H_4BP. The reaction would yield the same Fe^{II}-OO-4a cofactor adduct discussed above and possibly result in the same heterolytic decomposition pathway. The current experimental data unfortunately cannot differentiate these two pathways. Recent NMR studies on the active site of TH have measured the distance between the phenylalanine C3/C4 positions and the metal center at 6.8 ± 1.2 Å.[119] This constraint positions the amino acid in approximately the right place for a perferryl-oxo or ferric peroxide to act upon it during enzyme turnover.

If the activation steps are based on iron chemistry, release of superoxide or hydrogen peroxide might be a potential side reaction. There is conflicting evidence regarding H_2O_2 formation during the coupled and uncoupled reactions.[115,120,121] Superoxide dismutase is more effective than

catalase in preventing damage to the enzyme,[121] and small amounts of released superoxide have been detected during turnover.[115] Both of these results are consistent with a ferric-superoxide intermediate. These findings support an active role for the iron center in a reaction with O_2, but could also be explained by non-specific ferrous ion activity.

α-Keto Acid-Dependent Reactions

The α-keto acid-dependent enzymes, of which there are at least eight variants, comprise one of the largest classes of non-heme iron proteins.[101] These enzymes are characterized by their requirement for Fe^{II}, ascorbate, dioxygen and an α-keto acid, usually α-ketoglutarate (2-KG). In one example, (p-hydroxyphenyl)pyruvate hydroxylase, the keto acid moiety is an integral part of the substrate.[101] The general reaction catalyzed by these enzymes hydroxylates substrate and decarboxylates 2-KG, with one oxygen atom from O_2 being transferred to substrate and the other to the carboxylate group of the newly formed succinate (eq 1.26).[122,123] The best studied system to date is prolyl 4-hydroxylase which oxidizes proline residues of pre-collagen, but again, since all the enzymes in this class are expected to function similarly, discussion can be generalized to the other systems. Two reviews are available.[124,125]

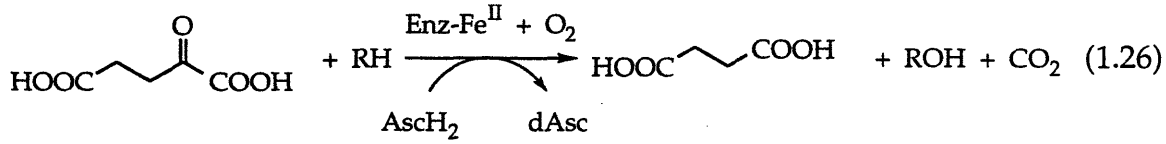

(1.26)

The mononuclear iron center in these enzymes has a rather accessible coordination sphere. In studies with cofactor analogs, it was found that both 2-KG and ascorbate bind directly to iron, and it was assumed that there must

also be an available coordination site for dioxygen.[124,126] Binding of 2-KG to the apoenzyme prevented subsequent incorporation of iron, so it was postulated that 2-KG occludes the metal binding site.[127] In prolyl hydroxylase, iron binding to the enzyme was proposed to require three ligands, at least one of which may be cysteinyl thiolate.[128-130] The identity of the other ligands is unknown and much work remains to be done. The only biophysical data available for the iron center come from EPR studies. In the absence of substrate or 2-KG, a signal appears at g = 4.3, typical of high spin ferric ion.[131] Upon addition of 2-KG, the amplitude of this signal increases, possibly indicating stronger coordination of ferric ion to the enzyme in its presence. Upon further addition of $AscH_2$, the g = 4.3 signal decays with concomitant growth of a signal at g = 2. The role of ascorbate therefore appears to be to reduce the ferric form of the enzyme.

Despite the lack of detailed information about the coordination environment of the iron center in prolyl hydroxylase, a mechanism consistent with all the experimental evidence has been proposed (Figure 1.7).[124] The mechanism consists of 5 main steps: 1) dioxygen binding to form ferric superoxide; 2) attack of superoxide on bound 2-KG; 3) decomposition of 2-KG into CO_2 and a succinate-bound ferryl; 4) attack by ferryl on the C-4 of proline; and 5) product release. Under normal turnover conditions, the iron returns to its original ferrous state at the end of the catalytic cycle. Several lines of evidence support this mechanism. First, substoichiometric amounts of ascorbate are consumed during turnover, whereas, in the absence of substrate, 1 mol of ascorbate is consumed per mole of CO_2 produced.[132-134] If the enzyme is reconstituted with ferrous ions, the initial rate of oxidation is constant whether or not ascorbate is present, but falls off within the first minute.[135] This behavior indicates two parallel

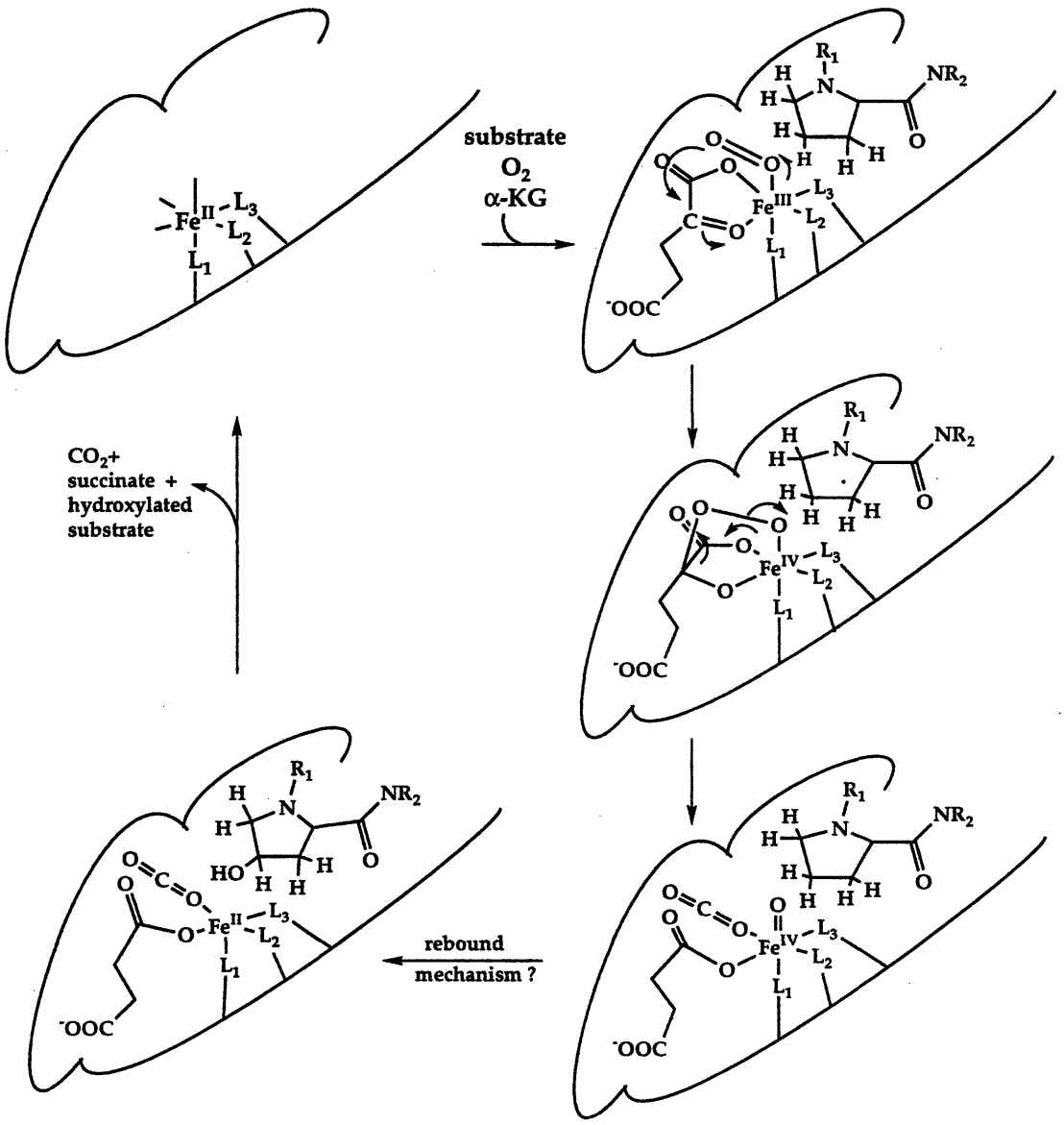

Figure 1.7. Proposed mechanism for the oxidation of proline by prolyl hydroxylase. Ligands L_1, L_2, and L_3 are amino acid residues. R_1 and R_2 are the peptide attachments of the proline substrate. (Adapted with permission from ref 124.)

pathways, a productive one leading to hydroxylated substrate and regenerated ferrous ion, and a non-productive one that leaves the enzyme stranded in the ferric state unless ascorbate is present to reactivate it. Such a stepwise mechanism is consistent with kinetic and EPR data showing a multiphase reaction, including an initial activation step, and CO_2 release at different rates than the appearance of dehydroascorbate.[131,134] Furthermore, the mechanism explains the very small observed intermolecular deuterium kinetic isotope effect. The rate-determining step involves enzyme binding and release of the cofactors and substrates, none of which is involved in the C-H bond breaking step.[124] The active ferryl species turns over whether or not substrate is in place, leading to the substoichiometric reduction of $AscH_2$.[136] Additional work to reveal the structural features of this and other 2-KG enzymes is necessary to understand fully the attributes of this system that are responsible for its robust nature and widespread use in biology. Furthermore, the enzymes are good targets for potential trapping of non-heme ferryl species through adjustments in the cofactor-enzyme interactions. Several cofactor analogs have already been studied in detail from a kinetic perspective,[126,133,137] but do not appear to have been used in attempts to obtain spectroscopic evidence for this elusive high-valent iron species. Model studies using ferrous benzoyl formate complexes have been able to duplicate the 2-keto acid decarboxylation reaction with concomitant oxidation of phenols to biphenols.[138,139] The nature of the active intermediate has not yet been determined, however.

The portion of the mechanism that remains murky pertains to the reaction of the ferryl species with substrate. For prolyl hydroxylase, it is difficult to approach this question because the substrate is a protein, typically $(Pro\text{-}Pro\text{-}Gly)_x$, in the in vitro assays.[140] Possibly this phase of the

mechanism might be clarified through investigation of alternative enzymes such as thymine 7-hydroxylase.[141] This enzyme hydroxylates the exocyclic methyl group of thymine, but recent work has shown that it can epoxidize olefins, oxidize thiol ethers to sulfones and sulfoxides, and demethylate the 1-methyl group of 1-methylthymine.[142] It therefore mimics all the activities associated with the putative ferryl species of the non-heme system cytochrome P-450.[42] Currently, only an outline of this activity has been elucidated, but the mechanistic results are sure to add greatly to our understanding of species involved in the reactions of non-heme iron proteins with dioxygen.

Isopenicillin N Synthase

The final mononuclear enzyme to be discussed is isopenicillin N synthase (IPNS), a polypeptide with a molecular weight of 37-40 kDa depending on the species from which it is isolated.[143-145] This iron(II)-containing enzyme differs substantially from those previously discussed in that, although dioxygen is consumed in the reaction, the substrate, δ-[5-amino-5-(hydroxycarbonyl)pentanoyl]-L-cysteinyl-D-valine (ACV), is not oxygenated. Instead, a process called desaturative cyclization occurs in which the loss of hydrogen atoms results in ring closure.[143-145] The overall reaction shown in eq 1.27 results in the stereospecific formation of both the β-lactam and thiazoline rings. The two ring-forming steps occur with retention of

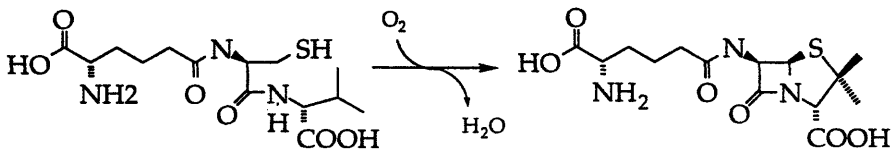

(1.27)

ACV Isopenicillin N

configuration, and the complete process consumes 1 equiv of dioxygen.[146,147] Since two covalent bonds are formed, the transformation results in no net change in iron oxidation state although transient, high-valent species are proposed as discussed below.

Whereas many of the mononuclear iron(II) enzymes discussed above have poorly understood metal centers, extensive spectroscopic data on IPNS provide as clear a picture of the active site as possible without a crystal structure. Mössbauer,[148,149] EPR,[148-150] NMR,[150,151] EXAFS[152,153] and optical spectroscopy,[148-150] summarized in Table 1.2, have been used to construct a model (Figure 1.8) in which the low spin octahedral iron(II) center is coordinated to one aspartate and three histidine residues in the resting state. There are two conserved cysteine residues that affect the reactivity of the enzyme, but are not essential to catalysis, as shown by mutagenesis experiments.[154,155] Upon addition of substrate, spectroscopic changes occur at the iron center consistent with direct coordination.[148-153] It has been postulated that, under anaerobic conditions, the peptide substrate coordinates through the cysteinyl sulfur. Binding of NO has been used to probe the structures of the O_2 and substrate adducts formed immediately prior to turnover, with somewhat conflicting results.[149,151] NO is postulated to displace either a histidine[151] or an aspartate residue.[149] In either case, coordinated water or hydroxide occupies the remaining coordination site(s).

The foregoing spectroscopic studies have not provided much evidence regarding the nature of the enzyme mechanism, however, and in work with the natural substrate, no intermediates, such as a monocyclic peptide, have been observed.[144] On the other hand, substrate analogues and isotopic labeling experiments have revealed several features of the reaction mechanism.[144,156-163] A current model, which is comprised of multiple

Table 1.2. Spectroscopic Properties of Isopenicillin N Synthase.[a]

	Parameter	IPNS no substrate	IPNS + NO no substrate	IPNS + NO + ACV	IPNS + ACV
Mössbauer	D, cm^{-1}		14	14	
	E/D		0.015	0.035	
	ΔE_Q, mm s^{-1}	2.70	-1.0	-1.2	3.40
	η		0.1	1.0	
	δ, mm s^{-1}	1.30	0.75	0.65	1.10
	T, K	4.2	4.2	4.2	4.2
EPR	g	n.o.	4.09	4.22	n.o.
			3.95	3.81	
			2.0	1.99	
	E/D		0.015	0.035	
	S		3/2	3/2	
Optical	λ, nm	none > 280	340	508 (1600)	none >280
	(ε, M^{-1} cm^{-1})		430	720	
			600		

[a]Data from ref. 148,149. n.o. = not observed. ACV = δ-[5-amino-5-(hydroxycarbonyl)-pentanoyl]-L-cysteinyl-D-valine

steps, is presented in Figure 1.9. Two hydrogen atom positions exhibit large kinetic isotope effects when deuterated substrate is used. Cleavage of these two C-H bonds, designated as steps 1 and 2 in Figure 1.9, is therefore important in initiating the respective ring closure reactions. As indicated, four-electron oxidation of the substrate-iron complex occurs prior to the closure of either heterocycle. Two of the oxidizing equivalents are used to oxidize the cysteinyl sulfur of the substrate while the other two electrons convert Fe^{II} to ferryl, Fe^{IV}. An internal rearrangement then occurs to generate a monocyclic intermediate bound to the ferryl through the sulfur

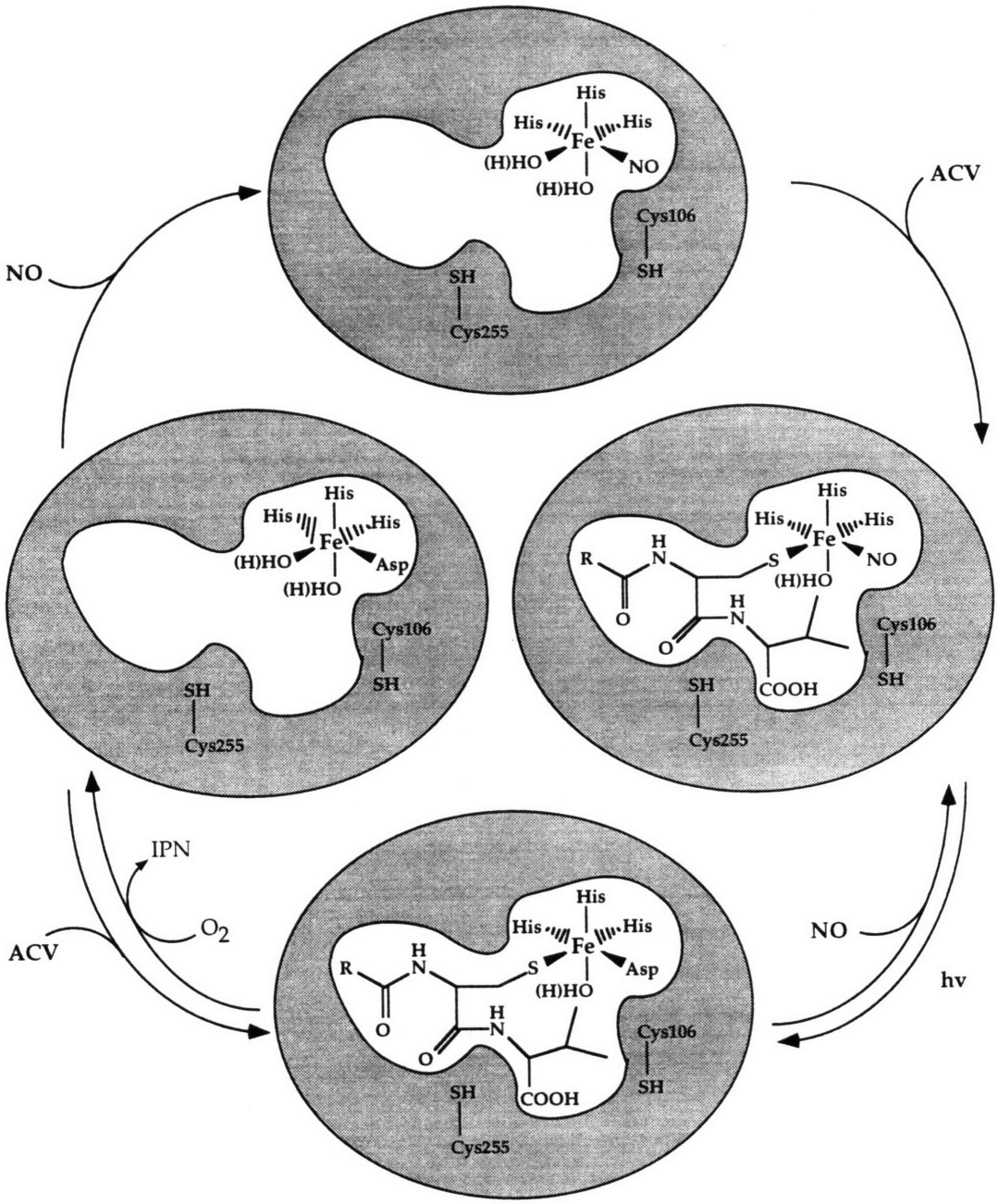

Figure 1.8. Proposed structure of the isopenicillin N synthase (IPNS) active site in its native, substrate bound, and nitrosyl forms. The relative positions of the ligands around the iron center are arbitrary. (Adapted with permission from ref. 149.)

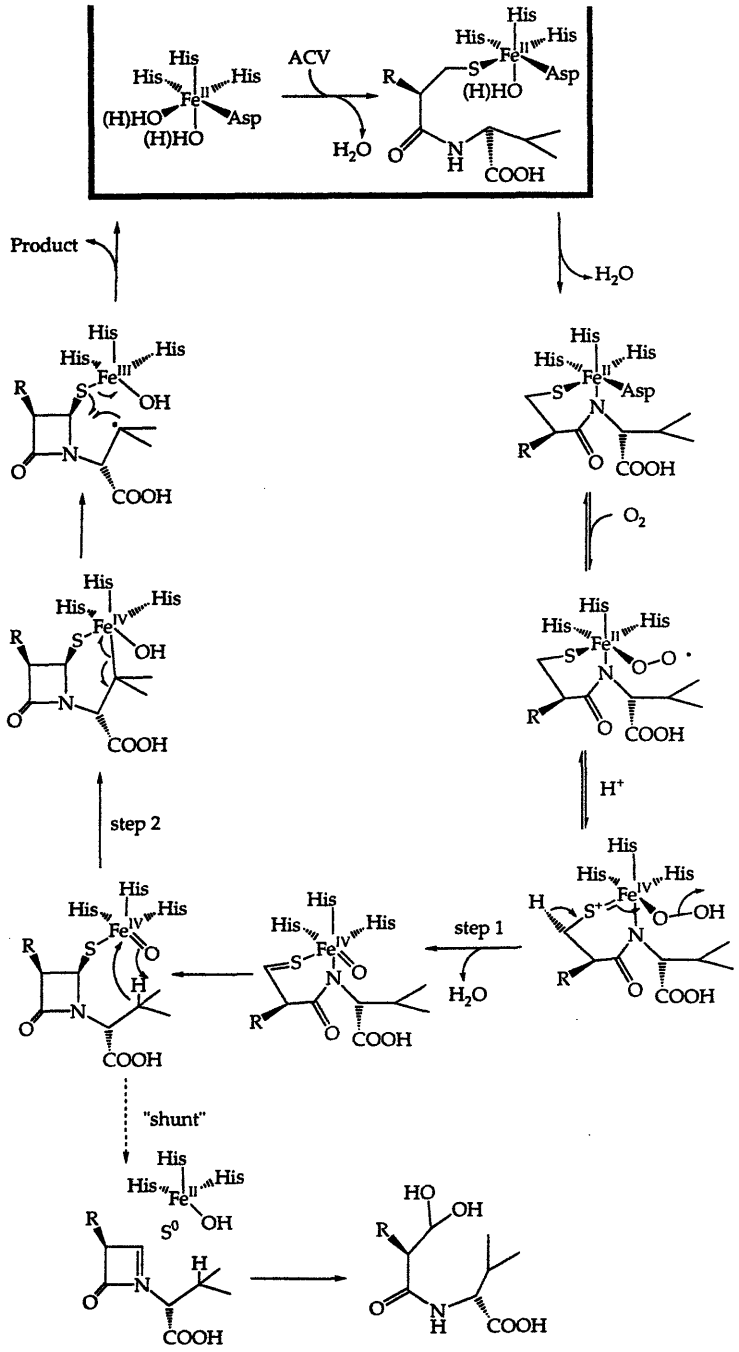

Figure 1.9. Mechanism proposed for the desaturative cyclization of ACV by isopenicillin N synthase. Steps 1 and 2 refer to processes affected by isotopic labeling of the depicted hydrogen atom. The shunt pathway is written as a branch between steps 1 and 2, but is generally not observed for the ACV substrate. The existence of this pathway is postulated on the basis of studies using substrate analogs and deuterated ACV. (Adapted with permission from ref. 163.)

atom. Evidence for this intermediate can be derived from so called "shunt" substrates that fail to undergo closure of the thiazolidine ring. These tripeptide substrates fall into several classes including some deuterated at the valine C-3 position or others containing homocysteine instead of cysteine.[144,163] The ferryl complex is then proposed to insert into the carbon-hydrogen bond at the valine C-3 position to form the organo-iron species shown in Figure 1.9. This intermediate then cleaves the Fe-C bond homolytically to eliminate, after rearrangement, product and water, while returning the enzyme to its initial iron(II) oxidation state.

The participation of a ferryl in this phase of the reaction has been supported by several experiments using amino acid analogues in place of valine. One of these derivatives, designed to show the role of a ferryl through the interception of the radical intermediate, contained a cyclopropyl group attached to the substrate.[156,164] Upon incubation with IPNS and dioxygen, a 3:1 ratio of ring-opened to unrearranged products was observed, indicative of a radical intermediate. An intermediate containing a weak iron-carbon bond capable of radical dissociation could explain these results and has been proposed.[156,165] Certain other derivatives, notably those containing allylglycine residues in place of valine, were oxygenated by IPNS in reactions remarkably similar to those of cytochromes P450.[144] In these cases, the incorporated oxygen atom derived primarily from dioxygen.

Proteins with Diiron Centers

Hemerythrin

Hemerythrin (Hr) is the oxygen carrier protein in marine invertebrates including sipunculids, annelids, priapulids and brachiopods. It functions in a manner directly comparable to the mammalian proteins myoglobin and hemoglobin.[14,16,57,166,167] In most species, the protein is an

octamer although monomeric and other oligomeric forms are known. Each subunit, ranging in molecular weight from 13.5 - 13.9 kDa, contains two ligand-bridged iron atoms.[16] There are two major classes of hemerythrins, those exhibiting cooperative binding of O_2 and those that do not. Unless otherwise specified, all studies mentioned here refer to non-cooperative hemerythrins.

The crystal structures of oxyhemerythrin[168] and higher resolution structures of oxy, deoxy, met and azidomet forms of the protein have been solved.[50,169-172] This extensive structural work revealed that the basic 3-dimensional motif of the protein is evolutionarily conserved[173] and confirmed many predictions made based on a variety of biophysical studies. Together with the available spectroscopic,[174-180] kinetic[181-185] and thermodynamic[181,182] data on the reaction of the dinuclear iron center in Hr with dioxygen, the structural details make this protein one of the best understood of all non-heme iron systems.[14,16,166,167,187]

The structure of Hr is shown in Figure 1.10. The dinuclear iron center, which resides within a 4-helix bundle, has several distinguishing features. In the reduced, deoxy form, the core is asymmetric, having one 5-coordinate and one 6-coordinate iron atom. Two protein carboxylates and one solvent-derived hydroxide bridge link the two iron atoms. In the met and oxy forms, the bridge is deprotonated. Terminal ligation sites are filled by nitrogen atoms donated from the imidazole side chains of five histidine residues and, in the met and oxy forms, by an additional, exogenous ligand. Key distances and angles are presented in Table 1.3. One of the more important findings of the structural work was proof that, upon reaction of dioxygen with the diiron(II) core, hydroperoxide coordinates in a bent, end-

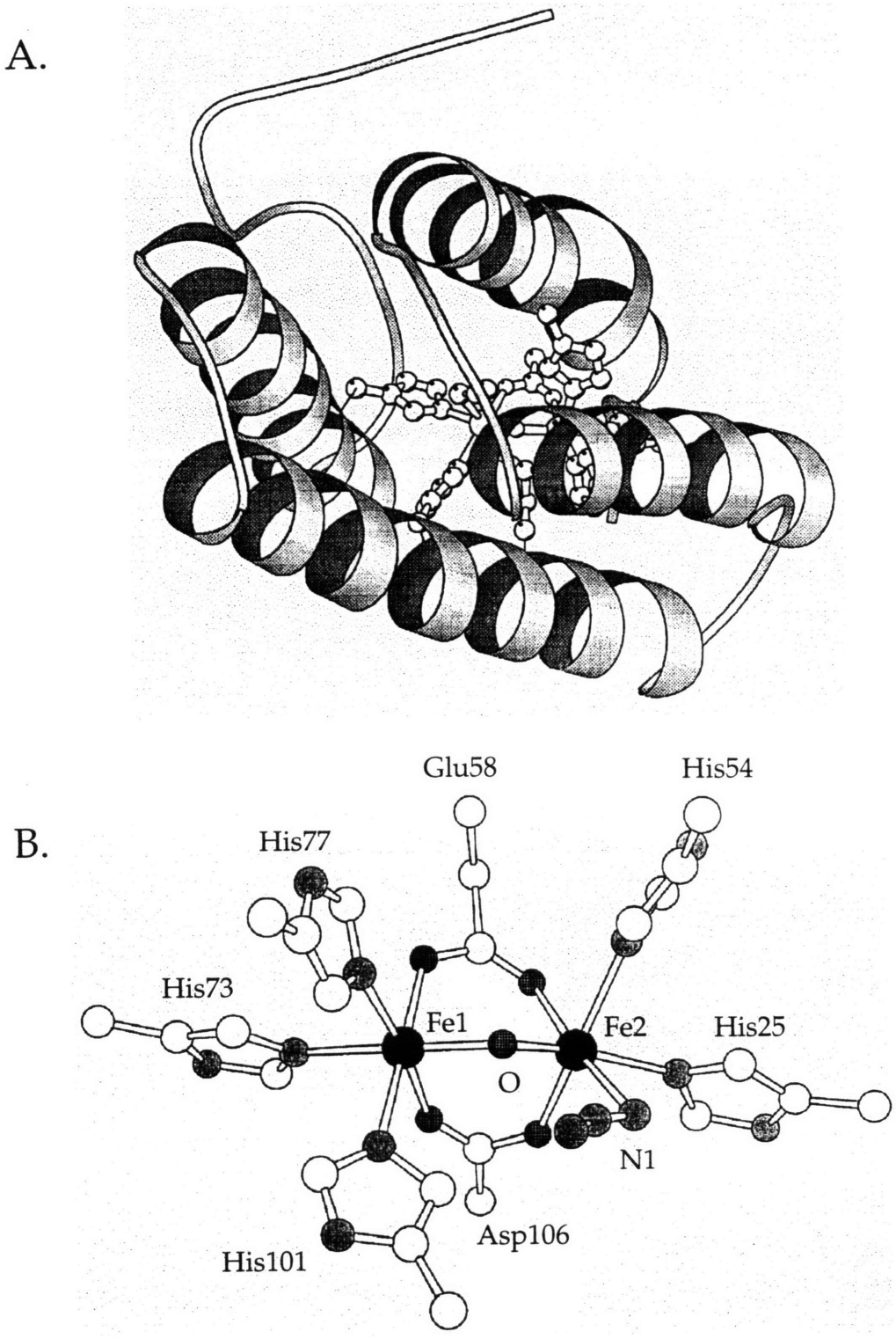

Figure 1.10. (A.) MOLSCRIPT[186] drawing of azidometHr showing the active site and protein fold and (B.) schematic diagram of the diiron center in azidometHr.

Table 1.3. Average Bond Distances (Å) and Angles (deg) in the Different Forms of Hr.[a]

	deoxyHr <Å>	oxyHr <Å>	metHr <Å>	azidometHr <Å>
Fe1-Glu58	2.33	2.20	2.26	2.17
Fe1-His73	2.23	2.22	2.22	2.24
Fe1-His 77	2.21	2.18	2.15	2.20
Fe1-His101	2.24	2.21	2.15	2.22
Fe1-Asp106	2.17	2.13	2.08	2.15
Fe1-O	2.15	1.88	1.92	1.80
Fe2-His25	2.15	2.14	2.07	2..21
Fe2-His54	2.28	2.25	2.23	2.24
Fe2-Glu58	2.140	2.20	2.04	2.25
Fe2-Asp106	2.14	2.15	2.08	2.09
Fe2-O	1.88	1.79	1.66	1.79
Fe1-Fe2	3.320	3.27	3.25	
Fe1-O-Fe2 (deg)	111	125	127	135
O-peroxy O2		2.80		
Fe2-peroxy O1		2.15		
Fe2-N1				2.34

[a]Data taken from refs. 50 and 170. See Figure 1.10 for labeling scheme.

on fashion to one of the ferric ions. Binding of dioxygen to deoxyHr is a two-electron transfer reaction, predicted as early as 1955 based on extraction studies with iron chelators.[188] More conclusive evidence was later provided by spectroscopic work (Table 1.4). Mössbauer spectra of deoxyHr display a

Table 1.4. Spectroscopic Properties of the Different Forms of Hr.

		deoxyHr	oxyHr	metHr	azido-metHr	ref.
Raman	ν_s(Fe-O-Fe), cm^{-1}		486	510	507	190
	ν_{as}(Fe-O-Fe), cm^{-1}		753	750	768	190
	ν(O-O), cm^{-1}		844		2050[a]	174
optical	$^6A_1 \rightarrow {}^4T_2({}^4G)$ λ, nm (ε, M^{-1} cm^{-1})		750 (210)		680 (190)	14
	$^6A_1 \rightarrow {}^4T_1({}^4G)$ λ, nm (ε, M^{-1} cm^{-1})		990 (10)		1010 (10)	14
magnetics	J, cm^{-1}[b]	-15	-90	-130		14
CD	ν(Fe-L), cm^{-1}		503		375	14
	Abs max., nm (ε, M^{-1} cm^{-1})		500 (2200)		445 (3700)	14
	CD max., nm ($\Delta\varepsilon$, M^{-1} cm^{-1})		520 (-2.5)		500 (-4.3)	14
	excitation max., nm		525		490	14
Mössbauer	Fe1 δ, mm s^{-1}	1.14	0.51	0.46	0.51	14
	Fe1 ΔE_Q, mm s^{-1}	2.76	0.91	1.57	1.96	14
	Fe2 δ, mm s^{-1}		0.52		0.51	14
	Fe2 ΔE_Q, mm s^{-1}		1.93		1.47	14
EPR		silent	silent			14

[a] ν(N-N), from ref. 181. [b] These values are reported using the convention $H = -2JS_1 \bullet S_2$.

single quadrupole doublet at 4.2 K with isomer shift (δ = 1.14 mm/s) and quadrupole splitting parameters (ΔE_Q = 2.76 mm/s) indicative of high spin Fe^{II}.[189] The spectrum of oxyHr, on the other hand, has two distinct doublets with similar isomer shifts (δ = 0.51, 0.52 mm/s) but different quadrupole splitting parameters (ΔE_Q = 0.91, 1.93 mm/s), consistent with an asymmetric, antiferromagnetically coupled diferric site.[16,189] Resonance Raman

spectroscopy revealed the presence of a ν_{O-O} stretching band at 844 cm^{-1}, characteristic of bound peroxide ion.[178] Assignment of this band was further verified by isotopic labeling experiments.[174,175]

The bent peroxide moiety in oxyHr can have two extreme orientations relative to the iron core, *syn* or *anti*, binding modes **e** and **f**, respectively, in Figure 1.3. The crystal structure of oxyHr revealed exclusively the *syn* orientation, which allows for hydrogen bonding between the hydroperoxide ligand and the oxo bridge. The O–O distance between these units is 2.8 Å,[50] well within the range of hydrogen bonding interactions. Proof for the existence of a hydrogen bond to the coordinated hydroperoxide was provided by resonance Raman studies of oxyHr. Spectra of samples prepared in H_2O versus D_2O were compared. The ν_s (Fe-O-Fe) bend in oxyHr shifts by 4 cm^{-1} toward higher energy in D_2O.[176] With the sole exception of hydroxymetHr, a derivative that can also use a proton to form a hydrogen bond with the oxo-bridge, no other form of the protein exhibited such a deuterium isotope effect. The reaction of deoxyHr to form oxyHr can therefore be written as indicated in eq 1.28, in which a proton from the hydroxo bridge is shuttled to the newly formed peroxide upon binding and reduction of dioxygen.

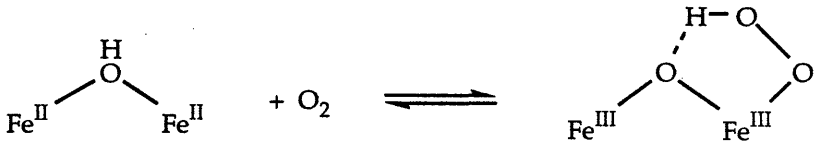

(1.28)

The protonation state of the bound peroxide in oxyHr has some interesting consequences. Protonation removes electron density from the oxygen p-orbitals, which otherwise might form π-bonds to the metal d-orbitals. Such weakening of the π–interaction might facilitate dissociation of

dioxygen and return to the ferrous, deoxy form of the protein.[177] Non-cooperative hemerythrins do not exhibit any pH dependent kinetic or thermodynamic changes in their dioxygen-binding properties. This striking insensitivity to pH has been ascribed to the internal proton transfer mechanism of eq 1.28.[191]

Kinetic studies of the dioxygen-binding reaction have been carried out for several forms of Hr.[181-185] Kinetic constants measured by temperature-jump relaxation, stopped-flow, and laser-photolysis techniques are in relatively good agreement with one another. A summary of the results is given in Table 1.5, together with corresponding values for the oxygenation reactions of hemoglobin and myoglobin for comparison purposes. The rate of Hr oxygenation is limited by the diffusion of O_2 to the diiron(II) binding site.[183] As expected for an oxygen transport or storage protein, oxyHr has good stability ($K_d \approx 10^{-6}$) and oxidation to the inactive met form is highly disfavored. Some of the early studies on the kinetics of oxygenation reported biphasic behavior that was ascribed to multiple binding geometries or sample heterogeneity;[181] for these cases, initial reaction velocities were measured. Biphasic kinetics were also observed in laser photolysis investigations of Hr and attributed to solution viscosity effects.[192] In at least one experiment significant changes in the kinetic parameters occurred under different salt conditions.[182] The enthalpy and entropy of the oxygenation reaction have been measured for some hemerythrins (*T. zostericola*, *S. nudus* and *P. gouldii*) and are in reasonably good agreement. [181,182,183]

Kinetic isotope effect (KIE) experiments carried out on the oxygenation reaction revealed an interesting difference from results for hemoglobin and myoglobin.[191] In Hr, only the dissociation rate constant (k_{off}) was affected by

Table 1.5. Kinetic and Thermodynamic Data on the Reaction of Dioxygen with Hemerythrin.

species	$k_{on} \times 10^{-6}$ ($M^{-1}\ s^{-1}$)	k_{off} (s^{-1})	$K_d \times 10^6$ (M)	$\Delta H^{\ddagger}_{on}$ (kcal/mol)	$\Delta S^{\ddagger}_{on}$ (eu)	$\Delta H^{\ddagger}_{off}$ (kcal/mol)	$\Delta S^{\ddagger}_{off}$ (eu)	ΔH (kcal/mol)	ΔS (eu)	Hill Coefficient	conditions	ref.
Lingula unguis (octamer, cooperative)	0.44	15	34								0.08 M phosphate, pH 6.8 at 17° C, stopped-flow	185
	0.63	61	97							1.86[a] (1.11)	0.08 M Phosphate, 0.1 M NaCl, pH 6.8 and/or pH 7.6 at 15° C	184
Siphonosoma cumanense (trimer, non-cooperative)	11.3	9.1	1.24								T-jump 0.08 M phosphate, 0.1 M NaCl, pH 6.8 at 15° C	184
Themiste zostericola (monomer, non-cooperative)	78	315	4.0	4	-11	16.8	9	-23	-20		T-jump Tris, pH 8.2, I = 0.1 M at 25° C	183
Themiste zostericola (octamer, non-cooperative)	7.5	82	10.9							1.1	T-jump Tris, pH 8.2, I = 0.1 M, at 25° C	183
Golfingia gouldii (octamer, non-cooperative)	7.4[b]	51	6.9	8.2	1	20.6	19	-12.4	-18	1.1	T-jump Tris, pH 8.2, I = 0.015 M, at 25° C	182
	12	43.1	3.6								T-jump 0.1 M Na_2SO_4, pH 8.55, at 25° C in H_2O	191
	12	35	2.9								T-jump, stopped-flow 0.1 M Na_2SO_4, pH 8.55, at 25° C in D_2O	191
Siphonosoma nudus (octamer, non-cooperative)	26	120	4.6			12.7[c]		-10.5		1.15	T-jump, stopped-flow 0.1 M phosphate, pH 7.0, at 25° C	181
	29[d]			-4.4 ± 0.5[c]							T-jump Tris, pH 8.2 or Phosphate pH 7.0	192
deoxymyoblobin sperm whale muscle	19	11	0.58	6-7[e]		19-21[e]					laser photolysis 0.1 M phosphate + 0.1 M KNO_3, pH 7.0 at 20° C	194
deoxyhemoglobin human erythrocyte, 4th oxygen	33	50	1.5								T-jump 0.1 M phosphate, pH 7.0 at 21.5 ° C stopped-flow	195

[a]The first values is for pH 7.6, the value in parentheses is for pH 6.8. [b]A strong ClO_4^- effect was observed in this study. [c]This value is an activation energy, not an activation enthalpy. [d]A strong viscosity effect was observed during this study. [e]Data point from ref. 193.

changing to D_2O as solvent ($k_H/k_D = 1.2$); k_{on} was unaffected. In the heme systems, both the binding and the dissociation rates had KIE values of ≈ 1.2.[191] These small isotope effects are consistent with hydrogen bonding interactions stabilizing the oxygenated forms of the proteins, but equally well could reflect internal proton transfer reactions within the active site. The lack of a KIE for the O_2 binding reaction in Hr indicates that the proton transfer step is more important for dioxygen release than uptake by the protein.

One puzzling aspect of Hr oxygenation chemistry is the nature of the cooperativity displayed for certain species. This behavior is pH dependent. Lowering the pH results in a sharp loss of cooperativity between pH 7.6 and 7.0,[184] implying that cooperativity depends upon a specific protonation event. The cooperative versus non-cooperative oxygenation reaction rate is strikingly different for *T. zostericola* (Table 1.5). The rate of binding is 10 times faster for the non-cooperative form of the protein. This difference in activity has been ascribed to a two state model for allostery,[184] suggesting that the rate of interconversion between the two affinity forms is much slower than the rate of dioxygen binding. More recently, it was shown that, although the subunits were initially thought to be identical, in the cooperative species they are in fact not so.[197] The source of the cooperativity is therefore presumed to be an interaction at the subunit interface. Studies of the allostery by resonance Raman spectroscopy revealed a shift in the O-O stretching frequency as a function of pH in cooperative systems.[179] No such shift was observed for non-cooperative hemerythrins nor was a pH dependent effect observed for the Fe-O stretching vibration. In each case, cooperativity was observed only at higher pH values under dioxygen

saturating conditions.[179] From this evidence, it was proposed that the cooperativity reflects a structural change that takes place after O_2 binding, in contrast to the nature of the cooperativity found in hemoglobin where the binding affinity of the deoxy Hb is affected by a structural change.[198]

The specific model for cooperativity postulated to explain these results is shown in Figure 1.11. In this model, a hydrogen bond from the bound hydroperoxide to an unidentified protein residue is responsible for the shift to a high affinity form of Hr. This hydrogen bonding arrangement is preferred to one involving the hydroperoxide ligand and the oxo-bridge because a change in the latter interaction would be expected to alter the Fe-O stretching vibration, which was not observed. Furthermore, no cooperative effects occurred in other oxidized forms of the protein such as azidometHr. The model is consistent with this behavior since it depends upon the specific geometric relationships between the hydrogen bond donor and acceptor pairs of the hydroperoxide ligand and protein residue.

The foregoing proposals to explain the nature of the cooperativity are compatible with one another. Hydrogen-bond formation between the protein side chain and the bound hydroperoxide should be fast, but propagation of the structural changes down the α-helix might not be as rapid. The nature of the changes in the coordination environment of a diiron(II) site transmitted to another subunit is uncertain and likely to be subtle. The motion of the helix following the formation of the proposed second hydrogen bond to the coordinated hydroperoxide might result in a more favorable alignment of the equivalent hydrogen bond at a distant site, but there is no experimental evidence to support such a proposal. Further

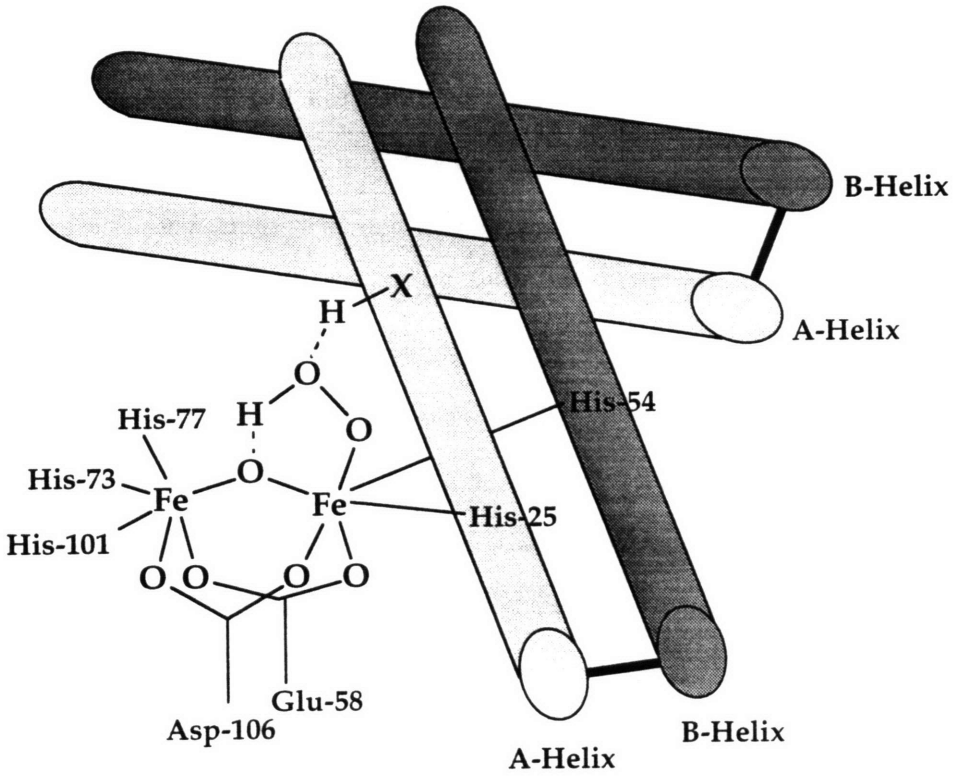

Figure 1.11. Schematic model for the dinuclear iron center in a cooperative oxyHr. The A- and B-helices of the α-subunit are assumed to be in contact with the A- and B-helices of the β-subunit. The unknown residue X is postulated to form a hydrogen bond to the bound hydroperoxide as discussed in the text. (Adapted with permission from ref. 179.)

work on the nature of the cooperativity is required to define the reorganization involved, and could be approached by site-directed mutagenesis experiments.

As a final consideration, the specificity of the reaction of deoxyHr with dioxygen will be addressed. A problem common to most dioxygen-utilizing ferrous proteins is oxidation to the inactive, ferric (met) form. In the case of Hr, such oxidation can result from dissociation of hydrogen peroxide from oxyHr. The dissociation rate of HO_2^- has been estimated to be approximately $1.0 \times 10^{-5}\ s^{-1}$.[14] This slow dissociation rate is postulated to be a result of the extremely hydrophobic nature of the hemerythrin dioxygen-binding pocket. Reactions of hemerythrins with alternative oxidants are quite slow in the absence of anionic ligands but significantly enhanced by their presence.[199] The semimet, $Fe^{II}Fe^{III}$, form has also been investigated, but is unstable with respect to disproportionation without an external reductant or oxidant. This instability reflects the preference of the diiron core in Hr to undergo two-electron redox steps,[166] a feature that is both interesting and important. The propensity of dioxygen to be reduced in two-electron steps was mentioned above, and it can now be seen that this preference is shared by the dinuclear iron center in Hr. In this system, the electron transfer properties of the dinuclear metal site and the exogenous ligand are beautifully tuned to accommodate one another. As discussed below, not all dinuclear iron sites in proteins and models present metastable mixed-valent forms.

The foregoing discussion illustrates several important features about the reaction of O_2 with a diiron(II) center. DeoxyHr reduces dioxygen to the peroxide level and the resulting hydroperoxide is stabilized by the protein sheath. As will be shown, most of the other systems use all four oxidizing

equivalents of the O_2 molecule. The stability of the ferric hydroperoxide complex in Hr results in part from hydrogen bonding to the oxo bridge, inaccessibility to reactive diiron(II) units in adjacent subunits, and possibly the nitrogen-rich histidine ligand environment of the core. These features render Hr unique among non-heme iron systems and are shared to some extent by the coordination spheres of the reversible dioxygen-binding heme proteins Hb and Mb. As will be discussed, one small molecule system, the hydroxo-bridged diiron(II) complex $[Fe_2(Me_3TACN)_2(OH)(OAc)_2]^+$, mimics several of the structural and spectroscopic properties of the deoxyHr core quite accurately. It lacks an open coordination site on iron(II) ion for dioxygen binding, however. Kinetic studies on its oxidation (discussed below) indicate that, following a carboxylate shift reaction to free an O_2-binding site, the compound reacts with dioxygen but fails to do so in a reversible manner because the oxygenated intermediate attacks a second equivalent of the diferrous complex to form, ultimately, 2 $[Fe_2(Me_3TACN)_2(O)(OAc)_2]^{2+}$.[200-202] These results show that simply recreating the coordination environment of iron in the Hr core is not necessarily sufficient to model the activity of the protein. Secondary interactions such as hydrogen bonding relationships might be necessary to stabilize properly a peroxide species, rendering it less reactive toward reductive decomposition.

Methane Monooxygenase

This enzyme system is currently one of the most intensively studied non-heme iron proteins. Recent investigations of the three-dimensional structure of the hydroxylase and its catalytic mechanism have yielded significant insights into the workings of this enzyme. MMO is a mixed

function oxidase; one atom of O_2 is transferred to substrate and the other forms water. As indicated in eq 1.29, the system converts methane to methanol in a process that is coupled to the oxidation of NADH.

$$CH_4 + O_2 + H^+ + NADH \longrightarrow CH_3OH + H_2O + NAD^+ \quad (1.29)$$

Several forms of MMO exist including soluble and membrane bound varieties.[203,204] Only the soluble form contains iron, the other having copper as its redox active metal ion. Most studies have focused on MMO isolated either from *Methylococcus capsulatus* (Bath) or *Methylosinus trichosporium* (OB3b), which differ in the temperatures at which they operate (45° versus ambient, respectively), their morphology and metabolic pathways following methane hydroxylation. The active site structures and hydroxylation mechanisms of MMOs from the two different organisms share many common features, but there are some interesting differences manifest in the mechanistic studies to be discussed below. One of the current goals in this field is to define the unifying features of the reaction and to understand or reconcile conflicting results.[205-209]

The MMO enzyme system contains 3 proteins, a hydroxylase, housing two dinuclear non-heme iron centers, a reductase containing one FAD and one [2Fe-2S] cluster, and protein B, a coupling unit that facilitates electron transfer from the reductase to the hydroxylase and modulates the properties of the latter.[210-213] In this review we focus primarily on the dinuclear iron core in the hydroxylase and its reactions with dioxygen. For more general discussions, other recent works can be consulted.[11,14-17,209-218]

The hydroxylase protein has an $\alpha_2\beta_2\gamma_2$ composition with a molecular weight of 251 kDa.[211,219] The crystal structure of the oxidized *M. capsulatus*

(Bath) enzyme has recently been solved to 2.2 Å,[49] confirming, and considerably elaborating on, the structure that had been proposed based on spectroscopic and other evidence (Table 1.6). As shown in Figure 1.12, the diiron(III) centers reside in the α subunits, which are related by a non-crystallographic 2-fold symmetry axis, at a distance of 45 Å from one another. In the original structure solution, the distance between iron atoms in each dinuclear core was 3.4 Å, in good agreement with EXAFS studies of the oxidized hydroxylase.[218] The two iron atoms were bridged by a glutamate side chain, E144, a hydroxide ion, and an acetate ion from the crystallization buffer. The terminal ligands were comprised of two histidine nitrogens (H147 and H246), three carboxylate oxygen donors (E114, E243, E20), and a water molecule which is hydrogen bonded to E114 and E243. Subsequently, other isomorphs have been observed. In one, the exogenous acetate shifted out of the coordination sphere leaving an μ-aquo, μ-hydroxo dibridged core. these variations highlight the lability of the core ligands and point toward the functional importance of carboxylate shift reactions in the enzyme mechanism. The reduced structure contains two six-coordinate iron atoms bridged by two bidentate glutamate side chains.[220] Whereas the ligand side chains making up the bulk of the coordination environment are equivalent between the oxidized and reduced forms, the bridge geometries are very different. In particular, the coordination of E243 is quite unusual and seems to be isolated in a semi-shifted binding mode.

The presence of a hydroxo, rather than an oxo, bridge in the ferric enzyme was initially suggested from optical, EXAFS and magnetic studies. These experiments revealed the absence of the visible absorption band, short

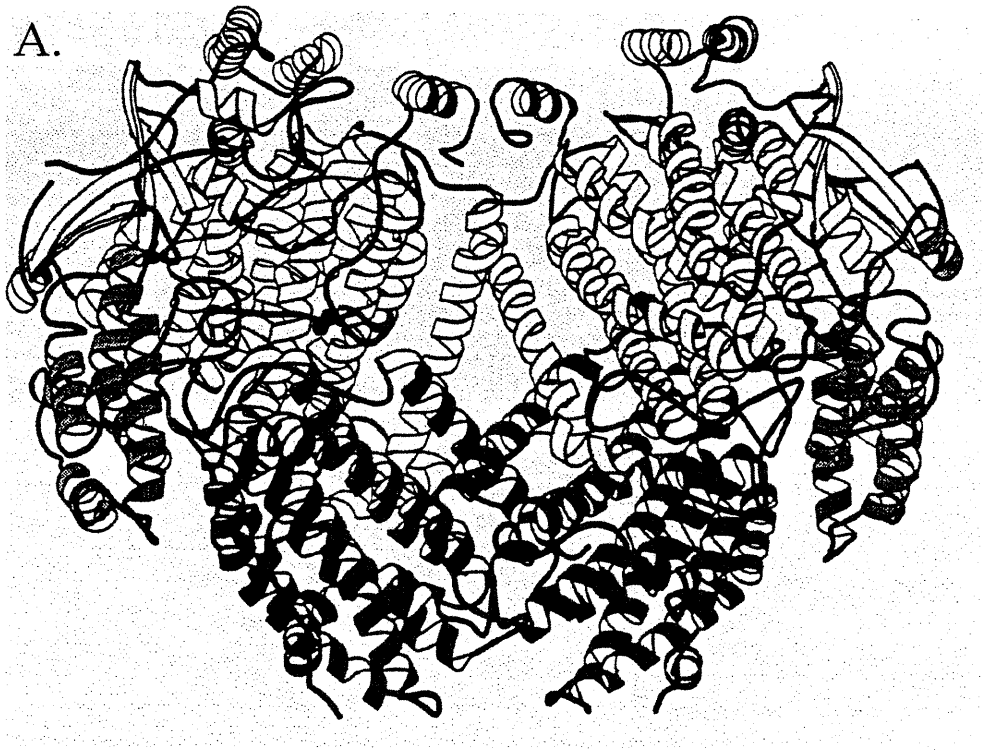

Figure 1.12. A. MOLSCRIPT[186] ribbon drawing showing the protein fold of the MMO hydroxylase protein and the diiron center from *M. capsulatul (Bath)*. B. Schematic drawing showing the quatenary structure of the active MMO Hydroxylase-Reductase-Protein B complex from *M. capsulatus (Bath)*. C. Schematic representation of the diiron center in the $Fe^{III}Fe^{III}$ state. D. Schematic representation of the diiron core in the reduced state.

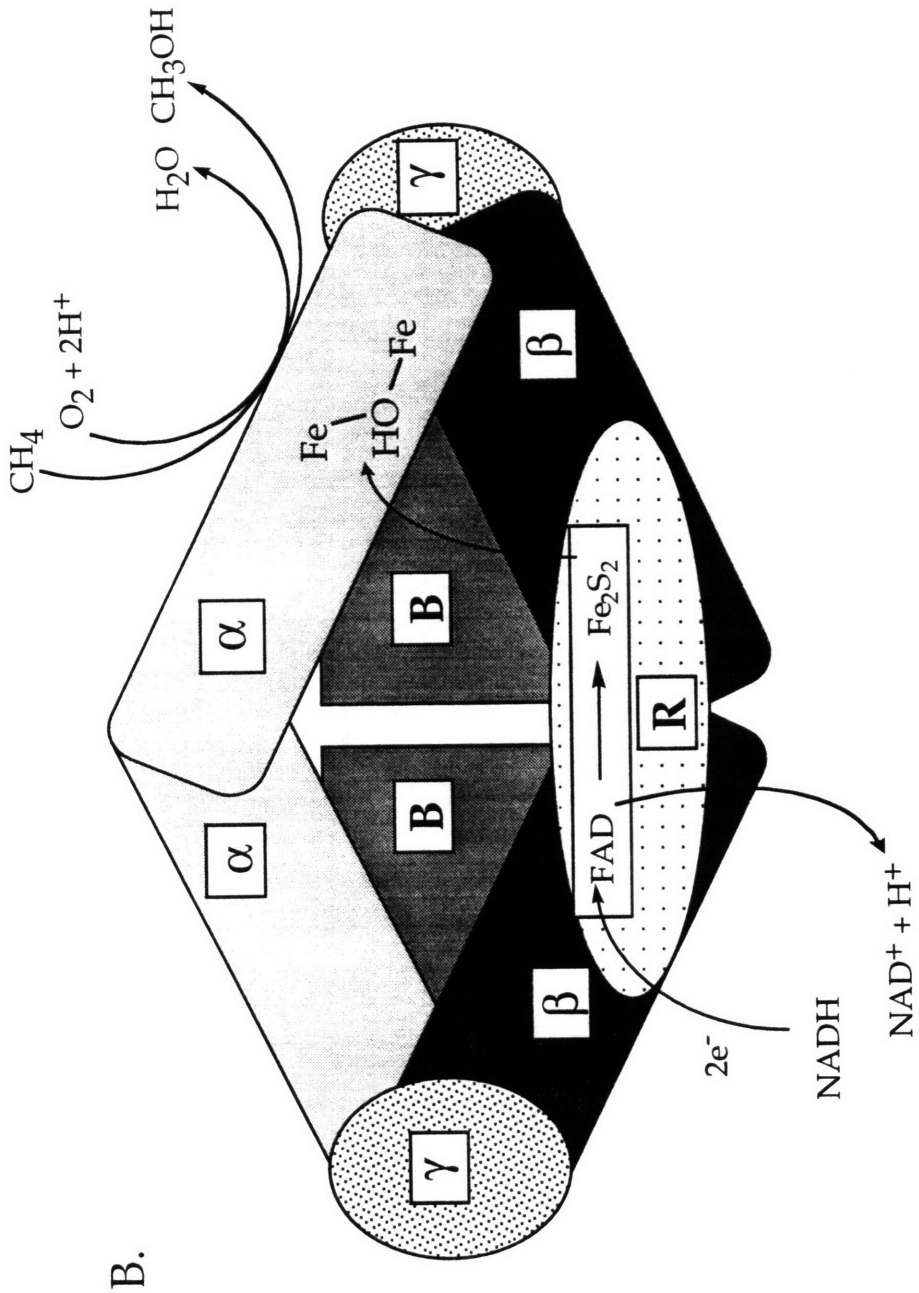
B.
CH4
O2 + 2H+
H2O
CH3OH
α
α
β
β
γ
γ
B
B
Fe
HO
Fe
R
Fe2S2
FAD
2e-
NADH
NAD+ + H+

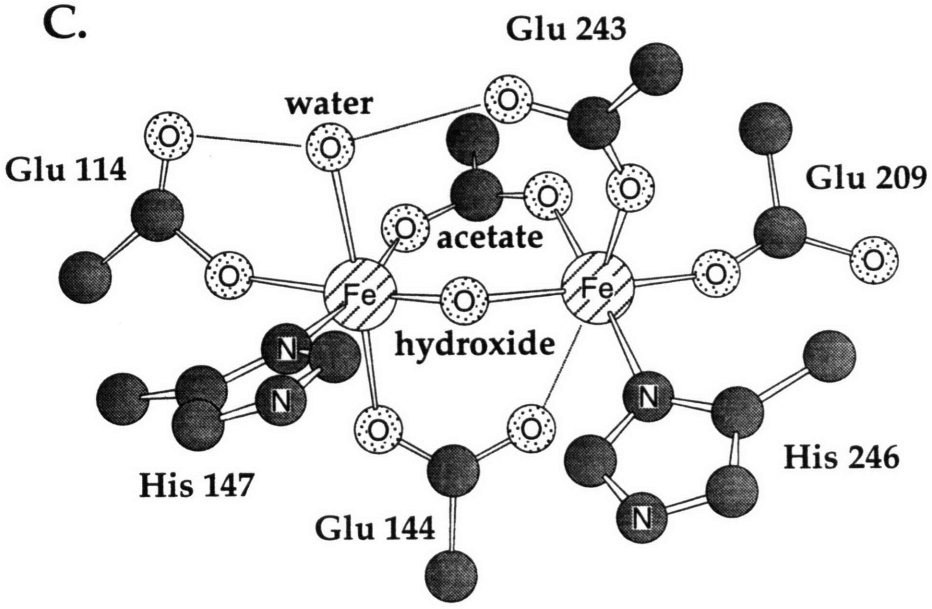
C.
Glu 243
water
Glu 114
Glu 209
acetate
Fe
Fe
hydroxide
N
N
N
His 147
His 246
Glu 144

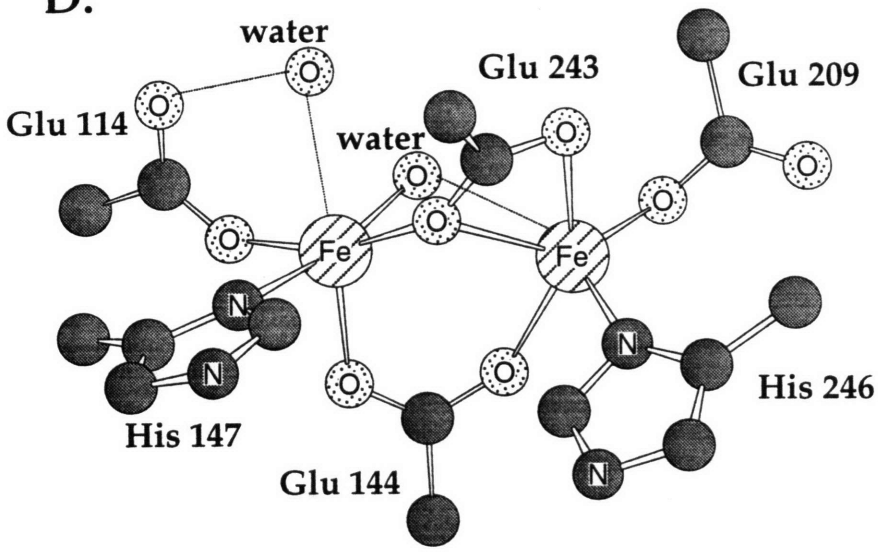
D.
water
Glu 243
Glu 209
Glu 114
water
Fe
Fe
N
N
N
His 147
His 246
Glu 144

Table 1.6. Spectroscopic Properties for the Different Forms of MMO Hydroxylase.

		M. trichosporium (OB3b)				*M. capsulatus* (Bath)			
		H_{red}	H_{mv}	H_{ox}	ref.	H_{red}	H_{mv}	H_{ox}	ref.
optical	λmax, nm			282	211			280	218
magnetics	J[a], cm^{-1}	0.35	-30	-7 ± 3	221-223		-32		218
Mössbauer	Fe1 δ, mm s^{-1} (T, K)	1.3 (4.2)	0.48 (150)	0.51 (4.2)	221	1.30 (80)		0.50 (80)	218
	Fe1 ΔEQ, mm s^{-1}	3.10	-1.3	1.16	221	3.014		1.05	
	Fe2 δ, mm s^{-1}	1.3	1.19	0.50	221				
	Fe2 ΔEQ, mm s^{-1}	2.4-3.0	2.4	0.87	221				
ENDOR	A, MHz		13-23[b]		230		14-30[b]		229
EPR	g_x		1.75		224		1.95		225
	g_y		1.86		224		1.88		225
	g_z		1.94		224		1.78		225
	g_{av}	16	1.85	4.3	224		1.83		217
Redox Potentials	E°, mV vs. NHE	21	76		226	-135	48		212
	E°, mV vs. NHE + additives	-115[c]	-52[c]		226		<100[d]		212

[a]These values are reported using the convention H = $-2JS_1 \bullet S_2$. [b]This signal arises from the hydroxide bridge; other resonances not listed (see text). [c]Potential in the presence of B. [d]Two electron addition in the presence of B, reductase and substrate.

Fe-Fe distance, and large antiferromagnetic exchange coupling, features characteristic of diiron(III) centers containing oxo and carboxylate bridges.[217,218,224,228] The identity of the monoatomic bridge was recently established by ENDOR studies of the mixed-valent form of the hydroxylase which revealed spectra displaying anisotropic coupling of the unpaired electron to an exchangable proton assigned to hydroxide ion.[229,230] The ENDOR results also indicated the coordination of at least one water molecule to the dinuclear iron center, a feature also revealed by the X-ray structure of the *M. capsulatus* (Bath) hydroxylase.

The dinuclear iron center is positioned in the center of a 4-helix bundle in the α-subunit. The $[Fe_2(OH)]^{5+}$ moiety is bound by two Glu-X-X-His sequences, an i, i+3 motif found in many metalloenzymes.[231,232] The exogeneous acetate bound to the diiron center may indicate the site at which dioxygen, substrate, or methoxide product interacts with the core, and further studies are in progress to address these questions. The carboxylate side chain of E243, hydrogen bound to the coordinated water, in the oxidized form readily undergoes carboxylate shifts upon redox cycling of the system (Figures 1.12C and 1.12D).[220] Analogous behavior is also observed in RNR (see below).[233,234] The hydrophobic pocket adjacent to the active site of the hydroxylase is larger than the one found in R2 (see below), and contains a cysteine at the position corresponding to the location of Y122 in R2. Entry of substrate to this pocket may occur through the α-subunit where there are several contiguous hydrophobic cavities. The canyon that straddles the non-crystallographic 2-fold axis on one face of the enzyme is a possible site for binding component B. Docking of B along canyon walls comprised of two of the helices involved in iron coordination would allow the modulation of activity as discussed below.

Investigations of the redox properties of the diiron center in MMO hydroxylase reveal three accessible oxidation states, $Fe^{III}Fe^{III}$, $Fe^{III}Fe^{II}$, and $Fe^{II}Fe^{II}$.[225] As isolated, the enzyme is in the fully oxidized state, whereas the reduced form is the one that reacts with dioxygen. The mixed-valent hydroxylase is inactive, but has important physical properties, such as the ENDOR spectrum mentioned above, that have been used to characterize the protein. For the *M. capsulatus* (Bath) hydroxylase, the iron redox couples occur at +48 and -135 mV versus NHE[212] and are shifted toward slightly more negative potentials upon addition of substrate. Addition of a 1:1 mixture of protein B and reductase had a striking influence on the redox properties of the diiron core, however. In the presence of the fully constituted protein system without substrate, the iron could not be reduced by dithionite in the presence of mediators even at -200 mV. In the presence of substrate, however, reduction occurred, and the potentials of the two redox steps were altered such that it was easier to add the second electron than the first. The system thus bypassed the inactive mixed-valent form of the hydroxylase; substrate binding triggered the reduction of iron and primed the enzyme for oxidation chemistry. Since alkanes are unlikely to bind directly to the dinuclear iron center, the effect must be indirect. For example, substrate binding might displace a bound water molecule or lead to a carboxylate shift.[235] Related studies have recently been reported for the *M. trichosporium* OB3b system, for which iron redox couples of +76 and +21 mV were obtained.[226] The addition of protein B shifted the reduction potentials of the dinuclear iron center by -132 mV. In the presence of B and reductase, the shift from a one-electron to a two-electron process was less clearly apparent, in contrast to the results for the *M. capsulatus* (Bath) protein. The differences between the two studies must be addressed by

further work, the most important of which was the use of a protein B/reductase mixture instead of the isolated protein components. The redox properties of MMO just discussed are quite different from those described above for Hr. The most notable difference is the relative stability of the mixed-valent species of the hydroxylase. Once generated, this $Fe^{II}Fe^{III}$ species can be purified and studied even though it is catalytically inactive.

Several general features of the MMO hydroxylation mechanism are understood. Dioxygen reacts with the reduced form of the enzyme, leading to the formation of a diiron(III) peroxide intermediate (Figure 1.13). This intermediate, H_{peroxo}, has been characterized by optical, Mössbauer and resonance Raman spectroscopies.[236] Isotope labeling studies showed that the peroxide is coordinated in a symmetric fashion. H_{peroxo} then decays into a second intermediate designated Q.[207,237] Q has been proposed to be either a diferryl or a diferric species bridged by two oxyl radicals. One of the oxygen atoms derived from dioxygen then gets incorporated into substrate by a sequence of events currently being probed by several different experiments. The roles that substrate radicals and/or a ferryl intermediate might play are of primary interest. When no reductase is present, the reduced hydroxylase alone will function in a single turnover experiment yielding stoichiometric amounts of product and the diiron(III) form of the enzyme. The reductase is thus essential only for recycling the enzyme. It has become clear, however, that important effects are occurring which render the hydroxylase more efficient in the presence of the other two proteins.[212,213] Protein B, in particular, greatly accelerates the rate of hydroxylation. Elucidating the details of these interactions will require more work. One of the current

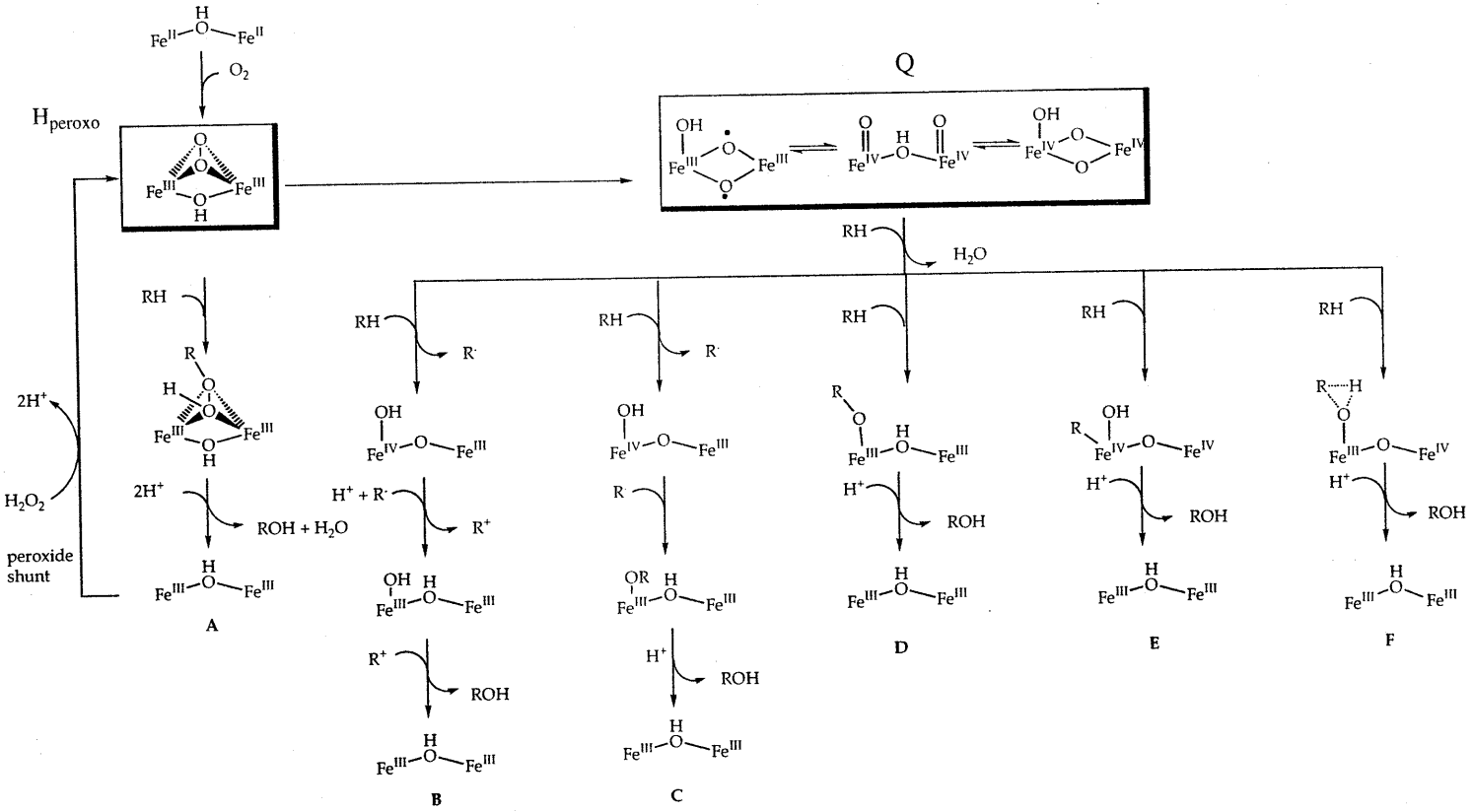

Figure 1.13. Mechanistic proposals for the hydroxylation of hydrocarbon substrates by MMO. Only the iron center and hydroxide bridge are shown. The other ligands have been removed for greater clarity. Pathway B follows the proposal put forth for *M. trichosporium.* in ref. 205. The radical, R•, refers to a substrate radical, but could potentially be either hydroxyl radical or a protein based species. Pathway C is the rebound mechanism directly analogous to that proposed for cytochrome p-450. Pathways A, D, E and F are possiblites suggested for *M. capsulatus* based on ref. 208. During enzyme turnover, the final oxidized state is returned to the active ferrous form by NADH reduction mediated by the reductase and coupling proteins.

approaches to this problem is to study the enzyme kinetics during single turnover experiments. This work has begun to yield information regarding discrete steps of the hydroxylation process. Previous studies using multiple turnover conditions revealed that electron transfer from the reductant to the diiron(III) hydroxylase is faster than the rate of hydroxylation.[214,215] The reduction step is therefore not rate limiting, leaving substrate binding, substrate release or some step in the oxygenation as potential rate-limiting processes of the complete catalytic system.

Elaboration of the MMO hydroxylase mechanism is usually written in a manner that mimics the rebound mechanism postulated for cytochrome P-450[42,205,238-240] because of similarities in the overall stoichiometry and substrates for the two systems. Both hydroxylate a wide variety of hydrocarbons and incorporate oxygen atoms from the dioxygen molecule with minimal solvent exchange. For the *M. trichosporium* hydroxylase, there is some evidence to justify the comparison with the generally accepted, if unproven, cytochrome P-450 mechanism. Radical clock studies using 1,1-dimethylcyclopropane gave ring opened products consistent with the formation of both radical and carbocation intermediates.[205] Although the yield of the ring-opened species was small, this result could be attributed to the use of a relatively sluggish radical clock. It was therefore proposed that the mechanism of MMO hydroxylation was similar to, but more complicated than, a simple rebound process. Following generation of a high valent ferryl intermediate, a hydrogen atom is abstracted to yield a substrate radical which is then oxidized by 1 electron and oxygenated. The rate constant measured for this rebound reaction is 2×10^{10} s^{-1}.[205]

Further support for a substrate radical intermediate was provided from studies using chiral ethane.[206] In this work, the stereochemistry of the

hydroxylation of (R)- and (S)-[1-^{2}H, 1-^{3}H]-ethane by the *M. trichosporium* enzyme was examined. Retention of configuration predominated, but 35% inversion also occurred and an intramolecular deuterium kinetic isotope effect (KIE) of 4.2 was measured (Table 1.7).[206] The result supports a role for a substrate radical constrained within the enzyme active site, but does not provide additional evidence for or against the possible presence of a carbocation. In addition, the observed KIE indicates a role for C-H bond cleavage in the rate determining step of the hydroxylation reaction. This value falls outside the KIE range of 7-14 reported for P-450 systems.[42] By using a value of 0.5 kcal/mol for rotation around the C-C bond in the ethyl radical, one can calculate a radical rebound rate based on the percentage inversion, which yields a value of 6 x 10^{12} s^{-1}.[241] This rate is significantly faster than that measured from the aforementioned radical clock study.

In another study, *trans*-1,2-disubstituted- and 1,2,2-trisubstituted cyclopropanes, some of the fastest known radical clock substrates, were used to measure radical rebound rates for both the *M. trichosporium* and the *M. capsulatus* (Bath) enzymes.[208] No evidence was obtained for radicals or carbocations with *M. capsulatus* MMO, although some previous studies using EPR spin traps had reported radical species.[242] The extremely fast ring opening rates [(4-5) x 10^{11} s^{-1}] for the substituted cyclopropyl radical clocks makes them ideal for studying putative short-lived intermediates in the oxidation pathway. The ratio of the rearranged to the unrearranged product alcohol is used to calculate the recombination rate for a potential substrate radical and, in this case, gave a maximum lifetime for the intermediate of 2.5 x 10^{-14} s.[208] The rebound must therefore take place in less than the duration of a single vibration, an unrealistically fast reaction rate for a cytochrome P-

Table 1.7 Percentage Distribution of ^3H Label in the Methylene Group of the 2R)-2-Acetoxy-2-phenylethanoate Derivative of the Samples Generated by MMO

	^3H % in methylene group			
product / substrate	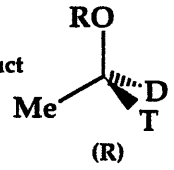 (R)	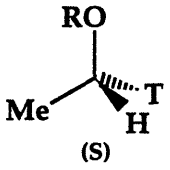 (S)	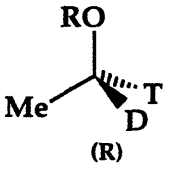 (R)	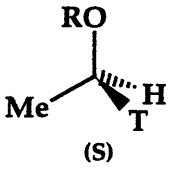 (S)
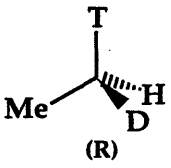 (R)	53	12	26	9
	retention = 68%		inversion[b] = 32%	
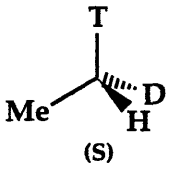 (S)	27	7	52	14
	inversion[b] = 36%		retention = 64%	

[a]Inversion/retention data have been corrected for the enantiomeric purity of the substrates. Data taken from ref. 206. [b]Indicates configuration inversion is due to flipping of the intermediate radical

450 type mechanism. It is possible that binding of the radical clock substrate to the enzyme somehow slows down the rate of ring opening, but this caveat was deemed unlikely based on a semi-quantitative analysis using Marcus theory and the fact that neither *trans*-2-phenyl- nor 2,2-diphenylmethylcyclopropane gave ring opened products.[208] Through the use of specifically deuterated substrates in this study, intermolecular and intramolecular KIE values were also measured for the *M. capsulatus* (Bath) system. The KIE_{inter} value was 1.0 and KIE_{intra} was 5.1. The latter value can

system. The KIE_{inter} value was 1.0 and KIE_{intra} was 5.1. The latter value can be compared to the intramolecular KIE of 4.2 ± 0.2 obtained for MMO from *M. trichosporium*[206] and the 7-14 range of cytochrome P-450.[42]

Use of the diphenylmethylcyclopropane radical clock substrate probe with the *M. trichosporium* OB3b hydroxylase enzyme showed a small amount of rearranged product indicative of a radical intermediate. The calculated rebound rate constant was (6-10) x 10^{12} s^{-1}, a value consistent with the chiral ethane experiments discussed above.[206] The consistency between the *M. trichosporium* radical clock and chiral ethane data lends credence to the interpretation of the experimental findings for the *M. capsulatus* MMO.

Unlike ribonucleotide reductase (see below), no stable enzyme-bound radical has been observed for the MMO hydroxylase. Recent freeze quench Mössbauer and stopped-flow optical spectroscopic studies of the *M. trichosporium* hydroxylase have detected an intermediate (Q), assigned as a symmetric Fe^{IV}-Fe^{IV} compound based on its isomer shift (δ = 0.17 mm/s) and single quadrupole doublet (ΔE_Q = 0.53 mm/s) at 4.2 K.[207] Magnetic Mössbauer experiments revealed the transient to be diamagnetic.[207] Although arguments to exclude a diiron(III) assignment were presented, the bis-oxyl bridged species cannot be ruled out. If the diferryl assignment can be verified, then pathway C in Figure 1.13 would be a good candidate for the mechanism.

Another similarity between the *M. trichosporium* MMO hydroxylase reaction and the P-450 mechanism is the ability of peroxide ion to activate the chemistry through a shunt pathway (Figure 1.13). For the *M. trichosporium* enzyme, this peroxide shunt afforded hydroxylation products, but only at very high hydrogen peroxide concentrations.[239] Peroxide was consumed at a rate that varied with the ratio of H_2O_2 to substrate, indicating

the presence of an uncoupled reaction that did not lead to product formation. Furthermore, in the presence of protein B, the product ratio differed for oxidation of propane; the dioxygen reaction showed 3-fold greater selectivity for hydroxylation at the primary carbon relative to the hydrogen peroxide induced reaction.[213] These results raise the question of whether the hydroxylation mechanism with the diiron(III) enzyme and H_2O_2 is identical to that operating when O_2 is added to the reduced enzyme. Appropriate controls were run to assure that the reaction occurred within the protein active site, but were insufficient to prove that the enzyme re-entered the normal catalytic mechanism. To verify such a convergence of mechanisms, parallel KIE or stereochemical selectivity experiments would be required. It should also be noted that other oxo-transfer agents such as iodosylbenzene, sodium periodate, sodium chlorite and t-butyl hydroperoxide, all of which are active in the P-450 shunt mechanism, are ineffective in initiating hydroxylation chemistry in MMO.[243] This result raises doubts about the possible participation of a ferryl intermediate in the reaction mechanism. Attempts to hydroxylate substrates via a peroxide shunt mechanism by addition of H_2O_2 to the oxidized M. *capsulatus* enzyme gave only low product yields.[243,244]

Several alternative pathways consistent with the radical trap and KIE data for the *M. capsulatus* hydroxylase have been set forth (Figure 1.13, pathways A, D, E and F). Pathways D-F are examples of hydroxylation mechanism that might employ a ferryl intermediate, but do not require the intermediacy of a substrate radical. Pathway A is an alternative in which the ferryl intermediate is also omitted. The ability of an η^2,η^2-diferric peroxide to hydroxylate alkanes has not been definitively proven. Precedence exists for

similar reactivity (hydroxylation of arenes) in dicopper(I) dioxygen chemistry, however.[245]

Another scheme that might be considered for the hydroxylation chemistry is set forth in Figure 1.14. In particular, we suggest the possible participation of a radical involving Cys-151. This amino acid occupies the equivalent region of space as the tyrosyl radical of RNR, based on sequence homology and recent X-ray crystallographic results.[48,49] Pathway ***a*** considers a diradical mechanism similar to one discussed below for ribonucleotide reductase. One radical is Cys-151 and the other is postulated to be an iron-bound oxyl, a seven-electron oxygen atom, distinct from the six-electron oxene of the ferryl species. The two units, Fe^{III}-O· and Fe^{IV}=O, are likely to have quite different reactivities. Mechanism ***a*** depicted in Figure 1.14 would account for the lack of rearranged products in the radical clock study for *M. capsulatus* MMO because the C-H bond is broken in a concerted manner yielding a coordinated alcohol and the cysteine thiol. The small amount of rearrangement observed in the *M. trichosporium* system could result from misalignment of the substrate within the active site such that C-H bond cleavage proceeds in two fast sequential steps with a transient substrate radical intermediate. Since only a small fraction of the product is formed from a substrate radical intermediate, the remainder resulting from the concerted attack, less rearranged alcohol is produced than would be expected from a purely radical process. This characteristic would artificially inflate the rate constants for the rebound step measured in a radical clock study. Pathway ***b*** in Figure 1.14 is similar to the classic rebound mechanism except that the sulfur radical facilitates recombination of the bound oxyl and alkyl radicals. Similar steps have recently been postulated for dopamine β-monooxygenase,[246] but with a tyrosyl rather than a cysteinyl radical. There is

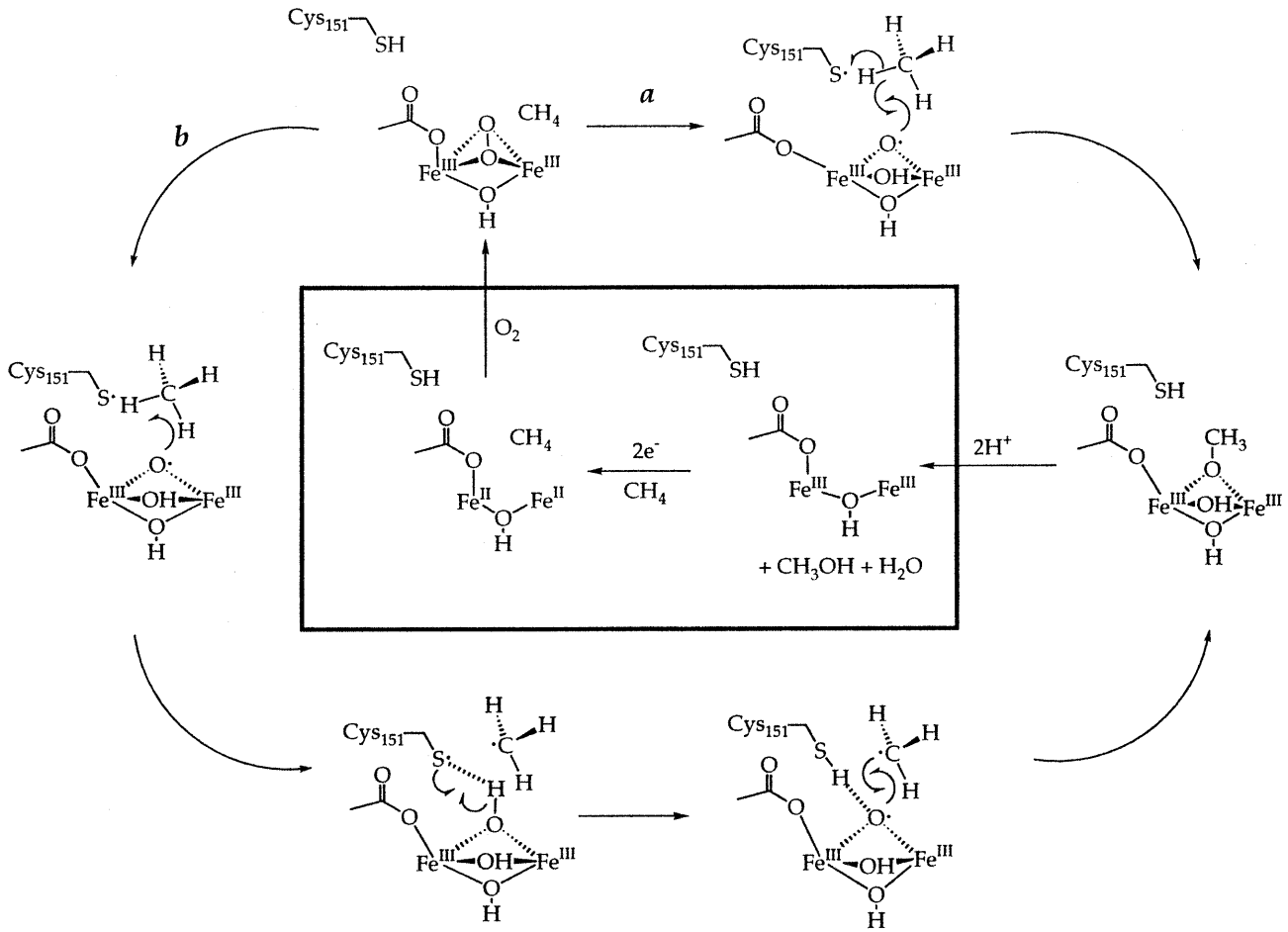

Figure 1.14. Two speculative diradical mechanisms for the activation of methane by the MMO hydroxylase that involves reductive activation of dioxygen by the active site cysteine residue. Pathway ***a*** involves concerted cleavage of the C-H bond. Pathway ***b*** is a form of the standard rebound mechanism, modified to facilitate formation of the C-O bond according to ref. 246. Although the oxyl moiety is depicted as bridging the two iron atoms, alternative structures in which it occupies a terminal position are not excluded.

currently no experimental evidence to support or refute these mechanisms. Another variation on this diradical mechanism could employ the dioxyl intermediate discussed above where the second oxyl radical takes the place of the cysteinyl radical. One final mechanism which must be mentioned is a recent proposal that a hypervalent carbon atom is involved in the transition state.[247,248] This species would have a different propensity toward rearrangement than a radical intermediate. It would not ring open most radical traps, but could undergo stereochemical inversion by a pseudorotation mechanism.

To summarize, there is currently no mechanism that explains all the data from the two MMO systems. The results may depend on substrate, protein B, and temperature. The *M. capsulatus* (Bath) enzyme operates at 45° C whereas the *M. trichosporium* enzyme has good activity at 30°. Because the systems can hydroxylate a variety of substrates, the active site must be large, as indicated by the X-ray study, and relatively flexible. Cytochromes P-450 behave very differently in this regard. There are many variants of cytochrome P-450, most tuned for a single substrate.[42] The broad specificity of the MMO hydroxylase might lead to variable alignment of the substrate and active oxidant. Without a highly confining substrate binding pocket in the active site, variable experimental results might be observed. As further evidence accrues, it is reasonable to expect that a single unifying mechanism will be found. In proposing new mechanisms, care should be taken to address what are currently contradictory findings for the systems. Contacts between the protein components of the quaternary system are likely to be important, and elucidating the role of the coupling protein should enhance understanding of how these protein-protein interactions modulate the hydroxylation chemistry at the dinuclear iron active site.

Ribonucleotide Reductase

In methane monooxygenase, the diiron center actively participates in substrate oxidation. The role of the metal cofactor in ribonucleotide reductase (RNR) from *Escherichia coli* is quite different, however, despite structural and chemical similarities in the active sites of the two enzymes. As the name implies, RNR reduces ribo- to deoxyribonucleotides in the first committed step in DNA biosynthesis.[233,249-253] The chemical transformation and a model for its mechanism are depicted in Figure 1.15. Note that no metal cofactor is involved in the dehydroxylation reaction, which is catalyzed by a protein radical designated **X** located on subunit R1 of the enzyme. The dinuclear iron cofactor is involved in the activation step by which this radical is generated in the *E. coli* enzyme and is located on a different protein subunit known as R2. This subunit houses a stable tyrosyl radical that is generated by reaction of dioxygen with the diferrous core, the process of interest in the present context.

The X-ray crystal structure of the R2 protein has been determined in both the reduced and oxidized (met) forms.[234,254,255] The protein structure and coordination geometry of the dinuclear iron center are shown in Figure 1.16. The latter resembles the Hr and MMO cores, but with several distinguishing features. Although both Hr and R2 contain an oxo-carboxylato-bridged dinuclear iron center, Hr has a total of 5 histidine ligands whereas there are only two histidines coordinated to the dinuclear iron center in R2. The rest of the coordination sphere is composed of oxygen donors. In this respect, the active site is identical to that of the MMO hydroxylase. In its reduced form, R2 lacks the hydroxide bridge that links the ferrous ions in deoxyHr (Figure 1.16B). Oxidation to met- or oxyHr is

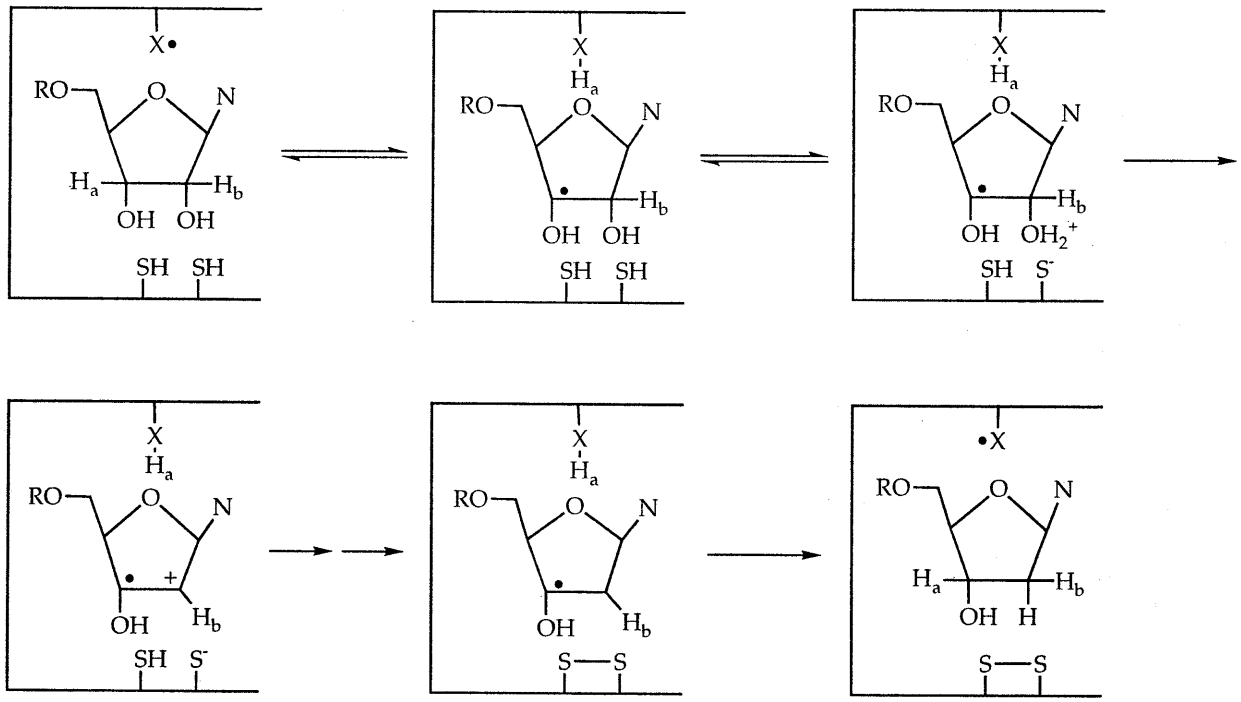

Figure 1.15. Postulated mechanism for RR involving radical cation intermediates. (Adapted with permission from ref. 251.)

A.

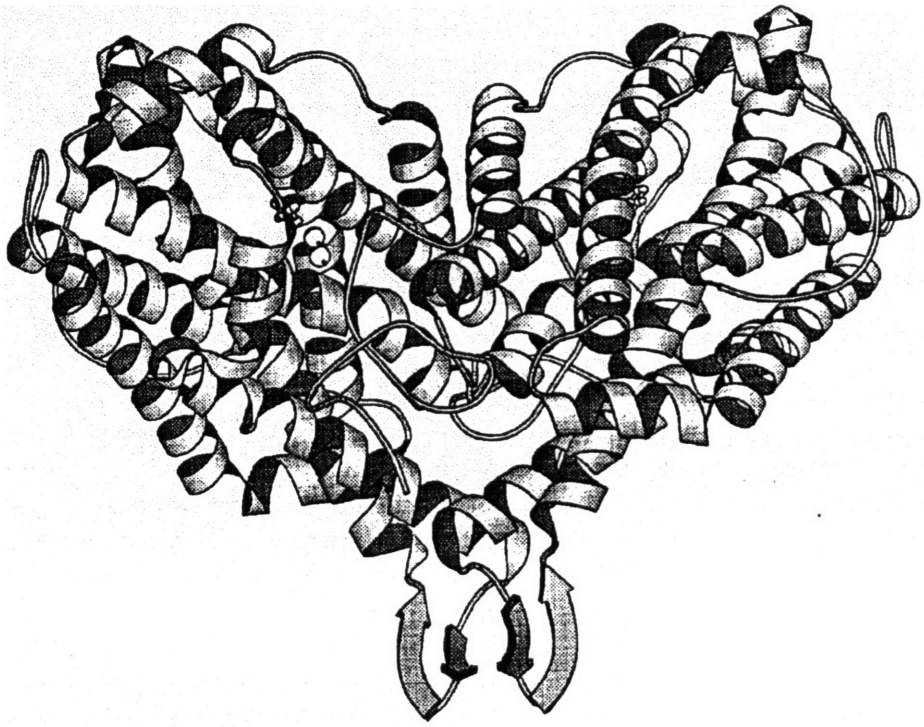

Figure 1.16. A. MOLSCRIPT[186] diagram of the ribonucleotide reductase R2 protein showing the protein fold. B. Active site structure of oxidized and reduced R2 protein from *E. coli*. Distances are given in Ångstroms. (Adapted with permission from ref. 233.)

B.

Reduced R2

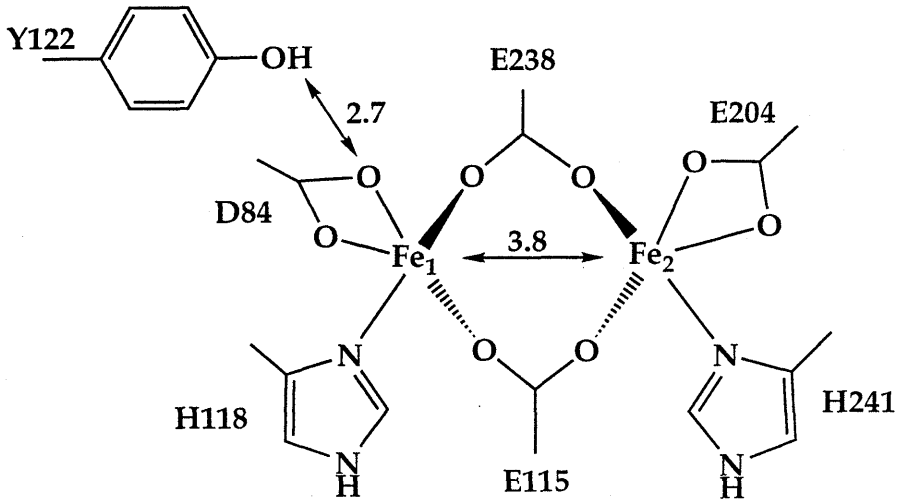

Met R2

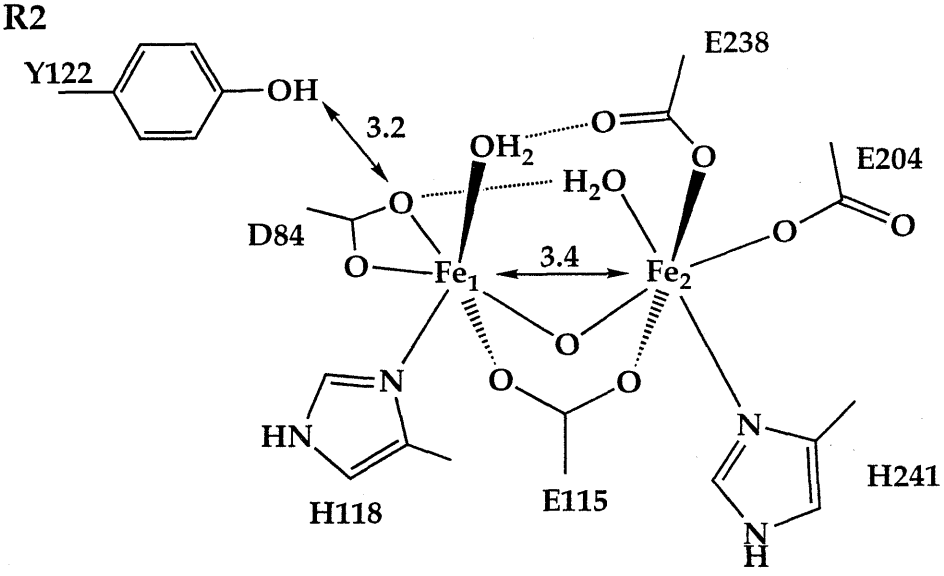

accompanied by only very small RMS displacements of the iron atoms and ligand side chains.[50] In the R2 protein, however, oxidation leads to a distinct carboxylate shift for Glu-238. One oxygen atom dissociates such that the carboxylate becomes a terminal rather than a bridging ligand (Figure 1.16b). Like those in Hr and MMO, the R2 diiron center is surrounded by hydrophobic residues, with the exception of the functionally important tyrosine residue located 5.3 Å from Fe1. The differences in the iron coordination environments of Hr and R2 centers are undoubtedly of functional significance,[48] as discussed further below.

The presumed function of the non-heme iron center in R2 is to generate the tyrosyl radical through a redox cycle such as that depicted in Figure 1.17. This figure also shows interconversions among the apo, reduced, met, and active forms of the enzyme. Spectroscopic characteristics of the dinuclear iron center in each of these states are presented in Table 1.8. During normal enzyme turnover, the iron remains in the diferric state while the tyrosyl radical appears to be responsible, either directly or indirectly, for the catalytic activity.[251-253] Generation of the tyrosyl radical from inactive forms of the enzyme can be accomplished by addition of dioxygen to reduced R2.[249] The net reaction, described by eq 1.30, requires four electrons, three of which come from the tyrosine and two ferrous ions

$$\text{Y122-H} + 2\text{Fe}^{\text{II}} + \text{O}_2 + \text{e}^- + \text{H}^+ \rightarrow \text{Y122}\cdot + \text{Fe}^{\text{III}}\text{-O-Fe}^{\text{III}} + \text{H}_2\text{O} \qquad (1.30)$$

and the fourth from another source. This fourth electron can be contributed by an external reductant such as ascorbate, or by a third equivalent of ferrous

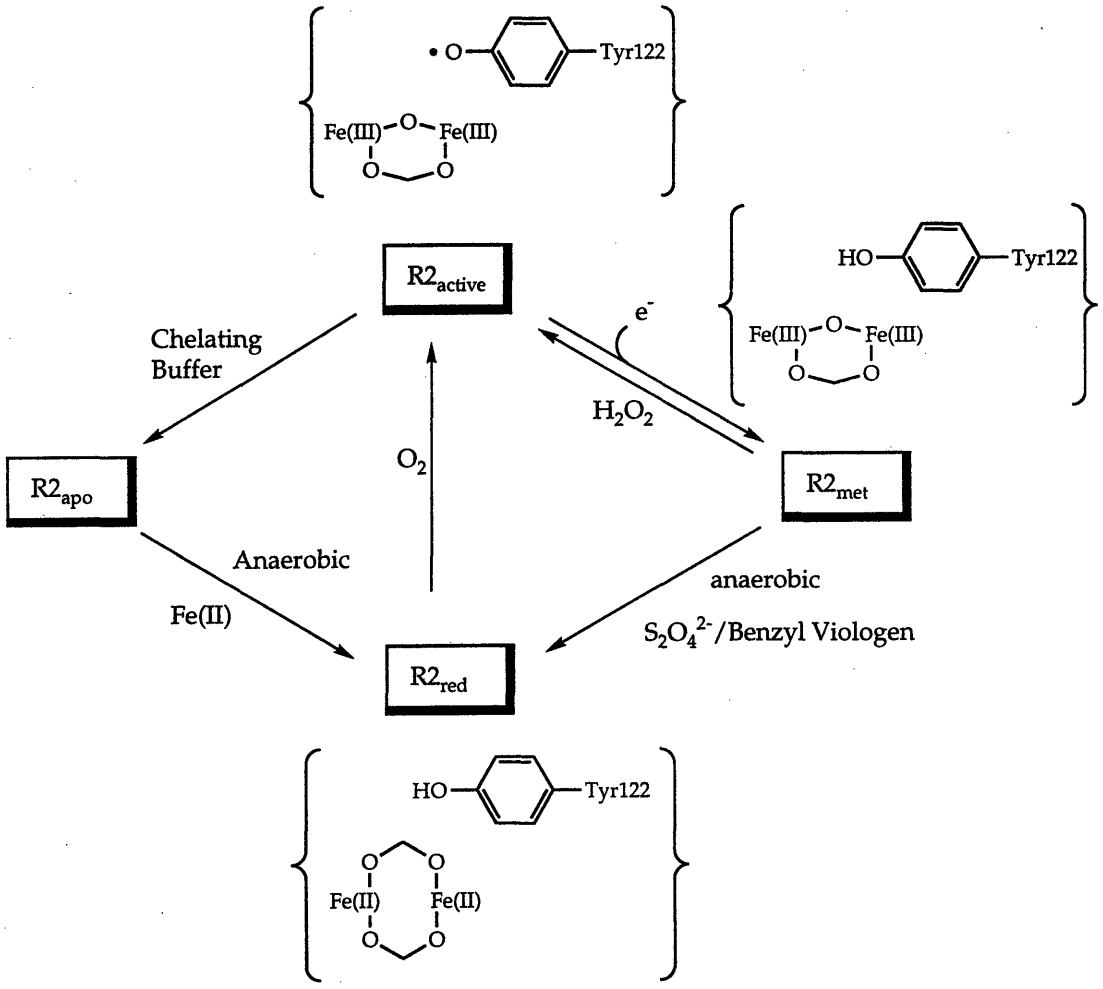

Figure 1.17. Redox states of the diiron core of ribonucleotide reductase from *E. coli.* (Adapted with permission from ref. 256.)

Table 1.8. Spectroscopic Properties for the Different Forms of Ribonucleotide Reductase R2.

		$R2_{red}$	R2 active	$R2_{met}$	ref.
Raman	ν_s(Fe-O-Fe) cm^{-1}		496	496	14
	ν_{as}(Fe-O-Fe), cm^{-1}		756	756	253
optical	λ, nm (ε, M^{-1} cm^{-1})		[a]	325 (9400) 370 (7200) 500 (800) 600 (300)	14
magnetics	-J, cm^{-1}	10		110	14
Mössbauer	Fe1 δ, mm s^{-1}	1.26		0.53	14,253
	Fe1 ΔE_Q, mm s^{-1}	3.13		1.66	14,253
	Fe2 δ, mm s^{-1}			0.44	14
	Fe2 ΔE_Q, mm s^{-1}			2.45	14,249
EPR	g		2 4.3	4.3	14

[a]Same transitions as $R2_{met}$ plus an additional band at 412 nm(ε = 4100 M^{-1} s^{-1}). [b] $H = -2JS_1S_2$.

ion.[256-258] Since ascorbate is capable of reducing ferric to ferrous ions,[259] it is possible that Fe^{II} is always the electron donor. In the presence of excess ascorbate, however, ferric ion generated in the process is reduced before it can be detected to confirm this mechanism.

Further elaboration of the mechanism of tyrosyl radical formation has come from kinetic studies that have identified two spectroscopic

intermediates.[258] The system lends itself nicely to kinetic analysis because of its many spectroscopic features. The tyrosyl radical has a strong visible absorption band at 412 nm, the (μ-oxo)diiron(III) core has absorption bands at 320 and 365 nm, and an intermediate (**U**) with an absorption maximum at 565 nm has been observed. A mutant Y122F, which lacks the key tyrosine residue and is therefore incapable of forming the active form of the enzyme, is also available.[258] When this mutant was used in the kinetic studies, **U** was still observed at 565 nm, but the band due to the stable tyrosyl radical at 412 nm was no longer present. This experiment proved that **U** could be generated independently from the tyrosyl residue of the active enzyme. The second intermediate (**X**) was discovered through freeze quench EPR studies. A sharp, isotropic signal at g = 2.00 distinct from the tyrosyl radical signal was observed. This EPR spectrum exhibited quadrupolar broadening when ^{57}Fe was used, indicating that it was derived from an organic radical bound to the iron center. The EPR signal assigned to the tyrosyl radical grew in at the same rate that **X** disappeared. These observations were interpreted by the mechanism shown on the right hand side of Figure 1.18. The measured rate constants for each process indicated in the scheme are all kinetically competent. Intermediate **U** was originally assigned as a diferric peroxide species based on comparison of its optical spectrum with those of several (μ-1,2-peroxo)diferric model compounds,[54,260] although a μ-1,1-structure has also been suggested.[180,261] These models are discussed in more detail below. An alternative assignment for this intermediate, supported by recent Mössbauer experiments,[262] is a protonated tryptophan cation radical, a species that has an optical absorbance maximum at 560 nm.[263] W48 is in a position suitable to partake in the reaction. In such a pathway, the diferric peroxide would still be a transient intermediate that decays into the diferric

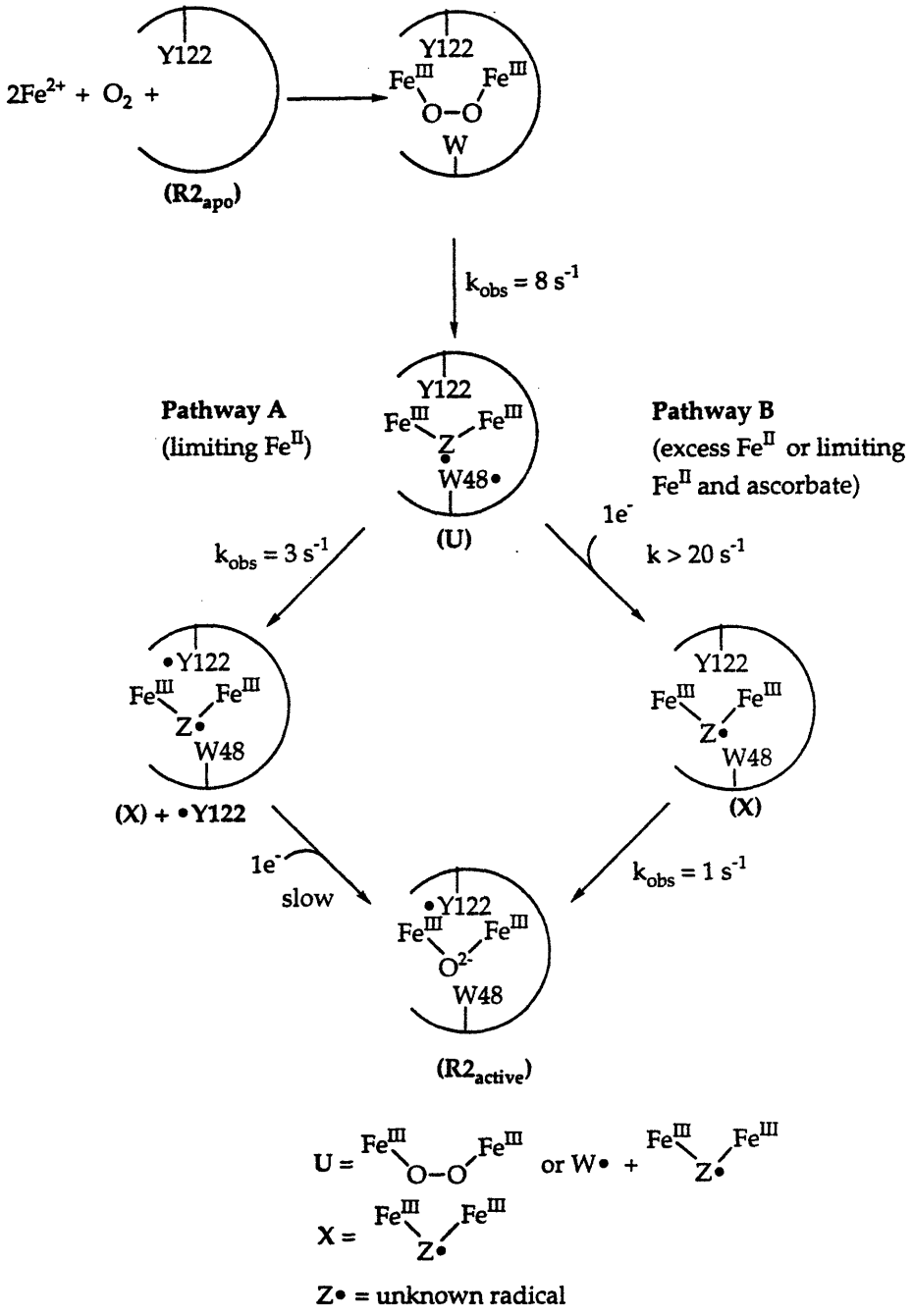

Figure 1.18. Proposed mechanism for the reconstitution and activation of *E. coli* ribonucleotide reductase by dioxygen. Intermediate **U**, observed by optical spectroscopy, has been postulated to be either a ferric peroxide species or a tryptophan cation radical. If **U** is the latter, the diferric peroxide species would probably be an unobserved precursor. (Adapted with permission from ref. 258.)

diradical enzyme species without being observed. The proposed radical ligand species (Z·) has not yet been assigned. Perhaps it is a coordinated oxyl radical, as proposed for the MMO hydroxylase in Figure 1.14.

Regardless of whether species **U** is a peroxide or a tryptophan radical, the mechanism shown in Figure 1.18 does not require a high valent iron-oxo intermediate. Furthermore, freeze quench Mössbauer experiments of intermediate **X** indicate a spin-coupled diferric site.[258] Most of the mechanisms for the decay of putative diferric peroxide intermediates invoke heterolytic O-O bond cleavage leading to a perferryl species.[261,264,265] Support for this mechanism is based on experiments using peroxides, peracids and other oxygen atom donors to activate metR2, a process that would bypass intermediate **U** of the dioxygen dependent reaction.[265] Resonance stabilization of the Fe^{V}-Fe^{III} species is afforded through the Fe^{IV}-O-Fe^{IV} form. The two working hypotheses could be reconciled if the peroxo intermediate were to decay heterolytically to generate a ferryl species that rapidly afforded **X** by the influx of a single electron either from the tyrosine (pathway A Figure 1.18) or from an external reductant (pathway B Figure 1.18).[261] This concept leads to a difficult question regarding the dioxygen activation chemistry, namely, when do the electrons actually enter the system? Does the O-O bond break because an electron is added from an external source such as tyrosine, ascorbate or a third mole of Fe^{II} when excess iron is present, or does the diferric peroxide unit disproportionate, generating a species that abstracts an electron from whatever donor is closest? Future work is required to determine the true sequence of events. No structural evidence exists for a ferryl species in reactions of dioxygen with reduced RNR R2 protein nor from ferrous model compounds (see below); however, if the decay of such a species were more rapid than its rate of

formation, the chance of observing it spectroscopically would be small. Spectra assigned to a non-heme iron-oxo (ferryl) complex have been reported in the reaction of hydrogen peroxide with a ferric model compound,[266] although recent work indicates that the species is more complex than originally believed.[267]

The reaction of the reduced form of an R2 mutant, F208Y, with dioxygen provides additional detail about O_2 activation by ribonucleotide reductase.[233,268,269] In this mutant, a tyrosine replaces phenylalanine-208 in the hydrophobic pocket surrounding the dinuclear iron binding site. Upon addition of dioxygen, a strong visible absorption band at 720 nm appeared and the enzyme became inactivated. Crystallographic and chemical analyses proved that the mutant had tyrosine hydroxylase activity such that Y208 was oxidized to 3,4-dihydroxyphenylalanine (DOPA) upon exposure to dioxygen (Figure 1.19). It was postulated that decomposition of the diferric peroxide produced a ferryl species that activated Y208 by two-electron oxidation followed by nucleophilic attack of water or hydroxide ion or that Y208 had been directly oxygenated by an oxene mechanism.[269] These results imply that the chemistry used to generate the stable Y122 radical in the native enzyme is non-specific and is directed by the relative positioning of reactive species in the active site. Attempts to trap hydroxyl radicals, potential electron shuttles during the reaction, have been unsuccessful and there is no evidence for OH· inactivation of the protein. Therefore, a direct electron-transfer mechanism from the iron center to the site of radical abstraction is preferred.

Having discussed the F208Y mutant and its interesting tyrosine hydroxylase activity, the treatment of the R2 protein concludes with a few comments about how the structure of the metal center might affect the

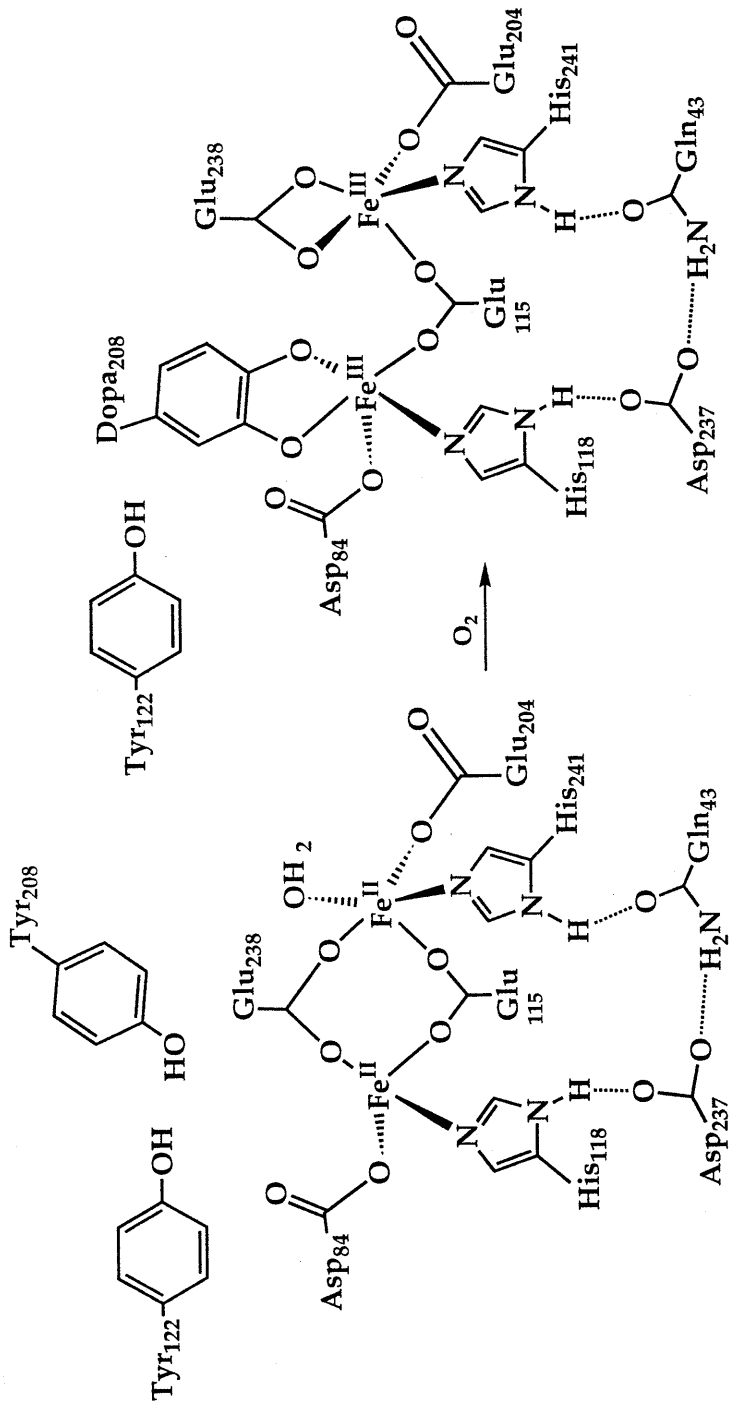

Figure 1.19. Proposed mechanism for the phenylalanine hydroxylase activity of the R2 F208Y mutant. The structure of the reduced form is a model adapted from the crystallographically characterized Mn^{II} derivative of the native protein. (Reprinted with premission from ref. 269. Copyright 1993 American Chemical Society.)

reactivity of its ferrous form with dioxygen. For Hr, it has been proposed that the hydrophobic nature of the core stabilizes a hydroperoxide diiron(III) adduct.[14] A similar situation probably contributes to the stability of the tyrosyl radical in the R2 site. The ability of the F208Y mutant RNR to be hydroxylated, however, is consistent with the notion that its diiron site functionally resembles that of the MMO hydroxylase core more than that of Hr. MMO hydroxylase and RNR have similar coordination spheres dominated by oxygen rather than histidine nitrogen donors. This coordination environment affects the reduction potentials of the iron atoms,[217] but it has not yet been shown unequivocally through model studies that oxygen donor atoms favor hydroxylation activity. In fact, many of the functional hydroxylation catalysts have pyridyl ligands or are inactive when pyridine is omitted from the solvent mixture.[270] In addition, the ability of the Hr structure to stabilize diferric hydroperoxide through internal hydrogen bonding does not seem to be possible in RNR and may not be for the diiron site of MMO hydroxylase either. It is unclear at present whether the diiron(III) peroxide unit is stabilized in Hr because of the difficulty of oxidizing iron to the +4 state (redox related) or whether the Hr core simply does a more effective job of stabilizing the potentially reactive species, trapping it in a low energy, inactivated state.

Ferritin-A Polynuclear Iron Protein

Ferritins are a family of iron storage proteins found in many organisms. Detailed accounts of their chemistry and biology can be found in recent reviews.[271,272] Ferritins are composed of a mineral iron(III) oxide/hydroxide core, similar to ferrihydrite ($FeO(OH)\cdot H_2O$), containing up to 4500 iron atoms in microcrystalline particles approximately 65-70 Å in diameter surrounded by a protein shell. The ferritin protein provides an

extremely soluble and concentrated store of intracellular ferric ions and is a fundamental component of iron homeostasis. The apoprotein from horse spleen Ft has been crystallographically characterized. It consists of 24 subunits made up of H and L polypeptide chains, the ratio of which varies greatly from species to species.[271,272] In general, ferritins with a greater proportion of H subunits display more rapid iron uptake[273] while those species composed predominantly of L-subunits sequester greater quantities of iron in their cavity.[274] The structure of horse spleen apoFt is shown in Figure 1.20. The interior regions of the chains are predominantly hydrophobic with the exception of a conserved group of closely spaced hydrophilic residues located on the H polypeptides. Iron is generally assumed to bind apoFt as iron(II) that is catalytically oxidized at a center on the H subunits. It has been proposed that the conserved regions define the active site for this ferroxidase activity.[275-277] Iron(II) also binds to hydrophilic residues on the L chains, as evident by slow packing of apoLF, but the oxidation step involved in core formation is uncatalyzed. Recent X-ray structural analysis has revealed that the quaternary structure of Ft is preserved in other species.[277] Distinct channels in the protein coat have been postulated as entry points for diffusion of Fe^{II} into the cavity.[278] The ferroxidase activity data support such potential roles for the channel, although other plausible entry routes have been discussed.[279] The oxidation of ferrous ions by dioxygen at such sites results in the initial deposition of the mineral core and is the focus of the present discussion. It should be noted that L chains in heterogeneous ferritins modulate the H-chain ferroxidase activity.[280] Therefore, the comparisons between species must be made with appropriate caution, especially when the H/L composition varies.

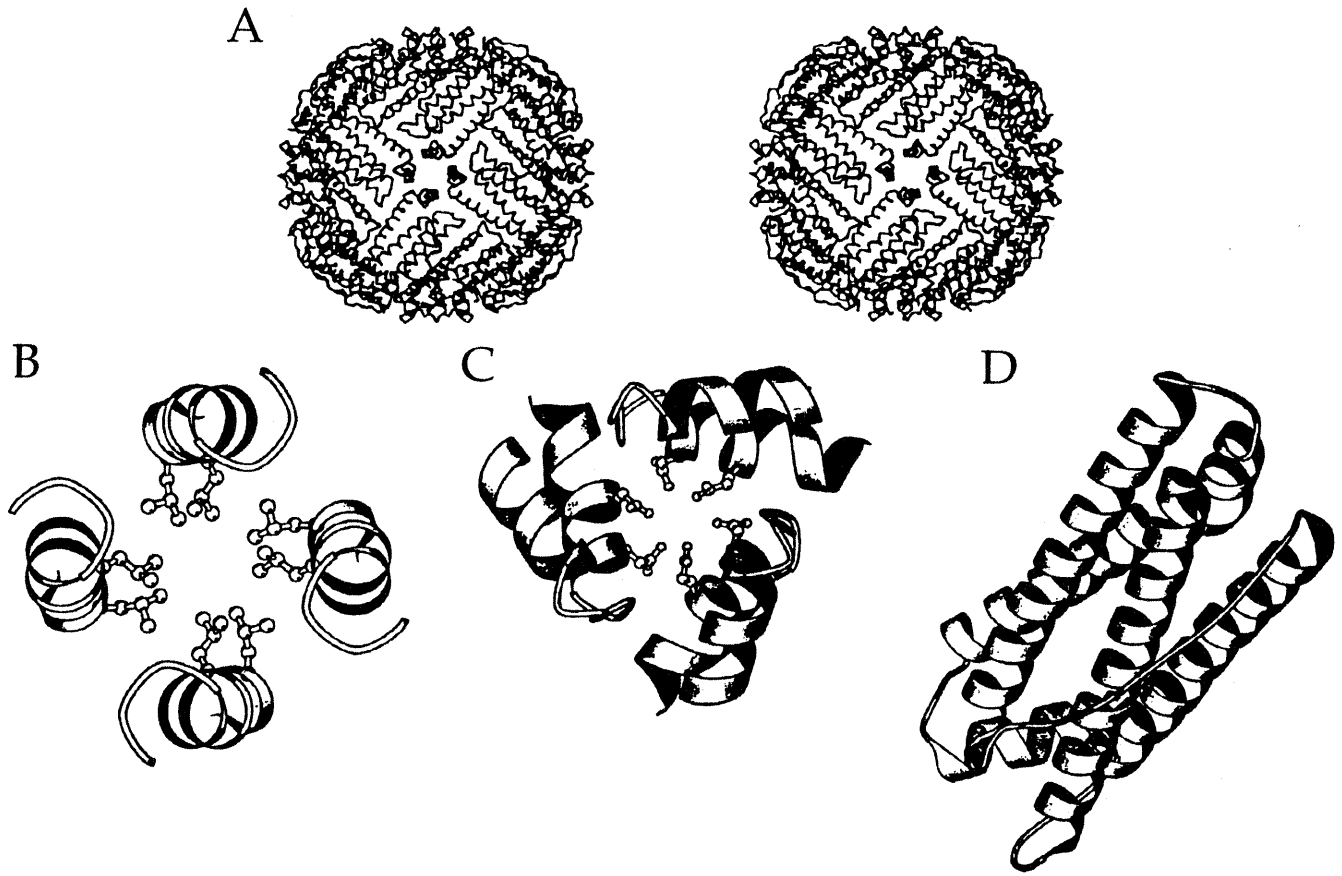

Figure 1.20. Structure of apoHoSF. A. Stereo view of the quaternary structure viewed down the 4-fold axis. (Reprinted with permission from ref. 274 Copyright 1990 Plenum.) B. Molscript[186] diagram depicting the hydrophobic channel along the 4-fold symmetry axis. C. Molscript[186] diagram depicting the hydrophobic channel along the 3-fold symmetry axis. D. Ribbon representation of the structure of a single subunit.

Early studies in vitro revealed that the only way to pack iron into ferritin was to supply Fe^{II} and an oxidant.[281,282] In the case of partially loaded Ft, alternative oxidants could be employed, but only dioxygen was effective with the apoprotein.[271] The reaction proceeds by an oxidation-hydrolysis mechanism whereby ferrous ions are first oxidized to the ferric state and then packed into the crystalline core during a hydrolytic process. For complete loading of ferritin the stoichiometry is approximately $4Fe^{II}:1O_2$.[271] The stoichiometry of the oxidation reaction at low iron loading levels appears variable, however, with reported values ranging from 1.5-4.0 $Fe^{II}:O_2$.[283] These disparate results for HoSF were explained by careful studies of the stoichiometry at different iron loading levels, from which a unifying explanation emerged.[283] In particular, there appear to be competing pathways, as illustrated in eqs 1.31-1.35 where eq 1.33 is the sum of eqs 1.31 and 1.32. At low iron loading, the stoichiometry of the oxidation is 2 mol of Fe^{II} per mole of O_2 (eq 1.33), but under conditions of higher iron loading the ratio shifts to 4:1 (eq 1.34). This shift in stoichiometry can be seen quite clearly

$$Fe^{II} + O_2 + 2H_2O \rightarrow Fe^{III}O(OH) + HO_2 + 2H^+ \quad (1.31)$$

$$Fe^{II} + HO_2 + 2H_2O \rightarrow Fe^{III}O(OH) + H_2O_2 + 2H^+ \quad (1.32)$$

$$2Fe^{II} + O_2 + 4H_2O \rightarrow 2Fe^{III}O(OH) + H_2O_2 + 4H^+ \quad (1.33)$$

$$4Fe^{2+} + O_2 + 6H_2O \rightarrow 4Fe^{3+}O(OH) + 8H^+ \quad (1.34)$$

$$Fe^{2+} + H_2O_2 + H_2O \rightarrow Fe^{3+}O(OH) + OH\cdot + 2H^+ \quad (1.35)$$

in Figure 1.21, where the stoichiometry is plotted as a function of iron loading for HoSF. At low iron(II) concentrations, where nucleation of the

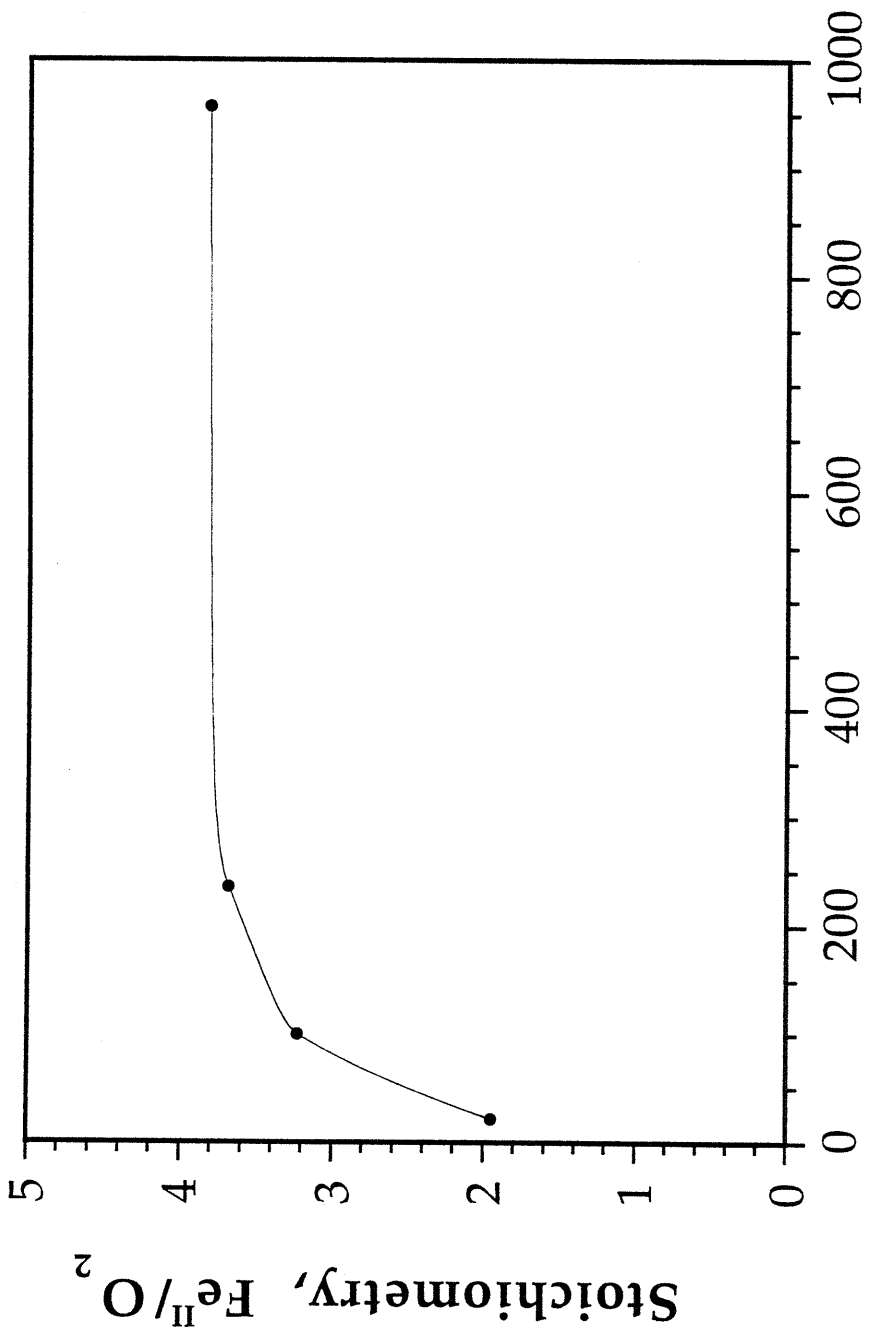

Figure 1.21. Stoichiometry of Fe^{II} uptake into apoHoSF measured as a function of inital iron loading. The conditions were as follows: 1 mM Fe^{II}, 1 μM to 42 μM apoferritin, 0.1 M MOPS, 0.15 M NaCl, pH 7.22, O_2/Fe^{II} ratio = 2.10. (Data taken from ref. 283.)

core occurs, a bimolecular reaction takes place between Fe^{II} and O_2, generating a (μ-oxo)diiron(III) species and hydrogen peroxide. This pathway is discussed in detail below for it pertains to the catalytic ferroxidase activity of ferritin H chains. The second pathway for oxidation is proposed to be a heterogeneous reaction catalyzed on the surface of growing ferrihydrite crystallites. In this reaction, ferrous ions are stoichiometrically oxidized to ferric ions with the consumption of 4 Fe^{II} ions per dioxygen molecule, but much less is known about the details.[281,283]

The ferroxidase activity of ferritins has been studied by Mössbauer, EPR and optical spectroscopy. A (μ-oxo)diiron(III) intermediate along the oxidation-hydrolysis pathway was detected by freeze-quench Mössbauer and UV difference experiments.[276,284,285] EPR studies on HoSF identified two intermediates, a mononuclear ferric species and a mixed-valence diiron(II,III) complex.[286] By optical spectroscopy, a ferric-tyrosinate complex was observed in recombinant bullfrog erythrocyte H-ferritin (rHF).[277,287,288] The burst kinetics of the latter species were sufficiently fast to have precluded detection by the oximetry techniques employed in earlier studies.[280,289] Following the iron-tyrosinate burst, a slow relaxation is observed (≈ 12 hours for full relaxation) before a second burst of equal magnitude occurs. Together with structural and spectroscopic work on rHF mutants lacking the proposed ferrous binding sites on the H chains, these spectroscopic investigations led to a model for the initial phases of ferritin core formation, the nature of which is illustrated schematically in Figure 1.22. It should be noted that this model incorporates kinetic and spectroscopic data from homogeneous (rHF) and heterogeneous (H/L) ferritins as well as mutant H strains, and may be a simplification of the actual events. It is useful

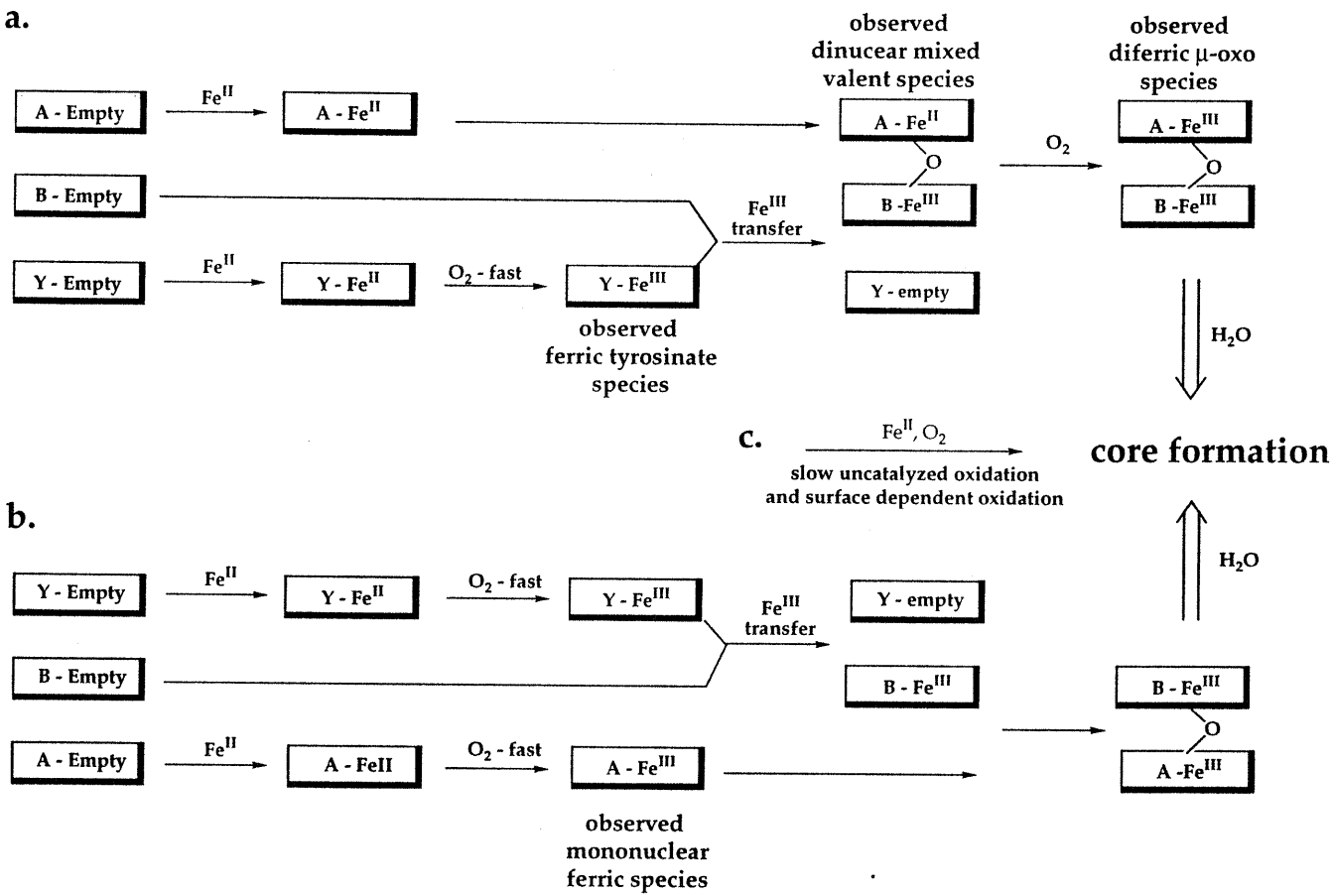

Figure 1.22. Diagrammatic representation of a model for the initial phases of ferritin loading via the ferroxidase center of H-chain ferritins based on spectroscopic data from rHF and HoSF, among others. A, B and Y refer to the binding sites identified and discussed in the text. Site B is depicted as being empty, but an alternative mechanism could be drawn in which the iron transits from A to B before oxidation. The observed intermediates in core formation are noted. Pathway c. refers to the major route of oxidation after the initial nucleation phase.

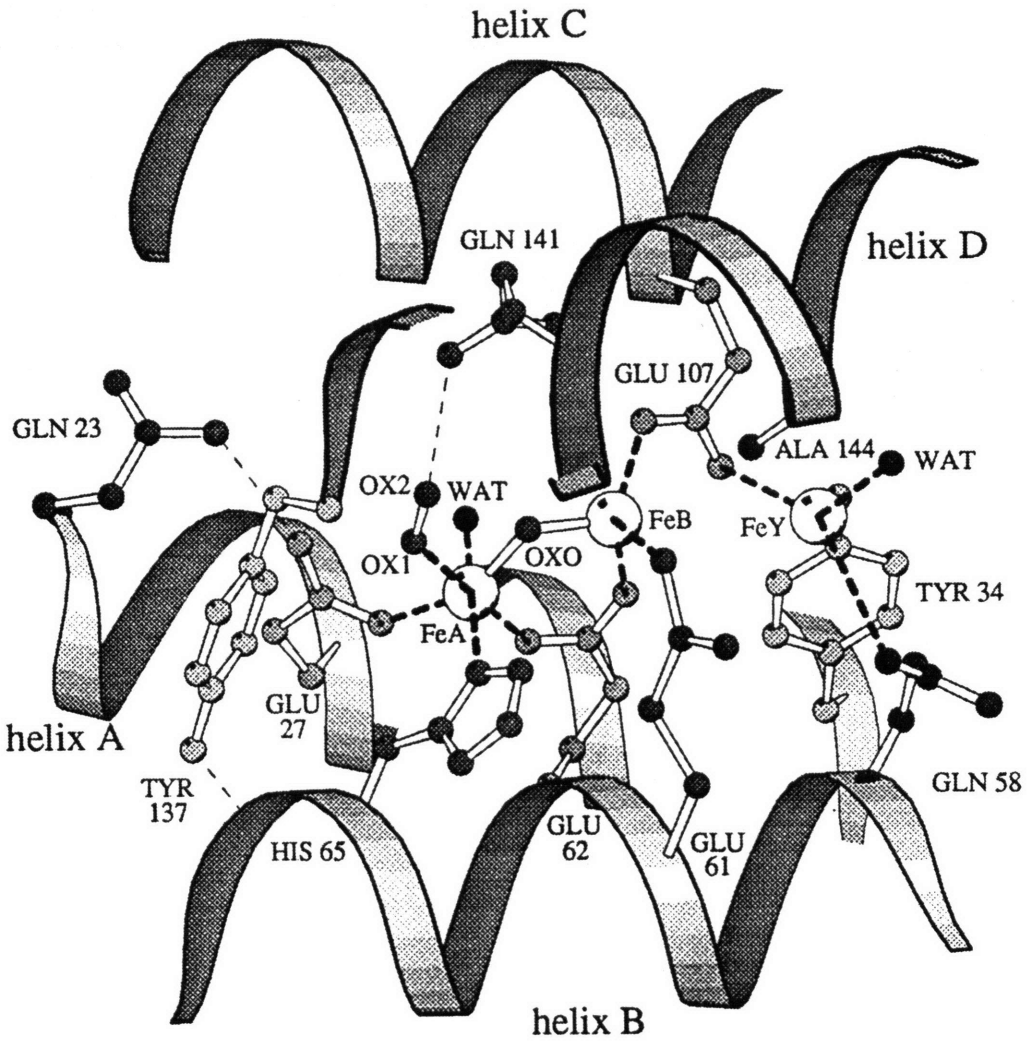

Figure 1.23. Identification of possible loci for the A, B, and Y iron-binding sites in recombinant H-chain ferritin.

nonetheless in helping to reconcile the differences observed in the varying ferritin systems currently under study.

There appear to be three specific sites for the binding of iron to Ft at low iron loading levels, designated A, B and Y. They were assigned, in part on the basis of the binding of Tb^{III}, an inhibitor of iron uptake,[271] to these locations in the crystal and are shown in Figure 1.23. Oxidation of iron(II) is proposed to occur at the A and Y sites. Kinetic studies using optical spectroscopy revealed the formation of a ferric tyrosinate complex that absorbed at 550 nm.[277,287,288] Initial burst kinetics monitored at this wavelength revealed much faster rates than for the formation of other intermediates in the ferritin loading reaction. This ferric tyrosinate species then decayed at a rate kinetically competent for the formation of the (μ-oxo)diiron(III) intermediate observed in the Mössbauer spectrum.[277] Site-directed mutagenesis experiments provided further support for these functional domains. Modification of any of the residues involved in stabilizing the dinuclear complex (FeA-FeB) resulted in significant losses in catalytic activity and recovery of L-chain like behavior, as measured by optical spectroscopy.[277] Studies using oximetry to monitor the kinetics revealed that ferritin molecules mutated at site B (E61A, E64A, E67A) did not lose significant levels of ferroxidase activity, whereas site A mutants (E62K, H65G, K86Q) lost most of their activity.[280] Ferritins with mutations at both sites lost all of their ferroxidase activity.[280] Mutation of the tyrosine residue did not affect the formation of the dinuclear species or the total amount of Fe^{II} oxidized, but the yield of total ferrihydrite was diminished.[277] As expected, the Y34F mutant did not display a tyrosine→iron(III) charge transfer band at 550 nm prior to dimer formation. Since the mutation of tyrosine did not inhibit dimer formation, there must be alternative ways to

catalyze ferrous ion oxidation, albeit more slowly than at the Y site. Possibly, all the iron is oxidized at Y and then migrates to the A and B sites in the wild type rHF. A recycling time of approximately 12 hours is required to see comparable initial burst effects, however.[288] This recovery time is not observed in other ferroxidase intermediates and supports a model in which parallel oxidation reactions at the A and Y sites are involved. Ferritin core packing also did not seem to be affected by mutation of the tyrosine residue. The distance between the A and Y sites is at least 7 Å, too long to be linked by a bridging ligand derived from a single dioxygen molecule. None of the current evidence requires simultaneous oxidation of the two ferrous ions, and oxidation by one-electron steps would explain the observations of mononuclear ferric complexes and mixed-valence species.[286] All of these data are consistent with the chemical transformations discussed above, eqs 1.31-1.35.

Kinetic parameters for the ferroxidase activity of several apoferritin species have been measured and are compiled in Table 1.9. The activity of the human liver ferritin (HLF) species was substantially higher than expected based on its subunit composition and the current understanding that catalytic ferroxidase activity derives from a site on the H-subunit. The large negative activation entropy for both recombinant H-chain ferritin (rHF) and horse spleen ferritin (HoSF) suggests substantial ligand reorganization following iron(II) binding. From the kinetics studies, it was concluded that oxidation occurs via two one-electron steps, as previously shown in eqs 1.31-1.33.[280]

Attempts to observe superoxide or hydroxyl radicals during Ft core formation have been made by using spin trapping agents.[283,290] Very low concentrations of trapped radicals were observed, but it was not possible to

Table 1.9. Kinetic Parameters for the Ferroxidase Activity of rHF, HLF, and HoSF.[a]

	rHF[b]	HLF[b]	HoSF[c]
K_{m,O_2} (μM)	6 ± 2	60 ± 12	140 ± 30
$K_{m,Fe}$ (μM)	80 ± 10	50 ± 10	350 ± 10
$k_{cat\text{-}ox}$ (s^{-1})	3.4 ± 0.2	0.52 ± 0.01	1.3 ± 0.06
$k_{cat\text{-}tyr}$ (s^{-1})	920 ± 50[d]		
Fe^{II}/O_2	2.1 ± 0.1	< 2.7 ± 0.1	2.0 ± 0.2[e]
E_a (kJ/mol)	26.4 ± 0.1	67.3 ± 0.5	36.6 ± 1.3
$\Delta H^{\ddagger}$ (kJ/mol)	23.9 ± 0.1	64.8 ± 0.5	34.2 ± 1.3
$\Delta S^{\ddagger}$ (J/mol K)	-136.0 ± 0.4	-11.0 ± 1.6	-108 ± 5
ref.	280	280	289

[a]rHf = recombinant H chain ferritin; HLF = human liver ferritin; HoSF = horse spleen ferritin. $k_{cat\text{-}ox}$ refers to oximetry measured k_{cat}. $k_{cat\text{-}tyr}$ refers to the k_{cat} for Fe^{III}-tyrosinate formation. [b]Conditions: 0.1 M NaCl, 50 mM MOPS, pH 7.05, 20° C. The composition of the HLF was 4% H- and 96% L-subunits. [c]Conditions as in footnote *a* , but the protein used consisted of 16%H- and 84% L-subunits. [d]Conditions: 0.2 M NaCl, 0.1 M MOPS, pH 7.0, T=25° C. Data point from ref. 283. [e]Data point from ref. 288.

identify definitively the particular species. The low concentration, 1 trapped radical per 5000 Fe^{II} atoms, was explained by noting that radical formation occurs within the protein shell, an environment favoring reaction of radical species with iron via Fenton and Haber-Weiss mechanisms.[63] One of the functional roles of the protein shell may be to react with the oxygen radicals so generated and prevent oxidative damage to other more sensitive biomolecules.[40,290] Because of the inability to trap superoxide ion as dissociated HO_2, a diferric peroxide intermediate was proposed. Such a mechanism would imply that the dinuclear mixed-valent species results

from the oxidation of iron(II) in site A followed by binding of Fe^{II} at site B, rather than by transfer of iron(III) from the Y site as postulated by others.[272,276,277,287,288]

Few reliable kinetic studies on the rate of packing iron into partially loaded ferritin are currently available, partly because of the multiple steps and competing pathways for core formation. Since these pathways depend upon the extent of iron loading, it is difficult to evaluate the published data. Individual intermediates have been studied by different techniques, and a particularly good kinetic investigation on ferritin-catalyzed iron oxidation has appeared.[291] One especially significant finding from this study was the observation that phosphate anions greatly accelerated the rates of ferrous ion oxidation, intermediate decay, and core formation. The phosphate-dependent oxidation acceleration is reminiscent of the autoxidation reactions of aqua-iron(II) species discussed previously and might arise for similar reasons. The rate of ferroxidase catalyzed reaction is several orders of magnitude more rapid than the uncatalyzed reaction, however. Alternatively, phosphate ions might facilitate formation of core particle crystallites, and the effect of phosphate on the oxidation reaction may simply be to clear out ferric intermediates from the catalytic sites.[291]

A final point concerning the ferritin core loading reaction is the fate of the oxygen atoms derived from the dioxygen molecule. Labeling studies using $^{18}O_2$ have conclusively shown that, under both high (1200-1900 Fe/molecule) and low (220-240 Fe/molecule) loading conditions, the oxygen atoms from dioxygen do not appear in the ferritin core with greater than 3-4% efficiency.[292] Thus, the hydrolysis step leading to ferrihydrite formation is distinct from the oxidation process. In a separate study at low iron concentrations, it was shown that hydrogen peroxide was released during the

oxidation process based on the ability of catalase to alter the $Fe^{II}:O_2$ stoichiometry of the reaction from 2:1 to 4:1.[283] Since the oxygen atoms from dioxygen are lost to diffusible hydrogen peroxide, this finding supports the premise that the oxygen atom in the (μ-oxo)diiron(III) intermediate as well as the oxide ions in the ferrihydrite core result from hydrolysis or protonolysis of the ferric peroxide species. A question that might be raised at this point is why is the ferric peroxide intermediate formed in the early stages of ferritin core deposition unstable towards loss of hydrogen peroxide, whereas a similar species in oxyHr is perfectly stable? One possibility is that the non-polar nature of the peroxide coordination environment in Hr retards release of the HOO^- anion, whereas the hydrated environment within the ferritin core leads to protonolysis of the hydrogen peroxide.[14,271] Furthermore, there does not appear to be any clear mechanism for the stabilization of the hydroperoxide. A related question is why, under low iron packing conditions, is O_2 not converted to water but instead departs as hydrogen peroxide?

If this oxidation reaction occurs in independent one-electron steps at the A and Y sites, superoxide ion might also be produced. Since HoSF has weak superoxide dismutase activity, free O_2^- produced will be converted to dioxygen and hydrogen peroxide before detection.[289] When superoxide was added to apoFt, the SOD activity converted it to dioxygen before iron(II) oxidation was observed. Therefore, the inability to observed free superoxide does not preclude its generation. Addition of exogeneous bovine SOD had no effect on either the kinetics of O_2 consumption or iron oxidation, and it was postulated that O_2^- produced remained bound to iron or was dismutated before leaving the confines of the ferritin shell.[289]

Bleomycin - A Metallopeptide with Biological Activity

Bleomycin (BLM) is an anticancer antibiotic used clinically in the treatment of squamous cell carcinomas and malignant lymphomas.[293] Its structure is shown in Figure 1.24. Studies using synthetic analogs have helped to define functional roles for the three domains of BLM, the central one of which, consisting of a pyrimidine, a β-aminoalanine and a β–hydroxyimidazole, is involved in metal binding.[294,295] The other domains are thought to facilitate DNA binding and the specificity of uptake by cells.[294-296] Although BLM strongly coordinates many transition metal ions, it is the ferrous complex that is considered to be the functional form of the drug.[298-300] In the presence of dioxygen, ferrous BLM is transformed into "activated-BLM" that is capable of DNA strand scission.[301-304] Activated-BLM can also oxygenate substrates such as olefins and phosphines.[297,305-310] A primary step in the chemistry leading to DNA damage is abstraction of the 4'-hydrogen atom of the deoxyribose ring. Transformation of ferrous-BLM into the activated-BLM is less well understood, but the process is relevant to mechanisms discussed above for non-heme iron enzymes. Features of this reaction are also found in the dioxygen chemistry of non-biological ferrous complexes, as discussed in the next section.

Structural information about the ferrous and ferric forms of bleomycin is based on analogy to the copper(II), zinc(II) and cobalt(III) derivatives which have been characterized by X-ray crystallography (Cu) and NMR spectroscopy (Zn, Co).[294,311] Since the X-ray structure determination was carried out on a peptide precursor of BLM, and not the final antibiotic, it lacks information about the potential metal-binding roles of the sugar and bithiazole moieties.[311,312] Spectroscopic similarities between the copper

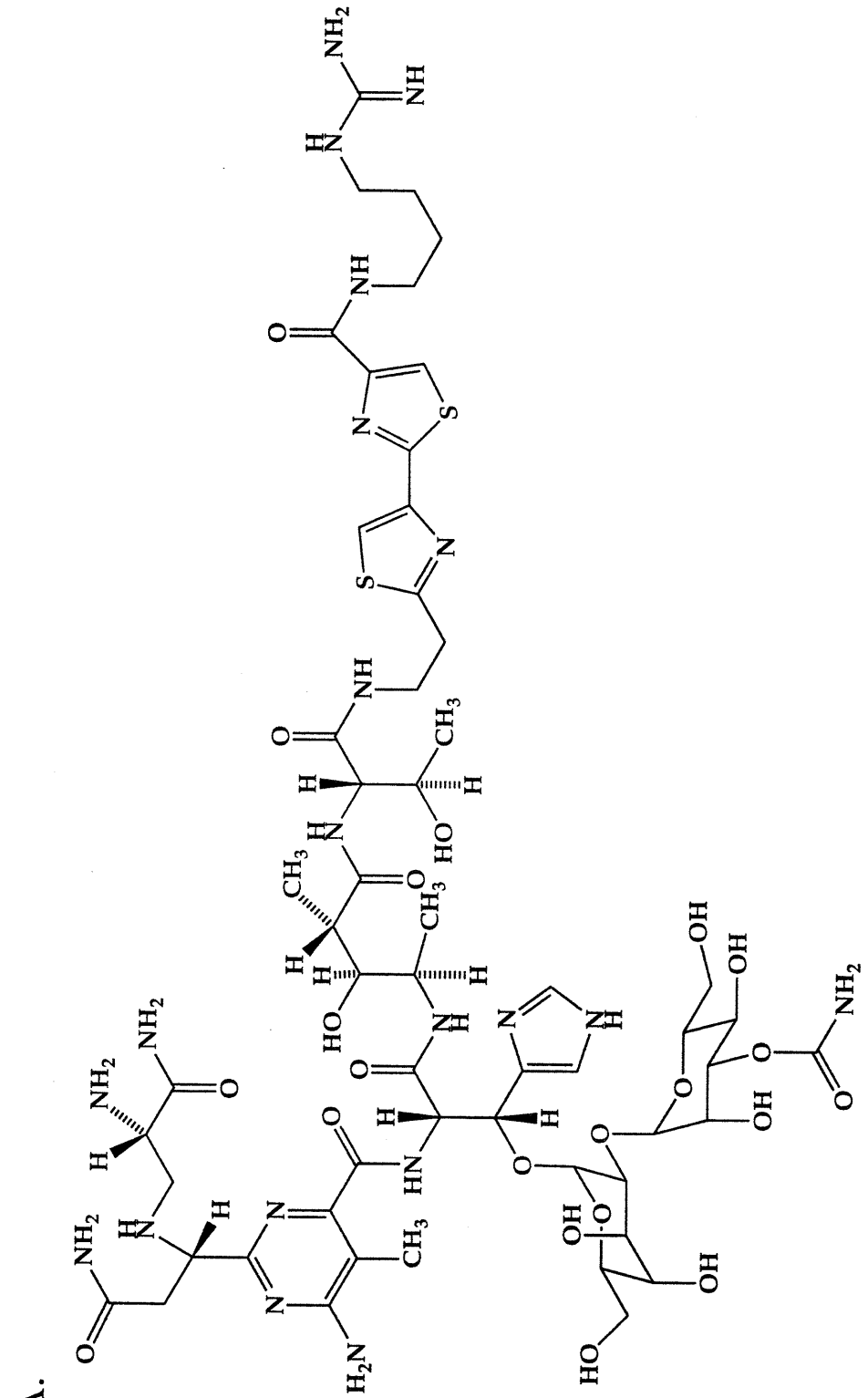

Figure 1.24. A. Structure of bleomycin-B_2, where the B_2 refers to the nature of the specific terminal amine attached to the bithiazole moiety. B. Proposed structure for BLM-Fe^{II}-O_2. (Adapted with permission from ref. 297.)

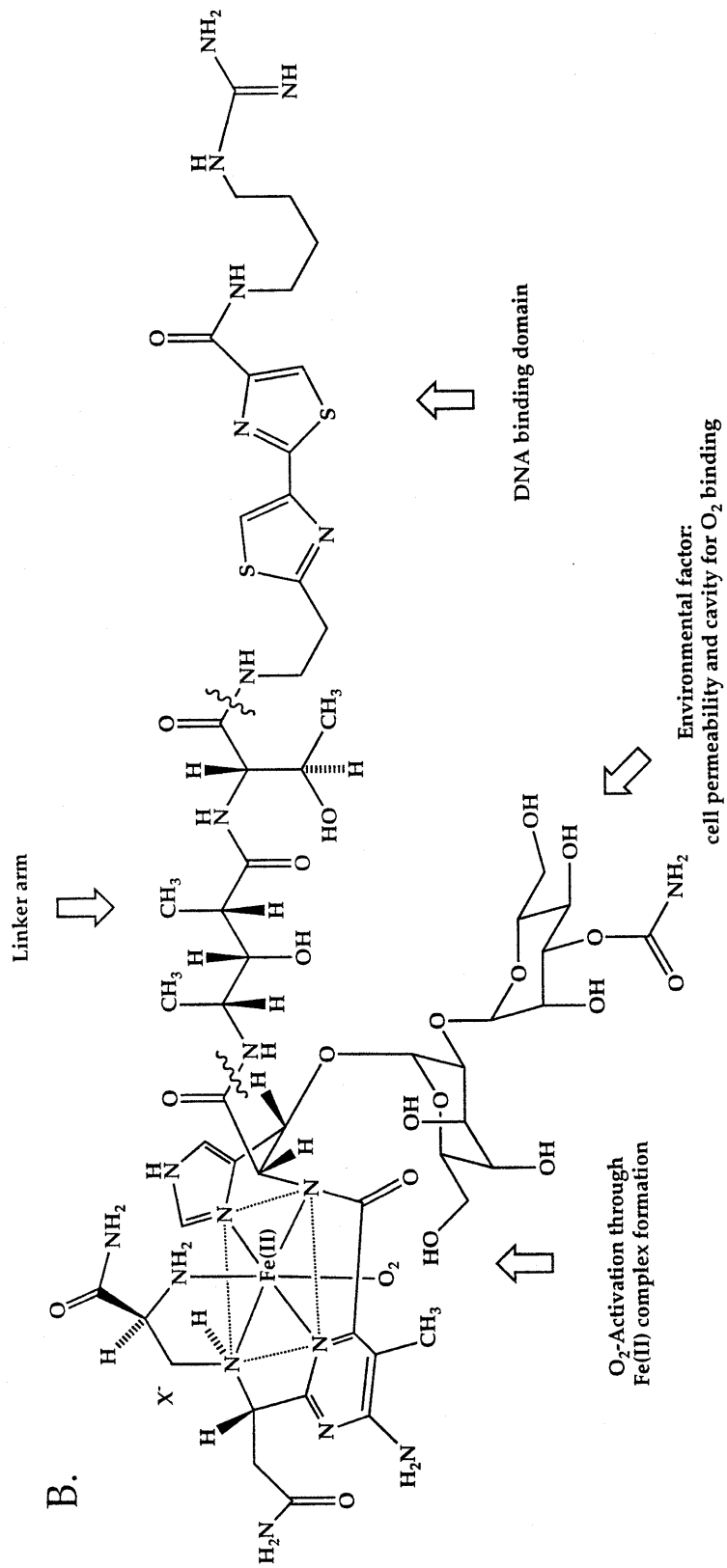
B.
Linker arm
DNA binding domain
Environmental factor:
cell permeability and cavity for O_2 binding
O_2-Activation through
Fe(II) complex formation
Fe(II)
O_2
X^-

derivative of the peptide precursor and the parent molecule, however, suggest that the former is a valid model.[313] As indicated in Figure 1.24B, the ligands in the equatorial plane afford a coordination environment that resembles porphyrin systems. In fact, the spectroscopic and reactivity properties of metal BLM derivatives are often compared to those of heme systems, especially chloroperoxidase.[305] The comparison extends to axial ligand effects so prominent in tuning the chemistry of iron porphyrins.[46,294] Although the saccharide portion of the molecule is usually neglected in discussions of BLM metal ion binding, this domain might have a functional role in the activation of dioxygen.[314] Weaker EPR signals and reduced reactivity toward DNA for the deglyco-BLM versus native BLM under identical conditions were attributed to diminished stability of the activated BLM. Moreover, the deglyco-BLM-Fe^{III} complex did not undergo the pH dependent high spin to low spin transition that occurred in the parent Fe^{III}-BLM complex.[314] It was therefore suggested that the sugar residues provide stabilizing hydrogen-bonding interactions with the dioxygen moiety of activated BLM, but further work is required to test this hypothesis.

BLM has proved to be a remarkable system for studying reactions of non-heme iron(II) with dioxygen because of the ability to characterize several intermediates, first observed through a combination of EPR and optical spectroscopic studies.[301,302] These species and their relationships to one another are shown diagramatically in Figure 1.25 together with the relevant spectroscopic parameters. In the ferrous form, the BLM complex can reversibly bind several dioxygen analogs (NO, CO, RNC) in a manner similar to iron-porphyrin complexes.[302] The initial reaction of the Fe^{II}-BLM complex with dioxygen results in the formation of a pink, EPR-silent species.

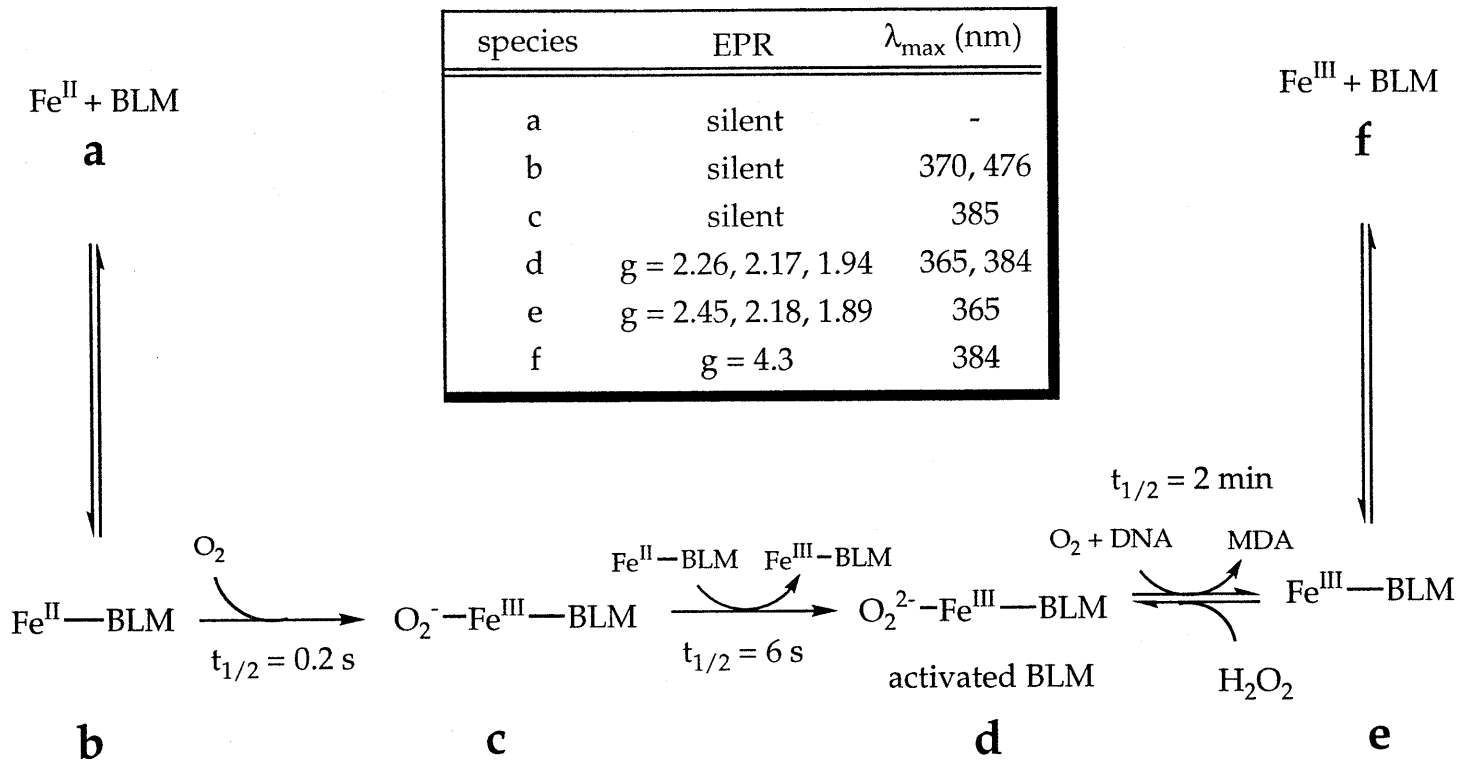

Figure 1.25. Proposed mechanism for the activation of Fe^{II}-BLM. (Adapted with permission from ref. 303.)

It forms according to the rate law shown in eq 1.36 with a $t_{1/2}$ of 0.2 s at 2° C.[301] The rate of this reaction is independent of pH from 6-8 and, from

$$\frac{d[\mathbf{c}]}{dt} = k_1[\mathrm{Fe^{II}}\text{–BLM}][\mathrm{O_2}] \tag{1.36}$$

Mössbauer studies, the pink intermediate was proposed to be a Fe^{III}-superoxide complex.[304] A second intermediate (**c'**), having an indistinguishable optical spectrum but a different EPR spectrum from that of **c**, has been reported.[315] It is not clear what the relationship between these two species is, but since they both decompose to the same product, it is possible that they are coordination isomers of one another, where the mode of O_2 bonding affects both the stability and EPR parameters. This intermediate (**c**) can also be intercepted by the addition of nucleophiles such as ethyl isocyanide, which can bind the ferric center, leading to the displacement of dioxygen and formation of a completely inactive ferrous-BLM-isocyanide complex.[303] The ability of ethyl isocyanide to affect the bleomycin chemistry only occurs at this stage of the reaction; once the dioxygen has been reduced to the peroxide level, the energy barrier for reoxidizing it to O_2 is prohibitive. The decay of **c**, which has a half-life of 6 s and follows the rate law in eq 1.37, affords activated-BLM.[303] This species appears to be a one-electron reduced form of **c** and has been designated a

$$\frac{d[\text{activated–BLM}]}{dt} = k_2[\mathbf{c}] \tag{1.37}$$

ferric-peroxide.[303,304] The Mössbauer and EPR studies definitively rule out an Fe^{IV} assignment, since these spectra require the iron center to have an

odd number of electrons.[303,304] The electron donor needed to form activated BLM in the absence of reducing agents has been proposed to be another equivalent of Fe^{II}-BLM.[301,303] The use of a second ferrous ion to effect the thermodynamically preferred two-electron reduction of dioxygen is similar to the autoxidation reactions of ferrous ions discussed above as well as the mechanism of tyrosyl radical formation in RNR. This reaction is influenced slightly by the presence of DNA, as revealed by EPR studies on ^{57}Fe enriched samples, indicating direct interaction between the product, activated-BLM, and DNA.[303] As an alternative to the dioxygen route, activated BLM can also be generated by addition of H_2O_2 to Fe^{III}-BLM in a manner analogous to the peroxide shunt mechanism of iron-porphyrin and MMO systems.[42,239,294,316,317]

In the absence of DNA, activated-BLM undergoes autoxidation, leading to complete inactivation within several minutes.[303] The resulting species can be only partially reconstituted by addition of ferrous iron. This behavior contrasts with that of the ferric BLM product resulting from the reaction of activated BLM with DNA which, upon addition of fresh ferrous ions, is fully functional.[303] The stoichiometry of this autoxidation reaction, starting from ferrous iron, is 4 mol of Fe^{II} per mole O_2 consumed, once again similar to the oxidation reactions of aquated iron(II).[318] When $^{18}O_2$ is used, the label is found almost quantitatively in water, showing that the active species undergoes inactivation via a ligand oxidation rather than an oxygenation process. Were metallo-BLM to decompose by self-hydroxylation, labeled oxygen would be incorporated into the molecule and less would appear in the water. Oxygenation followed by hydrolysis is not ruled out, however.[318]

In the presence of DNA, activated BLM immediately initiates cleavage chemistry by abstracting the 4'-H atom of the ribose ring. Using [4'-^{3}H] DNA, kinetic isotope measurements revealed this reaction to be involved in the rate-determining step.[319] The sugar radical then decomposes as indicated in Figure 1.26 to form free nucleic acid bases or base propenals.[313] The oxygen molecule in pathway a of Figure 1.26 has been distinguished from dioxygen involved in BLM activation by pulse chase experiments.[294,320] The overall DNA cleavage reaction follows Michaelis-Menten kinetics with a K_m = 1.8 mM and V_{max} = 5000 mol min^{-1} Fe^{II}.[321] It has a half-life of 8 s, making the formation of activated BLM kinetically competent to carry out the reaction.

Early work proposed hydroxyl radicals or superoxide ion to be the active species involved in BLM-mediated DNA degradation,[302,322,323] but such a mechanism seems unlikely based on the low yields of trapped hydroxyl radicals and the inability of small molecule superoxide dismutases to intercept the chemistry.[324] More recently,[313] the reaction has been envisioned to occur by a rebound mechanism similar to that proposed for cytochrome P-450.[42,316] Further evidence has cast doubt on this hypothesis, however. Whereas cytochrome P-450 and its models incorporate oxygen atoms from O_2 into the substrate, the products of BLM cleavage receive their oxygen atom from solvent water under anaerobic conditions using H_2O_2 as the activating agent.[325] A rebound mechanism need not be invoked in this chemistry. For the hydrogen abstraction step to be rate-determining, formation of the proposed ferryl ion must be faster than abstraction and therefore it would be expected to build up to some steady state concentration. A ferryl species has never been observed spectroscopically, however.[310] If

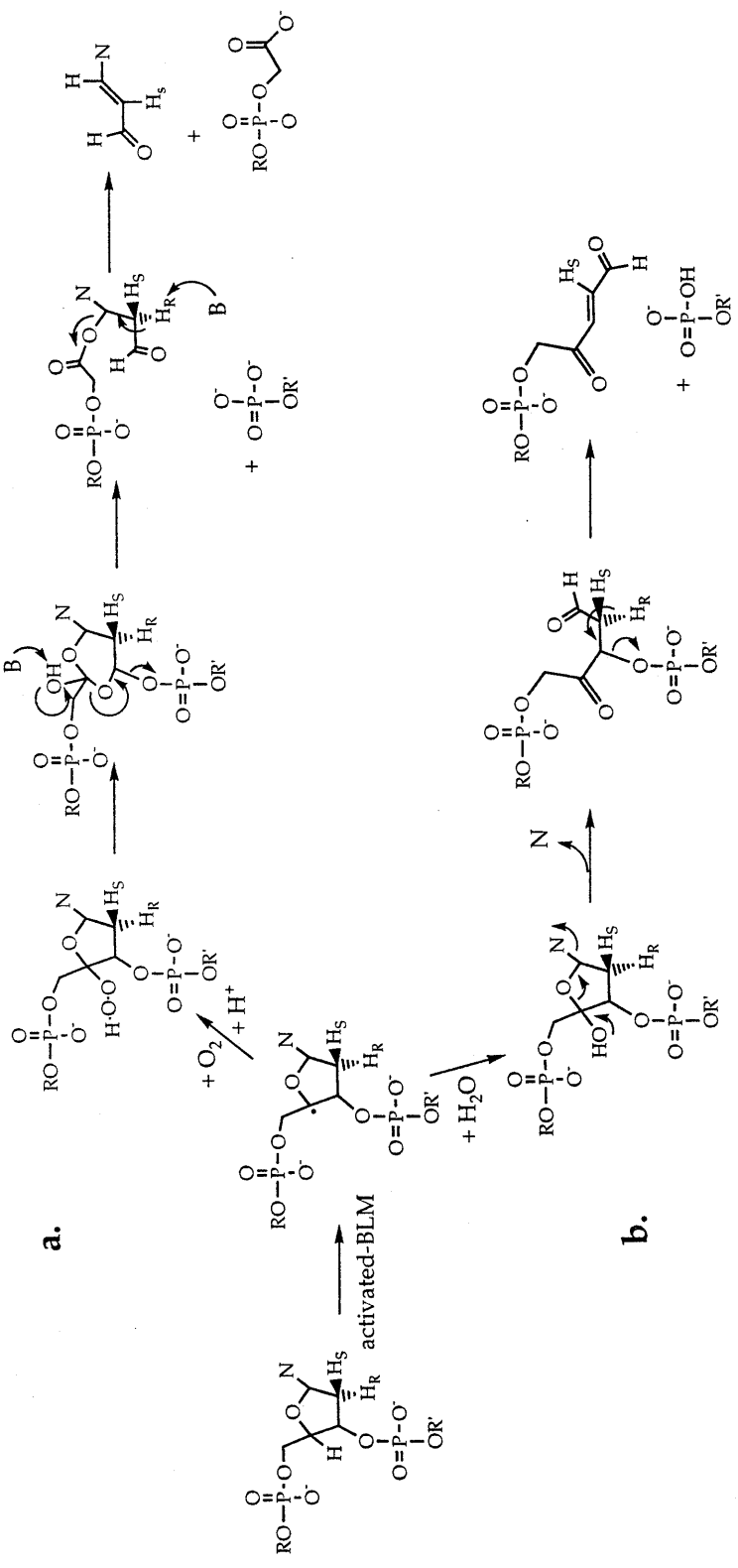

Figure 1.26. Proposed mechansim for the degradation of DNA by activated-BLM. Pathway **a** predominates under aerobic conditions and **b** under anaerobic conditions. (Adapted with permission from ref. 294.)

the oxygen atoms of activated-BLM were exchanging with solvent, the rebound mechanism would still be plausible, but experiments have shown that such is not the case.[310]

When provided with an alternative substrate to DNA, BLM oxidation chemistry ensues in a manner similar to that of cytochrome P-450 and its models. Another similarity between Fe-BLM catalyzed oxidation chemistry and P-450 systems is the ability to initiate the chemistry with a variety of alternative oxidants and oxo-transfer agents in place of dioxygen and a reductant.[307,313] It should be noted, however, that the distribution of products is not always identical for the dioxygen reactions and these shunt pathways. This point is clearly illustrated by studies using *cis*-stilbene.[307] The dioxygen promoted reaction yields solely benzaldehyde with complete incorporation of isotopic label. Hydrogen peroxide affords predominantly the *cis*-epoxide, and other oxo-transfer agents (PhIO, $NaIO_4$, ROOH) yield a mixture of the *cis*- and *trans*-epoxide, benzylphenyl ketone, and benzaldehyde. Furthermore, the isotopic distribution of the products is a function of the reductant used to initiate the reaction. These results imply that a bleomycin ferryl species can be generated, but raise serious concerns as to whether the oxo-transfer agents follow the same chemical mechanism as the dioxygen reaction. To generate 2 equiv of labeled benzaldehyde from stilbene and dioxygen, a cyclic peroxide is likely to be a key intermediate.[294] This intermediate cannot form under anaerobic conditions, and the mechanistic pathway will certainly be altered. Activated bleomycin might be capable of decomposing to a ferryl species, but for the case of stilbene oxidation at least, it appears that a dioxygen insertion reaction is operative.

The above discussion has presented evidence that argues against the involvement of a ferryl-induced rebound mechanism or diffusible oxygen-

derived radicals in the reaction of BLM with DNA. The challenge is to provide a plausible mechanism that fits all the observed data. It is still possible that activated-BLM decomposes to generate a ferryl intermediate that effects the chemistry by hydrogen atom abstraction in such a way that the substrate (or DNA) radicals produced react faster with water than with the Fe^{IV}-OH unit. One of the roles of the protein in P-450 systems might be to prevent such a water molecule from interacting with substrate radicals, but porphyrin model systems no bulkier than BLM exist which afford products attributed to ferryl species formed by the same mechanism. Direct reaction of a BLM ferric peroxide intermediate with DNA has rarely been invoked, but is one of the remaining contenders. When viewed with the benefit of information provided by studies of the small molecule catalysts, such as the Gif system discussed below, it seems possible that such a species may be reactive enough to catalyze the observed DNA degradation chemistry. In fact, early work on the Gif systems proposed ferryl intermediates before they were excluded by subsequent experimental work.[326,327]

Reaction of Biomimetic Iron(II) Complexes with Dioxygen

The systems discussed in this section were devised in various attempts to mimic the biological structures and functions described above. We present this work in three subsections according to the relative stability of the oxygenated species formed in the initial reaction of a ferrous precursor with dioxygen. The first section treats the most stable complexes, which form dioxygen adducts detected spectroscopically, usually at low temperature. A summary of the spectroscopic data on these compounds is provided in Table 1.10. The second section covers autoxidations of model compounds, reactions having transient intermediates but which do not

function to hydroxylate a substrate molecule. The last section discusses systems known to oxidize a hydrocarbon for which iron-dioxygen species have been inferred based on the measured catalytic properties. We make no attempt to include every catalytic reaction involving ferrous-dioxygen chemistry, for such a treatment would be prohibitively broad. Instead, we present selected reactions, chosen to illustrate the general scope, breadth and versatility of ferrous-dioxygen systems as oxidation catalysts. Reactions of hydrogen peroxide or superoxide ion with ferric complexes to form active oxygenation species are not explicitly treated, although they are mentioned in a few cases where the information was found to be insightful.

Stable Dioxygen Adducts

Pseudo-Heme Systems

Several mononuclear non-heme ferrous complexes in this class have been synthesized as models for the chemistry of porphyrin systems, Figure 1.27. Some bind dioxygen to form relatively stable mononuclear or dinuclear adducts.[328,329,336-339] Geometric information about these dioxygen adducts is not available and even their exact coordination modes are not well known. All but one of these compounds contain a N_4 donor macrocyclic ligand occupying the equatorial positions of the octahedral ferrous ion in the absence of dioxygen. Such a rigid planar coordination geometry is uncommon among non-heme systems, as manifest by the structural features of the biological molecules discussed above. Unlike the porphyrins, however, these macrocyclic ligands are not fully conjugated, a property that may destabilize the ferryl species. In this respect their reactivity may be more comparable to non-heme iron centers.

Table 1.10. Visible and Raman spectroscopy of the dioxygen adducts of non-heme iron model compounds.

compound	solvent	λ_{max}, nm (ε, M^{-1} cm^{-1})	ν(Fe-O)(^{18}O)	ν(O-O)(^{18}O)	binding mode	ref.
1	THF	534 (1590)		853	μ^4	51
2/O_2	toluene/pyridine 99:1	529				328
4/O_2	Acetone/Pyridine/ water (3:1:1)	523 (3200)				329
10b	water	540 (187)				330
12b	toluene	679 (3454)	418 (409)	876 (827)	μ-1,2	53
14a/H_2O_2	water	560 (2200)	476 (457)	895 (854)	μ-1,2	331
15b	CH_2Cl_2	588 (1500)	476 (460)	900 (850)	μ-1,2	54
16b	CH_2Cl_2/DMSO 9:1, v/v	562 (3200)			μ-1,2	54
16b	CH_2Cl_2/DMSO 8:2, v/v	572 (2060)	453, 481 (444)	877, 893 (834)	μ-1,2	54
$[Fe_2\{HB(3,5\text{-}iPr_2pz)_3\}_2(OBz)(OH)]/O_2$	pentane	$\approx$ 700				332
$[Fe_2(5\text{-Me-HXTA})(O_2)(OAc)]^{2-}$	DMSO or MeOH	480 (2370)	n.o.	884	μ-1,2	333
$[Fe(Ph_3PO)_4]_2(O_2)$	MeCN	576 (3540)	n.o.	884[a]	μ-1,2	334
$[Fe(OEP)O_2]^-$			n.o.	806 (759)	η^2	335
$[Fe(EDTAH)O_2]^{3-}$	water	520 (530)	n.o.	815 (794)	η^2	84
oxyHr	water	500 (2300)	503 (480)	844 (797)	η^1	190

[a]Raman spectrum taken in the solid state as a KCl mull.

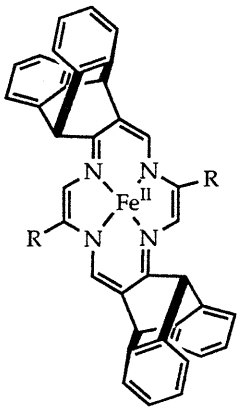

2

$R = (CH_2)_7CH_3$

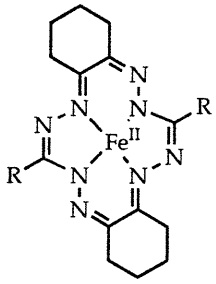

3

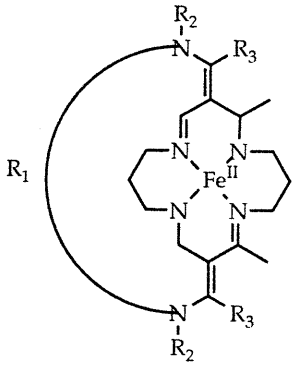

4: R_1 = m-xylylene, R_2 = Me, R_3 = Me
5: R_1 = m-xylylene, R_2 = benzyl, R_3 = phenyl
6: $R_1 = (CH_2)_3$, R_2 = Me, R_3 = Me
7: $R_1 = (CH_2)_4$, R_2 = Me, R_3 = phenyl
8: $R_1 = (CH_2)_5$, R_2 = Me, R_3 = phenyl

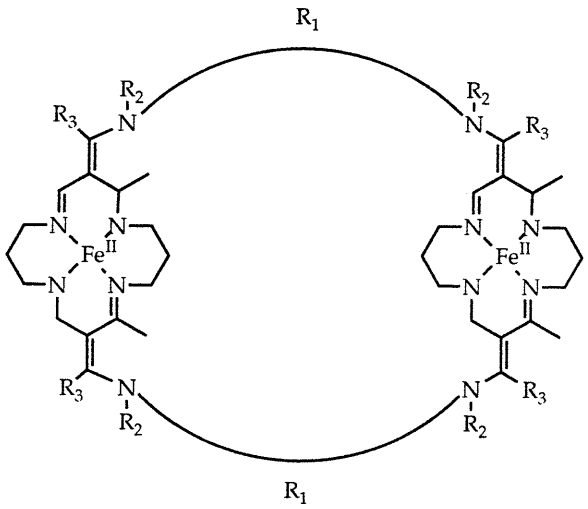

9: R_1 = m-xylylene, $(CH_2)_2$, $(CH_2)_3$, $(CH_2)_4$ among others
R_2 = H, R_3 = Me

Figure 1.27. Pseudo-heme ferrous complexes **2-9** which bind dioxygen to form stable adducts.

Some of the complexes shown in Figure 1.27 bind O_2 reversibly. Even these reversible systems undergo irreversible autoxidation, however (eq 1.38). This instability is minimized at low temperatures where the reversible binding of dioxygen still takes place.

$$\text{LFe(II)} + O_2 \rightleftharpoons \text{LFe(III)-}O_2^- \xrightarrow{\text{slow}} \text{irreversible oxidation} \quad (1.38)$$

Early workers[328] approached the construction of a non-heme iron reversible dioxygen carrier by the strategy that proved successful for heme analogs.[340-342] In the latter systems, the dioxygen adducts decompose in a bimolecular reaction involving a (μ-1,2-peroxo)diiron(III) porphyrinato complex that has been thoroughly characterized.[343,344] By constructing ligands with sufficient geometric bulk to prevent formation of the peroxide-bridged diiron(III) complex, such as capped or picket fence porphyrins,[341,345,346] the desired 1:1 adduct was stabilized. In a similar manner, sterically encumbered non-heme ligands and their respective ferrous complexes (**2** and **3**, Figure 1.27) were prepared having two different pocket depths (5 Å and 2.2 Å respectively). As expected, in the presence of pyridine as an axial base, the more sterically crowded ligand afforded reversible dioxygen binding at temperatures below -50° C. A 1:1 stoichiometry was demonstrated by dioxygen uptake experiments, and the adduct exhibited an optical band at 529 nm. Unfortunately, neither resonance Raman nor Mössbauer spectroscopy was used to characterize this compound, but its presumed mononuclear nature is consistent with the presence of a ferric-superoxide unit similar to that of Hb and synthetic iron-porphyrin-dioxygen complexes.[6] Compound **3**, having a shallower pocket,

was rapidly and irreversibly autoxidized at -78° C with the consumption of 0.5 equiv of O_2.[328] Clearly, ligand control of the environment around the dioxygen binding site attenuates the reactivity of the adducts.

The comparison of the reactivity of these two compounds, similar in all respects except for the depth of their O_2-binding pockets, reveals the importance of steric constraints in determining the course of the reaction of dioxygen with ferrous complexes. A second example of this property is afforded by the mononuclear cyclidene complexes.[329,338,339] Unlike the previous molecules, which had a simple cleft, these ligands are bicyclic, enclosing pockets of defined size based upon the length of the R^1 spacer (compounds **4** - **8**, Figure 1.27). Because of their versatility and ease of substitution at the different sites, iron complexes of these cyclidenes display a range of chemical reactions, for which complete and up-to-date reviews can be found elsewhere.[347,348]

Upon exposure of **4** to dioxygen at low temperature, an optical absorption band around 520 nm appears as well as less intense features in the 500-650 nm region.[329] The spectrum is quite similar to that of **2** discussed above. Gas uptake experiments revealed the new species to be a 1:1 adduct, which was diamagnetic and EPR silent.[329] This complex can best be formulated as a low spin ferric superoxide complex. The effect of axial bases on its dioxygen affinity parallels that of the porphyrin dioxygen carriers, with Cl^- < py < 1-MeIm.[329] When steric bulk was added to the R_2 and R_3 sites while maintaining a constant R_1 bridge, the autoxidation process was retarded without affecting the oxygen binding properties of the molecule.[338] The most stable adduct was formed with compound **5**, which bound dioxygen reversibly even at room temperature because of its slow ($t_{1/2}$ = 24 h) autoxidation process. The thermodynamic values for the reaction of this

complex with dioxygen are: $\Delta H = -17.5 \pm 0.4$ kcal/mole, $\Delta S = -76 \pm 2$ eu, $K_{O_2} = 0.050$ Torr^{-1}.[338] Although the reaction enthalpy is similar to values for Hr, the entropy is significantly more negative for this model compound. Such a large negative reaction entropy is consistent with the properties of other "lacunar" metal complexes.[338]

Because the autoxidation rate could be altered without changing the dioxygen binding properties of the iron center, this system provided a unique opportunity to carry out comparative mechanistic studies of the autoxidation and dioxygen binding reactions of the ferrous complexes. A series of ferrous cyclidene complexes with different exterior R groups and pocket sizes, including some with pockets too small for O_2 binding, was investigated.[347,349,350] For systems capable of binding dioxygen in the pocket, usually **4**, it was concluded that a ferric-peroxide species formed during autoxidation and that parallel, competing inner- and outer-sphere redox processes were involved. The binding and autoxidation reactions are shown in eqs 1.39 and 1.40, and the rate law derived from this competition is given in eq 1.41. Potential chemical routes to the peroxide species are listed in eqs 1.42-1.45.[347,350] An EPR spectral feature at g = 2.00 was assigned to the peroxide complex for experiments conducted in acetonitrile/pyridine/water and acetonitrile/1-MeIm solutions.[347] This signal was not observed in certain other solvent systems, however, and it is not clear whether the proposed intermediate was simply more reactive under such conditions, and therefore not observed, or whether its formation was somehow solvent specific. Although the process outlined for the autoxidation of **4** is chemically reasonable, spectroscopic evidence for the existence of the peroxide is weak.

$$LFe(II) + O_2 \underset{}{\overset{K_{O_2}}{\rightleftharpoons}} LFe(III)\text{-}O_2^- \quad (1.39)$$

$$LFe(II) + O_2 \xrightarrow{k'} LFe(III) + O_2^- \quad (1.40)$$

$$rate_{autox} = \frac{k'[Fe(II)][O_2]}{1 + K_{O_2}[O_2]} \quad (1.41)$$

$$LFe(II) + HO_2 \longrightarrow LFe(III)\text{-}(HO_2^-) \quad (1.42)$$

$$LFe(III)\text{-}(O_2^-) + HO_2 \longrightarrow LFe(III)\text{-}(HO_2^-) + O_2 \quad (1.43)$$

$$LFe(II) + HO_2 \longrightarrow LFe(III) + HO_2^- \quad (1.44)$$

$$LFe(III) + HO_2^- \longrightarrow LFe(III)\text{-}(HO_2^-) \quad (1.45)$$

In the work just discussed, it was postulated that the autoxidation step occurs by a separate pathway, parallel to the route leading to reversible dioxygen binding. The nature of this parallel reaction was approached by studying the effect of cavity size on autoxidation.[349] The species compared in this study were the tri-, tetra- and the pentamethylene bridged cyclidenes compounds **6** - **8** (Figure 1.27). The cavity sizes in these complexes are such that the smallest does not even allow O_2 to approach the iron center, whereas the largest allows access of both O_2 and solvent molecules. The effect of dioxygen concentration on the rates of autoxidation was dramatically different among these three systems, as shown graphically in Figure 1.28.[349] These results are consistent with the interpretation that autoxidation is a parallel pathway to dioxygen binding for the $(CH_2)_3$ (**6**) and $(CH_2)_4$ (**7**) cases (eqs 1.39-1.41). For the trimethylene bridged compound, K_{O_2} approaches zero and the rate law for autoxidation simplifies to a pseudo-

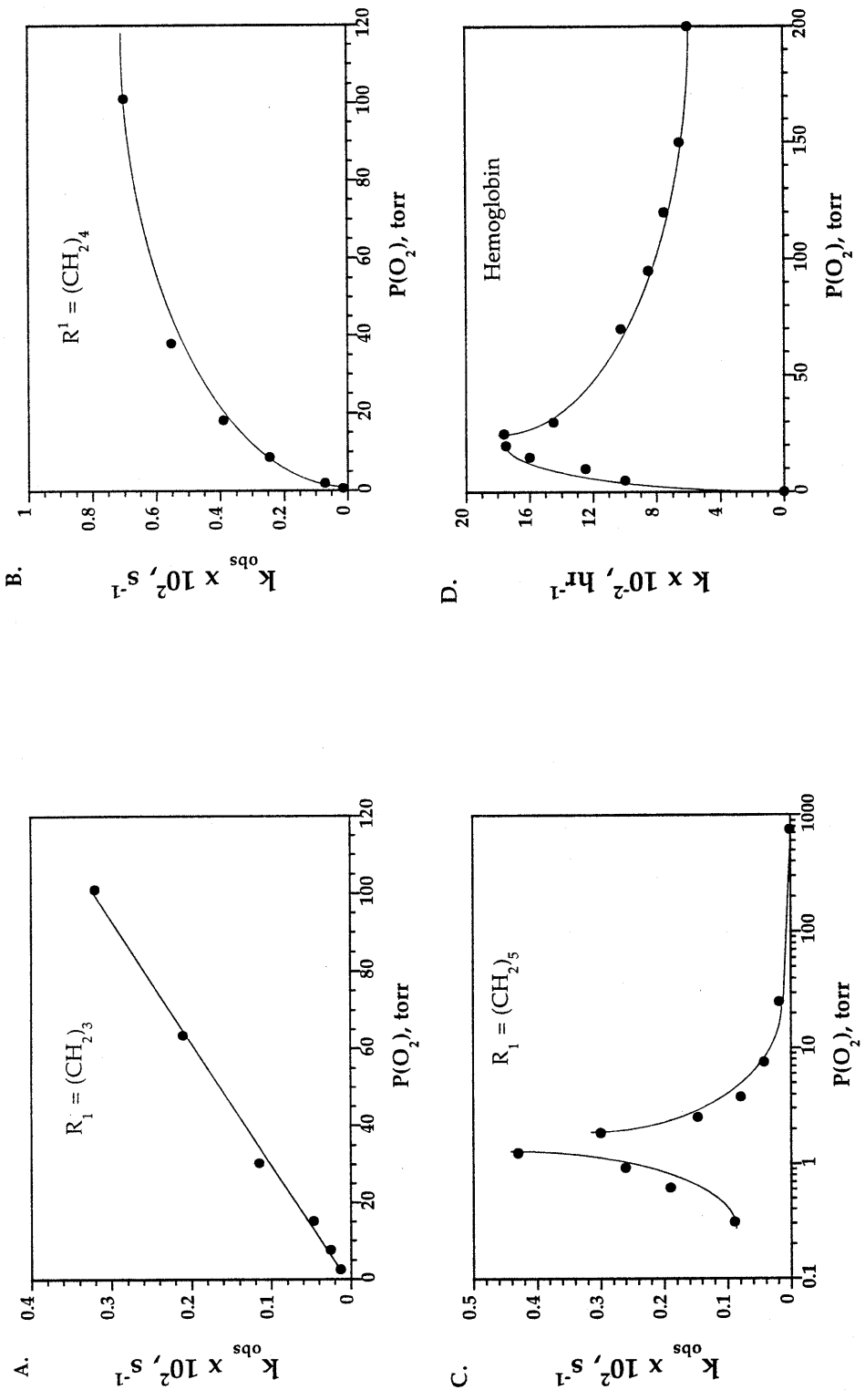

Figure 1.28. Plots of the observed rate constants for autoxidation as a function of dioxygen pressure for (A) compound **6**, (B) compound **7**, (C) compound **8**, and (D) hemoglobin. (Reprinted with permission from ref 349. Copyright 1993 American Chemical Society.)

first-order reaction. The extremely complicated behavior for the $(CH_2)_5$ complex (**8**), as for Hb, is explained by a solvent dependent competition for the dioxygen binding site. (eqs 1.46-1.48) Since the cavity in the $(CH_2)_4$ species (**7**) is only large enough to allow dioxygen access, solvent competition is removed and normal saturation behavior is observed.

$$LFe^{II} + S \underset{k_{-1}}{\overset{k_1}{\rightleftharpoons}} LFe^{II}\text{-}S \qquad (1.46)$$

$$LFe^{II}\text{-}S + O_2 \xrightarrow{k_2} LFe^{III}\text{-}S + O_2^- \qquad (1.47)$$

$$\text{rate} = \frac{k_1\left(k_2/k_{-1}\right)\left[Fe^{II}\right][S][O_2]}{\left(k_2/k_{-1}\right)K_{O_2}[O_2]^2 + \left\{\left(k_2/k_{-1}\right) + K_{O_2}\right\}[O_2] + 1} \qquad (1.48)$$

As a final note on the reversible O_2-binding behavior of the cyclidene complexes, we mention the dinuclear variant, compound **9** (Figure 1.27).[339] Complexes of this ligand undergo a different reaction with dioxygen, one not necessarily based on metal coordination. The two ferrous ions are separated by 8 - 15, Å depending on the length of the linker arms, and the iron atoms are postulated to act completely independently.[339] Superoxide is produced in the reaction but does not appear to coordinate to the metal ions. Autoxidation severely hampers the study of this system. To minimize this side reaction, very low oxygen tension was used to prevent the buildup of appreciable quantities of O_2^-. Interestingly, dioxygen binding in these

dinuclear cyclidenes showed an inverse first-order dependence on the concentration of added nitrogeneous base. Since no metal binding site was required for the electron transfer event, this result probably reflects changes in the redox properties of the ferrous center that accompany the base on/off equilibrium. For example, addition of excess pyridine to acetonitrile solutions shifted the Fe(II/III) couple by approximately -100 mV. Addition of 1-MeIm shifted it by -300 mV, the more negative value arising from stronger binding to iron(III) than to iron(II) of imidazole relative to pyridine. In less coordinating solvents, the magnitude of the pyridine-initiated shift of the redox potentials was greatly enhanced.[339] Since the ferrous form of the complex is stabilized by the binding of base, the driving force for the outer-sphere redox reaction is diminished, accounting for the inverse order in base concentration.

Although the effects of added base are well defined in reactions of porphyrins with dioxygen,[46] in non-porphyrin systems they are more difficult to observe and to rationalize. For heme iron the base effect results from coordination at the proximal site, trans to the dioxygen binding position. The composition of the coordination spheres varies greatly among non-heme iron oxygenases and dioxygen carriers, whereas variations in the ligand environment in porphyrin systems occur mainly in the axial sites. Therefore, in the non-heme systems, there are more states than simply base-on and base-off such that both the basicity of the ligand and its position in the coordination sphere will affect the reactivity of the iron site. The consequences of these considerations are largely unknown at present, however.

Non-Heme Systems

Very few ferrous complexes having non-porphyrin ligands react with dioxygen to form stable adducts.[37,53-55,260,330,351-353] Several claimed dioxygen adducts[354-357] could not be substantiated or were proved to be incorrect.[37] Unlike the pseudo-heme model complexes, all of these adducts appear to be peroxo rather than superoxo species. This behavior parallels that of heme versus non-heme dioxygen carrier proteins. For diiron complexes, this result was expected, but the formation of stable dinuclear peroxides from mononuclear iron(II) precursors was a surprise, although very similar bridging peroxide motifs had been observed as intermediates in the chemistry of porphyrin models with dioxygen.[343,344] Figure 1.29 displays the known or postulated structures of diiron(II) complexes and their corresponding (μ-peroxo)diiron(III) adducts to be discussed in this section.

When compound **10a** was exposed to dioxygen,[330] a violet species (**10b**) formed having λ_{max} = 540 nm (ε = 187 $M^{-1}\,cm^{-1}$). The adduct irreversibly decayed at room temperature over a period of 5 hours. For the corresponding ligand in which the pyridine ring was replaced by an aliphatic amine **11a** the dioxygen adduct was much shorter lived.[330] Upon exposure to dioxygen a red-purple adduct **11b** formed, but immediately faded as the colorless oxidized end product was generated.[330] Kinetic studies of the formation of **10b** indicated a process first-order in both [O_2] and [LFe^{II}] and polarographic studies of dioxygen uptake revealed a stoichiometry of $2Fe:1O_2$. The kinetic results were adequately fit by a simple two-step mechanism for the formation of the complex, where the first step is rate-limiting. The rate constant for this reaction in water, (I = 0.2 M, pH 8.0) at 25° C is $1.4 \pm 0.2 \times 10^2\ M^{-1}\ s^{-1}$.[330] The reaction was sensitive to pH, showing a 6-

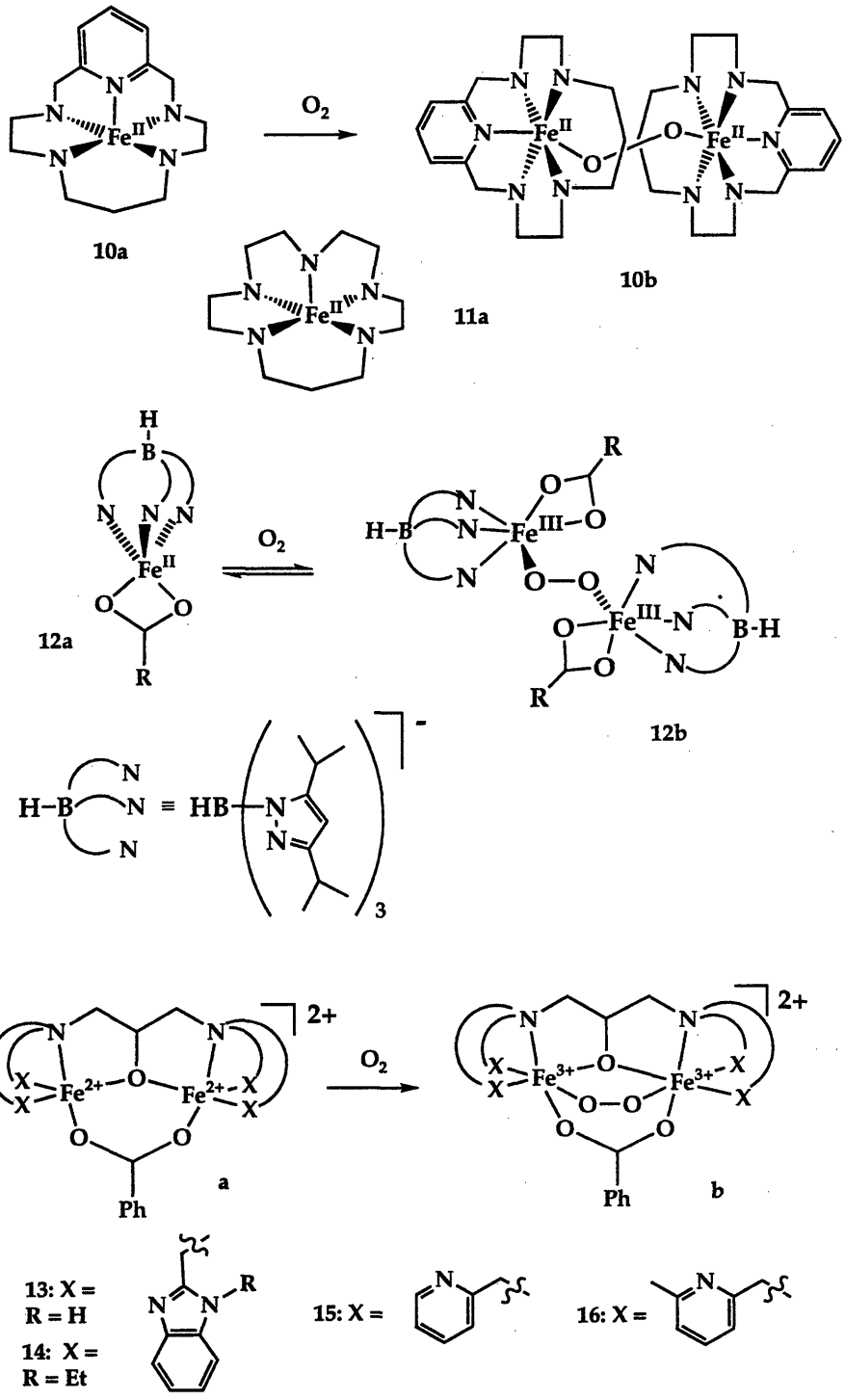

Figure 1.29. Structures of the non-heme ferrous complexes **10a-16a** and their dioxygen adducts **10b-16b**.

fold rate increase over the pH range 8.0-9.5. No explanation for this behavior was provided.

Another mononuclear complex that binds dioxygen and rapidly forms a dinuclear peroxide adduct is **12a**.[53,55] The precursor is a 5-coordinate ferrous ion bound to a sterically demanding tridentate, facially coordinating ligand {$HB(3,5\text{-}iPr_2pz)_3$} and a chelating carboxylate ligand. The structure of the precursor has been crystallographically determined. On exposure to dioxygen in non-coordinating solvents at temperatures below -20° C, **12a** reacts to form a dark blue-green (λ_{max} = 680 nm) 2:1 dioxygen adduct, **12b**.[53] Below -50° C, the binding is irreversible, but between -50 and -20° C, the ferrous starting material can be regenerated by application of vacuum or purging with an inert gas.[53,55] This system can be cycled at least 10 times with only minimal loss of activity. In coordinating solvents, **12b** is not formed at any temperature.[53]

The nature of the 2:1 adduct has been studied by a variety of physical methods in an attempt to determine its structure.[55] The resonance Raman spectrum revealed an O-O stretching band at 876 cm^{-1}, in the region for peroxide, and the assignment was supported by $^{18}O_2$ isotope shifts.[53] Unlike the pseudo-heme dioxygen adducts discussed above, this product was paramagnetic (S = 5/2) and exhibited weak (J = -33 cm^{-1}) antiferromagnetic coupling. EXAFS data supported the assignment of the structure as a (μ-1,2-peroxo)diiron(III) unit with a dihedral angle at the O-O bond of approximately 90° and an Fe-Fe distance of 4.3 - 4.4 Å.[55] Diiron(II) derivatives of **12a** also bind dioxygen, but the adducts appear to be less stable.[332] It is unclear whether solution equilibria lead to the formation of the same dioxygen adduct or whether the species are structurally different.

Compound **12b** is one of the more robust non-heme iron dioxygen complexes. Its autoxidation must be slow to explain reversible O_2 binding. The steric bulk of the hydrotris(diisopropylpyrazolyl)borate is probably responsible for the added stability, the reasons being similar to those discussed above for the phenyl and benzyl substituted cyclidene complexes. The electronic properties of the carboxylate ligand do not significantly affect the chemistry; changing the carboxylate ligand shifted the broad charge transfer band of the dioxygen adduct slightly, but did not alter its temperature sensitivity.[55]

A final class of stable ferric dioxygen adducts to be discussed form in the reaction of dioxygen with ferrous complexes of ligands derived from N,N,N',N'-X_4-2-hydroxy-1,3-diaminopropane, where X is one of several nitrogeneous bases. Most extensively studied are complexes where X= 2-benzimidazolylmethyl (HPTB) (**13a**), 2-(N-ethyl-benzimidazolyl)methyl (Et-HPTB) (**14a**), 2-pyridylmethyl (HPTP) (**15a**) and 2-(6-methylpyridyl)methyl (HPTMP) (**16a**). As a series, the diferrous compounds **13-16** nicely illustrate how ligand alterations can affect the reactivity of the metal center.

The first dioxygen adduct generated for this class was with the HPTB system.[351] The starting material was reportedly [Fe^{II}_2(HPTB)Cl_5], but was largely uncharacterized. Later studies of the oxygenation reactions employed μ-carboxylato analogs.[54,331] The bridging carboxylate group renders the model more biomimetic, although an alkoxo bridge has not yet been observed in a non-heme iron protein. The steric bulk of the benzimidazolyl rings prevented coordination of a second carboxylate to the dinuclear ferrous center, providing some indication of the crowding around the iron atoms.

At low temperature (T < -80°C), the HPTP, HPTMP and Et-HPTB diiron(II) complexes all formed stable dioxygen adducts quite readily. Only

the HPTMP adduct exhibited reversible behavior, however, with $P_{1/2}$ = 42 torr (CF_3COO^- complex) and 6 torr ($PhCOO^-$ complex) at -35° C in CH_2Cl_2.[352,353] The Et-HPTB complex is relatively symmetric, having two pentacoordinate square pyramidal ferrous ions.[54,260] The more sterically demanding HPTMP complex, on the other hand, is solvated and has one octahedral and one square pyramidal iron atom. The higher coordination number results in a lengthening of the Fe-N bonds and helps alleviate the steric clash. This asymmetric solvation probably indicates more flexibility for this complex than for **13a**, a property that could facilitate the binding of small molecules to the metal center.

The three complexes differ not only in the degree to which formation of their O_2 adducts is reversible, but also in the stability of the adducts toward irreversible decomposition. Compound **14b** is indefinitely stable in methylene chloride or acetonitrile at -60° C and forms transiently at room temperature before decomposing.[54] Formation of the HPTMP adduct **16b** is reversible at -20° C and the product is completely stable at -60° C.[352] The HPTP-O_2 adduct **15b** is exceedingly reactive, however, and cannot be formed at -40° C in MeCN or at -80° C in CH_2Cl_2.[54,352] The addition of small amounts of DMSO or other polar aprotic solvents has a stabilizing influence on this entire series of dioxygen complexes, although the reason for this effect is currently unknown.[54]

The chemical reactivities of the diiron(III) peroxide species have been studied only preliminarily. Sub-stoichiometric oxo-transfer to PPh_3 occurred for all three compounds, with the HPTP complex showing the greatest activity.[54,352] The degree of oxo-transfer capability follows the relative temperature stabilities of the adducts (HPTP > HPTMP > Et-HPTB, HPTB). The HPTP complex can also oxidize phenols, but none of these complexes

shows any propensity to hydroxylate or oxygenate substrates such as alkanes, which are much poorer oxo transfer acceptors.[54,358] The lack of oxo-transfer reactivity of **14b** contrasts with a report in which $[Fe^{III}_2(HPTB)(OH)]^{4+}$ was able to catalyze the oxidation of 2,4-di-t-butylphenol to 3,5-di-t-butylcatechol by hydrogen peroxide.[24] Presumably, quite similar diferric peroxide complexes are present in both reactions, although the carboxylate ligand is absent in the reported catalytic system. Reinvestigation of the latter may be required to resolve the inconsistency.

Recently, a kinetic investigation of the reactions of **14a - 16a** with dioxygen has been undertaken.[359] The first step of the reaction, formation of the (μ-peroxo)diiron(III) species, was studied by stopped-flow spectroscopy at low temperature. The results revealed a much larger activation barrier for the reaction of **16a** with O_2 relative to the other two compounds. The significantly larger activation enthalpy and less negative entropy of activation arise from a postulated internal ligand rearrangement required to open a coordination site for dioxygen.

Peroxide derivatives of **13-16** were formed from the reaction of the diiron(III) species with hydrogen peroxide.[23,24,31,331,351] The wavelengths of the absorption maxima often differed slightly from those of complexes formed in the reaction of the diiron(II) complexes with O_2, however.[23,54,351] The variations might arise from solvent system differences, since addition of aqueous hydrogen peroxide introduces protons that are not present in the dioxygen reactions carried out in dry, aprotic organic solvents.

Non-Catalytic Oxidation of Iron(II) Complexes Following Unstable Dioxygen Adduct Formation

The oxidation kinetics of a well characterized model compound $[Fe^{II}(Me_3TACN)_2(OH)(OAc)_2](ClO_4)_2$ (**17a**) which does not form stable

peroxide adduct have recently been investigated.[202] The reaction is shown in eq 1.49. The goal of this work was to elucidate intrinsic factors involved in the oxidation of dinuclear iron(II) centers similar to those found in the biological systems but without the surrounding protein sheath. The reaction consumed 0.5 mol equiv of dioxygen, all of which was used to form the oxo bridge in the product, as verified by ^{18}O labeling experiments.[202] The kinetics of the oxidation reaction could be explained by proposing a pre-equilibrium step that afforded an open coordination site prior to dioxygen binding. In particular, the order in dioxygen depended upon the choice of solvent. In chloroform, the rate law followed eq 1.50, with a first order dependence on $[O_2]$, whereas in methanol, the reaction was independent of dioxygen concentration (eq 1.51). This behavior was readily explained by proposing an equilibrium for **17a** in which a carboxylate ligand shifts from bidentate bridging to monodentate terminal with concomitant coordination of methanol to the site vacated on one of the ferrous ions. This intermediate accounts for the more rapid rate of oxidation in methanol compared to

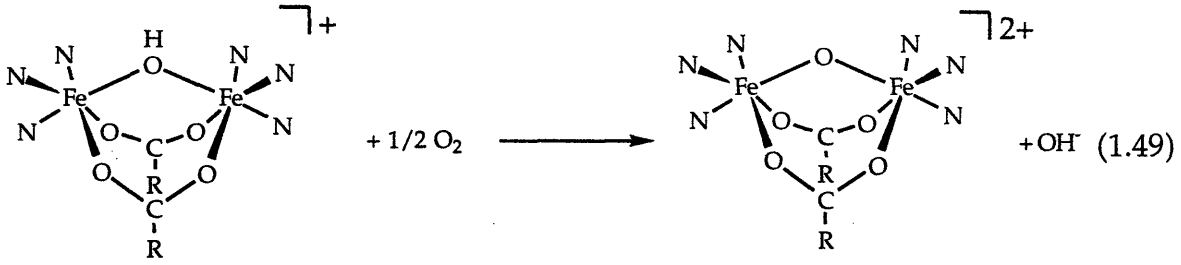

17a **17b**

(1.49)

$$\text{Rate} = k_{exp}[O_2][\mathbf{17a}]^2 \qquad (1.50)$$

$$\text{Rate} = k_{exp}[\mathbf{17a}]^2 \qquad (1.51)$$

chloroform. The transition state was postulated to be a mixed-valent tetranuclear η^2:η^2-peroxide-bridged complex.[202] Such a tetranuclear species, besides accounting for the kinetic data, has precedence in the only structurally characterized non-heme iron-peroxide model complex.[51] The tetranuclear intermediate is presumed to be the complex in which the critical O-O bond cleavage step occurs, but since its formation and not its decomposition was the rate limiting step, direct observation of bond scission was not possible.

The results of this study recall one of the main findings of the iron EDTA oxidation studies,[77] namely, that coordination of dioxygen to the metal is required. In reactions of **17a** with dioxygen, the need for a vacant coordination site is manifest by equilibria that precede the actual oxidation steps. The kinetic behavior of this complex is very different from that of the non-heme diiron proteins, where the diiron cores cannot approach one another to form the tetranuclear peroxide-bridged intermediate. The decomposition of this intermediate is analogous to the decay of iron porphyrin intermediates postulated to form during their reactions with dioxygen.[343,344]

The lesson learned from this kinetic study is one recognized by porphyrin chemists many years ago. To mimic the biological reactions, bulky ligands must be employed to avoid the kinetically favored bimolecular decay pathway. Dinucleating ligands provide some of the stability and bulk required, but many of the existing diiron(II) complexes in this class contain non-biomimetic bridges such as alkoxides or aryloxides. Moreover, in complexes of these dinucleating ligands, the RO^- bridge impedes access of O_2 to the dinuclear core from the direction typically found in proteins such as

Hr. The search for alternative dinucleating ligands is an area of active research.

Catalytic Hydroxylation Reactions with Fe^{II} and O_2 Involving Transient Fe-O_2 Intermediates

In many oxidations, the active species are too short-lived to be observed. In some cases, information on the active oxidants can be obtained indirectly from kinetics investigations, the distribution of products, or the identification of a decomposition product. Even when the spectroscopic signature of a species formed during the reaction can be monitored, it must be demonstrated to be on the reaction pathway. Unless the intermediate can be synthesized separately and shown to be capable of entering the reaction in the absence of its precursors, its proposed role is not definitively established.

The chemistry discussed in this section uses the reaction of dioxygen with a ferrous compound to oxygenate or oxidize an organic substrate in a catalytic manner. Commonly employed substrates include cyclohexane, cyclohexanol, cyclohexene, adamantane, and *cis*-stilbene. Information about the mechanism is gathered from relative reactivity at primary, secondary and tertiary aliphatic carbon positions, the ratio of alcohol to ketone products, the ability to form epoxides from alkenes, and isomerization taking place during the reaction. Together these features provide clues about the transient oxygen species involved in the reaction mechanism.

Udenfriend's Reaction

A catalytic system for synthesizing phenols, catechols and epoxides using ferrous ions, EDTA, ascorbic acid and dioxygen at neutral pH was first reported by Udenfriend.[360] This reaction has been well studied because of its similarity to that of many mononuclear monooxygenases. The actual species responsible for the activity, however, is still being debated 40 years after the

original discovery.[361-365] The reaction is mechanistically related to many of the autoxidations of chelated iron(II) discussed above (eqs 1.21 and 1.22). Two features differentiate the autoxidation and catalytic reactions, however. The first is the presence of a substrate, which reacts with one of the activated dioxygen intermediates, and the second is the presence of ascorbate, which reduces the ferric ions back to their ferrous form, closing the catalytic cycle. The oxidation and reduction phases of the reaction can be separated on the basis of work investigating the catalytic oxidation of ascorbate by dioxygen and iron.[259,366,367] In the absence of an oxidizable substrate, Udenfriend's reaction and the catalytic oxidation of ascorbate are identical. Iron(II) chelates are autoxidized to their iron(III) form, which then are reduced back to iron(II) by an intermediate iron(III)-ascorbate complex. This similarity is analogous to the coupled and uncoupled reactions discussed above for the pterin and α-ketoglutarate-dependent enzymes. No evidence was found for a complex between ferrous ions and ascorbate.[367,368] Instead, ferric ions produced by oxidation of iron(II) interact with ascorbate in a separate reaction leading to the reduction of the iron. Udenfriend's catalytic cycle can therefore be roughly approximated by eqs 1.52 and 1.53, where the former is the functional step and the latter reactivates the catalyst. Further support for

$$2LFe^{II} + O_2 + ArH + 2H^+ \rightarrow 2LFe^{III} + ArOH + H_2O \qquad (1.52)$$

$$2LFe^{III} + AscH_2 \rightarrow 2LFe^{II} + dAsc + 2H^+ \qquad (1.53)$$

the functional separation of these steps is the ability to substitute alternative reductants for ascorbic acid, a property also shared by many biological systems.[362,369] The efficiency of the Udenfriend reaction is extremely poor, however, often affording oxidized product yields of 5-10% based on

reductant.[361] Since the active oxidant is extremely reactive, a rate constant of $k = (3.9 \pm 0.6) \times 10^9$ dm^3 mol^{-1} s^{-1} having been measured for the Udenfriend reaction on thymine,[365] the low yield is probably based on a non-productive reaction with solvent or, more likely, autoxidation of the reductant. This problem is circumvented in biological systems by rendering the iron(II) center inactive in the absence of bound substrate and through the use of a separate reductase protein (see above discussion).

The active species in Udenfriend's reaction may or may not involve free hydroxyl radicals. The general methods used to approach this issue are to run parallel Fenton reactions, while attempting to trap the radical, or observe a rearranged substrate probe. The assumption here is that Fenton chemistry generates only free hydroxyl radicals and that a significant decrease in the amount of radical-generated products would indicate an alternative mechanism for Udenfriend's reaction. Product distribution studies revealed the presence of additional species formed in the Fenton chemistry and the ratios of common products formed by the two reactions were different.[361,362,370] It was therefore concluded that the active oxidant in Udenfriend's reaction was not the same one as in Fenton chemistry. On the other hand, use of a radical quenching technique to examine the effects of alcohols on the two systems gave identical results.[365] None of these investigations is totally convincing, however. Product distributions can be influenced by extremely small variations in reaction conditions or contaminants, and just because two chemical species are quenched at the same rate does not necessarily mean that the reactive species are identical.

Gif Chemistry

One of the most studied catalytic reactions is the so-called Gif system of Barton and co-workers.[327,371,372] Although there are many varieties of Gif

chemistry, some using oxidants other than dioxygen, there are several (Gif^{III}, Gif^{IV} and Gif-Orsay) which rely on the reaction of ferrous iron with dioxygen in a pyridine/acetic acid solvent. Some systems thought to use H_2O_2 as the oxygen donors were subsequently found to utilize dioxygen. When run under an atmosphere of $^{18}O_2$, the products contained exclusively ^{18}O-labeled oxygen.[373] In spite of extensive work on these systems, many of the mechanistic details remain murky. The structures of several intermediates proposed in the following discussion are quite speculative and have not been observed directly. They have been proposed in the primary literature to explain the observed products and isotopic distributions. These mechanisms should therefore be viewed as working hypotheses.

Gif catalysts react with alkanes affording primarily ketones along with small amounts of alcohols and other minor products, depending on the conditions. Furthermore, the preference for secondary over tertiary carbons has been measured to be as high as 22:1, but more typically the ratio is around 1.[327] A key piece of information regarding the nature of the Gif reaction was the observation of a cyclohexylhydroperoxide intermediate.[326,373] In the absence of an oxidant, this hydroperoxide decomposed in the presence of catalyst to form the observed ratio of products. Since the hydroperoxide affords both the major and minor products, it must lie along the reaction pathway at a point that precedes the divergence of products into alcohols and ketones. Mechanistic studies on other alkane activation systems employing iron catalysts have also proposed the intermediate formation of alkylhydroperoxides and/or metal bound alkylperoxides.[374,375] As currently formulated, the Gif mechanism does not involve direct reaction of dioxygen with a ferrous species in any of the mechanistically important steps (Figure 1.30); instead, O_2 oxidizes the Fe^{II}

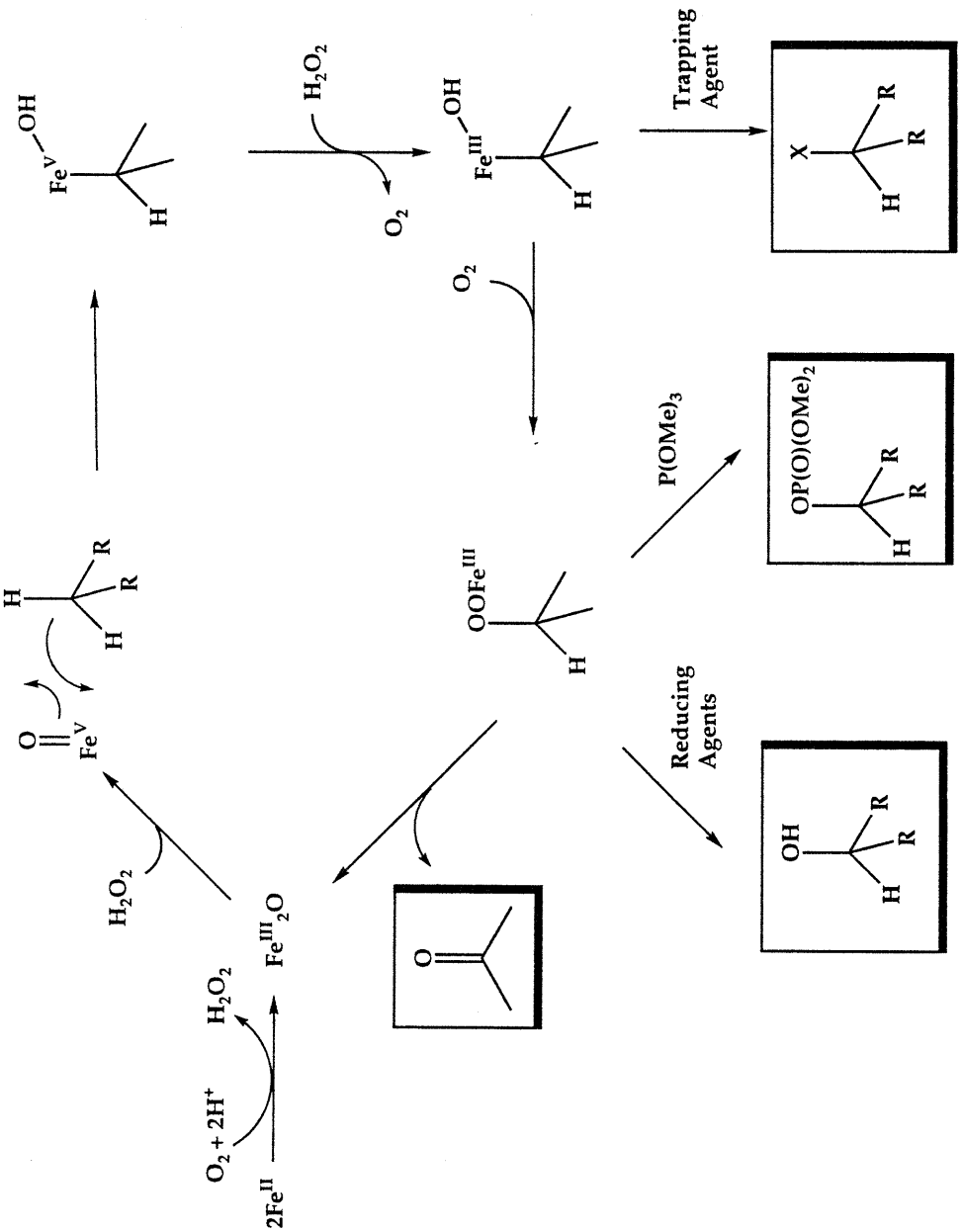

Figure 1.30. Proposed mechanism for the catalytic cycle of Gif oxidations. (Adapted with permission from ref. 327.)

pre-catalyst to a (μ-oxo)diiron(III) compound and hydrogen peroxide. These species then continue as if hydrogen peroxide and ferric ion were added initially.[38,327,376] Recent work, discussed below, may require that these Gif mechanistic proposals be altered, however.[270,377]

The picolinate (PA) and dipicolinate (DPA) systems, termed oxygenated Fenton reagents,[372,378] are quite similar to the Gif systems. The reactions are run in pyridine/acetic acid solutions with comparable product distributions, although the yields are higher. Instead of using Fe^{III} and peroxide, as in the Gif(II) system, the PA and DPA reactions employ Fe^{II} and hydrogen peroxide. Anaerobically, this mixture would be expected to undergo basic Fenton chemistry,[63] generating pyridyl or substrate radicals from hydroxyl radical. In the presence of dioxygen, however, the reaction is drastically modified.[270,372,377] Instead of cyclohexylpyridine being the primary product when cyclohexane is used as the substrate, cyclohexanone is produced.[377] The relative reaction rates of ferrous material with dioxygen and peroxide were measured, revealing a 1000-fold kinetic preference for reaction with the latter.[377] It was therefore proposed that a ferrous-hydroperoxide species reacts with dioxygen before decomposing via Fenton chemistry. A scheme delineating this hypothesis is shown in Figure 1.31. The active agent for hydrogen abstraction in this system is the ferric-peroxy-superoxide complex that, by analogy to Gif chemistry, leads to formation of a metallo-alkylperoxide, the decomposition of which yields products. Minor products can arise from simple Fenton chemistry or alternative modes of peroxide decomposition.

The Gif mechanism should be re-analyzed in light of these results and the $^{18}O_2$ labeling studies discussed above. The dioxygen affinity of ferrous ions is considerably greater than that of ferric complexes. Biological systems

that carry out such hydroxylations with iron usually require the reduced state of the enzyme. In one mechanism (Figure 1.30), oxygenation results from dioxygen insertion into the iron-carbon bond of an organometallic intermediate. Insertion reactions of this type are precedented in organometallic chemistry, but alternative routes to a metallo-alkylperoxide species, such as the one in Figure 1.31, can be envisioned and must be explored further. Whether one of these mechanisms, or some totally different route, is eventually accepted will have to await more detailed study of the reactions. To aid in that process, better defined catalysts will be helpful. The number of potentially equilibrating species in the parent Gif reactions is large, and elucidation of any rational mechanism is likely to be difficult until the system is simplified. The use of PA and DPA provides some stability for the metal complex resulting from chelation effects, and presumably the ligands remain coordinated during catalysis. These complexes are therefore a step toward the proper study of these reactions. As the full reaction schemes from the published work indicates, however, the chemistry still has little specificity and slight changes in conditions lead to new and different products.[377]

In the absence of peroxide, the ferrous compound $Fe^{II}(DPAH)_2$, will also react catalytically with dioxygen to convert cyclohexane to cyclohexanone. It has been postulated that the reaction results from in-situ generation of hydrogen peroxide as shown in eq 1.54.[270] Support for this mechanism, which is inconsistent with the common dinuclear intermediate observed for the autoxidation of porphyrins and several non-heme iron compounds discussed above,[330,343,344] comes from electrochemical experiments where a (μ-oxo)diiron(III) species, the normal product of the diferrous reaction pathway, is not observed. It is unclear why this complex

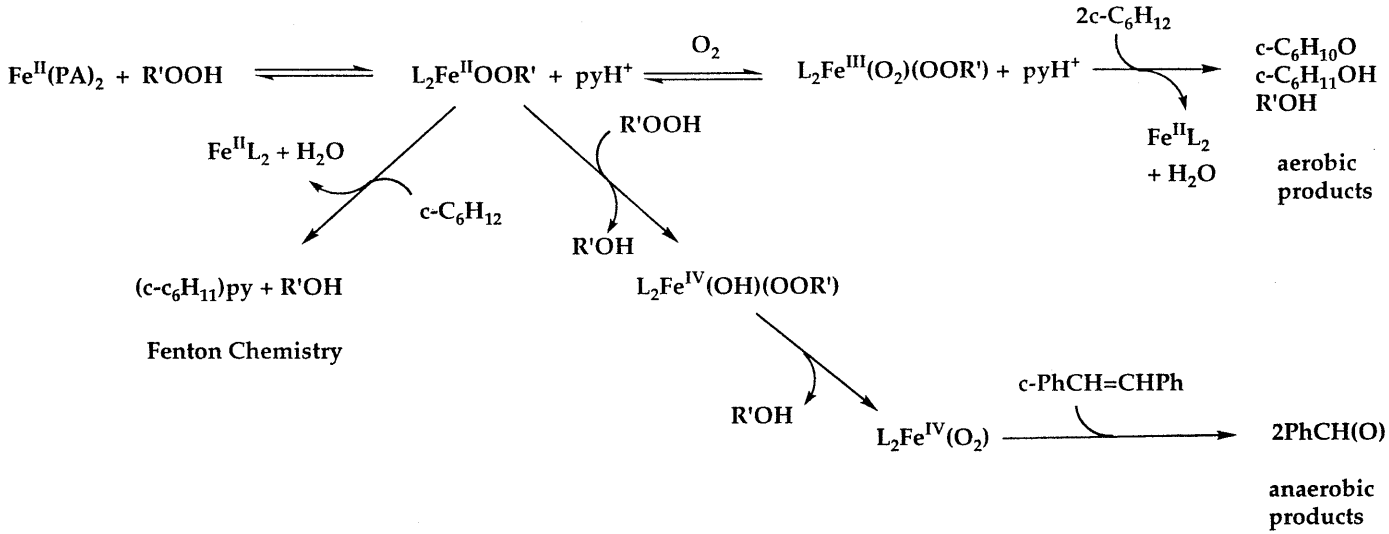

Figure 1.31. Proposed mechanism for the oxidation of alkanes by $Fe^{II}(PA)_2$. (Adapted with permission from ref. 377.)

reacts with dioxygen differently from other typical ferrous complexes or why the commonly observed and thermodynamically stable (μ-oxo)diiron(III) species is not formed.

$$[Fe^{II}(DPAH)_2] + O_2 \rightleftharpoons$$

$$[(DPAH)(DPA)Fe^{IV}(OOH)] + L_2Fe^{II} \longrightarrow HOOH + 2(DPA)(DPAH)Fe^{III} \quad (1.54)$$

Mimoun's System

Whereas Udenfriend's reaction can be written as two distinct steps, oxidation and reactivation as discussed above, a separate class of oxidations has been described in which an iron species coordinates simultaneously to both dioxygen and the reducing agent. As a result, more concerted redox steps can be envisioned. Several of the biological systems discussed employ a similar strategy in which multienzyme or multisubunit aggregates join the oxidizing and reducing functionalities. The interactions between subunits can then control the biochemistry to time the influx of electrons and avoid wasteful consumption of reductant. A model system of this type, capable of hydroxylating alkanes, alkenes and arenes, was first described by Mimoun[379] although other similar systems are known. The reaction is written in eq 1.55, where diphenylhydrazine is reduced to diazobenzene concomitant with substrate oxidation. This system tends to give alcohols rather than ketones

$$RH + PhNHNHPh + O_2 \xrightarrow[PhCOOH]{Fe^{II}\ cat} ROH + PhN{=}NPh + H_2O \quad (1.55)$$

and, like many other catalytic systems, is characterized by low yields and small turnover numbers.[380] As expected, this system exerts less control over

the autoxidation of the reductant than its biological counterparts and greater than stoichiometric consumption of reductant is usually observed. The secondary/tertiary oxidation ratio is typically around 1.[380]

Kinetic studies of this system have led to the proposal that an iron-hydroperoxide-hydrazine complex is the active species in the hydroxylation chemistry.[380] Electrochemical studies of Fe^{II}/diphenylhydrazine/hydrogen peroxide solutions support this finding, revealing that, in the presence of the disubstituted hydrazine, normal Fenton chemistry is subverted by an alternative reaction that leads to catalytic monooxygenation.[381] A proposed mechanistic scheme derived from kinetic studies is presented in Figure 1.32, but unfortunately no spectroscopic evidence has been obtained for any of the postulated intermediates. Structurally similar intermediates with different formal oxidation states are invoked in a $[Fe^{II}(DPAH)_2]$ catalyzed system, where diphenylhydrazine was used as the reductant.[382] In the latter study, greater oxidative selectivity was observed compared to Fenton chemistry. Much work remains to be done on systems of this kind before their reactivity is fully understood or the chemistry is rendered synthetically useful.

Conclusions and Future Directions

The foregoing discussion reveals the diversity of biochemical and biomimetic oxygenation reactions carried out by non-heme iron centers. Our understanding of these reactions is far from complete and examples of contradictory and confusing results have been included to illustrate the nature of the debate on the mechanisms of these reactions.

Over the past few years, the greatest advances have been in understanding the chemistry of dinuclear iron cores in Hr, RNR and MMO as well as their small molecule models. The extensive structural and

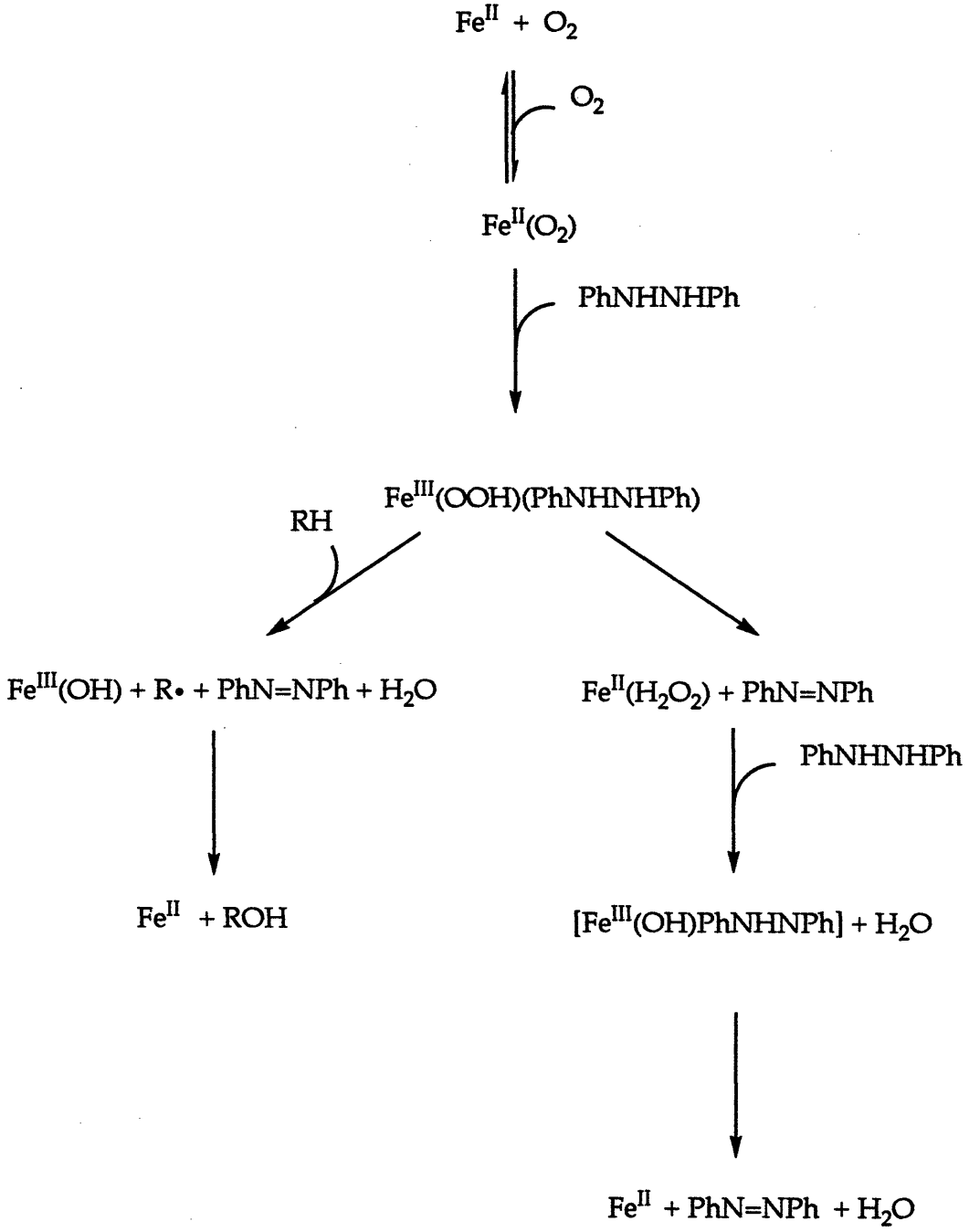

Figure 1.32. Proposed mechanism for the oxidation of alkanes by Mimoun's system. (Reprinted with permission from ref. 380. Copyright 1988 Pergamon.)

spectroscopic detail available for these three proteins has helped to unravel their individual reaction mechanisms, and we are beginning to understand why Hr reacts differently from RNR and MMO. The lower coordination numbers, preponderance of oxygen versus nitrogen donor atoms and possibly the involvement of amino acid derived radicals in RNR and MMO activate dioxygen for O-O bond cleavage. Another key factor may be that Hr, like Hb and Mb, has a well defined site for monodentate binding of O_2, whereas both RNR and MMO have the potential to form bridging peroxides. Perhaps such a species is a required precursor for oxygenation reactions in non-heme proteins. As a whole, there is less structural information available about mononuclear systems, and this area deserves more attention. Like MMO and RNR, the coordination environments of the mononuclear non-heme iron enzymes are flexible, with multiple sites of attachment for small molecules. The systems exhibit features that do not appear to play an important role in the chemistry of the dinuclear enzymes. The ability of substrates to activate the iron site toward dioxygen is of particular interest because the nonspecific oxidation of the reductant is one of the major drawbacks in most model catalytic hydroxylation reactions. In the enzymes, this property prevents the oxidation of the iron center when substrate is absent. In dinuclear systems such as MMO, binding of the other components and possibly substrate can affect the hydroxylase activity. Understanding the structural changes at the iron center that occur upon substrate and coupling protein binding will lead to more sophisticated design of model compounds and small molecule catalysts, allowing the greater tuning of the dioxygen reactivity of the ferrous ion.

For the modeling chemist, these systems provide a particular challenge. On the one hand, extreme bulk seems to be necessary to prevent

the unwanted bimolecular decay reactions of the active intermediates. At the same time, the ligand cannot be so sterically encumbered that dioxygen cannot bind; moreover, there must be room for a substrate to approach the active species. To accomplish these seemingly contradictory aims with anything less than a protein is a daunting task, but one that might be surmountable through the application of innovative ligand design. The functional models for the catalytic hydroxylation reactions currently have little resemblance to their biogenic progenitors. The path toward the marriage of the structural and functional modeling lies ahead.

References

(1) Most of this work has appeared in slightly altered form in ref. 2. (Copyright 1994, American Chemical Society).

(2) Feig, A. L.; Lippard, S. J. *Chem. Rev.* **1994**, *94*, 759-805.

(3) *Iron-Sulfur Proteins*; Lovenberg, W., Ed.; Academic: New York, 1977; Vol. 1-3.

(4) *Iron-Sulfur Proteins*; Spiro, T. G., Ed.; Wiley and Sons: New York, 1982; Vol. 4.

(5) *Heme Proteins*; Eichhorn, G. L.; Marzilli, L. G., Ed.; Elsevier: New York, 1988; Vol. 7, p 271.

(6) Rifkind, J. M. *Adv. Inorg. Biochem.* **1988**, *7*, 155-244.

(7) Holm, R. H.; Ciurli, S.; Weigel, J. A. *Prog. Inorg. Chem.* **1990**, *38*, 1-74.

(8) Springer, B. A.; Sligar, S. G.; Olson, J. S.; Phillips, G. N., Jr. *Chem. Rev.* **1994**, *94*, 699-714.

(9) Janssen, D. B.; Grobben, G.; Hoekstra, R.; Oldenhuis, R.; Witholt, B. *Appl. Microbiol. Biotechnol.* **1988**, *29*, 392-399.

(10) Janssen, D. B.; Witholt, B. In *Metal Ions in Biological Systems*; Sigel, H. and Sigel, A., Eds.; Marcel Dekker: New York, 1992; Vol. 28; pp 299-327.

(11) *Methane and Methanol Utilizers*; Murrell, J. C.; Dalton, H., Ed.; Plenum: New York, 1993.

(12) Fennell, D. E.; Nelson, Y. M.; Underhill, S. E.; White, T. E.; Jewell, W. J. *Biotechnology and Bioengineering* **1993**, *42*, 859-872.

(13) Lippard, S. J. *Angew. Chem. Int. Ed. Engl.* **1988**, *27*, 344-361.

(14) Sanders-Loehr, J. In *Iron Carriers and Iron Proteins*; Loehr, T. M., Eds.; VCH: New York, 1989; Vol. 5; pp 373-466.

(15) Que, L., Jr.; True, A. E. *Prog. Inorg. Chem.* **1990**, *38*, 97-200.

(16) Vincent, J. B.; Olivier-Lilley, G. L.; Averill, B. A. *Chem. Rev.* **1990**, *90*, 1447-1467.

(17) Kurtz, D. M., Jr. *Chem. Rev.* **1990**, *90*, 585-606.

(18) Howard, J. B.; Rees, D. C. In *Advances in Protein Chemistry*; Anfinsen, C. B., Edsall, J. T., Richards, F. M. and Eisenberg, D. S., Eds.; Academic: New York, 1991; Vol. 42; pp 199-280.

(19) Wilkins, R. G. *Chem. Soc. Rev.* **1992**, *21*, 171-178.

(20) Que, L., Jr. In *Bioinorganic Catalysis*; Reedijk, J., Eds.; Marcel Dekker: New York, 1993; pp 347-393.

(21) McClune, G. J.; Fee, J. A.; McCluskey, G. A.; Groves, J. T. *J. Am. Chem. Soc.* **1977**, *99*, 5220-5222.

(22) Shirazi, A.; Goff, H. M. *J. Am. Chem. Soc.* **1982**, *104*, 6318-6322.

(23) Nishida, Y.; Takeuchi, M.; Shimo, H.; Kida, S. *Inorg. Chim. Acta* **1984**, *96*, 115-119.

(24) Nishida, Y.; Takeuchi, M. *Z. Naturforsch.* **1987**, *42b*, 52-54.

(25) Balch, A. L. *Inorg. Chim. Acta* **1992**, *198-200*, 297-307.

(26) Nishida, Y.; Nasu, M.; Akamatsu, T. *Z. Naturforsch.* **1992**, *47b*, 115-120.

(27) Funk, M. O., Jr. ; Carroll, R. T.; Thompson, J. F.; Sands, R. H.; Dunham, W. R. *J. Am. Chem. Soc.* **1990**, *112*, 5375-5376.

(28) Que, L., Jr. *Adv. Inorg. Biochem.* **1983**, *5*, 167-199.

(29) Que, L., Jr. In *Iron Carriers and Iron Proteins*; Loehr, T. M., Eds.; VCH: New York, 1989; Vol. 5; pp 467-524.

(30) Nishida, Y.; Yamada, K.; Furuhashi, A. *Z. Naturforsch.* **1990**, *45b*, 1433-1436.

(31) Nishida, Y.; Yoshizawa, K.; Takahashi, S.; Watanabe, I. *Z. Naturforsch.* **1992**, *47c*, 209-214.

(32) Fridovich, I. *Adv. Enzymol.* **1986**, *58*, 61-97.

(33) Fox, B. G.; Shanklin, J.; Somerville, C.; Münck, E. *Proc. Natl. Acad. Sci., USA* **1993**, *90*, 2486-2490.

(34) Minotti, G.; Aust, S. D. *J. Biol. Chem.* **1987**, *262*, 1098-1104.

(35) Ursini, F.; Maiorino, M.; Hochstein, P.; Ernster, L. *Free Rad. Biol. Med.* **1989**, *6*, 31-36.

(36) Valentine, J. S. *Chem. Rev.* **1973**, *73*, 235-245.

(37) Jones, R. D.; Summerville, D. A.; Basolo, F. *Chem. Rev.* **1979**, *79*, 139-179.

(38) Simandi, L. I. *Catalytic Activation of Dioxygen by Metal Complexes*; Kluwer Academic: Dordrecht, 1992; Vol. 13, p 396.

(39) Foote, C. S. *Acc. Chem. Res.* **1968**, *1*, 104-110.

(40) Halliwell, B.; Gutteridge, J. M. C. *Biochem. J.* **1984**, *219*, 1-14.

(41) Halliwell, B.; Gutteridge, J. M. C. *Arch. Biochem. Biophys.* **1986**, *246*, 501-514.

(42) Ortiz de Montellano, P. R. In *Cytochrome P-450*; Ortiz de Montellano, P. R., Eds.; Plenum: New York, 1986; pp 217-271.

(43) Dawson, J. H.; Sono, M. *Chem. Rev.* **1987**, *87*, 1255-1276.

(44) Dolphin, D.; Forman, A.; Borg, D. C.; Fajer, J.; Felton, R. H. *Proc. Natl. Acad. Sci., USA* **1971**, *68*, 614-618.

(45) Traylor, T. G.; Lee, W. A.; Stynes, D. V. *J. Am. Chem. Soc.* **1984**, *106*, 755-764.

(46) Yamaguchi, K.; Watanabe, Y.; Morishima, I. *J. Am. Chem. Soc.* **1993**, *115*, 4058-4065.

(47) Sawyer, D. T. In *Oxygen Complexes and Oxygen Activation by Transition Metals*; Martell, A. E. and Sawyer, D. T., Eds.; Plenum: New York, 1988; pp 131-148.

(48) Nordlund, P.; Dalton, H.; Eklund, H. *FEBS Lett.* **1992**, *307*, 257-262.

(49) Rosenzweig, A. C.; Frederick, C. A.; Lippard, S. J.; Nordlund, P. *Nature* **1993**, *366*, 537-543.

(50) Holmes, M. A.; Trong, I. L.; Turley, S.; Sieker, L. C.; Stenkamp, R. E. *J. Mol. Biol.* **1991**, *218*, 583-593.

(51) Micklitz, W.; Bott, S. G.; Bentsen, J. G.; Lippard, S. J. *J. Am. Chem. Soc.* **1989**, *111*, 372-374.

(52) *Bioinorganic Chemistry of Copper*; Karlin, K. D.; Tyeklár, Z., Ed.; Chapman Hall: New York, 1993, p 506.

(53) Kitajima, N.; Fukui, H.; Moro-oka, Y. *J. Am. Chem. Soc.* **1990**, *112*, 6402-6403.

(54) Dong, Y.; Menage, S.; Brennan, B. A.; Elgren, T. E.; Jang, H. G.; Pearce, L. L.; Que, L., Jr. *J. Am. Chem. Soc.* **1993**, *115*, 1851-1859.

(55) Kitajima, N.; Tamura, N.; Amagai, H.; Fukui, H.; Moro-Oka, Y.; Mizutani, Y.; Kitagawa, T.; Methur, R.; Heerwegh, K.; Reed, C. A.; Randall, C. R.; Que, L., Jr.; Tatsumi, K. *J. Am. Chem. Soc.* **1994**, *116*, 9071-9085.

(56) Kurtz, D. M., Jr.; Shriver, D. F.; Klotz, I. M. *J. Am. Chem. Soc.* **1976**, *98*, 5033-5035.

(57) Kurtz, D. M., Jr.; Shriver, D. F.; Klotz, I. M. *Coord. Chem. Rev.* **1977**, *24*, 145-178.

(58) Goddard, W. A., III; Olafson, B. D. *Proc. Natl. Acad. Sci., USA* **1975**, *72*, 2335-2339.

(59) Abramowitz, S.; Acquista, N.; Levin, I. W. *Chem. Phys. Lett.* **1977**, *50*, 423-426.

(60) Chang, S.; Blyholder, G.; Fernandez, J. *Inorg. Chem.* **1981**, *20*, 2813-2817.

(61) *McGraw-Hill Dictionary of Scientific Technological Terms*; Parker, S. P., Ed.; McGraw-Hill, Inc.: New York, 1989.

(62) Weiss, J. *J. Chim. Phys.* **1951**, *48*, 6-10.

(63) Walling, C. *Acc. Chem. Res.* **1975**, *8*, 125-131.

(64) Brown, E. R.; Mazzarella, J. D. *J. Electroanal. Chem.* **1987**, *222*, 173-192.

(65) Weiss, J. *Experientia* **1953**, *9*, 61-62.

(66) Taube, H. *Science* **1984**, *226*, 1028-1036. (and ref. therein).

(67) George, P. *J. Chem. Soc.* **1954**, 4349-4359.

(68) Cher, M.; Davidson, N. *J. Am. Chem. Soc.* **1955**, *77*, 793-798.

(69) Huffman, R. E.; Davidson, N. *J. Am. Chem. Soc.* **1956**, *78*, 4836-4842.

(70) Macejevskis, B.; Dokuchaeva, A. N.; Liepina, L. *Latvijas, PSR Zinatnu Akad. Vestis. Kim. Ser.* **1965**, *4*, 453-460; *Chem. Abstr.* **1966**, 64, 2786d.

(71) McBain, J. W. *J. Phys. Chem.* **1901**, *5*, 623-638.

(72) Posner, A. M. *Trans. Fraday Soc.* **1953**, *49*, 382-388.

(73) Lamb, A. B.; Elder, L. W., Jr. *J. Am. Chem. Soc.* **1931**, *53*, 137-163.

(74) King, J.; Davidson, N. *J. Am. Chem. Soc.* **1958**, *80*, 1542-1545.

(75) Pound, J. R. *J. Phys. Chem.* **1939**, *43*, 969-980.

(76) Hammond, G. S.; Wu, C.-H. S. In *Adv. Chem. Ser.*; Gould, R. F., Eds.; ACS: Washington, D.C., 1968; Vol. 77; pp 186-207.

(77) Kurimura, Y.; Ochiai, R.; Matsuura, N. *Bull. Chem. Soc. Japan* **1968**, *41*, 2234-2239.

(78) Purmal, A. P.; Skurlatov, Y. I.; Travin, S. O. *Izvestiya Akademii Nauk. SSSR, Seriya Khimicheskaya* **1980**, *3*, 492-497.

(79) Ng, F. T. T.; Henry, P. M. *Can. J. Chem.* **1980**, *58*, 1773-1779.

(80) Nishida, Y.; Yoshizawa, K.; Takahashi, S. *J. Chem. Soc. Chem. Commun.* **1991**, 1647-1648.

(81) Burkitt, M. J.; Gilbert, B. C. *Free Rad. Res. Commun.* **1991**, *14*, 107-123.

(82) Lind, M. D.; Hoard, J. L.; Hamor, M. J.; Hamor, T. A.; Hoard, J. L. *Inorg. Chem.* **1964**, *3*, 34-43.

(83) Kosaka, H.; Katsuki, Y.; Shiga, T. *Arch. Biochem. Biophys.* **1992**, *293*, 401-408.

(84) Ahmad, S.; McCallum, J. D.; Shiemke, A. K.; Appelman, E. H.; Loehr, T. M.; Sanders-Loehr, J. *Inorg. Chem.* **1988**, *27*, 2230-2233.

(85) Fridovich, I. *Annu. Rev. Biochem.* **1975**, *44*, 147-159.

(86) Veldink, G.; Vliegenthart, J., F.G. *Adv. Inorg. Biochem.* **1984**, *6*, 139-161.

(87) Axcell, B. C.; Geary, P. J. *Biochem. J.* **1975**, *146*, 173-183.

(88) Bernhardt, F.-H.; Heymann, E.; Traylor, P. S. *Eur. J. Biochem.* **1978**, *92*, 209-223.

(89) Bernhardt, F.-H.; Meisch, H.-U. *Biochem. Biophys. Res. Commun.* **1980**, *93*, 1247-1253.

(90) Adrian, W.; Bernhardt, F.-H.; Bill, E.; Gersonde, K.; Heymann, E.; Trautwein, A.; Twilfer, H. *Hoppe-Seyler's Physiol. Chem.* **1980**, *361*, 211.

(91) Bernhardt, F.-H.; Kuthan, H. *Eur. J. Biochem.* **1981**, *120*, 547-555.

(92) Bill, E.; Bernhardt, F.-H.; Trautwein, A. X. *Eur. J. Biochem.* **1981**, *121*, 39-46.

(93) Twilfer, H.; Bernhardt, F.-H.; Gersonde, K. *Eur. J. Biochem.* **1981**, *119*, 595-602.

(94) Bernhardt, F.-H.; Nastainczyk, W.; Seydewitz, V. *Eur. J. Biochem.* **1977**, *72*, 107-115.

(95) Bernhardt, F.-H.; Erdin, N.; Staudinger, H.; Ullrich, V. *Eur. J. Biochem.* **1973**, *35*, 126-134.

(96) Twilfer, H.; Bernhardt, F.-H.; Gersonde, K. *Eur. J. Biochem.* **1985**, *147*, 171-176.

(97) Bill, E.; Bernhardt, F.-H.; Trautwein, A. X.; Winkler, H. *Eur. J. Biochem.* **1985**, *147*, 177-182.

(98) Arciero, D. M.; Lipscomb, J. D.; Huynh, B. H.; Kent, T. A.; Münck, E. *J. Biol. Chem.* **1983**, *258*, 14981-14991.

(99) Que, L., Jr.; Lipscomb, J. D.; Zimmermann, R.; Münck, E.; Orme-Johnson, N. R.; Orme-Johnson, W. H. *Biochim. Biophys. Acta* **1976**, *452*, 320-334.

(100) Wende, P.; Pfleger, K.; Bernhardt, F.-H. *Biochem. Biophys. Res. Commun.* **1982**, *104*, 527-532.

(101) Hayaishi, O.; Nozaki, M.; Abbott, M. T. In *The Enzymes*; Boyer, P. D., Eds.; Academic: New York, 1975; Vol. 12; pp 119-189.

(102) Lipscomb, J. D.; Orville, A. M. In *Metal Ions in Biological Systems*; Sigel, H. and Sigel, A., Eds.; Marcel Dekker: New York, 1992; Vol. 28; pp 243-298.

(103) Que, L., Jr.; Kolanczyk, R. C.; White, L. S. *J. Am. Chem. Soc.* **1987**, *109*, 5373-5380.

(104) Cox, D. D.; Que, L., Jr. *J. Am. Chem. Soc.* **1988**, *110*, 8085-8092.

(105) Jang, H. G.; Cox, D. D.; Que, L., Jr. *J. Am. Chem. Soc.* **1991**, *113*, 9200-9204.

(106) Zimmerman, R.; Huynh, B. H.; Münck, E.; Lipscomb, J. D. *J. Chem. Phys* **1978**, *69*, 5463-5467.

(107) Arciero, D. M.; Lipscomb, J. D. *J. Biol. Chem.* **1986**, *261*, 2170-2178.

(108) Arciero, D. M.; Orville, A. M.; Lipscomb, J. D. *J. Biol. Chem.* **1985**, *260*, 14035-14044.

(109) Mabrouk, P. A.; Orville, A. M.; Lipscomb, J. D.; Solomon, E. I. *J. Am. Chem. Soc.* **1991**, *113*, 4053-4061.

(110) Harris, W. R.; Carrano, C. J.; Cooper, S. R.; Sofen, S. R.; Avdeef, A. E.; McArdle, J. V.; Raymond, K. N. *J. Am. Chem. Soc.* **1979**, *101*, 6097-6104.

(111) Heistand, R. H., II; Lauffer, R. B.; Fikrig, E.; Que, L., Jr. *J. Am. Chem. Soc.* **1982**, *104*, 2789-2796.

(112) Shiman, R. In *Folates and Pterins*; Blakley, R. L. and Benkovic, S. J., Eds.; Wiley and Sons: New York, 1985; Vol. 2; pp 179-250.

(113) Dix, T. A.; Benkovic, S. J. *Acc. Chem. Res.* **1988**, *21*, 101-107.

(114) Blakley, R. L.; Benkovic, S. J. *Folates and Pterines*; Wiley and Sons: New York, 1985; Vol. 2.

(115) Dix, T. A.; Benkovic, S. J. *Biochem.* **1985**, *24*, 5839-5846.

(116) Dix, T. A.; Bollag, G. E.; Domanico, P. L.; Benkovic, S. J. *Biochem.* **1985**, *24*, 2955-2958.

(117) Nakata, H.; Fujisawa, H. *Biochim. Biophys. Acta* **1980**, *614*, 313-327.

(118) Pember, S. O.; Villafranca, J. J.; Benkovic, S. J. *Biochem.* **1986**, *25*, 6611-6619.

(119) Martínez, A.; Abeygunawardana, C.; Haavik, J.; Flatmark, T.; Mildvan, A. S. *Biochem.* **1993**, *32*, 6381-6390.

(120) Storm, C. B.; Kaufman, S. *Biochem. Biophys. Res. Commun.* **1968**, *32*, 788-793.

(121) Webber, S.; Harzer, G.; Whiteley, J. M. *Anal. Biochem.* **1980**, *106*, 63-72.

(122) Rhoads, R. E.; Udenfriend, S. *Proc. Natl. Acad. Sci., USA* **1968**, *60*, 1473-1478.

(123) Cardinale, G. J.; Rhoads, R. E.; Udenfriend, S. *Biochem. Biophys. Res. Commun.* **1971**, *43*, 537-543.

(124) Hanauske-Abel, H. M.; Günzler *J. Theor. Biol.* **1982**, *94*, 421-455.

(125) Kivirikko, K. I.; Myllylä, R.; Pihlajaniemi, T. *FASEB J.* **1989**, *3*, 1609-1617.

(126) Majamaa, K.; Günzler, V.; Hanauske-Abel, H. M.; Myllylä, R.; Kivirikko, K. I. *J. Biol. Chem.* **1986**, *261*, 7819-7823.

(127) Nietfeld, J. J.; De Jong, L.; Kemp, A. *Biochim. Biophys. Acta* **1982**, *704*, 321-325.

(128) Popennoe, E. A.; Aronson, R. B.; Van Slyke, D. D. *Arch. Biochem. Biophys.* **1969**, *133*, 286-292.

(129) Halme, J.; Kivirikko, K. I.; Simons, K. *Biochim. Biophys. Acta* **1970**, *198*, 460-470.

(130) Hobza, P.; Hurych, J.; Zahradnik, R. *Biochim. Biophys. Acta* **1973**, *304*, 466-472.

(131) De Jong, L.; Albracht, S. P. J.; Kemp, A. *Biochim. Biophys. Acta* **1982**, *704*, 326-332.

(132) Nietfeld, J. J.; Kemp, A. *Biochim. Biophys. Acta* **1981**, *657*, 159-167.

(133) Majamaa, K.; Hanauske-Abel, H. M.; Günzler, V.; Kivirikko, K. I. *Eur. J. Biochem.* **1984**, *138*, 239-245.

(134) Myllylä, R.; Majamaa, K.; Günzler, V.; Hanauske-Abel, H. M.; Kivirikko, K. I. *J. Biol. Chem.* **1984**, *259*, 5403-5405.

(135) Myllylä, R.; Kuutti-Savolainen, E.-R.; Kivirikko, K. I. *Biochem. Biophys. Res. Commun.* **1978**, *83*, 441-448.

(136) Yu, R.; Kurata, T.; Arakawa, N. *Agric. Biol. Chem.* **1988**, *52*, 721-728.

(137) Majamaa, K.; Turpeenniemi-Hujanen, T. M.; Latipää, P.; Günzler, V.; Hanauske-Abel, H. M.; Hassinen, I. E.; Kivirikko, K. I. *Biochem J.* **1985**, *229*, 127-133.

(138) Chiou, Y.-M.; Que, L., Jr. *J. Am. Chem. Soc.* **1992**, *114*, 7567-7568.

(139) Chiou, Y.-M.; Que, L., Jr. *J. Inorg. Biochem.* **1993**, *51*, 127.

(140) Tuderman, L.; Myllylä, R.; Kivirikko, K. I. *Eur. J. Biochem.* **1977**, *80*, 341-348.

(141) Warn-Cramer, B. J.; Macrander, L. A.; Abbott, M. T. *J. Biol. Chem.* **1983**, *258*, 10551-10557.

(142) Thornburg, L. D.; Lai, M.-T.; Wishnok, J. S.; Stubbe, J. *Biochem.* **1994**, *32*, 14023-14033.

(143) Baldwin, J. E. In *Recent Advances in the Chemistry of B-Lactam Antibiotics*; Bentley, P. H. and Southgate, R., Eds.; Royal Society of Chemistry: London, 1989; pp 1-22.

(144) Baldwin, J. E.; Bradley, M. *Chem. Rev.* **1990**, *90*, 1079-1088.

(145) Baldwin, J. E. *J. Heterocyclic Chem.* **1990**, *27*, 71-78.

(146) White, R. L.; John, E.-M. M.; Baldwin, J. E.; Abraham, E. P. *Biochem. J.* **1982**, *203*, 791-793.

(147) Bainbridge, Z. A.; Scott, R. I.; Perry, D. *J. Chem. Tech. Biotechnol.* **1992**, *55*, 233-238.

(148) Chen, V. J.; Orville, A. M.; Harpel, M. R.; Frolik, C. A.; Surerus, K. K.; Münck, E.; Lipscomb, J. D. *J. Biol. Chem.* **1989**, *264*, 21677-21681.

(149) Orville, A. M.; Chen, V. J.; Kriauciunas, A.; Harpel, M. R.; Fox, B. G.; Münck, E.; Lipscomb, J. D. *Biochem.* **1992**, *31*, 4602-4612.

(150) Ming, L.-J.; Que, L., Jr.; Kriauciunas, A.; Frolik, C. A.; Chen, V. J. *Inorg. Chem.* **1990**, *29*, 1111-1112.

(151) Ming, L.-J.; Que, L., Jr.; Kriauciunas, A.; Frolik, C. A.; Chen, V. J. *Biochem.* **1991**, *30*, 11653-11659.

(152) Scott, R. A.; Wang, S.; Eidsness, M. K.; Kriauciunas, A.; Frolik, C. A.; Chen, V. J. *Biochem.* **1992**, *31*, 4596-4601.

(153) Randall, C. R.; Zang, Y.; True, A. E.; Que, L., Jr.; Charnock, J. M.; Garner, C. D.; Fujishima, Y.; Schofield, C. J.; Baldwin, J. E. *Biochem.* **1993**, *32*, 6664-6673.

(154) Samson, S. M.; Chapman, J. L.; Belagaje, R.; Queener, S. W.; Ingolia, T. D. *Proc. Natl. Acad. Sci., USA* **1987**, *84*, 5705-5709.

(155) Kriauciunas, A.; Frolik, C. A.; Hassell, T. C.; Skatrud, P. L.; Johnson, M. G.; Holbrook, N. L.; Chen, V. J. *J. Biol. Chem.* **1991**, *266*, 11779-11788.

(156) Baldwin, J. E.; Adlington, R. M.; Domayne-Hayman, B. P.; Knight, G.; Ting, H.-H. *J. Chem. Soc., Chem. Commun.* **1987**, 1661-1663.

(157) Baldwin, J. E.; Adlington, R. M.; Bradley, M.; Norris, W. J.; Turner, N. J.; Yoshida, A. *J. Chem. Soc., Chem. Commun.* **1988**, 1125-1128.

(158) Baldwin, J. E.; Adlington, R. M.; Bradley, M.; Turner, N. J.; Pitt, A. R. *J. Chem. Soc., Chem. Commun.* **1989**, 978-981.

(159) Baldwin, J. E.; Bradley, M.; Turner, N. J.; Adlington, R. M.; Pitt, A. R.; Sheridan, H. *Tetrahedron* **1991**, *47*, 8203-8222.

(160) Baldwin, J. E.; Bradley, M.; Turner, N. J.; Adlington, R. M.; Pitt, A. R.; Derome, A. E. *Tetrahedron* **1991**, *47*, 8223-8242.

(161) Baldwin, J. E.; Lynch, G. P.; Schofield, C. J. *J. Chem. Soc., Chem. Commun.* **1991**, 736-738.

(162) Baldwin, J. E.; Adlington, R. M.; Marquess, D. G.; Pitt, A. R.; Russell, A. T. *J. Chem. Soc., Chem. Commun.* **1991**, 856-858.

(163) Baldwin, J. E.; Lynch, G. P.; Schofield, C. J. *Tetrahedron* **1992**, *48*, 9085-9100.

(164) Nonhebel, D. C. *Chem. Soc. Rev.* **1993**, 347-359.

(165) Baldwin, J. E.; Adlington, R. M.; Flitsch, S. L.; Ting, H.-H.; Turner, N. J. *J. Chem. Soc., Chem. Commun.* **1986**, *17*, 1305-1308.

(166) Wilkins, R. G.; Harrington, P. C. *Adv. Inorg. Biochem.* **1983**, *5*, 51-85.

(167) Stenkamp, R. E. *Chem. Rev.* **1994**, *94*, 714-726.

(168) Stenkamp, R. E.; Sieker, L. C.; Jensen, L. H.; McCallum, J. D.; Sanders-Loehr, J. *Proc. Natl. Acad. Sci., USA* **1985**, *82*, 713-716.

(169) Sheriff, S.; Hendrickson, W. A.; Smith, J. L. *Life Chem. Rep. Suppl. Ser.* **1983**, *1*, 305-308.

(170) Stenkamp, R. E.; Sieker, L. C.; Jensen, L. H. *J. Am. Chem. Soc.* **1984**, *106*, 618-622.

(171) Sheriff, S.; Hendrickson, W. A.; Smith, J. L. *J. Mol. Biol.* **1987**, *197*, 273-296.

(172) Holmes, M. A.; Stenkamp, R. E. *J. Mol. Biol.* **1991**, *220*, 723-737.

(173) Sheriff, S.; Hendrickson, W. A.; Stenkamp, R. E.; Sieker, L. C.; Jensen, L. H. *Proc. Natl. Acad. Sci., USA* **1985**, *82*, 1104-1107.

(174) Dunn, J. B. R.; Shriver, D. F.; Klotz, I. M. *Proc. Natl. Acad. Sci., USA* **1973**, *70*, 2582-2584.

(175) Dunn, J. B. R.; Shriver, D. F.; Klotz, I. M. *Biochem.* **1975**, *14*, 2689-2695.

(176) Shiemke, A. K.; Loehr, T. M.; Sanders-Loehr, J. *J. Am. Chem. Soc.* **1986**, *108*, 2437-2443.

(177) Reem, R. C.; McCormick, J. M.; Richardson, D. E.; Devlin, F. J.; Stephens, P. J.; Musselman, R. L.; Solomon, E. I. *J. Am. Chem. Soc.* **1989**, *111*, 4688-4704.

(178) Sanders-Loehr, J.; Wheeler, W. D.; Shiemke, A. K.; Averill, B. A.; Loehr, T. *J. Am. Chem. Soc.* **1989**, *111*, 8084-8093.

(179) Kaminaka, S.; Takizawa, H.; Handa, T.; Kihara, H.; Kitagawa, T. *Biochem.* **1992**, 6997-7002.

(180) Solomon, E. I.; Zhang, Y. *Acc. Chem. Res.* **1992**, *25*, 343-352.

(181) Bates, G.; Brunori, M.; Amiconi, E.; Antonini, E.; Wyman, J. *Biochem.* **1968**, *7*, 3016-3020.

(182) De Waal, D. J. A.; Wilkins, R. G. *J. Biol. Chem.* **1976**, *251*, 2339-2343.

(183) Petrou, A. L.; Armstrong, F. A.; Sykes, A. G.; Harrington, P. C.; Wilkins, R. G. *Biochim. Biophys. Acta* **1981**, *670*, 377-384.

(184) Zimmer, J. R.; Tachi-iri, Y.; Takizawa, H.; Handa, T.; Yamamura, T.; Kihara, H. *Biochim. Biophys. Acta* **1986**, *874*, 174-180.

(185) Tachi'iri, Y.; Ichimura, K.; Yamamura, T.; Satake, K.; Kurita, K.; Nagamura, T.; Kihara, H. *Eur. J. Biochem.* **1990**, *18*, 9-16.

(186) Kraulis, P. *J. of Appl. Cryst.* **1991**, *24*, 946-950.

(187) Wilkins, P. C.; Wilkins, R. G. *Coord. Chem. Rev.* **1987**, *79*, 195-214.

(188) Klotz, I. M.; Klotz, T. A. *Science* **1955**, *121*, 477-480.

(189) Clark, P. E.; Webb, J. *Biochem.* **1981**, *20*, 4628-4632.

(190) Shiemke, A. K.; Loehr, T. M.; Sanders-Loehr, J. *J. Am. Chem. Soc.* **1984**, *106*, 4951-4956.

(191) Armstrong, G. D.; Sykes, A. G. *Inorg. Chem.* **1986**, *25*, 3135-3139.

(192) Alberding, N.; Lavalette, D.; Austin, R. H. *Proc. Natl. Acad. Sci., USA* **1981**, *78*, 2307-2309.

(193) Antonini, E.; Brunori, M. *Hemoglobin and Myoglobin and Their Reactions with Ligands*; North-Holland: Amsterdam, 1971.

(194) Brunori, M.; Schuster, T. M. *J. Biol. Chem.* **1969**, *244*, 4046-4053.

(195) Gibson, Q. H. *J. Biol. Chem.* **1970**, *245*, 3285-3288.

(196) De Waal, D. J. A.; De Jong, L.; Hartog, A. F.; Kemp, A. *Biochem.* **1985**, *24*, 6493-6499.

(197) Zhang, J.-H.; Kurtz, D. M., Jr. *Biochem.* **1991**, *30*, 9121-9125.

(198) Matsukawa, S.; Mawatari, K.; Yoneyama, Y.; Kitagawa, T. *J. Am. Chem. Soc.* **1985**, *107*, 1108-1113.

(199) Bradíc, Z.; Conrad, R.; Wilkins, R. G. *J. Biol. Chem.* **1977**, *252*, 6069-6075.

(200) Chaudhuri, P.; Wieghardt, K.; Nuber, B.; Weiss, J. *Angew. Chem. Int. Ed. Engl.* **1985**, *24*, 778-779.

(201) Hartman, J. R.; Rardin, R. L.; Chaudhuri, P.; Pohl, K.; Wieghardt, K.; Nuber, B.; Weiss, J.; Papaefthymiou, G. C.; Frankel, R. B.; Lippard, S. J. *J. Am. Chem. Soc.* **1987**, *109*, 7387-7396.

(202) Feig, A. L.; Masschelein, A.; Bakac, A.; Lippard, S. J. *J. Am. Chem. Soc.* **1995**, manuscript in preparation.

(203) Dalton, H. In *Advances in Applied Microbiology*Academic: New York, 1980; Vol. 26; pp 71-87.

(204) Anthony, C. *The Biochemistry of Methylotrophs*; Academic: New York, 1982.

(205) Ruzicka, F.; Huang, D.-S.; Donnelly, M. I.; Frey, P. A. *Biochem.* **1990**, *29*, 1696-1700.

(206) Priestley, N. D.; Floss, H. G.; Froland, W. A.; Lipscomb, J. D.; Williams, P. G.; Morimoto, H. *J. Am. Chem. Soc.* **1992**, *114*, 7561-7562.

(207) Lee, S.-K.; Fox, B. G.; Froland, W. A.; Lipscomb, J. D.; Münck, E. *J. Am. Chem. Soc.* **1993**, *115*, 6450-6451.

(208) Liu, K. E.; Johnson, C. C.; Newcomb, M.; Lippard, S. J. *J. Am. Chem. Soc.* **1993**, *115*, 939-947.

(209) Liu, K. E.; Feig, A. L.; Goldberg, D. P.; Watton, S. P.; Lippard, S. J. In *The Activation of Dioxygen and Homogeneous Catalytic Oxidation*; Barton, D. H. R., Eds.; Plenum: New York, 1993; pp 301-320.

(210) Green, J.; Dalton, H. *Biochem. J.* **1989**, *259*, 167-172.

(211) Fox, B. G.; Froland, W. A.; Dege, J. E.; Lipscomb, J. D. *J. Biol. Chem.* **1989**, *264*, 10023-10033.

(212) Liu, K. E.; Lippard, S. J. *J. Biol. Chem.* **1991**, *266*, 12836-12839; 24859.

(213) Froland, W. A.; Andersson, K. K.; Lee, S.-K.; Liu, Y.; Lipscomb, J. D. *J. Biol. Chem.* **1992**, *267*, 17588-17597.

(214) Lund, J.; Dalton, H. *Eur. J. Biochem.* **1985**, *147*, 291-296.

(215) Lund, J.; Woodland, M. P.; Dalton, H. *Eur. J. Biochem.* **1985**, *147*, 297-305.

(216) Fox, B. G.; Lipscomb, J. D. In *Biological Oxidation Systems*; Reddy, C. C., Eds.; Academic: New York, 1990; Vol. 1; pp 367-388.

(217) Rosenzweig, A. C.; Feng, X.; Lippard, S. J. In *Applications of Enzyme Biotechnology*; Kelly, J. W. and Baldwin, T. O., Eds.; Plenum: New York, 1991; pp 69-85.

(218) DeWitt, J. G.; Bentsen, J. G.; Rosenzweig, A. C.; Hedman, B.; Green, J.; Pilkington, S.; Papaefthymiou, G. C.; Dalton, H.; Hodgson, K. O.; Lippard, S. J. *J. Am. Chem. Soc.* **1991**, *113*, 9219-9235.

(219) Green, J.; Dalton, H. *J. Biol. Chem.* **1985**, *260*, 15795-15801.

(220) Rosenzweig, A.; Frederick, C. A.; Lippard, S. J. *Biology and Chemistry* **1995**, *2*, 409-418.

(221) Fox, B. G.; Hendrich, M. P.; Surerus, K. K.; Andersson, K. K.; Froland, W. A.; Lipscomb, J. D.; Münck, E. *J. Am. Chem. Soc.* **1993**, *115*, 3688-3701.

(222) Hendrich, M. P.; Münck, E.; Fox, B. G.; Lipscomb, J. D. *J. Am. Chem. Soc.* **1990**, *112*, 5861-5865.

(223) Fox, B. G.; Liu, Y.; Dege, J. E.; Lipscomb, J. D. *J. Biol. Chem.* **1991**, *266*, 540-550.

(224) Fox, B. G.; Surerus, K. K.; Münck, E.; Lipscomb, J. D. *J. Biol. Chem.* **1988**, *263*, 10553-10556.

(225) Woodland, M. P.; Patil, D. S.; Cammack, R.; Dalton, H. *Biochim. Biophys. Acta* **1986**, *873*, 237-242.

(226) Paulsen, K. E.; Liu, Y.; Fox, B. G.; Lipscomb, J. D.; Münck, E.; Stankovich, M. T. *Biochem.* **1994**, *33*, 713-722.

(227) Paulsen, K. E.; Liu, Y.; Fox, B. G.; Stankovich, M. T.; Lipscomb, J. D.; Münck, E. *J. Inorg. Biochem.* **1993**, *51*, 307.

(228) Ericson, A.; Hedman, B.; Hodgson, K. O.; Green, J.; Dalton, H.; Bentsen, J. G.; Beer, R. H.; Lippard, S. J. *J. Am. Chem. Soc.* **1988**, *110*, 2330-2332.

(229) DeRose, V. J.; Liu, K. E.; Kurtz, D. M., Jr.; Hoffman, B. M.; Lippard, S. J. *J. Am. Chem. Soc.* **1993**, *115*, 6440-6441.

(230) Thomann, H.; Bernardo, M.; McCormick, J. M.; Pulver, S.; Andersson, K. K.; Lipscomb, J. D.; Solomon, E. I. *J. Am. Chem. Soc.* **1993**, *115*, 8881-8882.

(231) DeGrado, W. F. In *Advances in Protein Chemistry*1988; Vol. 39; pp 51-124.

(232) Cohen, C.; Parry, D. A. D. *Proteins: Structure, Function and Genetics* **1990**, *7*, 1-15.

(233) Åberg, A. Thesis, Stockholm University, 1993.

(234) Nordlund, P.; Åberg, A.; Eklund, H.; Regnström, K.; Hajdu, J. submitted for publication.

(235) Rardin, R. L.; Tolman, W. B.; Lippard, S. J. *New J. Chem.* **1991**, *15*, 417-430.

(236) Liu, K. E.; Valentine, A. M.; Qiu, D.; Edmondson, D. E.; Appelman, E. H.; Spiro, T. G.; Lippard, S. J. *J. Am. Chem. Soc.* **1995**, *117*, 4997-4998.

(237) Liu, K. E.; Valentine, A. M.; Wang, D.; Huynh, B. H.; Edmondson, D. E.; Salifoglou, A.; Lippard, S. J. *J. Am. Chem. Soc.* **1995**, in press.

(238) Green, J.; Dalton, H. *J. Biol. Chem.* **1989**, *264*, 17698-17703.

(239) Andersson, K. K.; Froland, W. A.; Lee, S.-K.; Lipscomb, J. D. *New J. Chem.* **1991**, *15*, 411-415.

(240) Wilkins, P. C.; Dalton, H.; Podmore, I. D.; Deighton, N.; Symons, M. C. R. *Eur. J. Biochem.* **1992**, *210*, 67-72.

(241) Newcomb, M., Wayne State University, personal communications, 1993.

(242) Deighton, N.; Podmore, I. D.; Symons, M. C. R.; Wilkins, P. C.; Dalton, H. *J. Chem. Soc. Chem. Commun.* **1991**, 1086-1088.

(243) Jiang, Y.; Wilkins, P. C.; Dalton, H. *Biochim. Biophys. Acta* **1993**, *1163*, 105-112.

(244) Liu, K.E, Lippard, S. J. Unpublished results.

(245) Tyeklár, Z.; Karlin, K. D. In *Dioxygen Activation and Homogeneous Catalytic Oxidation*; Simándi, L. I., Eds.; Elsevier Science: Amsterdam, 1991; pp 237-248.

(246) Tian, G.; Berry, J. A.; Klinman, J. P. *Biochem.* **1994**, *33*, 226-234.

(247) Shteinman, A. A. *Russian Chemical Bulletin* **1993**, *42*, 227-234.

(248) Shteinman, A. A. *FEBS Lett.* **1995**, *362*, 5-9.

(249) Atkin, C. L.; Thelander, L.; Reichard, P.; Lang, G. *J. Biol. Chem.* **1973**, *248*, 7464-7472.

(250) Eriksson, S.; Sjöberg, B.-M. In *Allosteric Enzymes*CRC: Boca Raton, FL, 1989; pp 189-215.

(251) Stubbe, J. In *Advances in Enzymology and Related Areas of Molecular Biology*; Meister, A., Eds.; John Wiley and Sons: New York, 1990; Vol. 62; pp 349-420.

(252) Stubbe, J. *J. Biol. Chem.* **1990**, *265*, 5329-5332.

(253) Fontecave, M.; Nordlund, P.; Eklund, H.; Reichard, P. In *Advances in Enzymology and Related Areas of Molecular Biology*; Meister, A., Eds.; Wiley and Sons: New York, 1992; Vol. 65; pp 147-183.

(254) Nordlund, P.; Sjöberg, B.-M.; Eklund, H. *Nature* **1990**, *345*, 593-598.

(255) Nordlund, P.; Eklund, H. *J. Mol. Biol.* **1993**, *232*, 123-164.

(256) Elgren, T. E.; Lynch, J. B.; Juarez-Garcia, C.; Münck, E.; Sjöberg, B.-M.; Que, L., Jr. *J. Biol. Chem.* **1991**, *266*, 19265-19268.

(257) Ochiai, E.-I.; Mann, G. J.; Gräslund, A.; Thelander, L. *J. Biol. Chem.* **1990**, *265*, 15758-15761.

(258) Bollinger, J. M., Jr.; Edmondson, D. E.; Huynh, B. H.; Filley, J.; Norton, J. R.; Stubbe, J. *Science* **1991**, *253*, 292-298.

(259) Taqui Khan, M. M.; Martell, A. E. *J. Am. Chem. Soc.* **1967**, *89*, 4176-4185.

(260) Menage, S.; Brennan, B. A.; Juarez-Garcia, C.; Münck, E.; Que, L., Jr. *J. Am. Chem. Soc.* **1990**, *112*, 6423-6425.

(261) Ling, J. Ph.D. Thesis, Oregon Graduate Institute of Science, 1993.

(262) Ravi, N.; Bollinger, J. M., Jr.; Huynh, B. H.; Edmondson, D. E.; Stubbe, J. *J. Am. Chem. Soc.* **1994**, *116*, 8007-8014.

(263) Bollinger, J. M., Jr.; Ravi, N.; Tong, W. H.; Edmondson, D. E.; Huynh, B. H.; Stubbe, J. *J. Inorg. Biochem.* **1993**, *51*, 6.

(264) Sahlin, M.; Sjöberg, B.-M.; Backes, G.; Loehr, T.; Sanders-Loehr, J. *Biochem. Biophys. Res. Commun.* **1990**, *167*, 813-818.

(265) Fontecave, M.; Gerez, C.; Atta, M.; Jeunet, A. *Biochem. Biophys. Res. Commun.* **1990**, *168*, 659-664.

(266) Leising, R. A.; Brennan, B. A.; Que, L., Jr.; Fox, B. G.; Münck, E. *J. Am. Chem. Soc.* **1991**, *113*, 3988-3990.

(267) Que, L., Jr. Univ. of Minnesota, personal communications, 1994.

(268) Ormö, M.; deMaré, F.; Regnström, K.; Åberg, A.; Sahlin, M.; Ling, J.; Loehr, T. M.; Sanders-Loehr, J.; Sjöberg, B.-M. *J. Biol. Chem.* **1992**, *267*, 8711-8714.

(269) Åberg, A.; Ormö, M.; Nordlund, P.; Sjöberg, B.-M. *Biochem.* **1993**, *32*, 9845-9850.

(270) Kang, C.; Sobkowiak, A.; Sawyer, D. T. *Inorg. Chem.* **1993**, submitted.

(271) Harrison, P. M.; Lilley, T. H. In *Iron Carriers and Iron Proteins*; Loehr, T. M., Eds.; VCH: New York, 1989; Vol. 5; pp 123-238.

(272) Theil, E. C. In *Advances in Enzymology and Related Areas of Molecular Biology*; Meister, A., Eds.; John Wiley and Sons: New York, 1990; Vol. 63; pp 421-450.

(273) Wagstaff, M.; Worwood, M.; Jacobs, A. *Biochem. J.* **1978**, *173*, 969-977.

(274) Artymiuk, P. J.; Bauminger, E. R.; Harrison, P. M.; Lawson, D. M.; Nowik, I.; Treffry, A.; Yewdall, S. J. In *Iron Biominerals*; Frankel, R. B. and Blakemore, R. P., Eds.; Plenum: New York, 1990; pp 269-294.

(275) Levi, S.; Luzzago, A.; Cesareni, G.; Cozzi, A.; Franceschinelli, F.; Albertini, A.; Arosio, P. *J. Biol. Chem.* **1988**, *263*, 18086-18092.

(276) Treffry, A.; Hirzman, J.; Yewdall, S. J.; Harrison, P. M. *FEBS Lett.* **1992**, *302*, 108-112.

(277) Harrison, P. M.; Bauminger, E. R.; Hechel, D.; Hodson, N. W.; Nowik, I.; Treffry, A.; Yewdall, S. J. In *Iron and Iron Protein Conference*; Israel, 1993.

(278) Harrison, P. M.; Bauminger, E. R.; Hechel, D.; Hodson, N. W.; Nowik, I.; Treffry, A.; Yewdall, S. J. In *Iron and Iron Protein Conference*; Israel, 1993 and ref. therein.

(279) Lawson, D. M.; Artymiuk, P. J.; Yewdall, S. J.; Smith, J. M. A.; Livingstone, J. C.; Treffry, A.; Luzzago, A.; Levi, S.; Arosio, P.; Cesareni, G.; Thomas, C. D.; Shaw, W. V.; Harrison, P. M. *Nature* **1991**, *349*, 541-544.

(280) Sun, S.; Arosio, P.; Levi, S.; Chasteen, N. D. *Biochem.* **1993**, *32*, 9362-9369.

(281) Macara, I. G.; Hoy, T. G.; Harrison, P. M. *Biochem. J.* **1972**, *126*, 151-162.

(282) Treffry, A.; Sowerby, J. M.; Harrison, P. M. *FEBS Lett.* **1979**, *100*, 33-36.

(283) Xu, B.; Chasteen, N. D. *J. Biol. Chem.* **1991**, *266*, 19965-19970.

(284) Bauminger, E. R.; Harrison, P. M.; Nowick, I.; Treffry, A. *Biochem.* **1989**, *28*, 5486-5493.

(285) Bauminger, E. R.; Harrison, P. M.; Hechel, D.; Nowik, I.; Treffry, A. *Biochim. Biophys. Acta* **1991**, *1118*, 48-58.

(286) Hanna, P. M.; Chen, Y.; Chasteen, N. D. *J. Biol. Chem.* **1991**, *266*, 886-893.

(287) Waldo, G. S.; Ling, J.; Sanders-Loehr, J.; Theil, E. C. *Science* **1993**, *259*, 796-798.

(288) Waldo, G. S.; Theil, E. C. *Biochem.* **1993**, *32*, 13262-13269.

(289) Sun, S.; Chasteen, N. D. *J. Biol. Chem.* **1992**, *267*, 25160-25166.

(290) Grady, J. K.; Chen, Y.; Chasteen, N. D.; Harris, D. C. *J. Biol. Chem.* **1989**, *264*, 20224-20229.

(291) Cheng, Y. G.; Chasteen, N. D. *Biochem.* **1991**, *30*, 2947-2953.

(292) Mayer, D. E.; Rohrer, J. S.; Schoeller, D. A.; Harris, D. C. *Biochem.* **1983**, *22*, 876-880.

(293) Umezawa, H. In *Bleomycin: Chemical, Biochemical and Biological Aspects*; Hecht, S. M., Eds.; Springer-Verlag: New York, 1979; pp 24-36.

(294) Stubbe, J.; Kozarich, J. W. *Chem. Rev.* **1987**, *87*, 1107-1136.

(295) Petering, D. H.; Byrnes, R. W.; Antholine, W. E. *Chem.-Biol. Interact.* **1990**, *73*, 133-182.

(296) Hamamichi, N.; Natrajan, A.; Hecht, S. M. *J. Am. Chem. Soc.* **1992**, *114*, 6278-6291.

(297) Suga, A.; Sugiyama, T.; Otsuka, M.; Ohno, M.; Sugiura, Y.; Maeda, K. *Tetrahedron* **1991**, *47*, 1191-1204.

(298) Sausville, E. A.; Peisach, J.; Horwitz, S. B. *Biochem. Biophys. Res. Commun.* **1976**, *73*, 814-822.

(299) Sausville, E. A.; Peisach, J.; Horwitz, S. B. *Biochem.* **1978**, *17*, 2740-2746.

(300) Sausville, E. A.; Stein, R. W.; Peisach, J.; Horowitz, S. B. *Biochem.* **1978**, *17*, 2746-2754.

(301) Burger, R. M.; Horwitz, S. B.; Peisach, J.; Wittenberg, J. B. *J. Biol. Chem.* **1979**, *254*, 12299-12302.

(302) Burger, R. M.; Peisach, J.; Blumberg, W. E.; Horwitz, S. B. *J. Biol. Chem.* **1979**, *254*, 10906-10912.

(303) Burger, R. M.; Peisach, J.; Horwitz, S. B. *J. Biol. Chem.* **1981**, *256*, 11636-11644.

(304) Burger, R. M.; Kent, T. A.; Horwitz, S. B.; Münck, E.; Peisach, J. *J. Biol. Chem.* **1983**, *258*, 1559-1564.

(305) Padbury, G.; Sligar, S. G. *J. Biol. Chem.* **1985**, *260*, 7820-7823.

(306) Heimbrook, D. C.; Mulholland, R. L., Jr.; Hecht, S. M. *J. Am. Chem. Soc.* **1986**, *108*, 7839-7840.

(307) Heimbrook, D. C.; Carr, S. A.; Mentzer, M. A.; Long, E. C.; Hecht, S. M. *Inorg. Chem.* **1987**, *26*, 3835-3836.

(308) Padbury, G.; Sligar, S. G.; Labeque, R.; Marnett, L. J. *Biochem.* **1988**, *27*, 7846-7852.

(309) Dawson, D. Y.; Hudson, S. E.; Mascharak, P. K. *J. Inorg. Biochem.* **1992**, *47*, 109-117.

(310) Sam, J. W.; Peisach, J. *Biochem.* **1993**, *32*, 1488-1491.

(311) Dabrowiak, J. C. *Adv. Inorg. Biochem.* **1982**, *4*, 69-113.

(312) Iitaka, Y.; Nakamura, H.; Nakatani, T.; Muraoka, Y.; Fujii, A.; Takita, T.; Umezawa, H. *J. Antibiot.* **1978**, *31*, 1070-1072.

(313) Stubbe, J.; Kozarich, J. W. *Chem. Rev.* **1987**, *87*, 1107-1136 and ref. therein.

(314) Kénani, A.; Bailly, C.; Helbecque, N.; Catteau, J.-P.; Houssin, R.; Bernier, J.-L.; Hénichart, J.-P. *Biochem. J.* **1988**, *253*, 497-504.

(315) Sugiura, Y.; Kikuchi, T. *J. Antibiot.* **1978**, *31*, 1310-1312.

(316) McMurry, T. J.; Groves, J. T. In *Cytochrome P-450*; Ortiz de Montellano, P., Eds.; Plenum: New York, 1986; pp 1-28.

(317) Natrajan, A.; Hecht, S. M.; van der Marel, G. A.; van Boom, J. H. *J. Am. Chem. Soc.* **1990**, *112*, 3997-4002.

(318) Barr, J. R.; Van Atta, R. B.; Natrajan, A.; Hecht, S. M. *J. Am. Chem. Soc.* **1990**, *112*, 4058-4060.

(319) Wu, J. C.; Stubbe, J.; Kozarich, J. W. *Biochem.* **1985**, *24*, 7569-7573.

(320) McGall, G. H.; Rabow, L. E.; Stubbe, J.; Kozarich, J. W. *J. Am. Chem. Soc.* **1987**, *109*, 2836-2837.

(321) Caspary, W. J.; Niziak, C.; Lanzo, D. A.; Friedman, R.; Bachur, N. R. *Mol. Pharmacol.* **1979**, *16*, 256-260.

(322) Lown, J. W.; Sim, S.-K. *Biochem. Biophys. Res. Commun.* **1977**, *77*, 1150-1157.

(323) Oberley, L. W.; Buettner, G. R. *FEBS Lett.* **1979**, *97*, 47-49.

(324) Rodriguez, L. O.; Hecht, S. M. *Biochem. Biophys. Res. Commun.* **1982**, *104*, 1470-1476.

(325) Rabow, L. E.; McGall, G. H.; Stubbe, J.; Kozarich, J. W. *J. Am. Chem. Soc.* **1990**, *112*, 3203-3208.

(326) Barton, D. H. R.; Csuhai, E.; Doller, D.; Balavoine, G. *J. Chem. Soc. Chem. Commun.* **1990**, 1787-1789.

(327) Barton, D. H. R.; Doller, D. *Acc. Chem. Res.* **1992**, *25*, 504-512.

(328) Baldwin, J. E.; Huff, J. *J. Am. Chem. Soc.* **1973**, *95*, 5757-5759.

(329) Herron, N.; Busch, D. H. *J. Am. Chem. Soc.* **1981**, *103*, 1236-1237.

(330) Kimura, E.; Kodama, M.; Machida, R.; Ishizu, K. *Inorg. Chem.* **1982**, *21*, 595-602.

(331) Brennan, B. A.; Chen, Q.; Juarez-Garcia, C.; True, A. E.; O'Connor, C. J.; Que, L., Jr. *Inorg. Chem.* **1991**, *30*, 1937-1943.

(332) Kitajima, N.; Tamura, N.; Tanaka, M.; Moro-oka, Y. *Inorg. Chem.* **1992**, *31*, 3342-3343.

(333) Murch, B. P.; Bradley, F. C.; Que, L., Jr. *J. Am. Chem. Soc.* **1986**, *108*, 5027-5028.

(334) Sawyer, D. T.; McDowell, M. S.; Spencer, L.; Tsang, P. K. S. *Inorg. Chem.* **1989**, *28*, 1166-1170.

(335) McCandlish, E.; Miksztal, A. R.; Nappa, M.; Sprenger, A. Q.; Valentine, J. S.; Stong, J. D.; Spiro, T. G. *J. Am. Chem. Soc.* **1980**, *102*, 4268-4271.

(336) Collamati, I.; Ercolani, C.; Rossi, G. *Inorg. Nucl. Chem. Lett.* **1976**, *12*, 799-802.

(337) Collamati, I. *Inorg. Chim. Acta* **1979**, *35*, L303-L304.

(338) Herron, N.; Cameron, J. H.; Neer, G. L.; Busch, D. H. *J. Am. Chem. Soc.* **1983**, *105*, 298-301.

(339) Herron, N.; Schammel, W. P.; Jackels, S. C.; Grzybowski, J. J.; Zimmer, L. L.; Busch, D. H. *Inorg. Chem.* **1983**, *22*, 1433-1440.

(340) Collman, J. P.; Gagne, R. R.; Reed, C. A.; Halbert, T. R.; Lang, G.; Robinson, W. T. *J. Am. Chem. Soc.* **1975**, *97*, 1427-1439.

(341) Almog, J.; Dyer, R. L.; Peters, M. *J. Am. Chem. Soc.* **1975**, *97*, 227-228.

(342) Collman, J. P. *Acc. Chem. Res.* **1977**, *10*, 265-272.

(343) Chin, D.-H.; La Mar, G. N.; Balch, A. L. *J. Am. Chem. Soc.* **1980**, *102*, 4344-4350.

(344) Paeng, I. R.; Shiwaku, H.; Nakamoto, K. *J. Am. Chem. Soc.* **1988**, *110*, 1995-1996.

(345) Almog, J.; Baldwin, J. E.; Huff, J. *J. Am. Chem. Soc.* **1975**, *97*, 228-229.

(346) Collman, J. P. *Acc. Chem. Res.* **1977**, *10*, 265-272. and ref. therein.

(347) Sauer-Masarwa, A.; Dickerson, L. D.; Herron, N.; Busch, D. H. *Coord. Chem. Rev.* **1993**, *128*, 117-137.

(348) Busch, D. H.; Alcock, N. W. *Chem. Rev.* **1994**, *94*, 585-623.

(349) Dickerson, L. D.; Sauer-Masarwa, A.; Herron, N.; Fendrick, C. M.; Busch, D. H. *J. Am. Chem. Soc.* **1993**, *115*, 3623-3626.

(350) Sauer-Masarwa, A.; Herron, N.; Fendrick, C. M.; Busch, D. H. *Inorg. Chem.* **1993**, *32*, 1086-1094.

(351) Sakurai, T.; Kaji, H.; Nakahara, A. *Inorg. Chim. Acta* **1982**, *67*, 1-5.

(352) Hayashi, Y.; Suzuki, M.; Uehara, A.; Mizutani, Y.; Kitagawa, T. *Chem. Lett.* **1992**, 91-94.

(353) Hayashi, Y.; Suzuki, M.; Uehara, A.; Mizutani, Y.; Kitagawa, T. submitted for publication.

(354) Drake, J. F.; Williams, R. J. P. *Nature* **1958**, *182*, 1084.

(355) Davies, R. C. Thesis, Waldham College, Oxford, 1963.

(356) McClellan, W. R.; Benson, R. E. *J. Am. Chem. Soc.* **1966**, *88*, 5165-5169.

(357) McKee, V.; Nelson, S. M.; Nelson, J. *J. Chem. Soc. Chem. Commun.* **1976**, 225-226.

(358) Holm, R. H.; Donahue, J. P. *Polyhedron* **1993**, *12*, 571-589.

(359) Feig, A.; Lippard, S. J. *J. Am. Chem. Soc.* **1994**, *116*, 8410-8411.

(360) Udenfriend, S.; Clark, C. T.; Axelrod, J.; Brodie, B. B. *J. Biol. Chem.* **1954**, *208*, 731-739.

(361) Hamilton, G. A.; Workman, R. J.; Woo, L. *J. Am. Chem. Soc.* **1964**, *86*, 3390-3391.

(362) Hamilton, G. A. *J. Am. Chem. Soc.* **1964**, *86*, 3391-3392.

(363) Hamilton, G. A. In *Molecular Mechanisms of Dioxygen Activation*; Hayaishi, O., Eds.; Academic: NY, 1974; pp 405-451.

(364) Kochi, J.; Sheldon, R. A. *Metal-Catalyzed Oxidations of Organic Compounds*; Academic: New York, 1981.

(365) Ito, S.; Ueno, K.; Mitarai, A.; Sasaki, K. *J. Chem. Soc., Perk. Trans. II.* **1993**, 255-259.

(366) Taqui Khan, M. M.; Martell, A. E. *J. Am. Chem. Soc.* **1967**, *89*, 7104-7111.

(367) Hamed, M. Y.; Silver, J.; Wilson, M. T. *Inorg. Chim. Acta* **1983**, *80*, 237-244.

(368) Hamed, M. Y.; Keypour, H.; Silver, J.; Wilson, M. T. *Inorg. Chim. Acta* **1988**, *152*, 227-231.

(369) Hamilton, G. *Adv. Enzymol.* **1969**, *32*, 55-96.

(370) Norman, R. O. C.; Radda, G. K. *Proc. Chem. Soc.* **1962**, 138.

(371) Sawyer, D. T.; Kang, C.; Qiu, A.; Sobkowiak, A. In *5th International Symposium on Redox Mechanisms and Interfacial Properties of Molecules of Biological Importance*; Schultz, F. A. and Tamijuchi, I., Eds.; The Electrochemical Society: Pennington, NJ, 1993.

(372) Sawyer, D. T.; Kang, C.; Llobet, A.; Redman, C. *J. Am. Chem. Soc.* **1993**, *115*, 5817-5818.

(373) Barton, D. H. R.; Beviere, S. D.; Chavasiri, W.; Csuhai, E.; Doller, D.; Liu, W.-G. *J. Am. Chem. Soc.* **1992**, *114*, 2147-2156.

(374) Fish, R. H.; Konings, M. S.; Oberhausen, K. J.; Fong, R. H.; Yu, W. M.; Christou, G.; Vincent, J. B.; Coggin, D. K.; Buchanan, R. M. *Inorg. Chem.* **1991**, *30*, 3002-3006.

(375) Fish, R. H.; Oberhausen, K. J.; Chen, S.; Richardson, J. F.; Pierce, W.; Buchanan, R. M. *Catalysis Letters* **1993**, *18*, 357-365.

(376) Barton, D. H. R.; Doller, D. In *Dioxygen Activation and Homogeneous Catalytic Oxidation*; Simándi, L., Eds.; Elsevier: New York, 1991; Vol. 66; pp 1-10.

(377) Kang, C.; Redman, C.; Cepak, V.; Sawyer, D. T. *Bioorg. Med. Chem.* **1993**, *1*, 125-140.

(378) Barton, D. H.; Sawyer, D. T. In *The Activation of O_2 and Homogeneous Catalytic Oxidation*; Barton, D. H. R., Martell, A. E. and Sawyer, D. T., Eds.; Plenum: New York, 1993; pp 1-7.

(379) Mimoun, H.; Seree de Roch, I. *Tetrahedron* **1975**, *31*, 777-784.

(380) Davis, R.; Durrant, J. L. A.; Khan, M. A. *Polyhedron* **1988**, *7*, 425-438.

(381) Sawyer, D. T.; Sugimoto, H.; Calderwood, T. S. *Proc. Natl. Acad. Sci., USA* **1984**, *81*, 8025-8027.

(382) Sheu, C.; Sawyer, D. T. *J. Am. Chem. Soc.* **1990**, *112*, 8212-8214.

CHAPTER II.

Kinetic Studies of Reactions of Dioxygen with Non-heme Diiron(II) Complexes Leading to the Formation of (μ–Oxo)diiron(III) Complexes

Introduction

Hemerythrin (Hr),[1-3] the R2 subunit of ribonucleotide reductase (RNR),[4-7] Δ-9-desaturase[8] and soluble methane monooxygenase (sMMO) hydroxylase[9-12] are members of an emerging class of non-heme diiron carboxylate proteins with important physiological roles.[2,13-15] Despite diverse biological functions, these proteins share a common structural motif and are all involved in reactions with dioxygen. The active centers of all four proteins contain pairs of iron atoms bridged by the carboxylate side chains of glutamate or aspartate. In their oxidized forms, additional monatomic oxo or hydroxo bridges, depending on the protein, are also present. The terminal sites are occupied by nitrogen atoms from histidine and oxygen atoms from additional carboxylate ligands and water. Isolated enzymes generally contain iron atoms in the +3 oxidation state, but the metal centers must be reduced to the diiron(II) state to observe activity.

The nature of the non-carboxylate bridging ligand differs among these proteins. In the case of deoxyHr, a dioxygen transport protein from marine invertebrates, a hydroxide ion bridges the two iron atoms. A vacant coordination site is present on one iron and is the place at which dioxygen binds. This binding is accompanied by two-electron oxidation of the diiron(II) center and proton transfer from the hydroxo bridge to the terminally coordinated peroxide. A hydrogen bond forms between the resulting hydroperoxide and the oxo bridge.[16] In the R2 protein, no monatomic bridge is observed in reduced state.[17] Upon reaction with dioxygen, however, a similar (μ-oxo)diiron(III) unit forms together with a functionally significant tyrosyl radical.[18-21] In sMMO hydroxylase, the bridging ligands vary with conditions. X-ray crystallographic studies have identified conditions under which the oxidized species can contain both (μ-hydroxo)bis(μ-

carboxylato)diiron(III) (μ-hydroxo)(μ-aqua)(μ-carboxylato)diiron(III), and (μ-hydroxo)diiron(III)cores.[10,22,23] In the reduced state, a bis(μ-carboxylato)diiron(II) core different from that of R2 is observed.[22,23] The core geometry of the Δ-9-desaturase enzyme is still unknown.

Significant progress has been made in modeling both the diiron(II) and diiron(III) forms of these proteins.[24-28] These studies have afforded valuable structural, spectroscopic and magnetic information, but only a few have focused on chemical reactivity, especially of diiron(II) with dioxygen.[14,15] Many of the important questions remaining to be answered for diiron carboxylate systems are dynamic in nature and can best be addressed by kinetic studies. Which bond is broken first in C-H activation, the O-O or the C-H bond? Which factors control the reversibility of O_2 binding? What are the intermediates along the reaction pathways? These questions are important to address directly for the protein, but detailed mechanistic studies on well-characterized models can also be of considerable value. Besides learning about the proteins through these studies, we also discover the deficiencies in the models which the next generation can incorporate features to overcome.

Only a few relevant kinetic studies have been published on model compounds and many of them concern ligand or bridge exchange reactions.[29,30] A detailed kinetic study of the autoxidation of cyclidene-based non-heme dioxygen carriers demonstrated the availability of an outer-sphere electron-transfer pathway when inner-sphere coordination of dioxygen was sterically prevented.[31-33] In other investigations, ferrous chelates generated in-situ afforded a metastable diferric peroxide species.[34,35] Preliminary results of a low-temperature kinetic study on reactions of dioxygen with a series of alkoxo-bridged compounds have been reported from our laboratory.[36]

In the present work, the kinetics of the reaction of dioxygen with two fully characterized diiron(II) model compounds have been studied. Both yield well-defined (μ-oxo)diiron(III) products, as shown in eqs 2.1 and 2.2. The

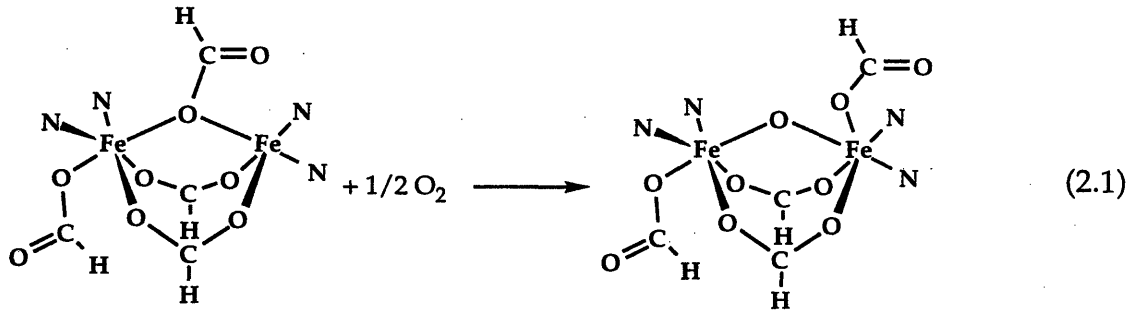

(2.1)

1a **1b**

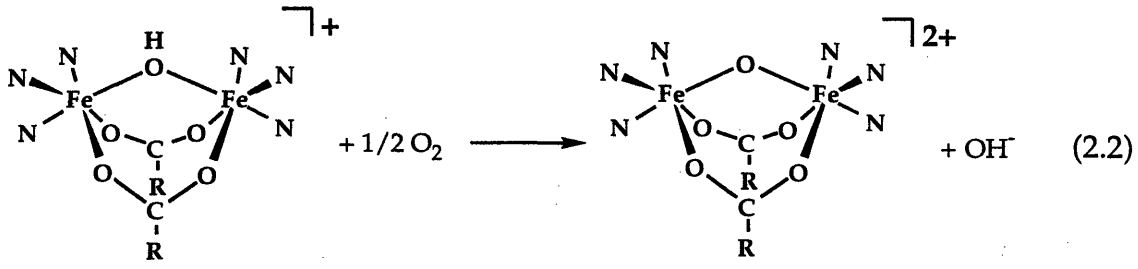

(2.2)

2a **2b**

reduced species are $[Fe_2(BIPhMe)_2(O_2CH)_4]$ (**1a**),[37,38] where BIPhMe = 2,2′-bis(1-methylimidazolyl)phenylmethoxymethane, and $[Fe_2(OH)(Me_3TACN)_2(OAc)_2](ClO_4)$ (**2a**),[39] Me_3TACN = 1,4,7-trimethyl-1,4,7-triazacyclononane. Upon reaction with dioxygen, these two complexes are oxidized in high yield (<95%) to $[Fe_2O(BIPhMe)_2(O_2CH)_4]$ (**1b**) and $[Fe_2O(Me_3TACN)_2(OAc)_2]^{2+}$ (**2b**), respectively. Kinetic results were obtained by stopped-flow spectrometry in which product formation was monitored. A portion of these results were previously published.[40] It should be noted that the preliminary discussion incorrectly identified the reaction order with respect to **1a** in this reaction.

Experimental

Preparation and Characterization of Compounds. 2,2′-Bis(1-methylimidazolyl)phenylmethoxymethane (BIPhMe) and $[Fe_2(BIPhMe)_2(O_2CH)_4]$ (**1a**) were prepared as previously described.[37,38] 1,4,7-Trimethyl-1,4,7-triazacyclononane (Me_3TACN) was synthesized according to a published procedure,[41] except for the detosylation step, which was carried out in 30% HBr in glacial acetic acid at reflux for 48 hours to yield 59.3% TACN•3HBr. This hydrobromide salt was used in the subsequent steps of the published procedure without further purification. $[Fe_2(OH)(Me_3TACN)_2(OAc)_2](ClO_4)$ (**2a**) was synthesized as previously reported.[39,42] Dry methanol was prepared by distillation from $Mg(OMe)_2$, and dry chloroform was obtained by distillation from CaH_2 after pre-drying with activated 4 Å molecular sieves.

Stopped-flow Kinetics Experiments. Two stopped-flow instruments were used during these experiments. Ambient temperature data (22 ± 1 °C) were collected by using an umbilical device, Applied Photophysics Rapid Kinetics Accessory RX-1000, fitted with Teflon flow lines and an argon-purged anaerobic attachment to avoid premature oxidation of air-sensitive solutions. Variable temperature data were collected with a Hi-Tech SF-41 Canterbury stopped-flow device fitted with Teflon-lined stainless steel flow lines. Once purged of dioxygen, these flow lines provided greater protection against premature oxidation and dioxygen leakage than standard Teflon lines and required no further purging with argon or nitrogen.

Optical absorption data were collected by using one of two independent detection systems depending on the time scale of the reaction. For reaction times greater than 1 min employing the RX-1000 device, a Hewlett Packard 8452A diode array spectrometer was used, allowing collection of multiwavelength data. Spectra as a function of time from 300 to 820 nm and

kinetic traces at single wavelengths were obtained. The resolution of this instrument was 2 nm and the fastest acquisition time was one spectrum every 2 s. For more rapid reactions and all experiments performed in the SF-41, a specially assembled fiber-optics spectrometer (components from Oriel Corp.) was used. It consisted of a visible light source (quartz-halogen lamp, 100W) irradiating a monochrometer (1/8 m, holographic grating 1200 lines/mm, blazed at 200 nm) connected to a fused-silica fiber-optics bundle. The monochromatic light was focused on the stopped-flow cell. A second fiber-optic bundle collected the transmitted light and irradiated a photomultiplier tube (Oriel 77341). Data were collected through software developed locally (Labview2 environment, National Instruments, Apple Macintosh IIfx computer) at a sampling rate such that approximately 1000 points were acquired over the course of the reaction with a linear time base. Data were analyzed with a statistical program (Kaleidagraph, Synergy Software) by non-linear least-squares regression on model-dependent equations. All reactions were followed for at least three half-lives at wavelengths appropriate for the detection of the products.

Solutions for the stopped-flow experiments were prepared anaerobically in a nitrogen-filled glove box (Vacuum Atmospheres) and loaded into gas-tight syringes (Hamilton) modified with Kel-F threaded adapters to fit the stopped-flow apparatus. Reaction orders with respect to the iron complexes were determined by the initial rate method,[43] by varying the concentration of complex solution. Pseudo-order conditions with a great excess of dioxygen ($\approx$ 5.7 mM in $CHCl_3$ and $\approx$ 5.2 mM in CH_3OH) were maintained throughout such experiments. Complex concentrations typically varied from 0.05 mM to 0.50 mM. Orders with respect to dioxygen were determined by saturating a reservoir containing pure solvent with a

dioxygen/nitrogen mixture. The O_2/N_2 ratio was controlled by the precise flow meters of a dynamic gas mixing system (Matheson, Inc.). The actual dioxygen concentrations in solution were calculated from the Ostwald's coefficient of O_2 in the appropriate solvent and the mole ratio of the gas mixture.[44] Reaction orders were obtained from the slopes of the $\ln(k_\psi)$ versus $\ln[O_2]$ plots, where k_ψ is the pseudo-order rate constant. When other additives were present, they were introduced as part of the oxygenated solutions. All experiments were repeated at least twice. Dioxygen concentrations were adjusted for solvent contraction in the variable temperature work based on a measured linear approximation of the solvent density.[45]

Manometric Analysis. Dioxygen uptake experiments in chloroform and methanol were conducted by using a mercury filled U-tube manometer and a calibrated sample cell. A detailed description of the apparatus and procedure is reported elsewhere.[38] In brief, the sample was loaded into the cell as a solution in a known volume of solvent (usually 11 mL for our cell). After degassing the sample by three freeze-pump-thaw cycles, the manometer was charged with a known pressure of dioxygen. The system was isolated from the gas inlet and the sample cell was opened to the manometer and allowed to equilibrate until the pressure remained constant. The change in pressure (ΔP) was corrected for dioxygen solubility in the solvent by subtracting the ΔP for a control reaction containing an equal volume of pure solvent and converted to moles of dioxygen based on a measured calibration constant derived from the ideal gas law. No differences in dioxygen uptake were detected when the solvent was changed. Data are reported as the mean of three separate uptake experiments.

Resonance Raman Experiments. Solutions of **2a** in methanol (≈ 5 mM) were prepared in the glove box in septum-sealed tubes. The samples were oxidized by addition of air or $^{18}O_2$ (91%) (Isotech). Spectra were recorded on an OMA III (EG&G PARC model 1460) analyzer and an intensified diode-array detector (EG&G PARC model 1455) attached to a 0.6 m single monochromator (SPEX, 2400 grooves/mm grating) with irradiation at 406.7 nm (Kr-ion laser, COHERENT Innova 90-K). To determine whether OH^- exchanges with the oxo bridge, 2 M NaOH in MeOH was added dropwise to ^{18}O-labeled **2b**.

NMR Studies. Solutions of **2a** (5-10 mM) in deuterated solvents (CD_3OD or $CDCl_3$) or ^1H solvents for ^2H NMR were prepared in a glove box under a nitrogen atmosphere. The septa-sealed tubes were removed from the box and flame sealed. Spectra were collected on a Varian XL300 spectrometer with a multinuclear probe. Temperatures were calibrated by using pure samples of methanol and the internal calibration routine of the instrument. Sweep widths of 1000 - 1333 ppm were scanned for features before focusing on individual peaks. Spectra were externally referenced to pure solvent or to tetramethylsilane.

Triphenylphosphine Oxidation. The possibility that triphenylphosphine might be oxidized to triphenylphosphine oxide was assayed either by GC (HP-5890, 12 m x 0.2 mm x 0.2 μm HP-101 column, fluid phase methylsilicone) or ^{31}P NMR spectroscopy. In a typical experiment, anaerobic solutions of the diiron(II) complex were prepared in the glove box in the presence of either 1 or 10 equiv of PPh_3. The sample was then removed from the box and opened to air. After complete oxidation of the iron(II) compound, the solutions were tested for the presence of Ph_3PO. Control reactions without iron were also carried out. Product spectra or GC retention times were compared to those of an authentic standard.

Measurement of the Solvent Contraction Correction Factor. A 5 mL sample of chloroform at 25 °C was accurately measured and placed in a narrow tube. The volume of this sample was determined at 5° temperature intervals between 25 and -45 °C and converted to density values based on the mass of the sample. A linear least-squares regression analysis of these data provided the temperature dependence of the solvent contraction.[45]

Computer Modeling. The tetranuclear transition state for the reaction of **2a** with dioxygen was modeled by using the CAChe MM2 package.[46] Initial structural parameters for the dinuclear domain were based on the crystal structure of the (μ-oxo)diiron(III) species **2b**. The peroxide O-O bond and the $Fe\text{-}O_{peroxo}$ initial parameters were based on the X-ray structure of $[Fe_6(O_2)(O)_2(OBz)_{12}(H_2O)_2]$ (**3**)[47] and then the Fe-O-O-Fe dihedral angle was artifically set to 0, 45 or 90 deg. Energy minimization was run from each of these starting points, fixing the dihedral angle so that it could vary no more than 10 degrees from the initial setting.

Results

Kinetics of the Reaction of 1a with Dioxygen in Chloroform. The stoichiometry of the conversion of **1a** into **1b** by dioxygen has been previously determined to be that shown in eq 2.1.[38] When chloroform solutions of **1a** and O_2 were mixed, a green-brown product appeared rapidly, the absorption spectrum of which corresponds to **1b**. This spectral transformation is shown in Figure 2.1. The build-up of the oxo-bridged complex was followed at 470 nm, a wavelength where only the product absorbs.[38] The data were mathematically fit to an expression of an integrated second-order build-up (eq 2.3) using up to 1000 experimental points per kinetic trace. A typical trace and the calculated fit are shown in the inset to Figure 2.1.

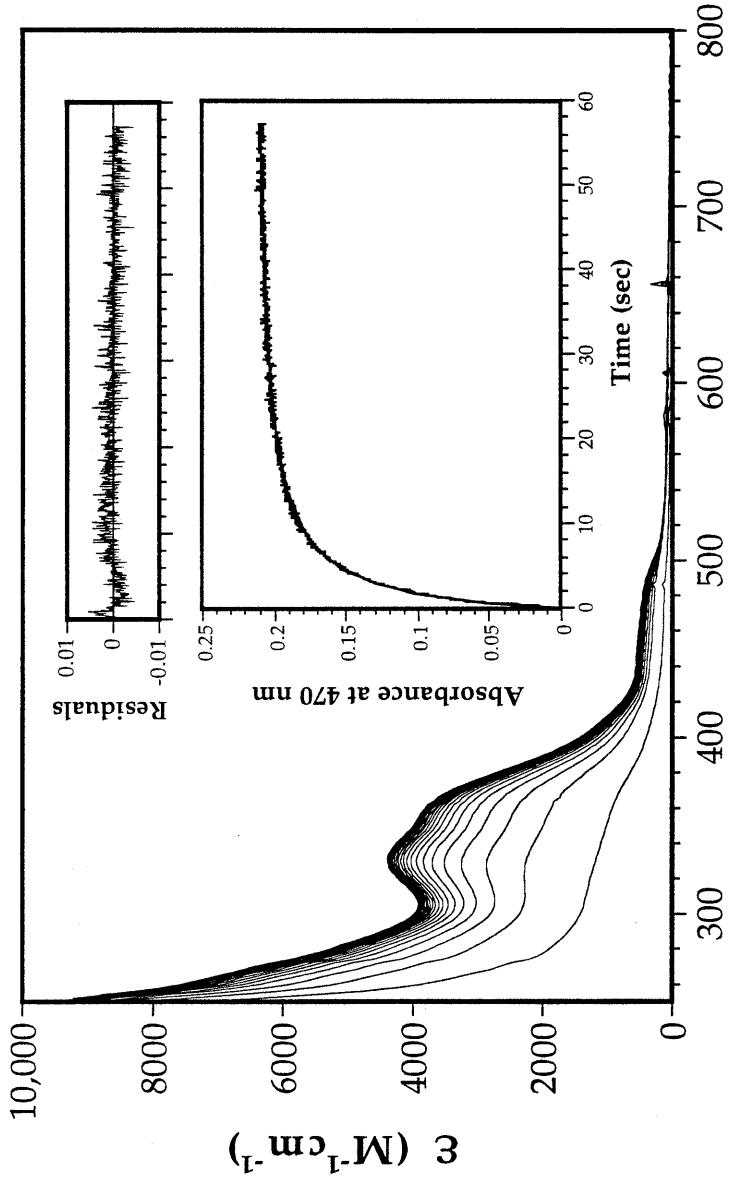

Figure 2.1. Spectral transformation during the reaction of 0.30 mM **1a** with dioxygen (5.7 mM) in $CHCl_3$ at 22 °C. The inset shows a kinetic trace obtained from a similar run collected at 470 nm with the single wavelength equipment. A fit to eq 2.3 is superimposed on the experimental data and the residual absorbance is shown.

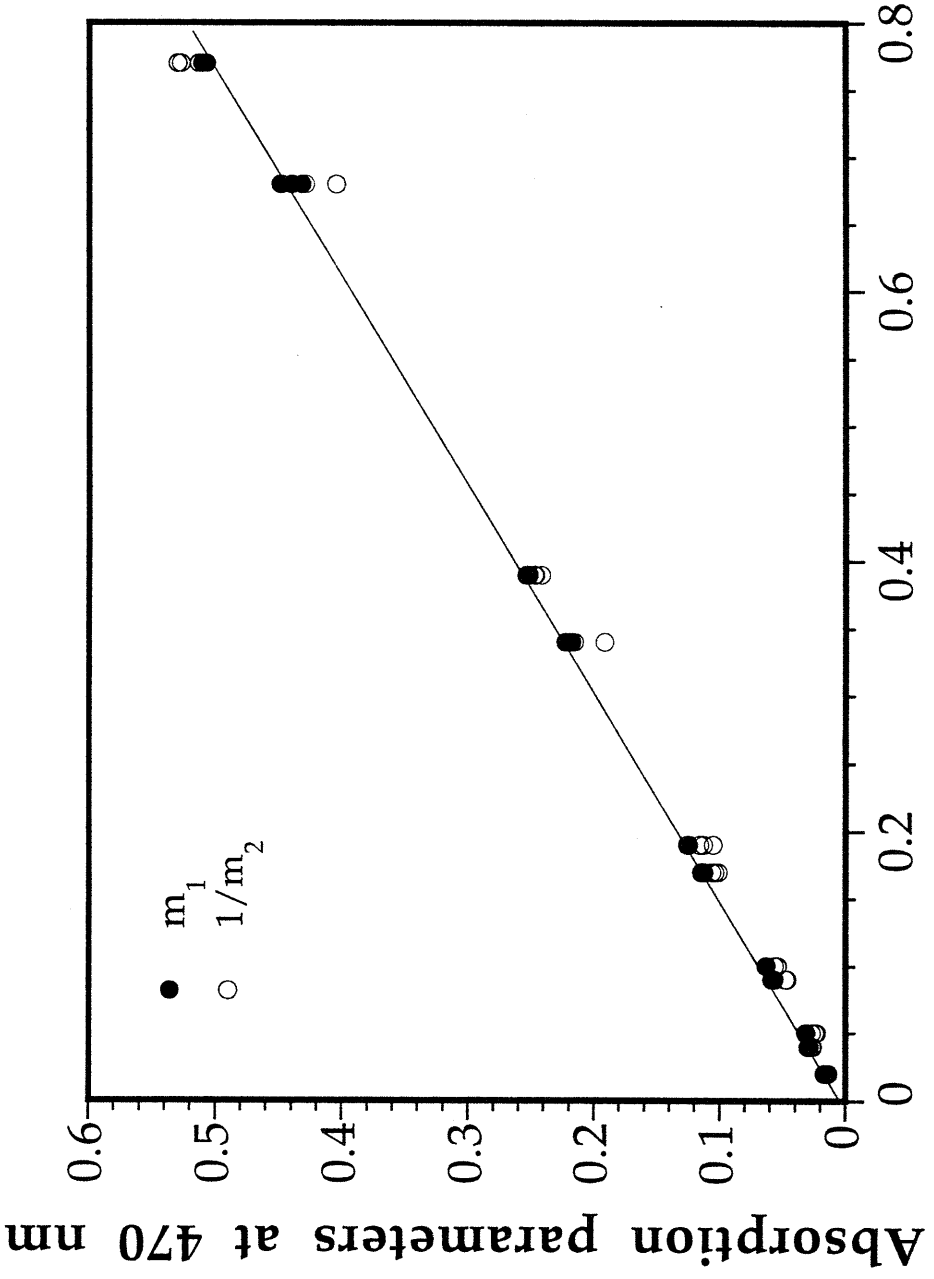

Figure 2.2. Beer's law analysis of the fitting parameters m_1 and $1/m_2$ for the oxidation of **1a** in $CHCl_3$ between 0.01 and 0.8 mM.

$$A(t) = m_1 - \frac{1}{m_2 + m_3 t} \tag{2.3}$$

In equation 2.3, A(t) is the measured absorbance at time t, m_1 represents the final absorbance for complete conversion of **1a** into **1b**, $1/m_2$ is the absorbance change during the reaction, and m_3 is related to k_{obs} by the extinction coefficient. At wavelengths where only the product absorbs, m_1 should equal $1/m_2$ at all concentrations and should obey Beer's law. A plot of m_1 and $1/m_2$ versus initial concentration of **1a** is given in Figure 2.2. An extinction coefficient of 657 ± 10 M^{-1} cm^{-1} was determined for **1b** at this wavelength, in reasonable agreement with the published value of 680 at 478 nm.[38] Values for the extinction coefficients reported here are per dinuclear molecule.

Reaction Order Versus Complex. The initial rate of the reaction (V_0) can be calculated from the fitting parameters according to eq 2.4. A plot of $\ln(V_0)$ versus ln([**1a**]) for data collected at 22 °C between 0.12 - 0.64 mM in the presence of large excesses of dioxygen (5.7 mM) is shown in Figure 2.3. This plot yields a reaction order of 2.0 ± 0.1 with respect to the diiron(II) complex. The rate constant for each of these conditions is provided in Table 2.S1.

$$V_0 = \left(\frac{dA(t)}{dt}\right)_0 = \frac{m_3}{(m_2)^2} \tag{2.4}$$

Reaction Order Versus Dioxygen. The saturation concentration of dioxygen dissolved in chloroform is 11.48 mM at 20°C.[44] In a stopped-flow experiment using a 1:1 ratio of the reaction components, however, the maximum accessible concentration of O_2 is only 5.74 mM since the diiron(II)

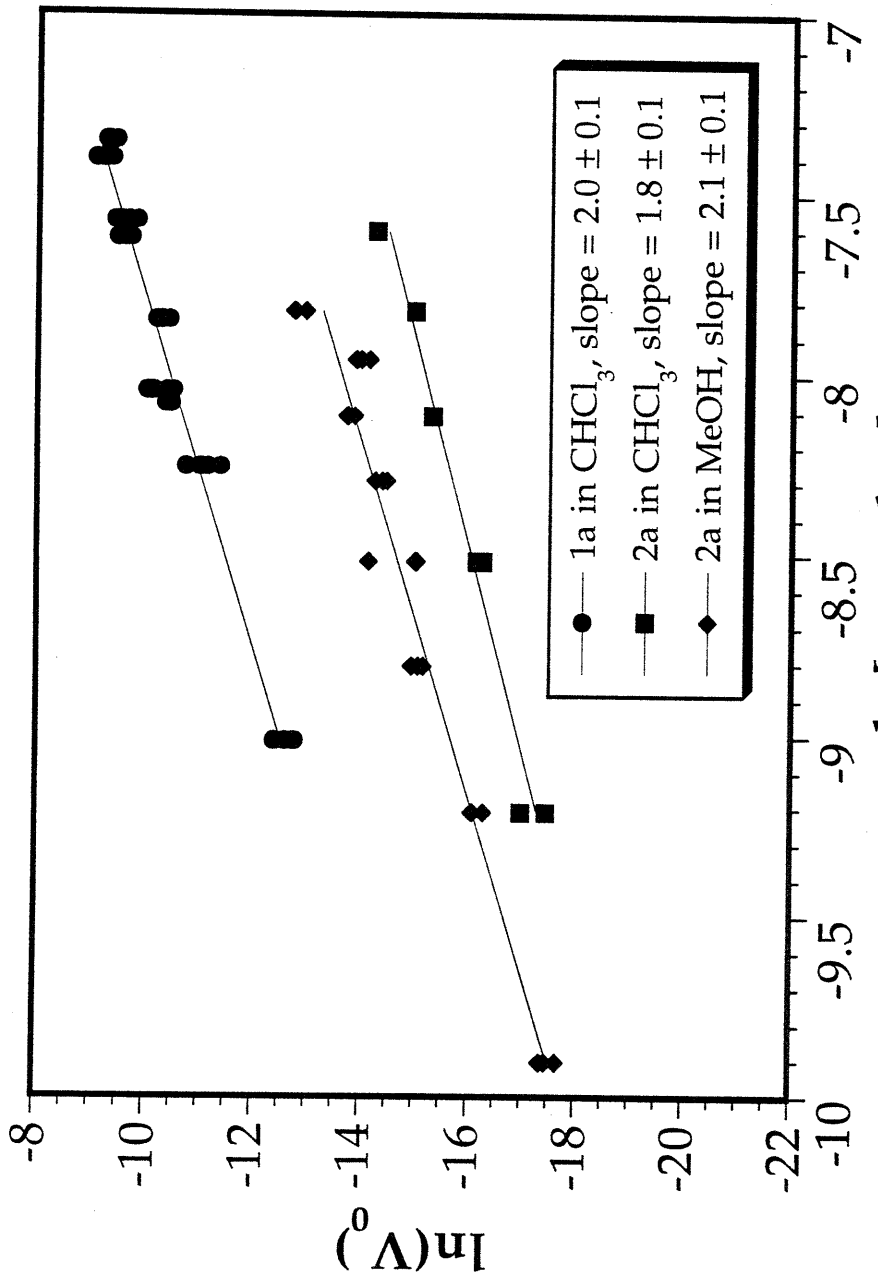

Figure 2.3. Plot of the ln(V_0) versus the ln([complex]$_0$) for the reactions of **1a** and **2a** with dioxygen in MeOH and $CHCl_3$. Linear least-squares fits (solid lines) are superimposed upon the experimental data, the slope of which equals the reaction order. Raw data are provided in Tables 2.S1 - 2.S3.

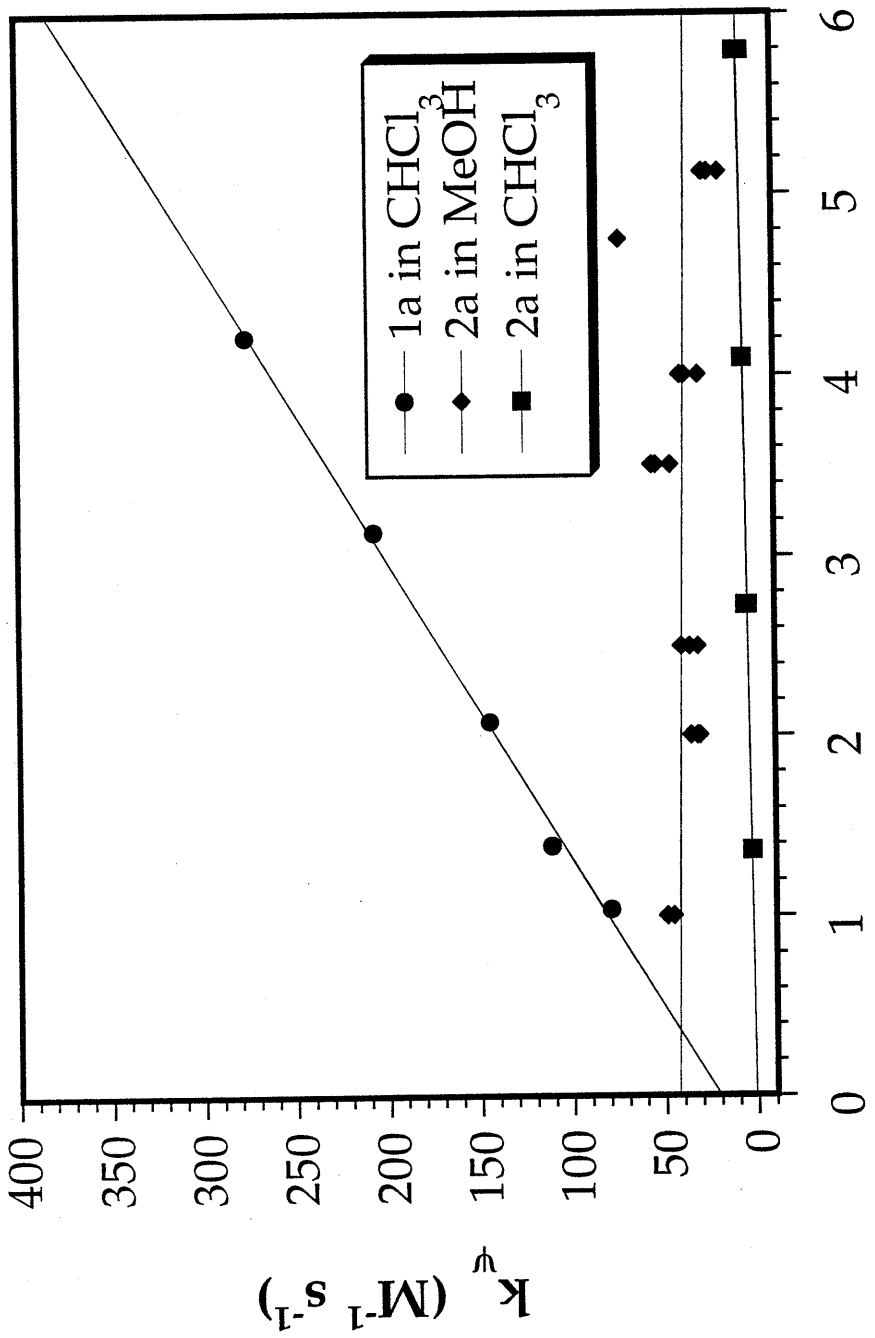

Figure 2.4. Plot of k_ψ versus $[O_2]$ for the reactions of **1a** and **2a** with dioxygen in $CHCl_3$ and MeOH. Data were collected at 22 °C. Linear least-squares fits (solid lines) are superimposed upon the experimental data. Raw data are provided in Tables 2.S4 - 2.S6.

solution must be free of dioxygen. Lower dioxygen concentrations, down to around 1.4 mM, were achieved by mixing N_2 and O_2 prior to dissolution in chloroform. Since the concentration of dioxygen greatly exceeded that of the diiron complex in all the experiments, it was approximated as a constant throughout the reaction. A plot of k_ψ versus $[O_2]$ (Figure 2.4) is linear, indicative of a reaction order of 1, and has a small positive intercept. This intercept (21 ± 5), if significant, might indicate the presence of a reversible step prior to dioxygen binding. Internal rearrangements required to provide dioxygen binding sites have been observed in other reactions of this type.[36,48] A plot of the $\ln(k_{obs})$ versus $\ln([O_2])$ is also linear and has a slope of 0.96 ± 0.10, confirming the conclusion that the reaction is first-order in dioxygen. The rate constant for each of these conditions is provided in Table 2.S4. The complete rate law for the oxidation of **1a** by dioxygen in chloroform is therefore given by eq 2.5. The reaction is third-order overall with a rate constant of (1.73 ± 0.31) x 10^5 at 20 °C.

$$\text{Rate} = k_\psi[\mathbf{1a}]^2 = k_{obs}[O_2][\mathbf{1a}]^2 \qquad (2.5)$$

Activation Parameters. Data were collected over a 75 °C temperature range to determine the activation parameters of the reaction of **1a** with O_2 (Table 2.S7). Since chloroform contracts significantly over this range, a correction factor was determined based upon a linear approximation for the solvent density as a function of temperature (Figure 2.S1). The experimentally determined equation for the density of chloroform as a function of temperature and the corresponding adjustment to the dissolved dioxygen concentration are given in eqs 2.6 and 2.7, respectively. Figure 2.5 shows an Eyring analysis of the data. The downward curvature of the plot in

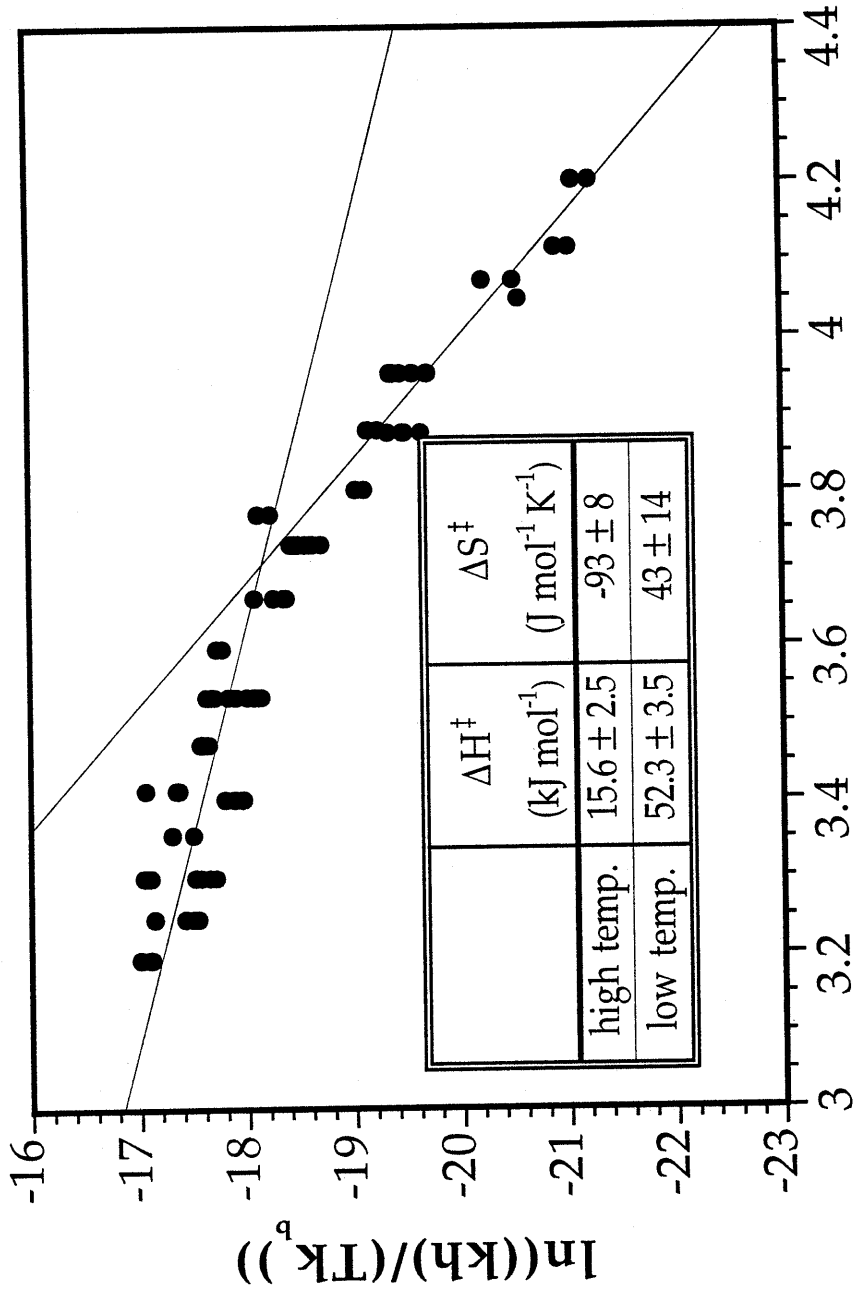

Figure 2.5. Eyring analysis for the reaction of 0.3 mM **1a** with 5.7 mM O_2 in $CHCl_3$ between -35 and 40 °C. Separate linear least-squares fits (solid lines) to high and low temperature regimes are superimposed on the experimental data. The high temperature range was defined as 5 - 40 °C and low temperature as -35 - 0 °C. Raw data are provided in Table 2.S7.

Table 2.1. Activation Parameters for the Reaction of **1a** and **2a** with Dioxygen in $CHCl_3$.[a]

Compound	temperature range (°C)	$\Delta H^{\ddagger}$ (kJ mol^{-1})	$\Delta S^{\ddagger}$ (J mol^{-1} K^{-1})	$\Delta G^{\ddagger}_{293}$ (kJ mol^{-1})
1a	5 - 40	15.6 ± 2.5	-93 ± 8	42.8 ± 4.8
1a	0 - -35	52.3 ± 3.5	43 ± 14	39.7 ± 7.6
2a	0 - 45	57.9 ± 1.4	-19 ± 5	63.4 ± 2.7

[a]The errors reported here are based on the the curve fitting as defined in the text. Because of the curvature of the plot and the potential error in defining the limits of the high and low temperature regimes, the actual error may be slightly greater.

$$\delta_T = 1.520(1) - 0.0018(1)*T \text{ (T in °C)} \quad (2.6)$$

$$[O_2]_T = \frac{[O_2]_{22°C}}{\delta_{22°C}} * \delta_T \quad (2.7)$$

shows an Eyring analysis of the data. The downward curvature of the plot in the center of the temperature range is apparent. This type of behavior indicates that the rate determining step changes over the temperature range employed.[43] The data from the high and low temperature regions were therefore treated separately to provide activation parameters for the independent steps. The calculated activation parameters are listed in Table 2.1.

At no time during the course of this reaction was an intermediate observed by optical spectroscopy. In freeze-quench experiments, however, a signal indicative of a mixed-valent species was previously reported during oxidation of **1a** in CH_2Cl_2.[38] In these experiments, the samples were frozen aproximately 30 seconds after exposure to air at -78 °C. From the activation parameters measured here and the concentrations used in the EPR experiments (1.7 - 5.5 mM) the half-life in these reactions can be estimated to be approximately 5 - 6 min. The main question, therefore, is whether the EPR

signal corresponds to a species along the oxidation pathway. This issues will be discussed further below.

Stoichiometry of the Reaction of 2a with Dioxygen. The oxidation of **2a** was previously shown to yield the (μ-oxo)bis(μ-carboxylato)diiron(III) complex **2b**.[39] The stoichiometry of this reaction was determined by manometry in both methanol and chloroform. Oxidation of one mole of the diferrous compound consumed 0.5 ± 0.1 mole of dioxygen in both solvents, thus the reaction proceeds as indicated in eq 2.2. These results show that, as for **1a**, all the oxidizing equivalents of molecular oxygen are consumed in converting diiron(II) to the (μ-oxo)diiron(III) core. Eq 2.2 further suggests that an equivalent of hydroxide is generated in the oxidation reaction. Resonance Raman experiments using $^{18}O_2$ have verified that the oxygen atom of **2b** derives from dioxygen and not from the bridging hydroxide ligand of the starting material (Figure 2.6). Since OH^- is generated by the reaction, we tested to see if free hydroxide exchanges with the μ-oxo ligand. Addition of several drops of 2 M NaOH solution to ^{18}O-**2b** resulted in no exchange of the oxo bridge. Addition of water has previously been shown to be an effective method of exchanging the bridging atom in (μ-oxo)diiron(III) complexes. Interestingly, the symmetric Fe-O-Fe vibration, which occurs in the expected frequency region for a tribridged (μ-oxo)diiron(III) compound,[27,49] appeared as a doublet in both the ^{16}O and ^{18}O samples, at 531, 518 and 512, 498 cm^{-1}, respectively. This splitting is observed in the solid state spectrum[50] as well as in the solution spectrum presented here. Since the feature is present in both states, it probably does not relate to a kinetic process of the system but rather to the coupling of the Fe-O mode to a second vibration in the molecule.

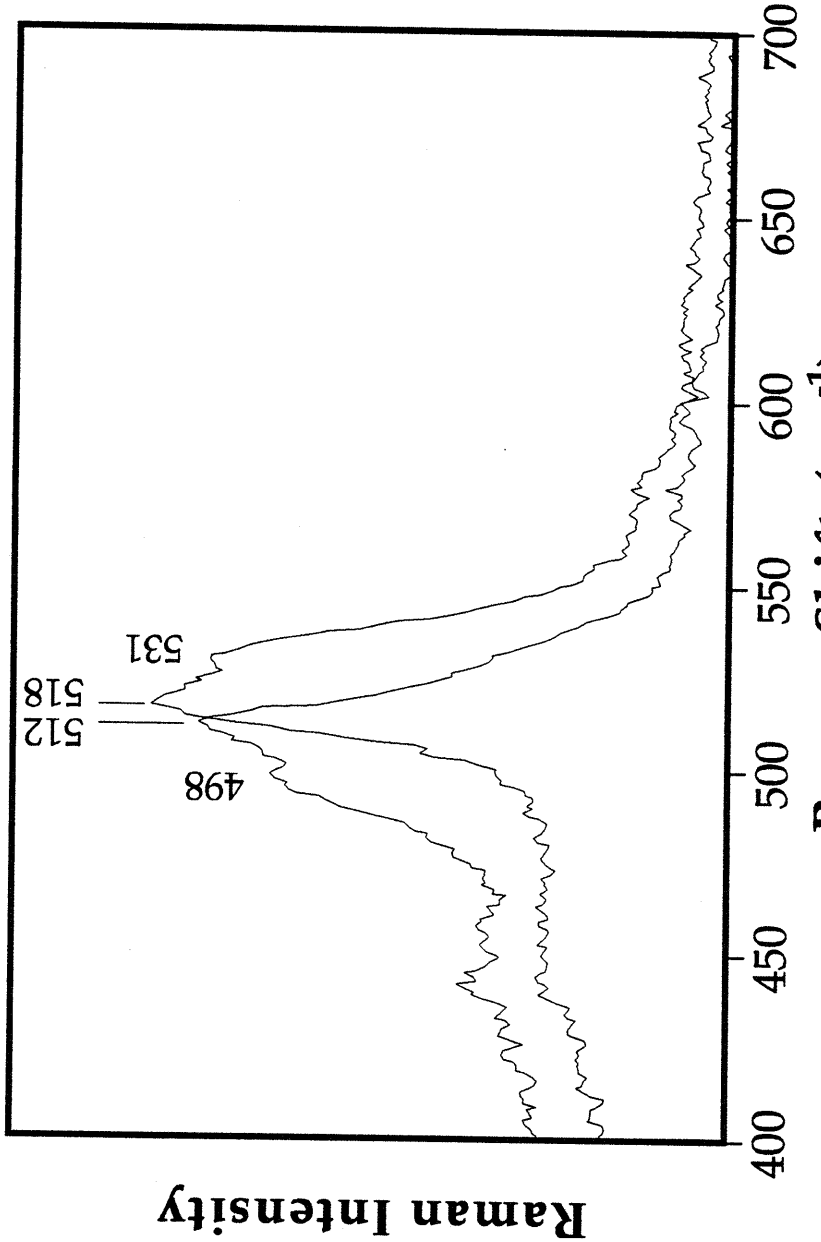

Figure 2.6. Resonance Raman spectra (406.7 nm irradiation) of **2b** (≈ 2 mM) from the reaction of **2a** with $^{16}O_2$ and $^{18}O_2$ in MeOH. Peaks at 531 and 518 cm $^{-1}$ correspond to the $^{16}O_2$ sample and the features at 512 and 498 cm^{-1} belong to the $^{18}O_2$ species.

Kinetics of the Reaction of 2a with Dioxygen in Chloroform and Methanol. The oxidation of **2a** to form **2b** was followed spectrophotometrically in a manner similar to that described above for **1a**. Figure 2.7 displays the spectral changes that accompany this transformation in chloroform solution. Kinetic traces were recorded at 474 nm and fit to a second-order build-up of (μ-oxo)bis(μ-carboxylato)diiron(III) product. Extinction coefficients of 1295 ± 20 in methanol, and 1197 ± 20 M^{-1} cm^{-1} in chloroform were determined from the fitting parameters as described for **1b**. Previously published values for the extinction coefficient of **2b** showed a significant dependence on the counter ion and solvent. For the hexafluorophosphate salt in water, ε_{475} = 1560 M^{-1} cm^{-1} and for the perchlorate salt in methanol, ε_{472} = 1450 M^{-1} cm^{-1}.[39]

Reaction Orders for Complex and Dioxygen. As shown in Figure 2.3, the reaction exhibits a second-order dependence on the concentration of the diferrous compound in both methanol and chloroform solution. The dependence of the reaction rate on the concentration of dioxygen differs in the two solvents, however (Figure 2.4). Under a large excess of dioxygen, the reaction is zero-order in $[O_2]$ in methanol, whereas in chloroform the reaction order is 0.9 ± 0.1. The saturation concentration of dioxygen in methanol is 10.4 mM at room temperature, defining the upper limit of accessible concentrations.[44] At high complex and low dioxygen concentrations in methanol, 1.25 and 0.1 mM respectively, the rate of the oxidation reaction becomes pseudo-first-order and the resultant traces can be fit to simple exponential growth curves. Because of limited solubility of **2a** and the difficulty of controlling dioxygen concentrations accurately at such low levels, independent reaction orders for the reactants could not be determined under these conditions. It is reasonable to assume, however, that the observed order

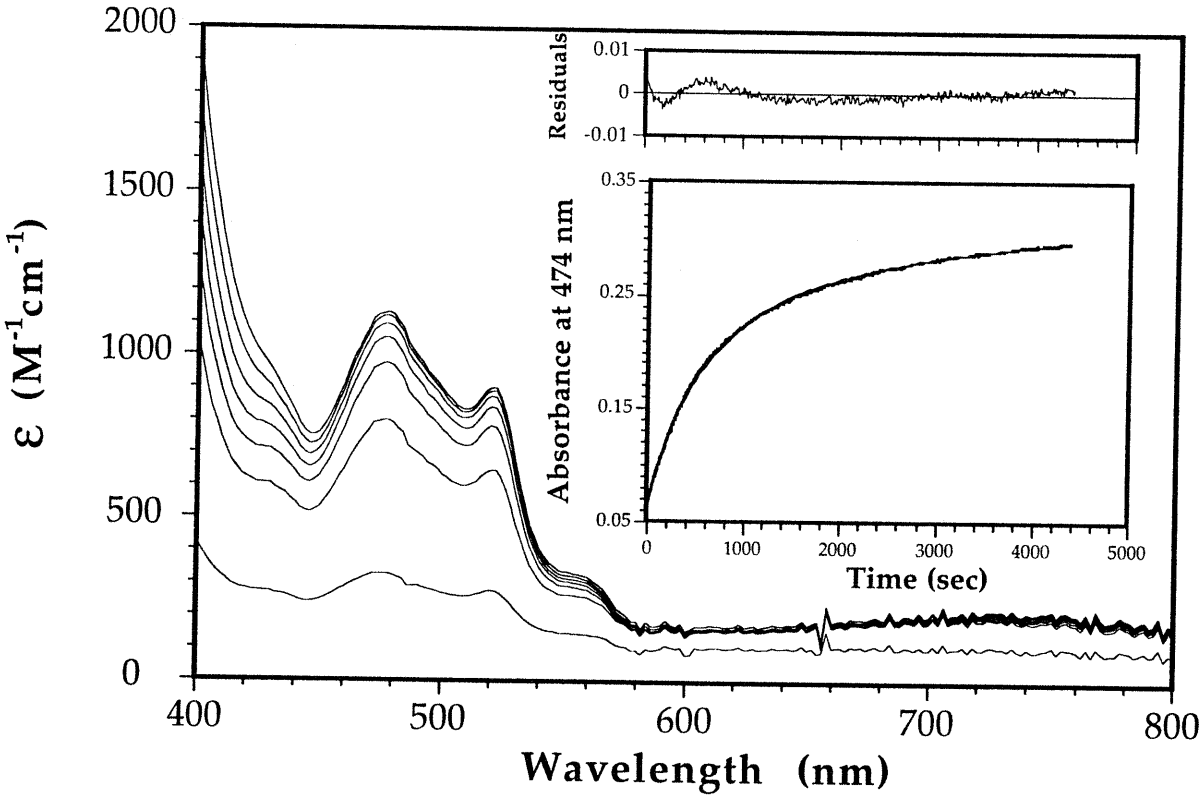

Figure 2.7. Spectral transformation during the reaction of 0.20 mM **1a** with dioxygen (5.3 mM) in MeOH at 22 °C. The inset shows a kinetic trace obtained from a similar run collected at 474 nm with the single wavelength equipment. A fit to eq 2.3 is superimposed on the experimental data and the residual absorbance is shown.

is due to dioxygen, and that the reaction is pseudo-zeroth-order in diiron(II) complex. From the foregoing results, the complete rate laws for the oxidation of **2a** to **2b** in methanol and chloroform can be expressed according to eqs 2.8 and 2.9, respectively. The mean values of the observed rate constants are 21.0 ± 8.6 M^{-1} s^{-1} in methanol and 1290 ± 508 M^{-2} s^{-1} in chloroform.

$$\text{Rate}_{\text{MeOH}} = \frac{d[\mathbf{2b}]}{dt} = k_{obs}[\mathbf{2a}]^2 \tag{2.8}$$

$$\text{Rate}_{\text{CHCl}_3} = \frac{d[\mathbf{2b}]}{dt} = k_{\psi}[\mathbf{2a}]^2 = k_{obs}[O_2][\mathbf{2a}]^2 \tag{2.9}$$

Temperature-Dependence of the Rate Constant. The temperature dependence of the reaction of **2a** with dioxygen was measured between 20 and 55 °C in methanol as shown in Figure 2.8. The Eyring plot of these data appears curved, but the inability to measure the kinetics at higher temperatures precluded further study of this phenomenon. The 55 °C data points were omitted from the subsequent curve fitting. The activation parameters are provided in Table 2.1.

Observation of Kinetic Intermediates. Figure 2.9 shows the time dependence of the dioxygen reaction over the region from 500 to 800 nm in an expanded view. A very small but reproducible broad feature was observed to grow in and then decay. Dinuclear iron-peroxide adducts exhibit a charge transfer band around 600 nm.[15,36,51-54] Unfortunately, the product **2b** absorbs in this region which complicates data analysis. Attempts to use global analysis failed, the small optical density changes being ascribed to the error term. By extracting single wavelength data at 670 nm, the complicated line shape could be fit to the sum of a first-order decay and a second-order growth (eq. 2.10), as shown in the inset to Figure 2.9. In this equation, $m_1 = A_\infty$, m_2 =

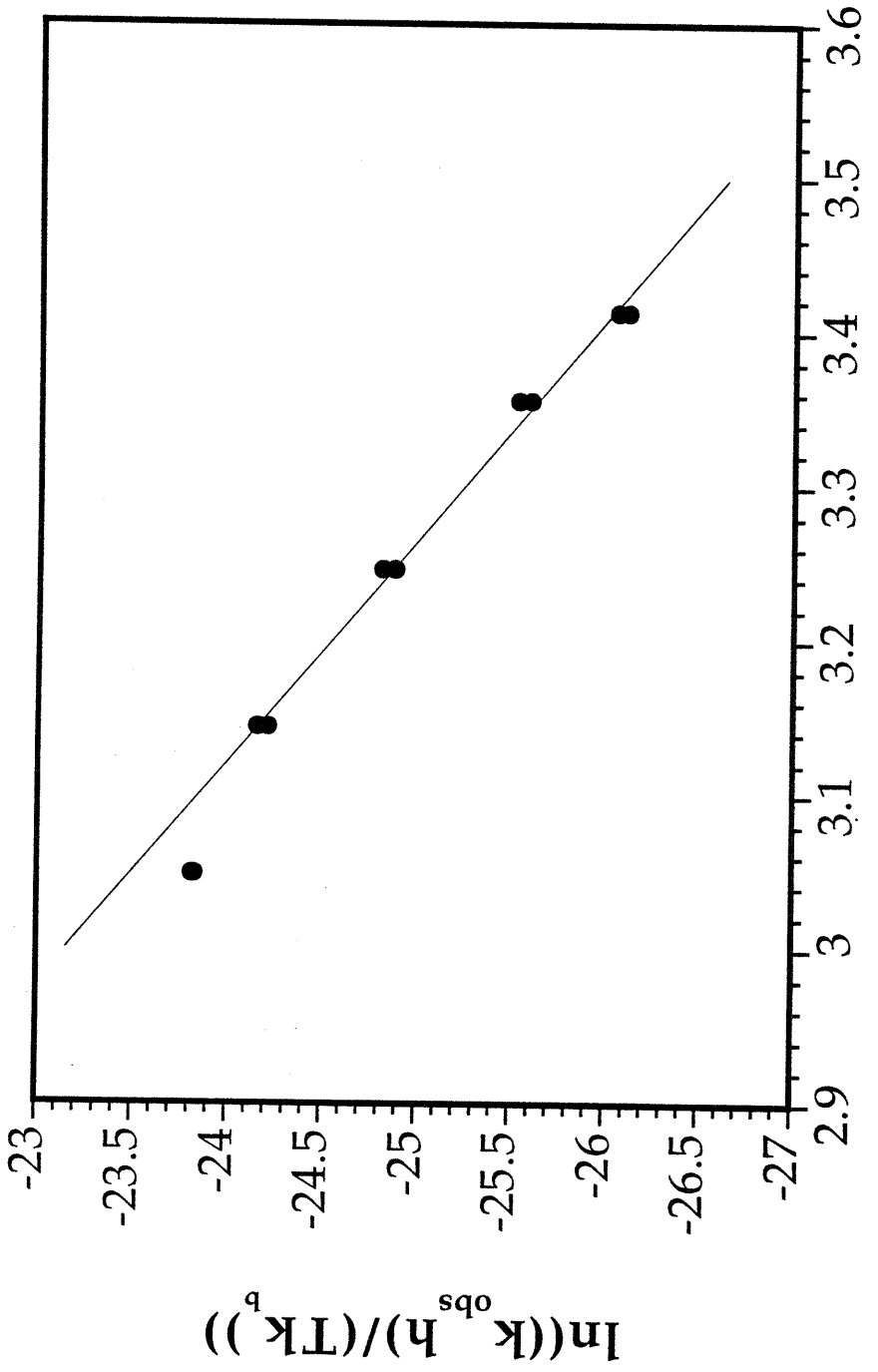

Figure 2.8. Eyring analysis for the reaction of 0.2 mM **2a** with 5.3 mM O_2 in MeOH between 20 and 55 °C. The linear least-squares regression shown for these data does not reflect the contribution of the 55°C data as discussed in the text. Raw data are provided in Table 2.S8.

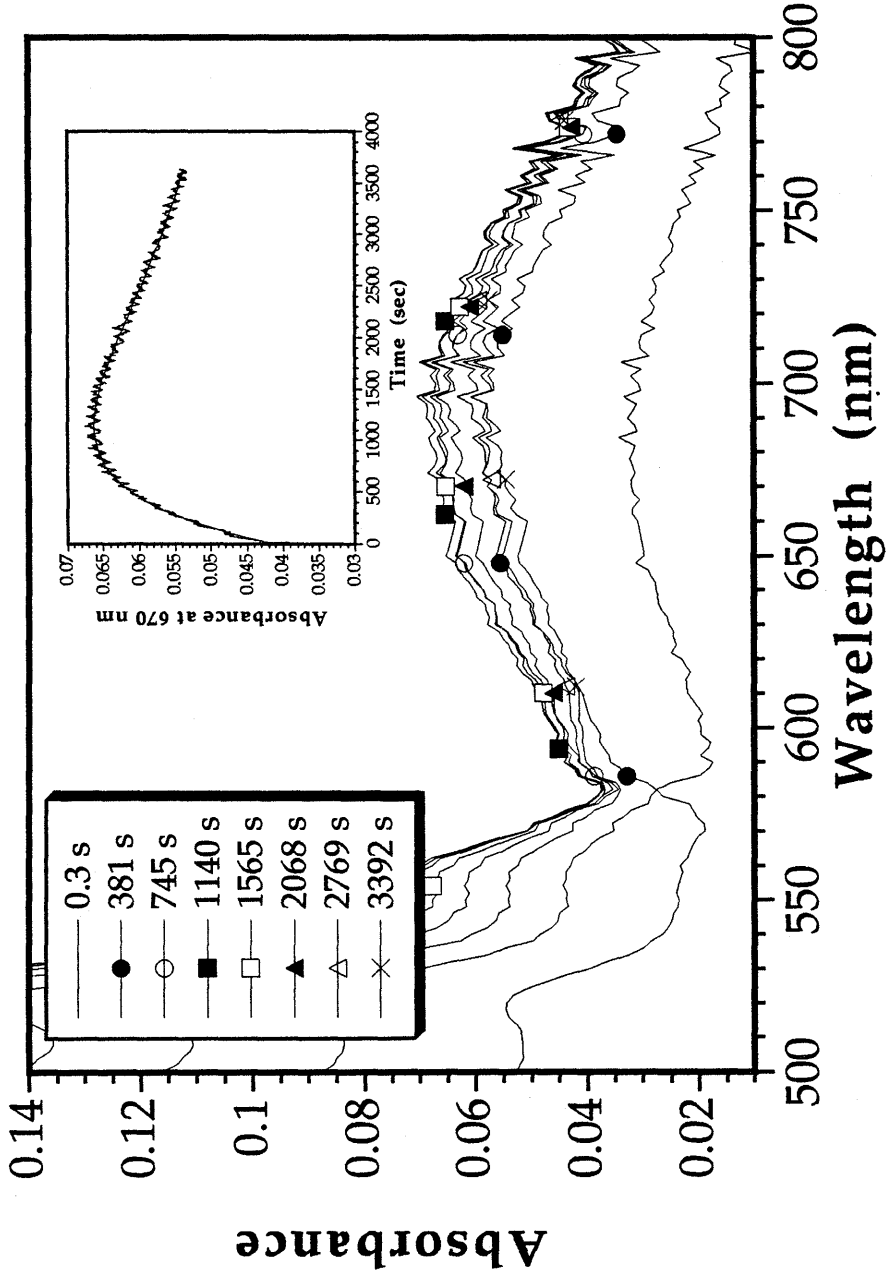

Figure 2.9. Expanded view of the optical spectrum of an intermediate during the reaction of **2a** (0.50 mM) with dioxygen (1.2 mM) in $CHCl_3$ at 22 °C. Inset trace shows the absorbance at 670 nm as a function of time. Superimposed on these data (solid line) is a least-squares fit based on eq 2.10.

$$A(t) = m_1 - \frac{1}{m_2 + m_3{*}t} + m_4{*}e^{-m_5{*}t} \qquad (2.10)$$

$1/\Delta\varepsilon_p$, the inverse of the absorbance change due to the reaction product, m_3 is the rate constant for the second-order component, $m_4 = 1/\Delta\varepsilon_I$, the absorbance change due to the intermediate and m_5 is the first-order rate constant of the decay phase. Since the rate constants have different units, it is easier to compare values for the half-lives of the reactions. Under the conditions measured, $t_{1/2}$ was approximately 900 s for the first-order decay and 1300 s for the second-order growth phases.

NMR Spectral Evidence for Carboxylate Exchange. Both of the iron atoms in **2a** are coordinately saturated. If the reaction of this complex with dioxygen were to proceed by an inner-sphere mechanism, a site for O_2 coordination must be available. A likely route for this process is by carboxylate shift, in which one of the bidentate bridging acetates becomes monodentate terminal.[55] Variable temperature ^1H and ^2H NMR studies were therefore carried out in order to determine whether the carboxylate bridges exchange with free acetate in solution at a rate sufficient to be considered fast with respect to the observed oxidation. Complete exchange can be considered the extreme carboxylate shift. The more common monodentate-bidentate shift must occur at a rate equal to or faster than the substitution reaction. The addition of sodium d_3-acetate to **2a** resulted in the loss of the broad ^1H signal at ≈ 23 ppm (T = -30 °C) associated with the bound acetate, indicating it to be in rapid exchange with free acetate. Concomitantly, a resonance at ≈ 23 ppm appeared in the ^2H spectrum. As the temperature was raised above -30 °C, broadening of the free and bound d_3-acetate signals occurred, although

coalescence of these resonances did not take place at temperatures up to 60 °C. The temperature dependent ^2H spectra are shown in Figure 2.10. Similar carboxylate ligand exchange was identified for **1a** in a previous study.[38]

Addition of Triphenylphosphine. Triphenylphosphine, a good acceptor in oxo-transfer reactions,[56] was added to test for the possible formation of a high-valent oxo (ferryl or perferryl) intermediate. No such species could be trapped. Triphenylphosphine oxide was not detected by gas chromatography or by ^{31}P NMR spectroscopy in reactions of **1a** or **2a** with dioxygen.

Discussion

Mechanistic Consideration of the Reaction of $[Fe_2(BIPhMe)_2(O_2CH)_4$ (1a) with Dioxygen. The primary feature of the reaction with dioxygen is the second-order dependence on the concentration of the diiron(II) species. Based solely on stoichiometric values, a mechanism was proposed for this oxidation reaction several years ago (Scheme 2.1).[38] The present kinetic data strongly support this earlier proposal. Since ternary collisions are statistically improbable, a net third-order reaction usually results from consecutive binary collisions, which is not uncommon. For all three species to appear in the overall rate equation, the second collision must be the rate-determining step in the observed transformation.

Two general reaction schemes fit the data. The first, and more probable one, consists of dioxygen reacting reversibly with the diferrous compound to form an intermediate, $\mathbf{I_1}$. This intermediate then reacts with another equivalent of the starting material to afford the product, probably passing through a tetranuclear transition state, $[\mathbf{I_2}]^{\ddagger}$. This later collision is the rate-determining step and $[\mathbf{I_2}]^{\ddagger}$ rapidly forms two equivalents of product (eq 2.11). The rate law corresponding to this sequence is given in eq 2.12 and reverts to

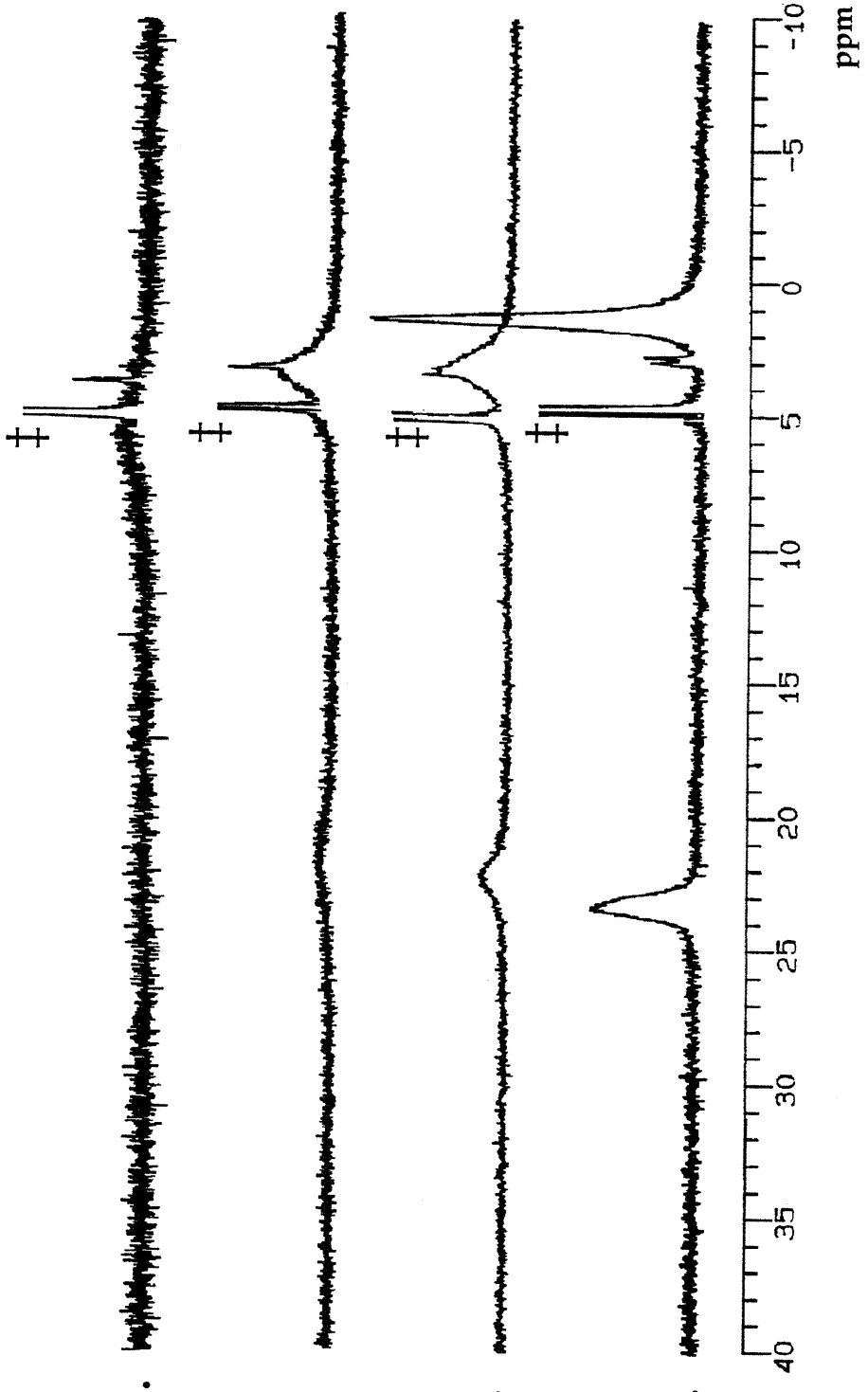

Figure 2.10. ^{2}H NMR of **[2a]** in MeOH solution in the presence of excess CD_3COONa. Temperature dependence of the free and bound acetate resonance. A = 50 °C, B = 30 °C, C = 10 °C, D = -30 °C. **[2a]** = 18.6 mM.

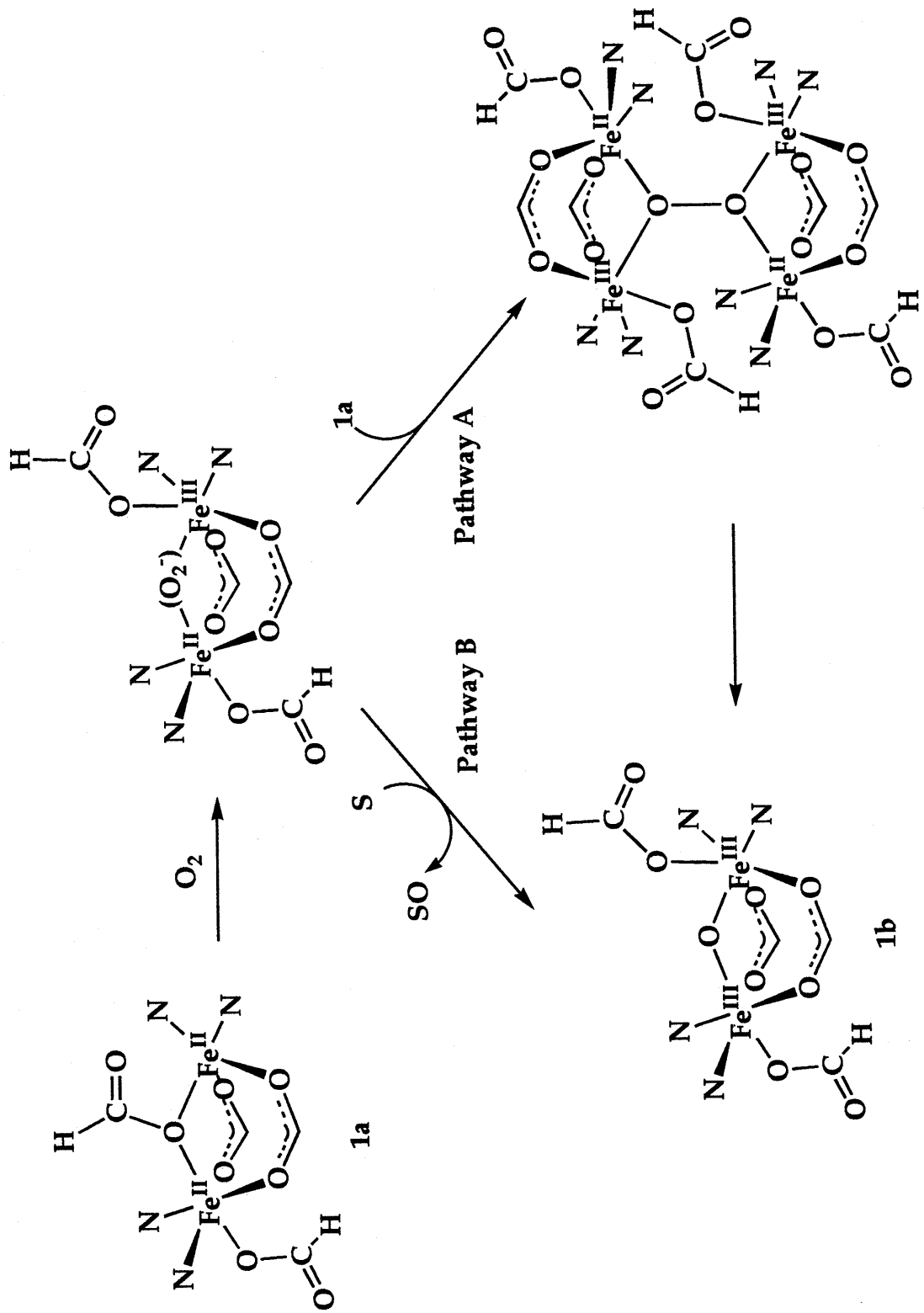

Scheme 2.1. (Reprinted with permission from ref. 38. © American Chemical Society, 1991)

$$\mathbf{1a} + O_2 \underset{k_{-1}}{\overset{k_1}{\rightleftharpoons}} I_1 \xrightarrow[k_2]{+\,\mathbf{1a}} 2\,(\mathbf{1b}) \tag{2.11}$$

$$\frac{d[\mathbf{1b}]}{dt} = k_\psi[\mathbf{1a}]^2 = \frac{2k_1k_2[\mathbf{1a}]^2[O_2]}{k_{-1} + k_2[\mathbf{1a}]} \tag{2.12}$$

the observed rate law under conditions where $k_{-1} >> k_2[\mathbf{1a}]$. Another reaction scheme that is kinetically indistinguishable from the one presented has two molecules of **1a** colliding to form a tetranuclear iron(II) species which then reacts with a dioxygen molecule (eq 2.13). The rate law derived from a steady-state analysis is shown in eq 2.14. We prefer the mechanism depicted in eq 2.11, however, since other diiron(II) compounds react similarly.[36,48]

$$2\,(\mathbf{1a}) \underset{k_{-1}}{\overset{k_1}{\rightleftharpoons}} I_1 \xrightarrow[k_2]{+\,O_2} 2\,(\mathbf{1b}) \tag{2.13}$$

$$\frac{d[\mathbf{1b}]}{dt} = k_\psi[\mathbf{1a}]^2 = \frac{2k_1k_2[\mathbf{1a}]^2[O_2]}{k_{-1} + k_2[O_2]} \tag{2.14}$$

A chemical interpretation of the pathway from eq 2.11 is given in Scheme 2.2. This proposed mechanism has some significant differences from that in Scheme 2.1. The most important difference is that the initial reaction with dioxygen is reversible. The intercept in the plot of k_ψ versus $[O_2]$ is slightly larger than 3σ. If this feature is significant, it implies yet another reversible step, K_0, not shown in Scheme 2.2 prior to k_1. This feature would be a rearrangement of the diiron(II) species into a state more reactive with O_2 and would most likely involve a carboxylate shift. However, a small error in the concentration of O_2 in solution could also lead to this intercept. The second difference between Schemes 2.1 and 2.2 is that pathway B is omitted in

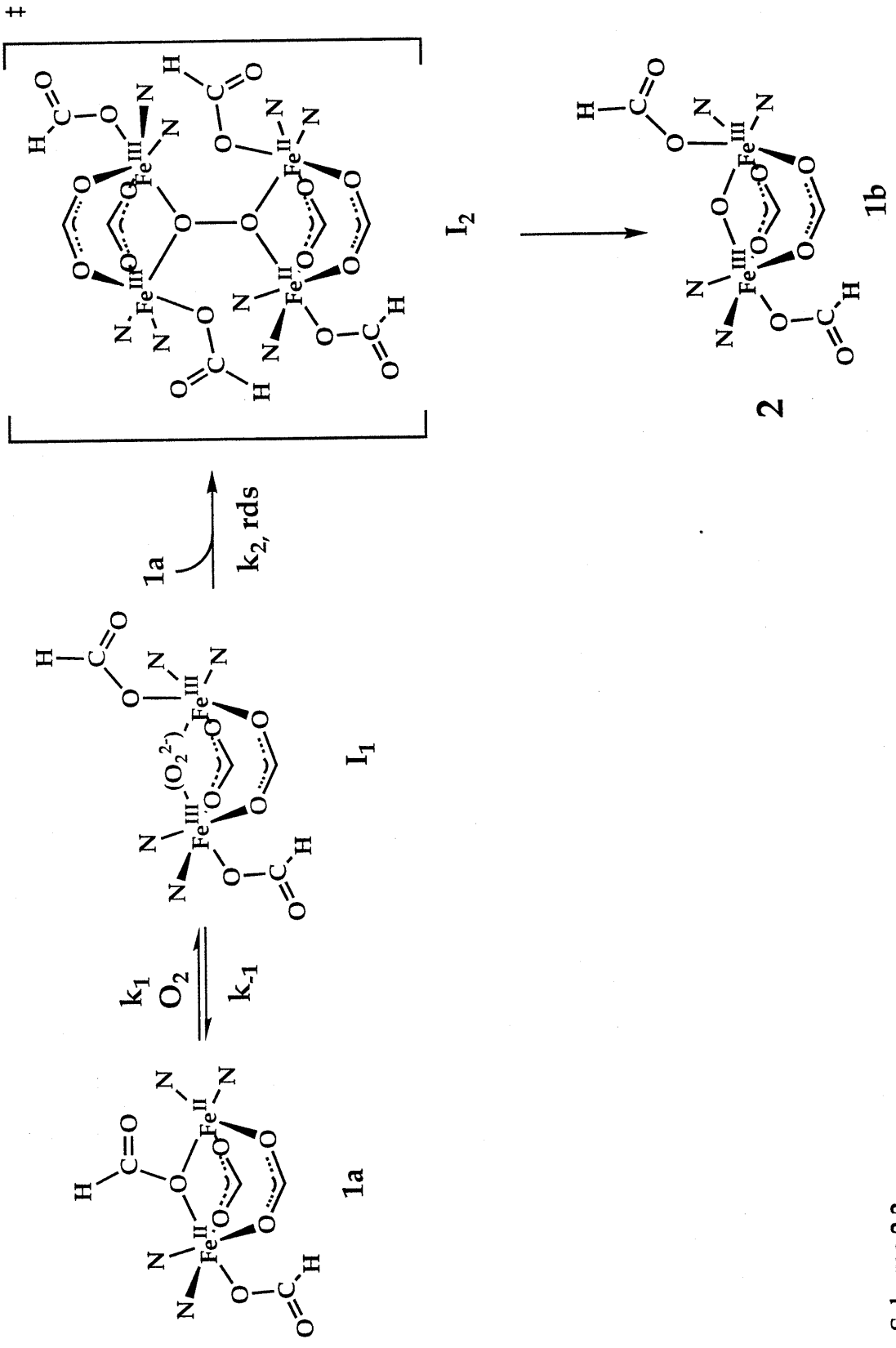

Scheme 2.2.

the latter. The intermediate I_1 does not appear to have the oxidizing power to carry out oxo transfer chemistry, even in the presence of very efficient oxo acceptors.

A final question concerning the reconciliation of the two reaction schemes is the oxidation states of the iron atoms. In the original scheme, the dioxygen binding step was proposed to be accompanied by one-electron transfer forming a superoxide adduct. This assignment was based on the EPR signal discussed above. $[\mathbf{I_2}]^{\ddagger}$ cannot be responsible for this mixed-valent signal. The overall third-order behavior identifies this species as the transition state, so no build-up is possible. $\mathbf{I_1}$ was drawn in Scheme 2.2 as a diferric peroxide in analogy to the reactions of other diiron(II) systems.[51,53,57,58] The 2-electron processes clearly dominate the behavior of these model compounds and the diiron proteins. Optical absorbtion in the 600 nm region characteristic of such adducts has not been observed during the reactions of **1a** with dioxygen, but its absence could arise from low steady-state concentrations. In our opinion, a rapid equilibrium between $\mathbf{I_1}$ and the mixed-valent superoxide adduct is most likely responsible for the observed EPR signal, although this electronic configuration cannot be excluded.

One of the main questions concerning compound **1a** is whether or not an open site exists for dioxygen binding. Formally, this complex has a vacant coordination site on one of the iron atoms, as revealed by the X-ray structure. In early studies of **1a** attempting to mimic the anion binding behavior of metHr, the complex was allowed to react with a variety of potential ligands.[38] No species containing a coordinated anionic or neutral ligand was observed, however. This behavior was ascribed to a steric hindrance by the dangling oxygen atom of the monodentate bridging formate ligand of the "pentacoordinate" iron atom.

Even though added ligands do not appear to bind **1a**, carboxylate exchange reactions are facile. The concept of the carboxylate shift was developed in part on the properties of **1a** which, upon addition of R'COONa, rapidly exchanges its formate bridges for the new carboxylate.[38,55] The complete exchange of a carboxylate presumably passes through an intermediate monodentate state. The open form is then the reactive intermediate in the exchange, and would be susceptible to replacement by an incoming ligand. This shifting of the carboxylate is also called upon in the oxidation mechanism. A shift from a bridging to a terminal mode is proposed to allow dioxygen adduct formation ($\mathbf{I_1}$). An analogous shift is required in the product forming step k_2.

The temperature-dependence of the reaction of **1a** with O_2 shows significant curvature (Figure 2.5 and Table 2.1) and can be best explained by the presence of two transformations contributing to the k_2 reaction. At low temperature, the activation parameters are typical of a dissociative reaction. A large activation enthalpy is observed with a modest favorable entropy term. Upon moving to the higher temperature regime, the measured values resemble an additive or associative process with a smaller enthalpic term and a large unfavorable entropy. Throughout the study, the kinetic traces are second-order with respect to **1a** and the reaction is third-order overall. This implies that both the dissociative and associative steps contribute to the k_2 process. The aforementioned equilibrium could involve either **1a** or $\mathbf{I_1}$, but since exchange processes involving Fe^{III} are generally slower than those of Fe^{II},[59] equilibria of $\mathbf{I_1}$ should be more easily frozen out than those of **1a**. $\mathbf{I_1}$ must therefore be involved in a rearrangement on approach to $[\mathbf{I_2}]^{\ddagger}$. One might predict that either a carboxylate shift or a change in the coordination mode of the peroxide ligand from a 1,2-bridging mode to a μ-1,1-geometry is

involved in this dissociative process. The observed rate law does not require this equilibrium process to have a stable intermediate, I_1', although such a species is also not precluded. Were it to exist, the kinetic constants pertaining to its formation and decay would be absorbed into the constant k_2 and subsequently into the k_{obs} values.

The formation of polynuclear peroxo intermediates is well documented in the literature of iron(II)-porphyrin systems[60-63] and a diiron(III) peroxo intermediate in the pathway of sMMO hydroxylase has recently been identified.[58] A non-heme iron peroxide compounds has also been structurally characterized, $[Fe_6(O_2)(O)_2(OBz)_{12}(H_2O)_2]$ (**3**) (Scheme 2.3).[47] The complex has an in-plane μ,μ-η^2:η^2-peroxide ligand surrounded by four ferric ions. Synthesized by addition of hydrogen peroxide to basic iron benzoate, this core is presumably stablized toward reductive cleavage of the O-O bond because the ferric ions cannot be easily oxidized to iron(IV). The structure of the proposed transition state $[\mathbf{I_2}]^{\ddagger}$ in Scheme 2.2 is similar to that of the $\{Fe^{III}_4O_2\}$ core in **3** (Scheme 2.3), existence of which lends support to our hypothesis. Since the proposed unstable species contains two ferric ions and two ferrous ions, in contrast to the four ferric centers in **3**, rapid O-O bond homolysis is expected with concomitant oxidation of the two iron(II) ions. Unfortunately, O-O bond cleavage occurs after the rate determining step in reaction 2.11, so the present kinetic data do not provide conclusive information regarding this process.

Mechanistic Consideration of the Reaction of $[Fe_2(OH)(Me_3TACN)_2(OAc)_2](ClO_4)$ (2a) with Dioxygen. For **2a**, the reaction is zero-order with respect to dioxygen in methanol but first-order in chloroform. It is second-order with respect to complex in both solvents. The results in chloroform are

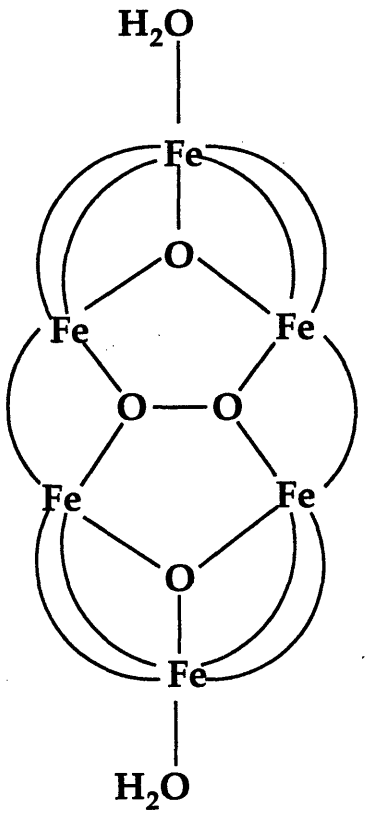

3

Scheme 2.3.

consistent with a mechanism analogous to that proposed for the reaction of **1a** with dioxygen (eq 2.11). This simple scheme does not account for the behavior in methanol, however. One possible explanation is the reaction shown in eq 2.13. If the k_1 step is rate-limiting, the order in O_2 would be zero. From a chemical perspective, however, this reaction is unattractive because it is hard to picture how O_2 can interact with the putative Fe_4 core. Furthermore, no evidence for this tetrairon species is present under anaerobic conditions. Another possibility is that **2a** reacts completely with O_2 to form $\mathbf{I_1}$ prior to the onset of the bimolecular decay reaction. This type of behavior is observed for some diiron(II) compounds (see Chapter III), but results in build-

up of the $\mathbf{I_1}$ intermediate. This species is not observed in MeOH. Finally, a reversible step prior to O_2 binding might account for a reduced order in O_2. Scheme 2.4 presents the correspondingly modified, solvent-assisted mechanism. We postulate that a carboxylate shift, facilitated by a coordinating solvent such as methanol, occurs. The direct, rapid reaction of **2a** with O_2 to form $\mathbf{I_1}$ in methanol is less likely. Optical studies in chloroform have observed an intermediate which is not detected in methanol. The transition state structure $[\mathbf{I_2}]^{\ddagger}$ is not drawn explicitly in Scheme 2.4, but is believed to be analogous to that shown in Scheme 2.2 for **1a**.

The rate equation derived from the reactions depicted in Scheme 2.4 by using a steady state approximation is given by eq 2.15. It can be simplified for the two different solvents, chloroform and methanol, as indicated in eqs 2.16 and 2.17, respectively. In both solvents, step k_4 is assumed to be rate determining such that $k_4[\mathbf{2a}] << k_{-3}$. This assumption requires binding of O_2

$$\frac{d[\mathbf{2b}]}{dt} = \frac{2k_3k_4\left(k_{-1} + k_2[O_2]\right)[\mathbf{2a}]^2[O_2] + 2k_1k_2k_4[\mathbf{2a}]^2[O_2]}{\left(k_{-3} + k_4[\mathbf{2a}]\right)\left(k_{-1} + k_2[O_2]\right)} \qquad (2.15)$$

in both solvents: $k_{-3} \gg k_4[2a]$

in $CHCl_3$: $k_{-1} \gg k_2[O_2]$

$$\text{rate}_{CHCl_3} \cong \frac{2k_4[\mathbf{2a}]^2[O_2]\left(k_{-1}k_3 + k_1k_2\right)}{k_{-1}k_{-3}} \qquad (2.16)$$

in MeOH: $k_2[O_2] \gg k_{-1}$ and $k_1 \gg k_3[O_2]$

$$\text{rate}_{MeOH} \cong \frac{2k_4[\mathbf{2a}]^2\left(k_3[O_2] + k_1\right)}{k_{-3}} \approx \frac{2k_1k_4[\mathbf{2a}]^2}{k_{-3}} \qquad (2.17)$$

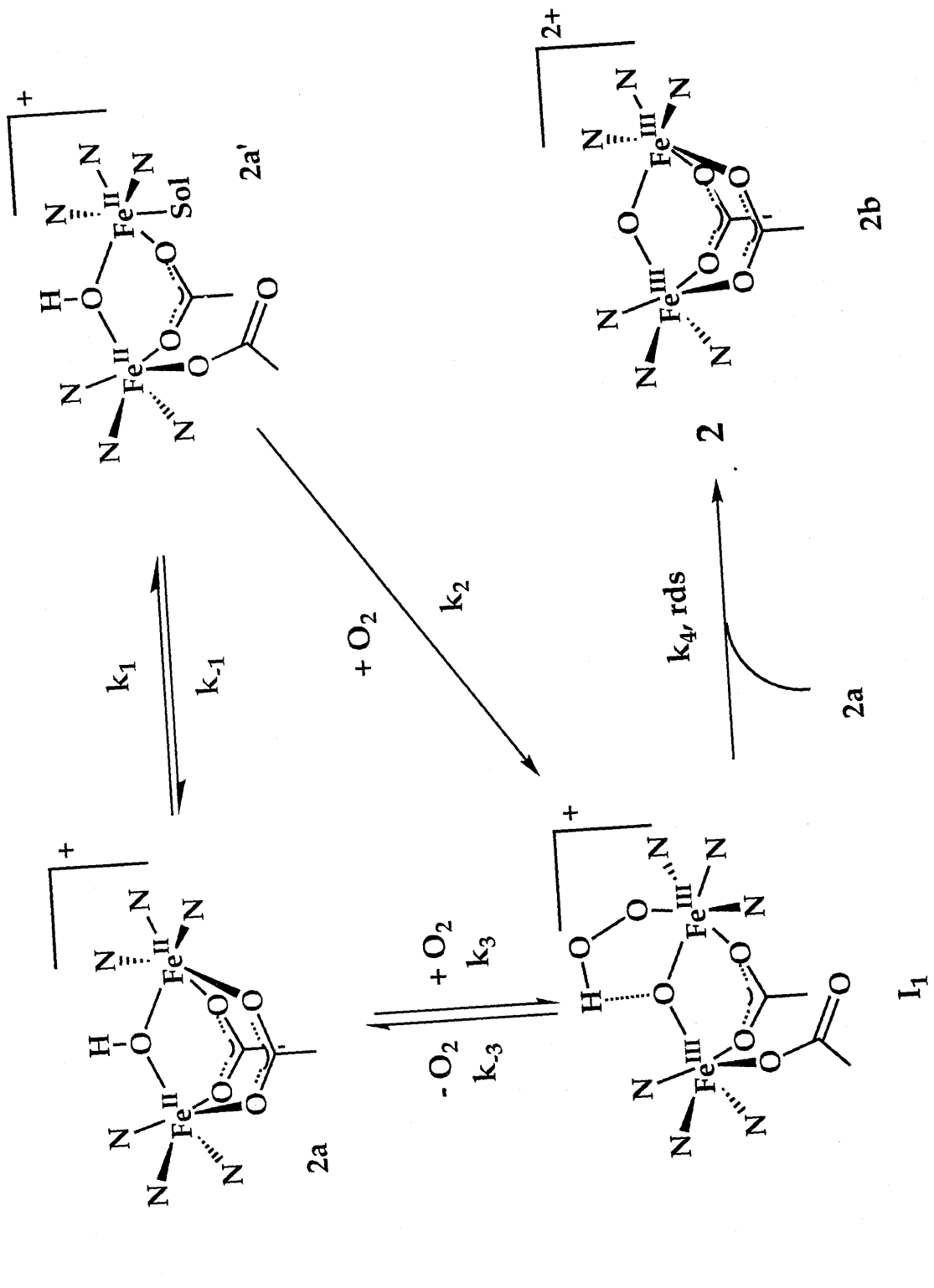

Scheme 2.4.

is fast compared to the bimolecular reaction leading to formation of the tetranuclear peroxide transition state and product **2b**. In chloroform, the solvent-assisted carboxylate shift equilibrium is unfavorable, [**2a'**] is small, and k_{-1} is large relative to $k_2[O_2]$. In methanol however, k_{-1} is small compared to $k_2[O_2]$ and k_1 is greater than $k_3[O_2]$. These inequalities yield eq 2.17, which accounts for the observed zero-order dependence on $[O_2]$ in this solvent. Scheme 2.4 also explains why the reaction rate in methanol is significantly faster than in chloroform, even though step 4 is rate determining in both cases. The open site required for O_2 coordination is pre-formed in **2a'**, making it more reactive toward O_2 or $\mathbf{I_1}$. Recent work has also addressed the role of solvents in carboxylate shift reactions. It was shown that polar protic solvents such as methanol favor monodentate versus bidentate coordination.[64] The observed change in the rate law for **2a** → **2b** under conditions of limiting dioxygen is also consistent with the mechanism in Scheme 2.4. This behavior arises from the new inequality $k_2[O_2] \ll k_{-1}$ and the condition that [**2a**] is approximately constant during the course of the reaction (eq 2.18).

$$\frac{d[\mathbf{2b}]}{dt} \approx \frac{2k_4\left(k_1 + k_3[O_2]\right)[\mathbf{2a}]^2}{\left(k_{-3} + k_4[\mathbf{2a}]\right)} \qquad (2.18)$$

As in the Eyring analysis of the reaction of **1a** with dioxygen, some curvature occurs in the temperature versus reaction rate plot for **2a** (Figure 2.8, Table 2.S8). Unfortunately, the high temperature regime could not be adequately studied since it extended beyond the upper limit of our current instrumentation. The activation enthalpy is similar in magnitude to that of

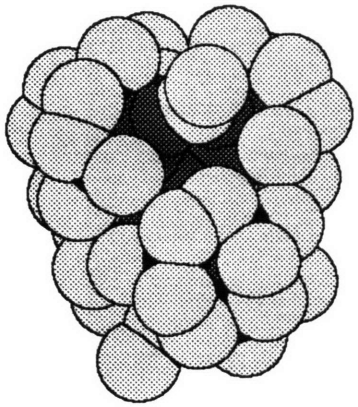

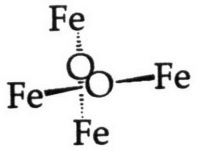

dihedral angle = 85.2°
relative energy: 587 kcal/mol

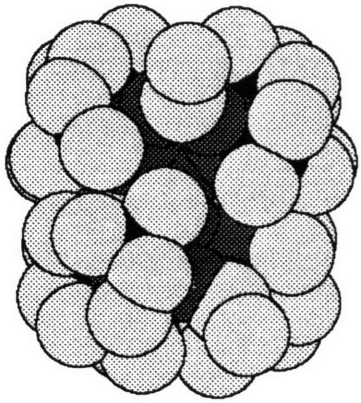

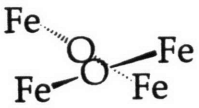

dihedral angle = 43°
relative energy: 670 kcal/mol

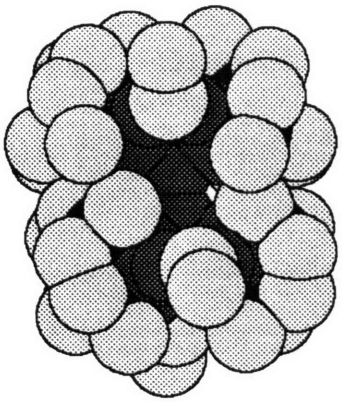

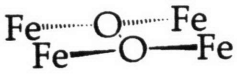

dihedral angle = 2.3°
relative energy: 794 kcal/mol

Figure 2.11. Results of CAChe molecular modeling of the $[\mathbf{I_2}]^{\ddagger}$ transition state for the reaction of **2a** with O_2. Space filling diagrams are oriented such that the O-O bond lies along the long axis of page.

1a where the dissociative component of the reaction dominates. The entropic term is unfavorable, but quite small.

Results of a computer modeling study on $[\mathbf{I_2}]^{\ddagger}$ for the reaction of **2a** with O_2 are shown in Figure 2.11. The question was whether this tetranuclear species could form due to potential steric contacts between the methyl groups on the Me_3TACN ligand. The quantitative energy values from MM2 calculations of this type are not accurate because of the inadequacies of the force field. Relative values between the orientational isomers do provide some measure of the favored states, however. The difference between the three states in Figure 2.11 is the Fe-O-O-Fe dihedral angle. The other geometric parameters are similar in the mimized structures. The calculations show that only one orientation of the Fe_2OOFe_2 core, that with an FeOOFe dihedral angle of approximately 90°, is reasonable. The other species have extremely high energy contacts involving ligand atoms. In all three minimized structures, the O-O bond distance was a long 1.60 Å. Locking in a shorter bond length of 1.48 Å resulted in higher energy species. Since this complex is proposed to be a transition state on the path to O-O cleavage, the elongated bond was not considered to be problematic.

The variable temperature NMR study of **2a** (Figure 2.10) supports the idea of a solvent-assisted equilibrium. As explained above, carboxylate exchange can be considered the extreme of a carboxylate shift reaction. The component steps in exchange of a bidentate bridging carboxylate consist of the breaking and forming of the two Fe-O bonds. The carboxylate shift, however, must occur at a rate equal to or greater than the complete substitution reaction. The slow exchange region can be monitored at low temperature in methanol and room temperature lies in the intermediate exchange region with respect to the NMR time scale. The coalescence of the free and bound

acetate signals is not observed in the NMR due to the inability to access the necessary temperatures in methanol solution. These results show that at room temperature and above, the carboxylate shift is facile relative to the formation of **2b**. At -30 °C and below the exchange is frozen out.

An intermediate in the reaction of **2a** with dioxygen was observed, but proved difficult to characterize spectroscopically. It appears only in chloroform solutions as a green transient with a weak absorption spectrum. The absorption maximum occurs at approximately 670 nm, a region associated with peroxide-to-iron(III) charge transfer bands.[51-53,57] The weakness of the signal could result either from a low concentration of the chromophore or a small extinction coefficient. The former is more likely since all known non-heme peroxodiiron(III) complexes with absorption features in this region have extinction coefficients between 1000 and 2000 M^{-1} cm^{-1}.[51-53,57] Attempts to observe ν(O-O) in the resonance Raman spectrum by exciting time-resolved or freeze-quenched samples at 647.1 nm were unsuccessful.

Recently, the asymmetric, coordinately unsaturated compound $[Fe_2(O)(OAc)_2(Me_3TACN)(bpy)](PF_6)_2$ was reported to have catalase activity.[65] The structure of the proposed diiron(III) peroxo intermediate in that study is quite similar to that of $\mathbf{I_1}$ of Scheme 2.4. Compound **2b** was unable to disproportionate hydrogen peroxide under the same conditions, because it is coordinately saturated.[65] The results of both this study and the present work clearly indicate the need for a vacant site(s) at the dinuclear iron center for binding of O_2 or H_2O_2. Without such a vacancy, intermediates involving carboxylate shifts will probably be required.

Comparison of Kinetic Results for the Two Compounds. The reactions of **1a** and **2a** with dioxygen are remarkably similar. Both traverse a

polynuclear iron-peroxide transition state on their way to the (μ-oxo)diiron(III) products. When studied under a narrow set of conditions, the reactions appear quite simple. As the temperature-dependent studies and the solvent effects indicate, however, these reactions are more complex. In view of the solvent-dependence of the **2a** oxidation, it seems possible that a similar effect could occur for **1a**. Unfortunately reaction of **1a** with O_2 in methanol led to the formation of an intractable yellow precipitate which was not further characterized. A detailed study of the oxidation kinetics in this solvent was therefore not undertaken.

In Schemes 2.2 and 2.4, we have assumed oxidation of iron by an inner- rather than an outer-sphere electron-transfer mechanism. Outer-sphere mechanisms have been proposed for the autoxidation of several mononuclear iron(II) model compounds.[66] Our results, however, are best explained by reactions involving direct coordination of dioxygen to the metal center. In an outer-sphere process, there should be no need for a vacant coordination site or for the equilibrium processes we must invoke to explain the kinetic results. Furthermore, the complete incorporation of isotopic label into the oxo bridge when $^{18}O_2$ is employed is only consistent with an inner-sphere pathway.

The mechanisms presented for oxidation of **1a** and **2a** are also comparable to those deduced from studies of iron(II) porphyrin complexes with dioxygen, where diferric porphyrinato-peroxo complexes have been observed.[61-63,67] Here the O-O bond cleavage proceeds in a heterolytic manner, and ferryl species are observed as intermediates. Although the presence of ferryl or perferryl species in the present systems cannot formally be excluded, such species could not be trapped by triphenylphosphine. The lifetimes of these intermediates would have to be exceedingly short to subvert

oxo-transfer chemistry. The mechanisms presented in Schemes 2.2 and 2.4 in which O-O bond cleavage affords the (μ-oxo)diiron(III) products directly, are therefore preferred.

Implications for Non-Heme Iron Enzymes. The two complexes studied here react with dioxygen by a pathway that clearly is inaccessible to the enzyme systems. The initial dioxygen binding step is related to the formation of intermediates like H_{peroxo} in the sMMO hydroxylase system,[68] but a cascade of reactions involving the formation of polynuclear iron species occurs in the case of the model compounds. Proteins prevent such reactions kinetically by sequestering the diiron center deep within the folded polypeptide. In this manner, slower reactions leading to substrate activation become dominant. The intermediate observed in the reaction of **2a,** tentatively assigned as a diferric peroxide, is long-lived for a species of this type. Its low steady-state concentration, due to the presence of a rapid back reaction, makes it difficult to study, however.

The kinetic results agree strongly with a role of carboxylate shifts in controlling the behavior of the oxidation reactions. It is likely that similar dissociative steps are involved in the protein systems. Since dioxygen reactivity can be tailored so dramatically by this phenomenon, it appears to be an ideal mechanism for the biological control of active site reactivity. Carboxylate shifts could arise from the binding or dissociation of other protein components, such as protein B or reductase in the MMO system, substrate or other allosteric effectors. The role of the coupling protein in sMMO is still not known, but the proposed binding site, based on the crystal structure of the hydroxylase component, is ideally suited for such a regulatory role. Situated along helices E and F of the canyon, binding of protein B would be readily transmitted to the diiron center through helix motion. Further

studies with the enzyme system are addressing these issues. Already, several carboxylate shift motifs have been observed in sMMO hydroxylase crystals by varying the crystallization conditions.[23]

Implications for Modeling Studies. The present experiments strongly argue that proper design of biomimetic models for diiron(II) oxygen activating proteins must take into account the need to block bimolecular reactions of the core. Such processes have been avoided, or at least diminished, in some model systems by using ligands bulkier than BIPhMe or Me_3TACN.[51-53,57] The use of more sterically hindered ligands is clearly a step in the proper direction, and a kinetic study of three such complexes is presented elsewhere.[48,69] In these systems, greater stability of the peroxide intermediates is achieved and the separation of the two kinetic steps is possible. A further step toward minimizing bimolecular decay of the intermediates could be achieved by immobilization of the ferrous material on a solid support. By sequestering the dinuclear center in this way, second-order reactions would be eliminated without preventing access of a potential substrate. Such studies would more accurately reflect the role of the protein without resorting to elaborate ligand design.

Another possible approach that has not yet been tried would be to run the reactions under conditions of greater viscosity. The result could be to decelerate bimolecular reactions such as those observed in the decay of the peroxide intermediates. If slowed sufficiently, a unimolecular pathway leading to the formation of alternative intermediates might be observed. Such species might be more capable of carrying out oxo-transfer reactions than those intermediates studied here.

Conclusions

This work provides kinetic results for the reaction of dioxygen with two dinuclear non-heme iron protein models. Despite structural similarities with the protein cores, an alternative reaction ensues for these compounds. The first step involves dioxygen binding to a vacant coordination site, made available by a carboxylate shift reaction. This shift can be either solvent-assisted or not, depending on the conditions. Cleavage of the O-O bond occurs after the rate-determining step, the formation of a tetranuclear peroxide transition state. Therefore, little can be deduced about this critical process. An intermediate has been spectroscopically identified in the oxidation of **2a**, but owing to its low steady-state concentrations, it was not characterized much beyond its optical absorbance. Based solely on the optical spectrum and kinetic behavior, it has been assigned as a diiron(III) peroxide species. The observations reported here provide new constraints for the modeling community and have offered quantitative information concerning the kinetics of the biomimetic reaction of dioxygen with non-heme iron(II) complexes.

Acknowledgements. This work was supported by grants from the National Institute of General Medical Sciences (GM 32134) and AKZO.

References.

(1) Stenkamp, R. E.; Sieker, L. C.; Jensen, L. H.; McCallum, J. D.; Sanders-Loehr, J. *Proc. Natl. Acad. Sci., USA* **1985**, *82*, 713-716.

(2) Sanders-Loehr, J. In *Iron Carriers and Iron Proteins*; Loehr, T. M., Eds.; VCH: New York, 1989; Vol. 5; pp 373-466.

(3) Stenkamp, R. E. *Chem. Rev.* **1994**, *94*, 714-726.

(4) Nordlund, P.; Sjöberg, B.-M.; Eklund, H. *Nature* **1990**, *345*, 593-598.

(5) Stubbe, J. In *Advances in Enzymology and Related Areas of Molecular Biology*; Meister, A., Eds.; John Wiley and Sons: New York, 1990; Vol. 62; pp 349-420.

(6) Stubbe, J. *J. Biol. Chem.* **1990**, *265*, 5329-5332.

(7) Fontecave, M.; Nordlund, P.; Eklund, H.; Reichard, P. In *Advances in Enzymology and Related Areas of Molecular Biology*; Meister, A., Eds.; Wiley and Sons: New York, 1992; Vol. 65; pp 147-183.

(8) Fox, B. G.; Shanklin, J.; Somerville, C.; Münck, E. *Proc. Natl. Acad. Sci., USA* **1993**, *90*, 2486-2490.

(9) Fox, B. G.; Froland, W. A.; Dege, J. E.; Lipscomb, J. D. *J. Biol. Chem.* **1989**, *264*, 10023-10033.

(10) Rosenzweig, A. C.; Frederick, C. A.; Lippard, S. J.; Nordlund, P. *Nature* **1993**, *366*, 537-543.

(11) Lipscomb, J. D. *Annu. Rev. Microbiol.* **1994**, *48*, 371-399.

(12) Liu, K. E.; Lippard, S. J. *Adv. Inorg. Chem.* **1995**, in press.

(13) Howard, J. B.; Rees, D. C. In *Advances in Protein Chemistry*; Anfinsen, C. B., Edsall, J. T., Richards, F. M. and Eisenberg, D. S., Eds.; Academic: New York, 1991; Vol. 42; pp 199-280.

(14) Que, L., Jr. In *Bioinorganic Catalysis*; Reedijk, J., Eds.; Marcel Dekker: New York, 1993; pp 347-393.

(15) Feig, A. L.; Lippard, S. J. *Chem. Rev.* **1994**, *94*, 759-805.

(16) Shiemke, A. K.; Loehr, T. M.; Sanders-Loehr, J. *J. Am. Chem. Soc.* **1986**, *108*, 2437-2443.

(17) Åberg, A. Thesis, Stockholm University, 1993.

(18) Bollinger, J. M., Jr.; Edmondson, D. E.; Huynh, B. H.; Filley, J.; Norton, J. R.; Stubbe, J. *Science* **1991**, *253*, 292-298.

(19) Bollinger, J. M., Jr.; Tong, W. H.; Ravi, N.; Huynh, B. H.; Edmondson, D. E.; Stubbe, J. *J. Am. Chem. Soc.* **1994**, *116*, 8024-8032.

(20) Bollinger, J. M., Jr.; Tong, W. H.; Ravi, N.; Huynh, B. H.; Edmondson, D. E.; Stubbe, J. *J. Am. Chem. Soc.* **1994**, *116*, 8015-8023.

(21) Ravi, N.; Bollinger, J. M., Jr.; Huynh, B. H.; Edmondson, D. E.; Stubbe, J. *J. Am. Chem. Soc.* **1994**, *116*, 8007-8014.

(22) Rosenzweig, A., Frederick, C, and Lippard, S.J. unpublished results.

(23) Rosenzweig, A.; Frederick, C. A.; Lippard, S. J. *Biology and Chemistry* **1995**, *2*, 409-418.

(24) Murray, K. S. *Coord. Chem. Rev.* **1974**, *12*, 1-35.

(25) Lippard, S. J. *Chem. in Britain* **1986**, *22*, 221-227.

(26) Lippard, S. J. *Angew. Chem. Int. Ed. Engl.* **1988**, *27*, 344-361.

(27) Sanders-Loehr, J.; Wheeler, W. D.; Shiemke, A. K.; Averill, B. A.; Loehr, T. *J. Am. Chem. Soc.* **1989**, *111*, 8084-8093.

(28) Que, L., Jr.; True, A. E. *Prog. Inorg. Chem.* **1990**, *38*, 97-200.

(29) Drüeke, S.; Wieghardt, K.; Nuber, B.; Weiss, J.; Fleischhauer, H.-P.; Gehring, S.; Haase, W. *J. Am. Chem. Soc.* **1989**, *111*, 8622-8631.

(30) Watton, S. P.; Masschelein, A.; Rebek, J., Jr.; Lippard, S. J. *J. Am. Chem. Soc.* **1994**, *116*, 5196-5205.

(31) Dickerson, L. D.; Sauer-Masarwa, A.; Herron, N.; Fendrick, C. M.; Busch, D. H. *J. Am. Chem. Soc.* **1993**, *115*, 3623-3626.

(32) Sauer-Masarwa, A.; Dickerson, L. D.; Herron, N.; Busch, D. H. *Coord. Chem. Rev.* **1993**, *128*, 117-137.

(33) Busch, D. H.; Alcock, N. W. *Chem. Rev.* **1994**, *94*, 585-623.

(34) Purmal, A. P.; Skurlatov, Y. I.; Travin, S. O. *Izvestiya Akademii Nauk. SSSR, Seriya Khimicheskaya* **1980**, *3*, 492-497.

(35) Nishida, Y.; Yoshizawa, K.; Takahashi, S. *J. Chem. Soc. Chem. Commun.* **1991**, 1647-1648.

(36) Feig, A.; Lippard, S. J. *J. Am. Chem. Soc.* **1994**, *116*, 8410-8411.

(37) Tolman, W. B.; Bino, A.; Lippard, S. J. *J. Am. Chem. Soc.* **1989**, *111*, 8522-8523.

(38) Tolman, W. B.; Liu, S.; Bentsen, J. G.; Lippard, S. J. *J. Am. Chem. Soc.* **1991**, *113*, 152-164.

(39) Hartman, J. R.; Rardin, R. L.; Chaudhuri, P.; Pohl, K.; Wieghardt, K.; Nuber, B.; Weiss, J.; Papaefthymiou, G. C.; Frankel, R. B.; Lippard, S. J. *J. Am. Chem. Soc.* **1987**, *109*, 7387-7396.

(40) Liu, K. E.; Feig, A. L.; Goldberg, D. P.; Watton, S. P.; Lippard, S. J. In *The Activation of Dioxygen and Homogeneous Catalytic Oxidation*; Barton, D. H. R., Eds.; Plenum: New York, 1993; pp 301-320.

(41) Wieghardt, K.; Chaudhuri, P.; Nuber, B.; Weiss, J. *Inorg. Chem.* **1982**, *21*, 3086-3090.

(42) Chaudhuri, P.; Wieghardt, K.; Nuber, B.; Weiss, J. *Angew. Chem. Int. Ed. Engl.* **1985**, *24*, 778-779.

(43) Connors, K. A. *Chemical Kinetics. The Study of Reaction Rates in Solution*; VCH Publishers: New York, 1990.

(44) *Oxygen and Ozone*; Battino, R., Ed.; Pergamon Press: Oxford, 1981; Vol. 7.

(45) Karlin, K. D.; Wei, N.; Jung, B.; Kaderli, S.; Niklaus, P.; Zuberbühler, A. D. *J. Am. Chem. Soc.* **1993**, *115*, 9506-9514.

(46) CAChe, V. 2.7; Tektronix, 1991.

(47) Micklitz, W.; Bott, S. G.; Bentsen, J. G.; Lippard, S. J. *J. Am. Chem. Soc.* **1989**, *111*, 372-374.

(48) See also Chapter III.

(49) Kurtz, D. M., Jr. *Chem. Rev.* **1990**, *90*, 585-606.

(50) Sanders-Loehr, J. Personal communication.

(51) Dong, Y.; Menage, S.; Brennan, B. A.; Elgren, T. E.; Jang, H. G.; Pearce, L. L.; Que, L., Jr. *J. Am. Chem. Soc.* **1993**, *115*, 1851-1859.

(52) Kitajima, N.; Tamura, N.; Amagai, H.; Fukui, H.; Moro-Oka, Y.; Mizutani, Y.; Kitagawa, T.; Methur, R.; Heerwegh, K.; Reed, C. A.; Randall, C. R.; Que, L., Jr.; Tatsumi, K. *J. Am. Chem. Soc.* **1994**, *116*, 9071-9085.

(53) Kitajima, N.; Fukui, H.; Moro-oka, Y. *J. Am. Chem. Soc.* **1990**, *112*, 6402-6403.

(54) Moro-Oka, Y.; Fujisawa, K.; Kitajima, N. *Pure & Appl. Chem.* **1995**, *67*, 241-248.

(55) Rardin, R. L.; Tolman, W. B.; Lippard, S. J. *New J. Chem.* **1991**, *15*, 417-430.

(56) Holm, R. H.; Donahue, J. P. *Polyhedron* **1993**, *12*, 571-589.

(57) Hayashi, Y.; Suzuki, M.; Uehara, A.; Mizutani, Y.; Kitagawa, T. *Chem. Lett.* **1992**, 91-94.

(58) Liu, K. E.; Valentine, A. M.; Qiu, D.; Edmondson, D. E.; Appelman, E. H.; Spiro, T. G.; Lippard, S. J. *J. Am. Chem. Soc.* **1995**, *117*, 4997-4998.

(59) Porterfield, W. W. *Inorganic Chemistry - A Unified Approach*; Academic: New York, 1993.

(60) Balch, A. L. *Inorg. Chim. Acta* **1992**, *198-200*, 297-307.

(61) Balch, A. L.; Chan, Y.-W.; Cheng, R.-J.; La Mar, G. N.; Latos-Grazynski, L.; Renner, M. W. *J. Am. Chem. Soc.* **1984**, *106*, 7779-7785.

(62) Chin, D.-H.; Del Gaudio, J.; La Mar, G. N.; Balch, A. L. *J. Am. Chem. Soc.* **1977**, *99*, 5486-5488.

(63) Chin, D.-H.; La Mar, G. N.; Balch, A. L. *J. Am. Chem. Soc.* **1980**, *102*, 4344-4350.

(64) Connolly, J. A.; Kim, J. H.; Banaszczyk, M.; Drouin, M.; Chin, J. *Inorg. Chem.* **1995**, *34*, 1094-1099.

(65) Mauerer, B.; Crane, J.; Schuler, J.; Wieghardt, K.; Nuber, B. *Angew. Chem. Int. Ed. Engl.* **1993**, *32*, 289-231.

(66) Sauer-Masarwa, A.; Herron, N.; Fendrick, C. M.; Busch, D. H. *Inorg. Chem.* **1993**, *32*, 1086-1094.

(67) Balch, A. L.; La Mar, G. N.; Latos-Grazynski, L.; Renner, M. W.; Thanabal, V. *J. Am. Chem. Soc.* **1985**, *107*, 3003-3007.

(68) Liu, K. E.; Valentine, A. M.; Wang, D.; Huynh, B. H.; Edmondson, D. E.; Salifoglou, A.; Lippard, S. J. *J. Am. Chem. Soc.* **1995**, in press.

(69) Feig, A. L.; Schindler, S.; van Eldik, R.; Lippard, S. J. *J. Am. Chem. Soc.* **1995**, to be submitted for publication.

Supplementary Materials for

CHAPTER II.

Kinetic Studies of Reactions of Dioxygen with Non-heme Diiron(II) Complexes Leading to the Formation of (μ–Oxo)diiron(III) Complexes

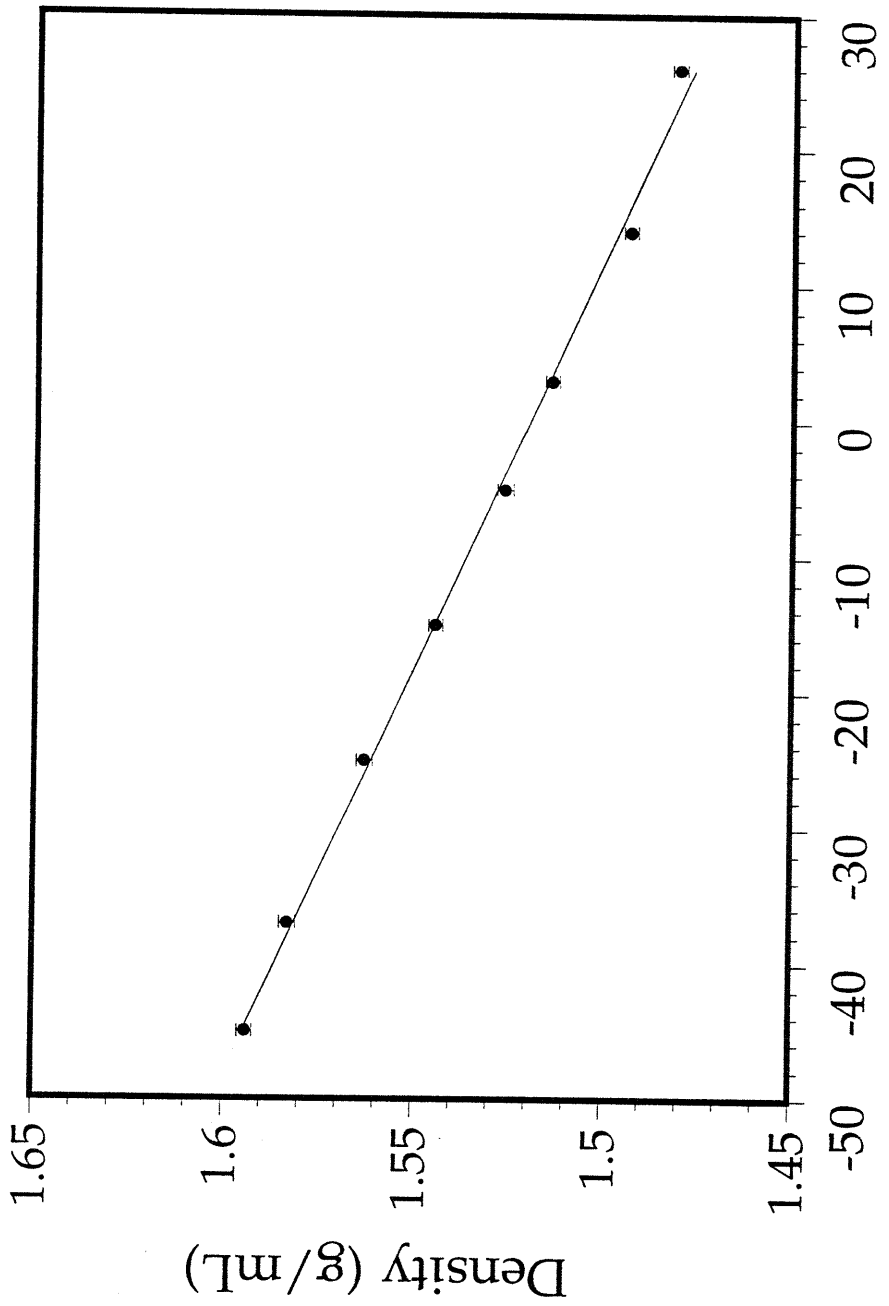

Figure 2.S1. Plot of the measure density of chloroform as a function of temperature between 25 and -45 °C. Error bars indicate one standard deviation based on 4 independent measurements at each temperature.

Table 2.S1. Mean Rate Constants as a Function of Complex Concentration for the Oxidation of **1a** in $CHCl_3$.[a]

[**1a**] (mM)	k_ψ (M^{-1} s^{-1})	$k_{obs}*10^{-6}$ (M^{-2} s^{-1})[b]	$t_{1/2}$ (s)	V_0*10^5 (M s^{-1})[c]
0.122	1250 ± 51	2.22± 0.09	11.3 ± 0.93	3.22 ± 0.57
0.260	1170 ± 130	2.10± 0.23	5.23 ± 0.83	16.3 ± 3.4
0.310	862 ± 7.3	1.54± 0.01	4.40 ± 0.08	30.0 ± 1.1
0.321	1140 ± 56	2.03± 0.10	3.46 ± 0.42	37.6 ± 6.7
0.390	991 ± 34	1.77± 0.06	3.85 ± 0.22	34.3 ± 2.9
0.490	800 ± 14	1.43± 0.03	3.00 ± 0.14	69.9 ± 7.5
0.514	928 ± 28	1.66± 0.05	2.78 ± 0.23	70.8 ± 9.7
0.610	697 ± 17	1.24± 0.03	2.67 ± 0.14	101 ± 11
0.642	844 ± 60	1.51± 0.05	2.55 ± 0.14	91.8 ± 6.2

[a]Dioxygen concentration was 5.6 mM, Temp = 22 °C.

[b]$k_{obs} = k_\psi/[O_2]$

[c]V_0 calculated based on eq 2.4.

Table 2.S2. Mean Rate Constants as a Function of Complex Concentration for the Oxidation of **2a** in $CHCl_3$.[a]

[**2a**] (mM)	k_ψ (M^{-1} s^{-1})	k_{obs} (M^{-2} s^{-1})[b]	$t_{1/2}$ (s)	V_0*10^9 (M s^{-1})[c]
0.10	9.77 ± 6.00	1880 ± 1150	1970 ± 936	33.9 ± 11
0.20	8.01 ± 2.40	1540 ± 462	1190 ± 218	92.3 ± 6.5
0.30	7.80 ± 0.090	1501 ± 17	752 ± 10	226 ± 2.0
0.40	4.58 ± 0.43	880 ± 83	831 ± 41	317 ± 1.3
0.50	3.38 ± 0.12	649 ± 23	660 ± 9.2	680 ± 43

[a]Dioxygen concentration was 5.6 mM, Temp = 22 °C.

[b]$k_{obs} = k_\psi/[O_2]$

[c]V_0 calculated based on eq 2.4.

Table 2.S3. Mean Rate Constants as a Function of Complex Concentration for the Oxidation of **2a** in MeOH.[a]

[**2a**] (mM)	k_{obs} (M^{-1} s^{-1})	$t_{1/2}$ (s)	V_0*10^9 (M s^{-1})[b]
0.050	171 ± 29	488 ± 61	25.2 ± 3.7
0.10	36.3 ± 4.1	536 ± 64	97.8 ± 11.5
0.15	25.6 ± 3.2	368 ± 43	293 ± 31
0.20	21 ± 10	383 ± 150	447 ± 248
0.25	14.8 ± 1.9	343 ± 39	584 ± 61
0.30	16.8 ± 1.3	238 ± 18	1056 ± 75
0.35	9.78 ± 1.3	353 ± 47	841 ± 103
0.40	22.9 ± 3.3	127 ± 18	2792 ± 329

[a]Dioxygen concentration was 5.2 mM, Temp = 22 °C.

[b]V_0 calculated based on eq 2.4.

Table 2.S4. Rate Constants for the Oxidation of [**1a**] in $CHCl_3$ as a Function of Dioxygen Concentration.

T (°C)	[**1a**] (mM)	$[O_2]$ (mM)	k_ψ (M^{-1} s^{-1})	k_{obs} (M^{-2} s^{-1}) $*10^{-3}$[a]
22	0.20	1.04	79.8	76.7
22	0.20	1.39	112	80.3
22	0.20	2.08	145	69.7
22	0.20	3.13	208	66.4
22	0.20	4.21	277	65.7

[a] $k_{obs} = k_\psi/[O_2]$

Table 2.S5. Rate Constants for the Oxidation of **2a** in $CHCl_3$ as a Function of Dioxygen Concentration.

T (°C)	[**2a**] (mM)	$[O_2]$ (mM)	k_ψ (M^{-1} s^{-1})	k_{obs} (M^{-2} s^{-1})[a]
22	0.13	5.79	8.41 ± 1.47	1453 ± 253
22	0.13	4.09	6.61 ± 0.31	1616 ± 76
22	0.13	2.73	5.16 ± 1.15	1890 ± 421
22	0.13	1.36	2.66 ± 0.27	1956 ± 198

[a] $k_{obs} = k_\psi/[O_2]$

Table 2.S6. Rate Constants for the Oxidation of **2a** in MeOH as a Function of Dioxygen Concentration.

T (°C)	[**2a**] (mM)	$[O_2]$ (mM)	k_{obs} (M^{-1} s^{-1})
22	0.25	5.2	24.1 ± 4.4
22	0.25	4.0	36.9 ± 5.1
22	0.25	3.5	52.4 ± 5.3
22	0.25	2.5	36.2 ± 4.5
22	0.25	2.0	32.8 ± 2.4
22	0.25	1.0	47.4 ± 2.4

Table 2.S7. Mean Rate Constants as a Function of Temperature for the Oxidation of **1a** in $CHCl_3$.[a]

T (°C)	$[O_2]$ (mM)[b]	k_ψ (M^{-1} s^{-1})	k_{obs} (M^{-2} s^{-1}) *10^{-3}[c]	$\ln((k_{obs}h)/Tk_b)$
40.0	5.48	1300 ± 72	237 ± 13	-17.05 ± 0.06
35.0	5.51	902 ± 160	164 ± 29	-17.4 ± 0.2
30.0	5.55	931 ± 274	168 ± 49	-17.4 ± 0.3
25.0	5.58	894 ± 124	160 ± 22	-17.4 ± 0.1
21.0	5.61	537 ± 37	95.8 ± 6.5	-17.90 ± 0.07
20.0	5.61	1003 ± 157	179 ± 28	-17.3 ± 0.1
15.0	5.65	711 ± 24	126 ± 4.2	-17.61 ± 0.03
10.0	5.68	524 ± 105	92 ± 18	-17.9 ± 0.2
5.0	5.72	600 ± 22	105.0 ± 3.9	-17.75 ± 0.04
0.0	5.75	355 ± 43	61.8 ± 7.4	-18.3 ± 0.1
-5.0	5.78	261 ± 25	45.2 ± 4.4	-18.6 ± 0.1
-7.8	5.80	382 ± 31	65.8 ± 5.3	-18.2 ± 0.1
-10.0	5.82	154 ± 8	26.5 ± 1.4	-19.1 ± 0.1
-15.0	5.85	101 ± 13	17.3 ± 2.2	-19.5 ± 0.1
-15.2	5.85	137 ± 7	23.4 ± 1.2	-19.2 ± 0.1
-20.0	5.89	96 ± 15	16.3 ± 2.5	-19.5 ± 0.2
-27.5	5.94	40 ± 8	6.8 ± 1.4	-20.4 ± 0.2
-30.0	5.95	21.9 ± 1.9	3.7 ± 0.3	-21.0 ± 0.1
-35.0	5.99	18.0 ± 1.9	3.0 ± 0.3	-21.2 ± 0.1

[a]Complex concentration was 0.30 mM at room temperature.

[b]$[O_2]$ adjusted for solvent contraction based upon eqs 2.5 and 2.6.

[c]$k_{obs} = k_\psi/[O_2]$

Table 2.S8. Mean Rate Constants as a Function of Temperature for the Oxidation of **2a** in MeOH.[a]

Temp (°C)	k_{obs} (M^{-1} s^{-1})	$\ln((k_{obs}h)/Tk_b))$
55	286.2 ± 2.6	-23.82 ± 0.01
45	194.7 ± 6.3	-24.18 ± 0.03
35	95.4 ± 3.5	-24.86 ± 0.04
25	45.5 ± 2.1	-25.56 ± 0.05
20	26.6 ± 1.0	-26.09 ± 0.04

CHAPTER III.

Mechanistic Studies of the Formation and Decay of Diiron(III) Peroxo Complexes in the Reaction of Diiron(II) Precursors with Dioxygen[1,2]

Introduction

Reduced dinuclear iron centers occur in several metalloproteins, including hemerythrin (Hr),[3-5] the R2 protein of ribonucleotide reductase (RNR) from *E. coli*,[6-9] and the hydroxylase (H) component of soluble methane monooxygenase (sMMO).[10-12] In each of these systems, the diiron center is directly involved in a reaction with dioxygen that is integral to the function of the protein.[13,14] Of major interest to scientists working in this field is what features of these proteins lead to the different modes of activity. Hr binds dioxygen, but subsequent reactions leading to cleavage of the O-O bond are disfavored. In RNR and MMO, however, four-electron reduction of dioxygen occurs with the utilization of the oxidizing equivalents for different purposes. In RNR, the dioxygen reaction oxidizes Tyr-122 to the functionally important tyrosyl radical, whereas in sMMO a substrate alkane is oxidized to an alcohol. A similarity between the RNR and MMO activities can be observed in the R2 F208Y mutant protein.[15] In this altered enzyme, exposure of the apo-enzyme to iron(II) and dioxygen converts the tyrosine residue to dihydroxyphenylalanine (DOPA).

Reactions of the reduced forms of RNR and sMMO with dioxygen occur by multistep processes.[16-22] The initial step in both cases is coordination of dioxygen to the diiron(II) center accompanied by two-electron oxidation. This process is similar to the dioxygen binding reaction of deoxyHr, but the resultant adducts in MMO and RNR differ from the η^1-hydroperoxide coordination mode found in oxyHr.[23,24] In both MMO and RNR, the peroxo species is unstable and decomposes to less well defined intermediates. In the case of MMO, H_{peroxo} decays to a species designated Q which has been postulated to be either a diferryl or a diiron(III) center bridged by two oxyl radicals.[12,17,18,22] Further spectroscopic and mechanistic work is

required to define the chemical nature of this transient. In RNR, a diferric center bridged by a single radical ligand has been proposed to be the intermediate in the oxidation mechanism.[16,19-21]

Several model compounds have been synthesized for the reduced cores of these enzymes.[25-36] None of them is a perfect structural mimic for the protein cores, and none exhibits the catalytic monooxygenase type activity observed in the proteins. Several of these complexes react cleanly with dioxygen, however, to afford well characterized products. We have therefore undertaken a systematic kinetic investigation of this reaction and report here our results on three closely related ones. All contain a (μ-alkoxo)(μ-carboxylato)diiron(II) core coordinated by N,N,N',N'-tetrasubstituted-1,3-diamino-2-hydroxypropane (HPTR) ligands. They are of particular interest for mechanistic studies of dioxygen reactivity because of the ability to isolate different phases of the reaction (Scheme 3.1). When first reported by other laboratories, it was noted that stable peroxide adducts formed following exposure to dioxygen at low temperature.[29,31] Spectroscopic studies of these complexes revealed the presence of a symmetrical peroxide, presumably bound in a μ–1,2 fashion. In the case of compound **1a**, the dioxygen binding was reversible.[29] Once dioxygen bound to either **2a** or **3a**, however, could not be released.[31,37,38] Thus, although the chemical differences among **1a - 3a** are subtle, consisting primarily of changes in the steric properties around the diiron center, the effects of these differences on the reactions with dioxygen are quite profound. Upon warming, all three of the metastable diferric peroxo complexes decompose. The temperature at which the intermediates decompose varies greatly, as noted previously.[31]

The question addressed here is whether one can understand these differences. In particular, what are the primary structural features that

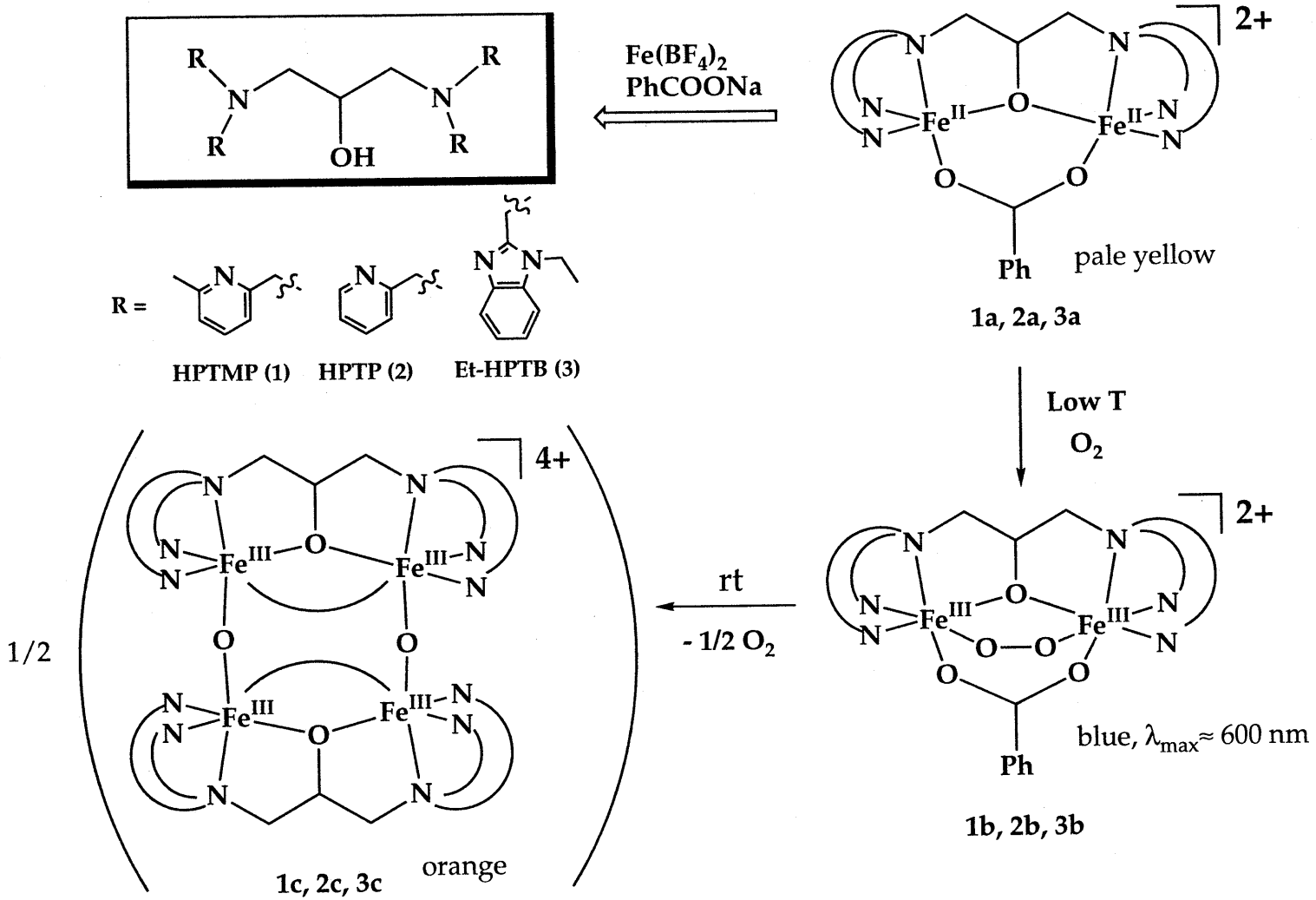
R
N
R
OH
R
N
R
Fe(BF4)2
PhCOONa
2+
N
Fe^II
O
Fe^II
N
Ph
pale yellow
1a, 2a, 3a
R =
HPTMP (1)
HPTP (2)
Et-HPTB (3)
Low T
O2
2+
Fe^III
O—O
blue, λmax≈ 600 nm
1b, 2b, 3b
rt
- 1/2 O2
1/2
4+
Fe^III
O
1c, 2c, 3c
orange

Scheme 3.1.

influence the reactivity of the diiron(II) compounds and the activated dioxygen complexes? In addition, what predictions can be made based on this evidence about how further modifications will lead to significant changes in the chemical properties of the diiron-O_2 adducts?

Experimental

General Considerations. All solvents were dried and distilled prior to use. For most studies, propionitrile (Fluka) was prepared by distillation from CaH_2. Significant levels of residual water were present after this treatment, as measured by Karl Fischer analysis (Galbraith Laboratories). Rigorously dry solvent for the determination of the effects of small amounts of added water was obtained by pre-drying over CaH_2, decanting the solvent into a distillation flask containing P_2O_5 (5 g/L), and refluxing overnight under N_2. The propionitrile was collected by distillation and then refluxed over CaH_2 (5 g/L). After 12 h, the solvent was collected by distillation and transferred to a glove box. Karl Fischer analysis of EtCN treated in this manner contained <34 ppm residual water. Et_2O, MeOH and MeCN used in the syntheses of **1a** - **3a** were dried by standard procedures.[39] Dioxygen was purified by passing the gas stream through a column of Drierite (1 m). Anaerobic manipulations were carried out in a nitrogen filled glove box (Vacuum Atmospheres) or by using standard Schlenk techniques. Labeled dioxygen (≈ 98% ^{18}O) was obtained from Isotech (Miamisburg, OH) and used without further purification.

Ligand Syntheses. N,N,N',N'-tetrakis[(6-methylpyrid-2-yl)methyl]-2-hydroxy-1,3-diaminopropane (HPTMP) (**1**), a known compound,[29] was synthesized by a new method described below. N,N,N',N'-tetrakis(2-pyridylmethyl)-2-hydroxy-1,3-diaminopropane (HPTP) (**2**) and N,N,N',N'-tetrakis(N-ethyl-2-benzimidazolyl-methyl)-2-hydroxy-1,3-diaminopropane (Et-HPTB) (**3**) were prepared according to literature procedures.[31]

6-Methyl-2-hydroxymethylpyridine. To a solution of 6-methyl-2-pyridinecarboxaldehyde (25.0 g, 0.207 mol) in ethanol (100 mL) at 0 °C 3.0 g of $NaBH_4$ was added. The solution was stirred for 1 h, after which time 100 mL H_2O was added. The solution was neutralized by addition of HCl and the product was extracted into Et_2O. The solution was dried over $MgSO_4$ and the solvent removed under reduced pressure yielding the product alcohol as a colorless oil (23.2 g, 0.189 mole, 91.5%). ^1H NMR (300 MHz, $CDCl_3$) δ 7.56 (t, 1 H, J = 7.5 Hz), 7.05 (t, 2 H, J = 7.8 Hz), 4.71 (s, 2 H), 2.54 (s, 3 H).

6-Methyl-2-bromomethylpyridine. The above alcohol was dissolved in 70 mL of 48% HBr. Concentrated H_2SO_4 (50 mL) was added slowly and the solution was refluxed overnight. The reaction mixture was poured into 100 mL of H_2O and then neutralized with saturated aq Na_2CO_3. The product was extracted into Et_2O and dried over $MgSO_4$. The solvent was removed under reduced pressure yielding a pink solid (29.0 g, 0.156 mol, 82.5%). ^1H NMR (250 MHz, $CDCl_3$) δ 7.57 (t, 1 H, J = 7.8 Hz), 7.23 (d, 1 H, J = 7.8 Hz), 7.05 (d, 1 H, J = 7.8 Hz), 4.51 (s, 2 H), 2.55 (s, 3H). EI MS *m/z* 185,187 (isotope ratio 1:1, M^+).

N,N,N′,N′-Tetrakis[(6-methylpyrid-2-yl)methyl]-2-hydroxy-1,3-diaminopropane. To a solution of 1,3-diamino-2-propanol (0.902 g, 10 mmol) in H_2O (25 mL), 6-methyl-2-pyridinemethylbromide (8.60 g, 46 mmol) and NaOH (4.5 g, 113 mmol) were added . The solution was refluxed overnight and, upon cooling, a biphasic mixture was obtained. The organic component was extracted 3 times into CH_2Cl_2, the extract was dried over $MgSO_4$, and the solvent was removed under reduced pressure. The product was purified by silica column chromatography (EtOAc/MeOH) yielding the pure compound as a viscous brown oil (3.73 g, 9.03 mM). ^1H NMR (250 MHz, $CDCl_3$) δ 7.45 (t, 4 H, J = 7.7 Hz), 7.17 (d, 4 H, J = 7.8 Hz), 6.93 (d, 4 H, J = 7.5 Hz), 3.90 (m, 1 H), 3.80 (dd, 4 H, J = 6.0 and 37.5 Hz), 2.45 - 2.62 (m, 8 H), 2.46 (s, 12 H). The NMR

spectrum of this material matches the previously reported one of material prepared by the alternative synthetic route. The overall three step yield was 68.2%.

Preparation of Iron(II) Compounds. The three complexes used in this study, $[Fe_2(HPTMP)(OBz)](BPh_4)_2$ (**1a**), $[Fe_2(HPTP)(OBz)](BPh_4)_2$ (**2a**), and $[Fe_2(Et\text{-}HPTB)(OBz)](BF_4)_2$ (**3a**), were synthesized by the methods previously reported[29,31] and purified by multiple (usually 3) recrystallizations from MeCN by vapor diffusion of Et_2O under a nitrogen atmosphere.

Optical Spectra. Optical spectra of compounds **1b** - **3b** were previously reported.[29,31] Prior to beginning kinetic work, these spectra were recollected by using an Hewlett Packard 8452A diode array spectrometer fitted with a specially modified dewar flask with quartz windows. Absorptions due to the metastable dioxygen adducts were observed at -77 °C. Values for the extinction coefficients were determined based on a Beer's law analysis of curve fitting parameters in the kinetic experiments in dry solvent. These values match those measured by static oxygenation experiments. We assume in our studies that the extinction coefficients do not vary significantly with temperature.

Manometry. Manometric experiments were carried out in propionitrile as previously described, but with minor modifications.[28,40] Because of the temperature sensitivity of the peroxide intermediates, dioxygen uptake for the first phase of the reaction was measured with the reaction flask cooled to -77 °C by immersion in a dry ice/acetone bath. After equilibrium was achieved, the decomposition of the peroxide was measured by warming the reaction vessel to 20 °C and monitoring the manometer. Dioxygen consumption was measured at least twice and is reported as the mean of the two values.

Isotope Exchange Studies. To determine whether isotope exchange occurred during the decomposition of **3b** to **3c**, samples (50 mg of **3a** in each sample dissolved in propionitrile) were prepared in separate reaction flasks and cooled to -77 °C. The samples were oxygenated with either $^{16}O_2$ or $^{18}O_2$ and both flasks were purged of excess O_2 by repeated vacuum/argon cycling. The $^{18}O_2$ sample was then transferred by cannula to the flask containing the unlabeled material. The head space above the reaction was evacuated by using a modified Toepler pump (Figure 3.1) while the sample was kept cold. The reaction flask was then isolated from the pump and the solution was stirred at room temperature for 2 h at which time the decay reaction appeared to be complete based on the color change. The head space of the vessel was evacuated and the gas was collected in the receiving tube connected to the outlet of the Toepler pump. The gas was then analyzed by mass spectrometry (Hewlett Packard 5971 mass spectrometer).

Stopped-Flow Kinetics Experiments. All ambient pressure kinetics experiments were carried out by using an SF-41 Canterbury instrument described previously.[40,41] The optical signal was detected by using the fiber-optics spectrometer. The effect of pressure on the formation of the peroxide intermediate **3b** was measured on a homemade high pressure stopped-flow instrument previously described.[42] The preferred solvent for these studies was propionitrile because of its low freezing point (-95 °C) and high boiling point (97 °C) and was used unless noted otherwise. The formation of intermediates **1b - 3b** was studied under pseudo-first-order conditions with the concentration of O_2 maintained in great excess of the iron complexes. Concentrations of the ferrous complexes, were generally varied from 0.02 - 0.50 mM. The dioxygen concentration at saturation (20 °C) is 8.8 mM.[43] Saturation concentrations in other solvents were calculated from the Ostwald

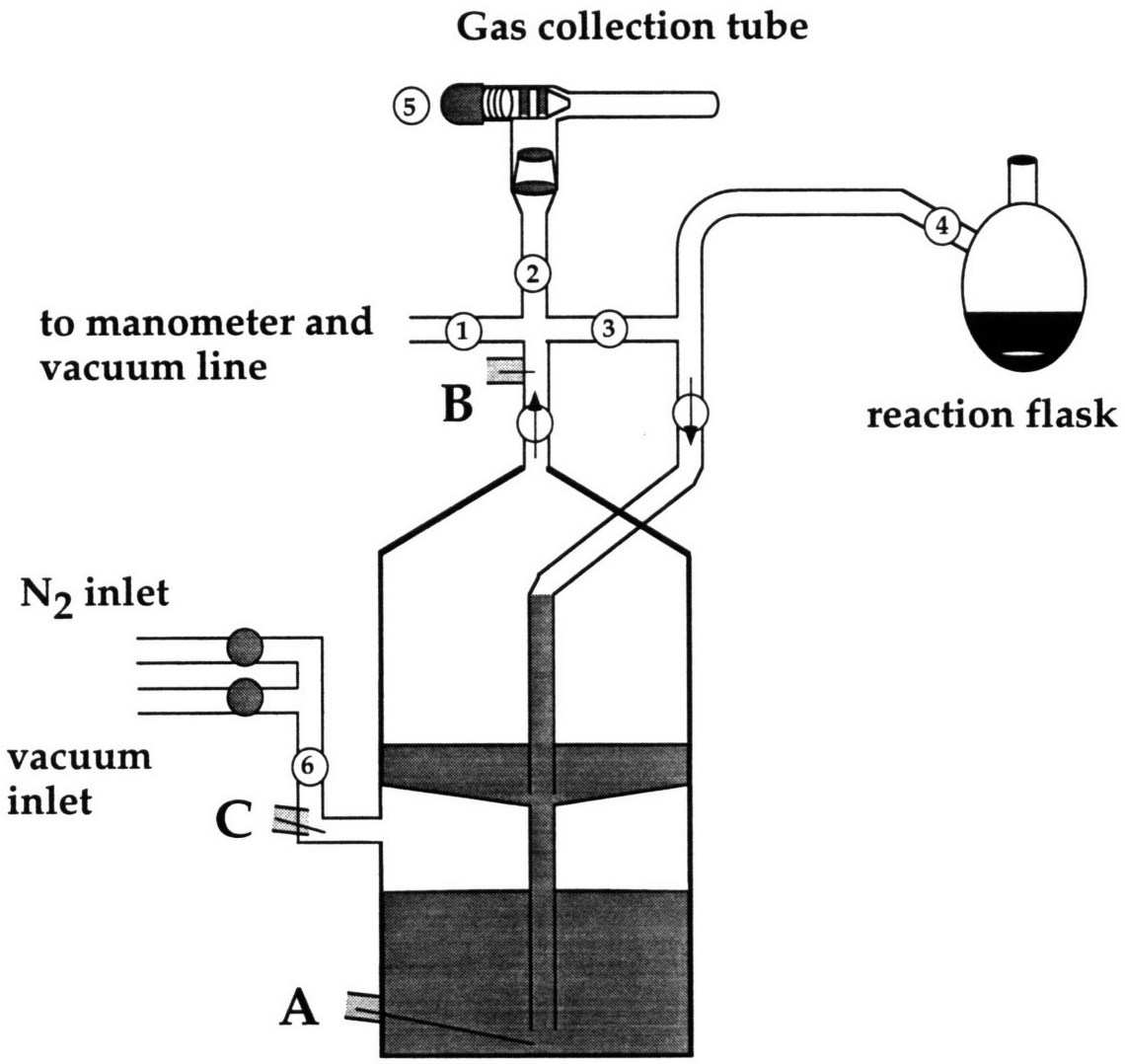

Figure 3.1. Schematic drawing of the Toepler pump used in the isotope scrambling studies. Open circles represent manual control valves. Shaded circles represent solenoids controlled by the electronic relay and A, B, and C are the electrical contacts used by the relay circuit.

coefficients (L) and eq 3.1, where χ is the mole fraction, R is the gas constant, T is the temperature, $P_{(g)}$ is the partial pressure, and $V°_{(l)}$ is the molar volume.[44] Dioxygen concentrations were studied over the 0.8 - 4.4 mM range

$$\chi = \left(\frac{RT}{P_{(g)} L V°_{(l)}} + 1 \right)^{-1} \tag{3.1}$$

at room temperature. A linear correction for the solvent contraction of propionitrile as a function of temperature was previously measured[43] and is given in eqs 3.2 - 3.3. This correction was applied to the dioxygen concentration whenever the rate constant depended upon this value. Once it was determined that the decay phase of the reaction was not $[O_2]$-dependent, the reaction conditions for these runs were varied beyond the pseudo-order limits, employing complex concentrations as high as 1.0 mM.

$$\rho = 0.8011(4) - 0.0009801(90)*T \text{ (T in °C)} \tag{3.2}$$

$$[O_2]_T = \frac{[O_2]_{22°C}}{\rho_{22°C}} * \rho_T \tag{3.3}$$

Rate constants were derived from optical traces obtained at 600 nm, a wavelength at which both the formation and the decomposition of the peroxide intermediate can be observed. The data were analyzed with Kaleidagraph (Abelbeck Software) running on a Macintosh IIfx computer and fit to model-dependent equations by nonlinear least-squares regression. The formation and decay phases of the reaction were studied independently by varying the temperature and time base. Traces used for curve fitting were all recorded to at least 3 half-lives. For the formation of the peroxide species,

optical density data were fit to eq 3.4, a generalized first-order growth expression. Errors provided for the kinetic constants are based on the standard deviation from the mean for multiple runs under identical

$$A(t) = m_1 + m_2\left(1 - e^{-m_3 t}\right) \tag{3.4}$$

$$[B]_t = m_1 + \frac{1}{m_2 + m_3 t} \tag{3.5}$$

$$[B]_t = m_1 + m_2\left(1 - e^{-m_3 t}\right) + \frac{1}{m_4 + m_5 t} \tag{3.6}$$

conditions. Errors for the activation parameters are based on the propagated errors from the linear fit of the Eyring plot. Beer's Law analysis of the fitting parameters allowed the determination of the extinction coefficients for **1b - 3b**. These values were used to convert the optical density to concentration prior to the curve fitting of decay traces to eq 3.5. Under certain conditions for compound **1a**, both the formation and decay could be observed with the same time base. Such data could be fit to the sum of a first-order growth and a second-order decay (eq 3.6). If the initial growth phase was masked and the data were fit to the simple second-order decay, identical rate constants were obtained. Under conditions of incomplete separation of the first and second phases of the reaction, the kinetic data reported for the decay reaction reflects the latter treatment. This analysis allowed the accurate fitting of the traces with fewer independent variables.

Reactions performed under strictly anhydrous conditions were used to provide zero points prior to studies of the effect of added water on the oxidation rates. Procedures for these experiments were slightly altered to ensure a minimum amount of residual water. Prior to these experiments, THF solutions of sodium benzophenone ketyl were passed through the flow

lines until the blue color showed no loss in intensity over a 6 minute period. The residual ketyl was then flushed from the system with a small volume of dry THF and then dry EtCN. The experiments were run immediately thereafter. Solvents for these experiments were freshly distilled as discussed above. Oxygenated water was added to the oxygenated propionitrile solution just prior to reaction with the dry, anaerobic iron solution.

Oxygen Atom Transfer to Thiophenol. In a typical reaction, a Schlenk flask was charged with 10 mL of a solution of **3a** (0.22 mM in EtCN) containing 0.8 mM MeOBz as in internal standard. This solution was brought out of the glove box and cooled to -77 °C. Excess (0.1 mL, 0.98 mmol, 440 equiv) degassed thiophenol was then added by syringe. The flask was flushed with dioxygen with constant stirring and aliquots were intermittently analyzed by GC or GC/MS.

Results

Oxygenation of the Diferrous Complexes 1a - 3a. The reaction of compounds **1a - 3a** with dioxygen at low temperature leads to the formation of **1b - 3b**, diferric species containing a symmetrically bridging peroxide ligand. Previous spectroscopic studies on these complexes are consistent with either a μ-η^1:η^1 or a μ-η^2:η^2 geometry, although the former is preferred based on the stretching frequency of the O-O bond in the Raman spectrum.[31] The reaction was followed by monitoring a peroxide-to-iron charge transfer band, a broad feature centered around 600 nm for all three complexes (Figure 3.2A). When studied under conditions where the dioxygen concentration is in great excess relative to the diiron(II) species, simple first-order kinetic traces are observed for the buildup of the peroxide intermediates (Figure 3.2B).

Rate constants were derived from time-dependent absorbance changes using a non-linear least-squares fitting procedure described in the

Experimental Section. Extinction coefficients at 600 nm for **1b - 3b** of 1550 ± 58, 1559 ± 41, and 1421 ± 22 M^{-1} cm^{-1}, respectively, were derived from the fitting parameters and a Beer's law analysis. These values were used to convert molar absorbances to concentrations for the determination of initial rates and for curve fitting of the second-order decay phase of the reaction, discussed below. This conversion was unnecessary for determining formation rate constants since these values are independent of complex concentration. Manometric analysis at low temperature (-77 °C) verified the previously reported 1:1 stoichiometry for the reactions forming **2b - 3b** (Table 3.1).[29,31]

Table 3.1. Manometric Studies on the Dioxygen Uptake of **1a - 3a**.[a]

Compound	Peroxide Formation Reaction	Peroxide Decay Reaction
1a	n.d.[b]	0.60 ± 0.10
2a	0.87 ± 0.10	0.45 ± 0.10
3a	0.80 ± 0.10[c]	0.40 ± 0.10

[a]In equivalents based on the mass of diiron(II) sample used in the experiment. [b]Previously measured to be 1.0, ref. 31. [c]Measured at -25 °C.

Experimental Rate Laws for the Formation of 1b - 3b. Kinetic runs were made by varying the complex concentrations over the range 0.05 - 0.50 mM. A plot of $\ln(V_0)$ versus ln([**3a**]) is depicted in Figure 3.3. The reaction was first-order with respect to complex in all cases. When the $[O_2]$ was varied, however, different behavior was observed for **1a** compared to the other two compounds. Clean first-order behavior with respect to dioxygen (Figure 3.4) was exhibited by **2a** and **3a**. The mechanism and rate law for the formation of **2b** and **3b** are therefore as described by eqs 3.7 and 3.8, respectively. Since a

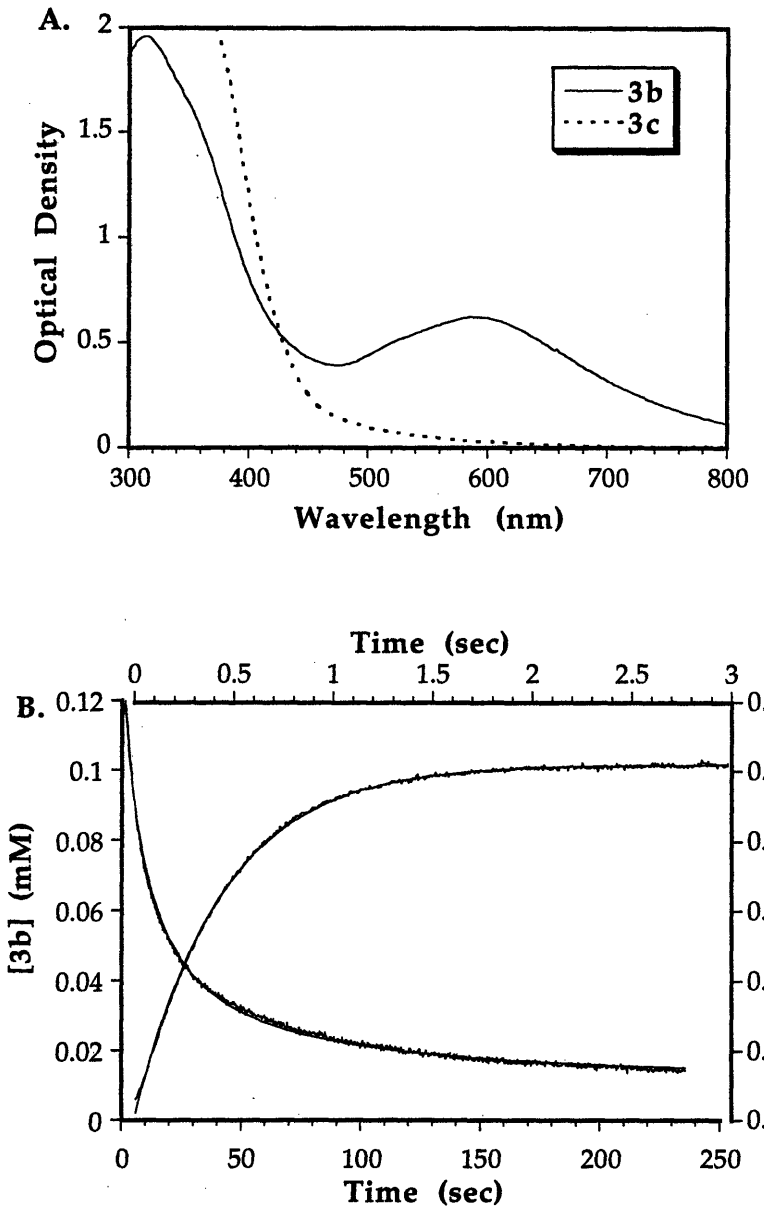

Figure 3.2. (A.) Optical spectrum of **3b**, and **3c** in EtCN. (B.) Sample kinetic traces for the growth (top and right axes) and decay (left and bottom axes) of **3b**. Experimental traces are overlaid by a least-squares fit of the data to the equations shown. Growth phase conditions: -55 °C, 0.40 mM **3a**, 4.52 mM O_2; Decay phase conditions: 55 °C, 0.125 mM **3a**, 4.21 mM O_2.

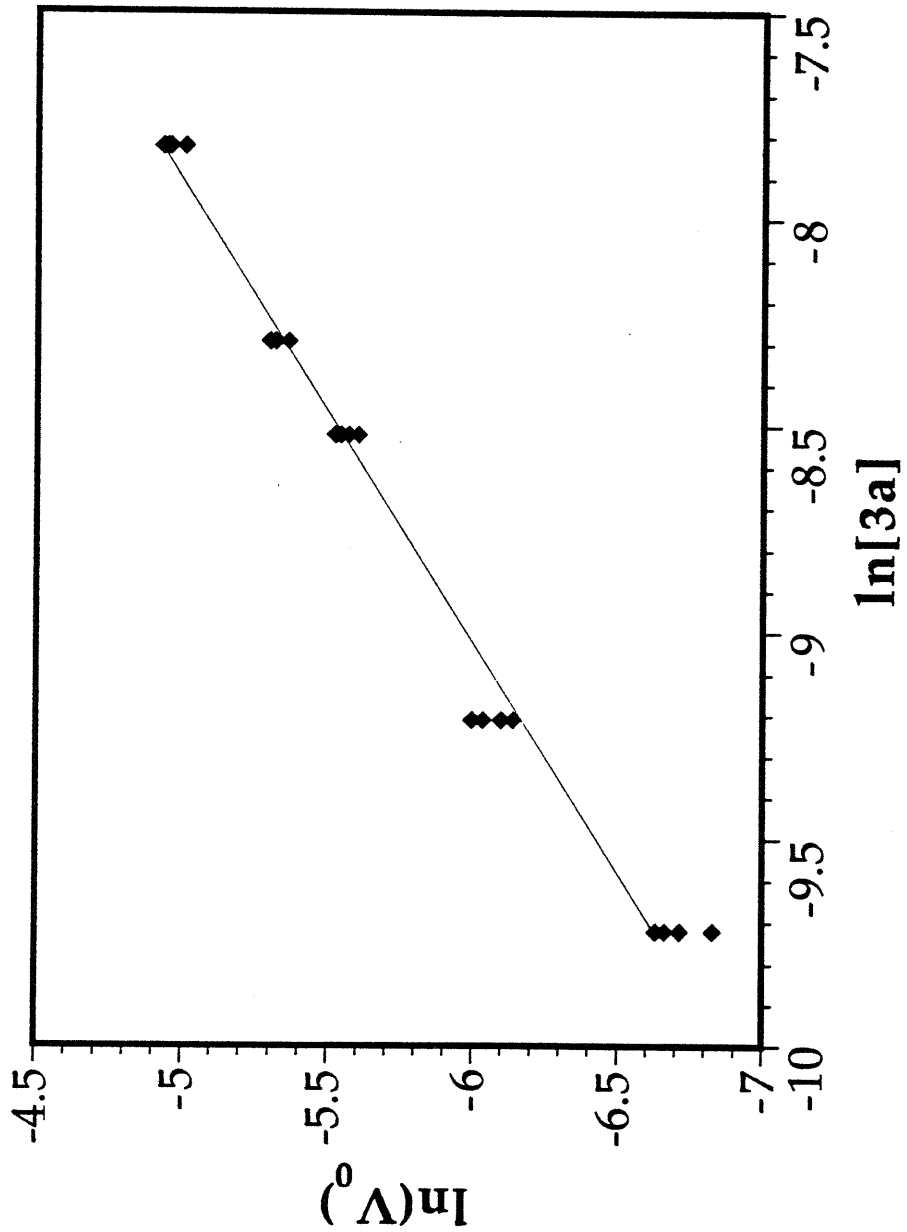

Figure 3.3. A plot of the $\ln(V_0)$ versus the ln[**3a**] (0.05 - 0.50 mM) used to determine the reaction order with respect to complex for the formation of **3b**. The slope of the linear regression corresponds the the reaction order. The reactions of **1a** and **2a** were also between 0.9 and 1.0 ± 0.1. Raw data are provided in Table 3.S1.

partial order with respect to dioxygen, 0.65 ± 0.10, was measured for the reaction of **1a** (Figure 3.4), the mechanism is slightly more complicated. The results can be accounted for by the processes shown in eqs 3.9 - 3.10, where a reversible step occurs prior to oxygenation. Steady state analysis yields the rate law shown in eq 3.11. Partial orders between 0 and 1 are observed in cases where $k_{-0} \approx k_{1'}[O_2]$.

$$A + O_2 \xrightarrow{k_1} B \tag{3.7}$$

$$\frac{d[\mathbf{B}]}{dt} = k_1[\mathbf{2a,3a}][O_2] \tag{3.8}$$

$$A \underset{k_{-0}}{\overset{k_0}{\rightleftharpoons}} A' \tag{3.9}$$

$$A' + O_2 \xrightarrow{k_{1'}} B \tag{3.10}$$

$$\frac{d[\mathbf{B}]}{dt} = \frac{k_0 k_{1'}[\mathbf{1a}][O_2]}{k_{-0} + k_{1'}[O_2]} \tag{3.11}$$

Transformations following the rate laws given by eqs 3.8 versus 3.11 can be differentiated by plotting $1/k_{obs}$ vs $1/[O_2]$. The rate laws expressed in this reciprocal fashion are given by eqs 3.12 and 3.13, respectively. As can be seen from these equations, the simpler system is mathematically required to have a zero intercept at all temperatures. For the more complicated reaction mechanism, however, the intercept of the plot corresponds to $1/k_0$. Since k_0 is temperature-dependent, so too will be the intercept of the $1/k_{obs}$ vs $1/[O_2]$ plot. Plots for **1a - 3a** are shown in Figure 3.5.

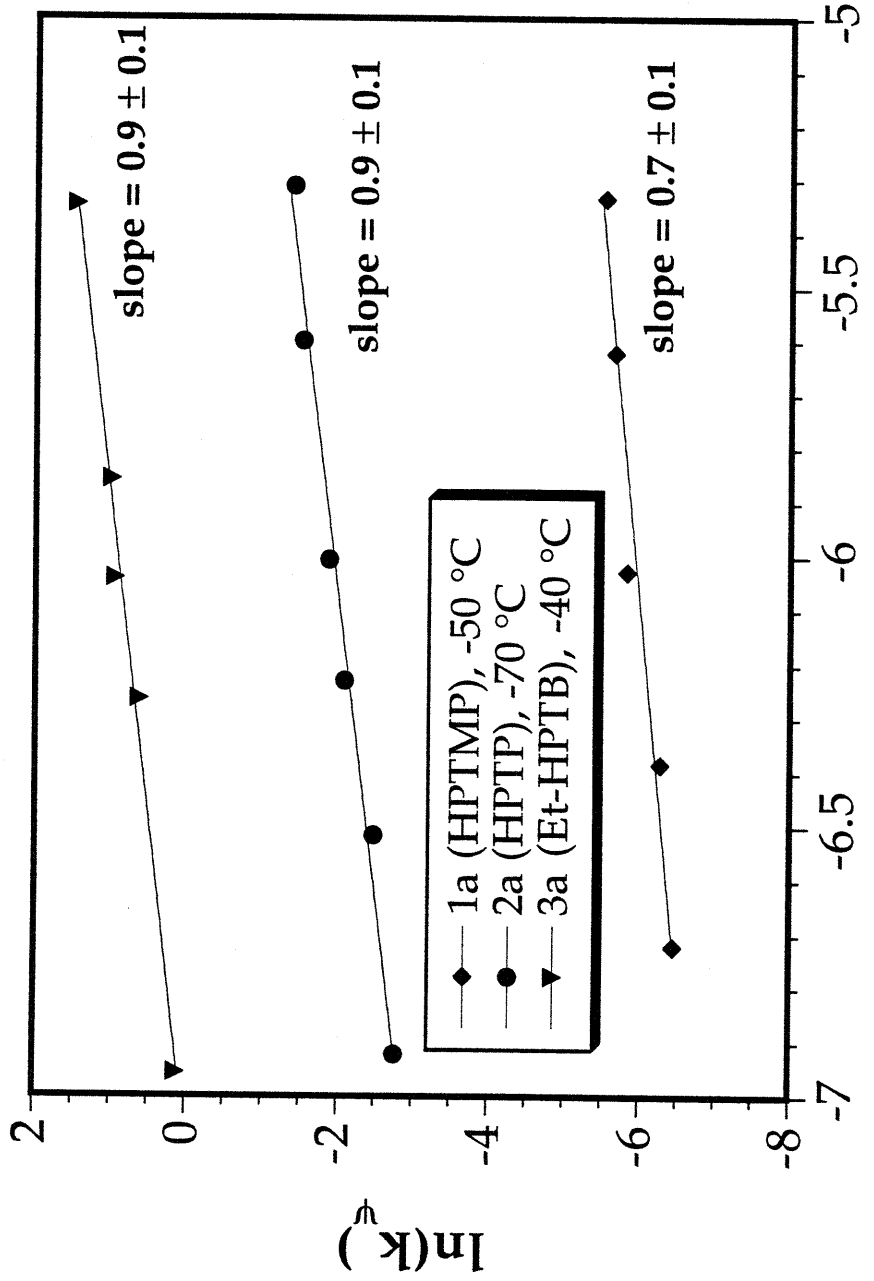

Figure 3.4. A plot of $\ln(k_{obs})$ versus $\ln([O_2])$ used to determine the reaction order with respect to dioxygen for **1a** - **3a**. Temperatures and complex concentrations are as indicated in the legend. When plotted as k_{obs} versus O_2, the same data yields y-intercept values close to zero in each case. Raw data are provided in Table 3.S2- 3.S4.

$$\frac{1}{k_{obs}} = \frac{1}{k_1[O_2]} \tag{3.12}$$

$$\frac{1}{k_{obs}} = \frac{1}{k_0} + \frac{k_{-0}}{k_0 k_{1'}[O_2]} \tag{3.13}$$

Activation Parameters for the Oxygenation of 1a - 3a. The temperature dependence of the reactions of **1a - 3a** with O_2 was investigated between -75 and 20 °C. An Eyring plot (Figure 3.6) of these data provided the activation parameters listed in Table 3.1. The results for the three compounds fall into two classes, divided as previously noted for the experimental rate laws. Compounds **2a** and **3a** have almost identical activation parameters, $\Delta H^{\ddagger} = 16$ kJ mol^{-1} and $\Delta S^{\ddagger} \approx -120$ J mol^{-1} K^{-1}.

The rate constant for oxygenation of **1a** has a dramatically different temperature dependence, reinforcing the contrast between the reaction mechanisms for this compound compared to the other two. The enthalpic contribution to the activation barrier is almost 3 times greater than that for **2a** and **3a**. The Eyring plot in Figure 3.6 assumes that the interaction of **1a** with O_2 is an elementary reaction with a single barrier. The situation has already been shown to be somewhat more complicated, however. By using the rate constants derived from the slopes and intercepts of Figure 3.5A at each temperature, the effective activation barriers for k_0 and $1/(K_0k_1)$ can be extracted. These values are also listed in Table 3.1. From the results, it can be seen that the enthalpic contribution of the overall process derives almost entirely from the k_0 step.

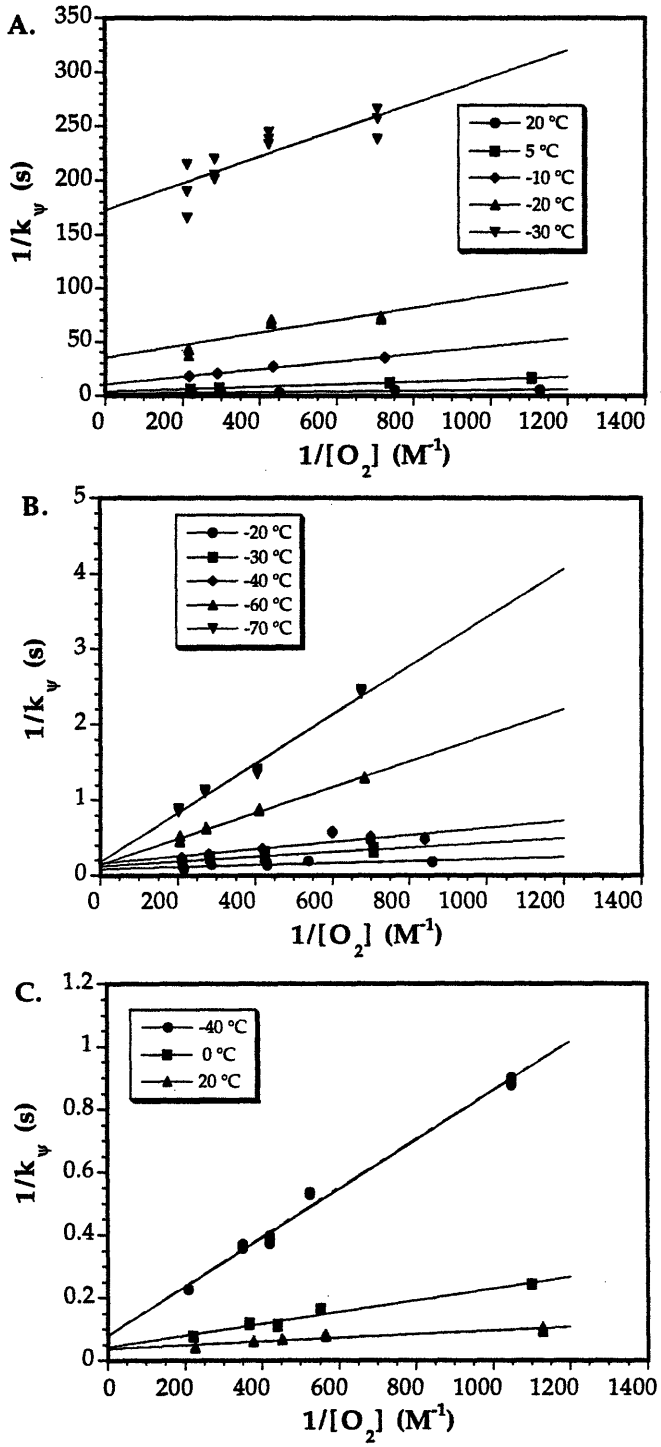

Figure 3.5. Double reciprocal analysis for the formation of **1b** (A), **2b** (B) and **3b** (C) based on eqs 3.11 and 3.12. Data were collected between -70 and 20 °C and at dioxygen concentrations between 0.1 mM and 0.48 mM. Data at each temperature were fit to a linear least-squares regression (solid lines). Raw data are provided in Tables 3.S5 - 3.S6.

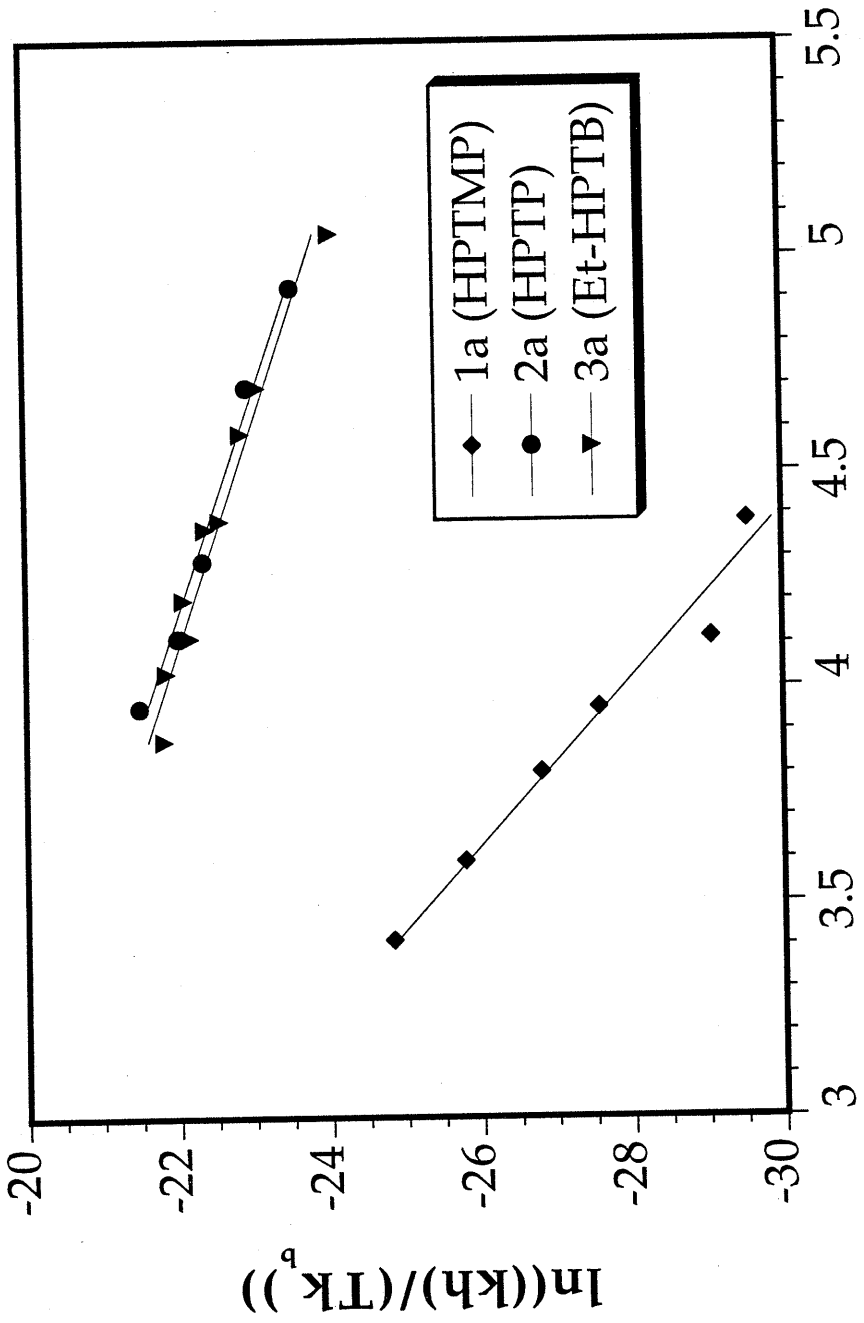

Figure 3.6. Eyring plot for the reaction of 0.16 - 0.25 mM **1a - 3a** with ≈ 4.4 mM dioxygen in propionitrile based on the observed second-order rate constants between -70 and 20 °C. Raw data are provided in Tables 3.S7 - 3.S9.

Table 3.2. Activation Parameters for the Formation and Decay of Peroxide Intermediats **1b - 3b** and Other Relevant Protein and Model Systems.

		$\Delta H^{\ddagger a}$	$\Delta S^{\ddagger a}$	$\Delta V^{\ddagger}$	$\Delta H^{\ddagger b}$	$\Delta S^{\ddagger b}$
		(kJ mol^{-1})	(J mol^{-1} K^{-1})	(cm^3 mol^{-1})	(kJ mol^{-1})	(J mol^{-1} K^{-1})
Oxygenation Reactions	**1a** → **1b**	42.2 ± 1.6	-63 ± 6		39.2 ± 1.6	-65 ± 6
					39.6 ± 2.4	-114 ± 9
	2a → **2b**	16.5 ± 0.4	-114 ± 2			
	3a → **3b**	15.4 ± 0.6	-121 ± 3	-12.8 ± 0.9		
	Hr → oxyHr[c]	16.8	-46	+13.3 ± 1.1[d]		
Peroxide Decomposition Reactions	**1b** → **1c**	113.3 ± 7.7	187 ± 27			
	2b → **2c**	51.9 ± 2.7	-47 ± 11			
	3b → **3c**	80.6 ± 3.9	74 ± 14		80.2 ± 7.0	73 ± 24
					370 ± 6	-8 ± 12
	MMO[e] Peroxo → Q	111	147			
	Q → Decay	75	8			

[a]Activation parameters in this column are derived from Eyring plots of observed rate constant (Figures 3.6 and 3.10). [b]Activation parameters for **1a** in this column correspond to the composite rate constant K_0k_1' (top value) and k_0 (bottom value) derived from Figure 3.5. For **3b**, the activation parameters correspond to K_3k_2' (top vlaue) and k_3 (bottom value) derived from Figure 3.11. [c] From *Themiste zostericola* in Tris buffer, pH 8.2, I = 0.1 M.[45] [d]From *Themiste zostericola* in Tris buffer, pH 8.5, I = 0.10 M.[54] [e] From *Methylococcus capsulatus* (Bath) in MOPS buffer, pH 7.0, I = 25 mM in the presence of protein B.[22]

Effect of Pressure on the Rate of Oxygenation. The effect of pressure on the rate of **3b** formation was studied in propionitrile between 10 and 140 MPa (Figure 3.7). From eq 3.14,[46] we computed the volume of activation to be -12.8 ± 0.9 cm^3 mol^{-1} at 20 °C, a value consistent with the simple addition mechanism discussed above. Volumes of activation for the formation of **1b** and **2b** could not be measured due to temperature limitations of the high-pressure system.

$$\left(\frac{\partial(\ln k)}{\partial P}\right)_T = \frac{\Delta V^{\ddagger}}{RT} \qquad (3.14)$$

Effect of Water on the Rate of Oxygenation. When **1a** crystallized from $MeOH/H_2O$, water coordinated to one of the iron atoms.[29] We therefore studied the effect of added water on the rate of formation of the peroxide intermediates. Reaction of **3a** was investigated, because its greater thermal stability allowed work at higher temperatures and therefore higher water concentrations. At temperatures of -30 and below, ice crystals formed in aqueous propionitrile solutions at the higher end of the water concentration range resulting in light scattering and the inability to collect useful data. The addition of up to 1% (v/v) water (0.5 M) at 20°C had no effect on the reaction rate (Figure 3.8A), indicating that if water were ligated, as it was in the solid state, it is readily displaced by dioxygen. An interesting observation during this study was that the extinction coefficient of the peroxide complex increased linearly by to to 60% over the range of water concentrations studied (Figure 3.8B).

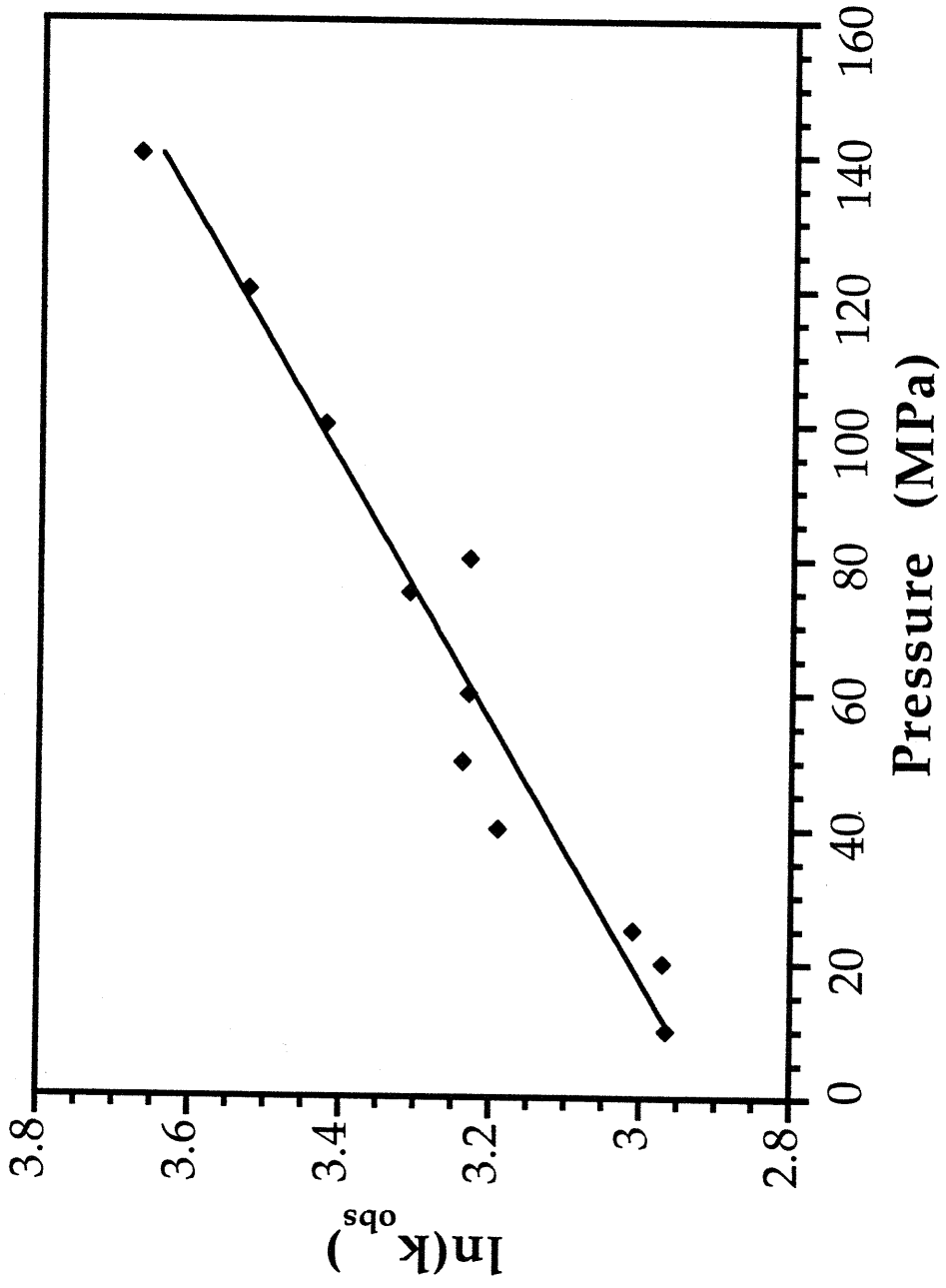

Figure 3.7. A plot showing the effect of pressure on the reaction of 0.20 mM **3a** with dioxygen between 10 and 140 MPa. Raw data are provide in Table 3.S10.

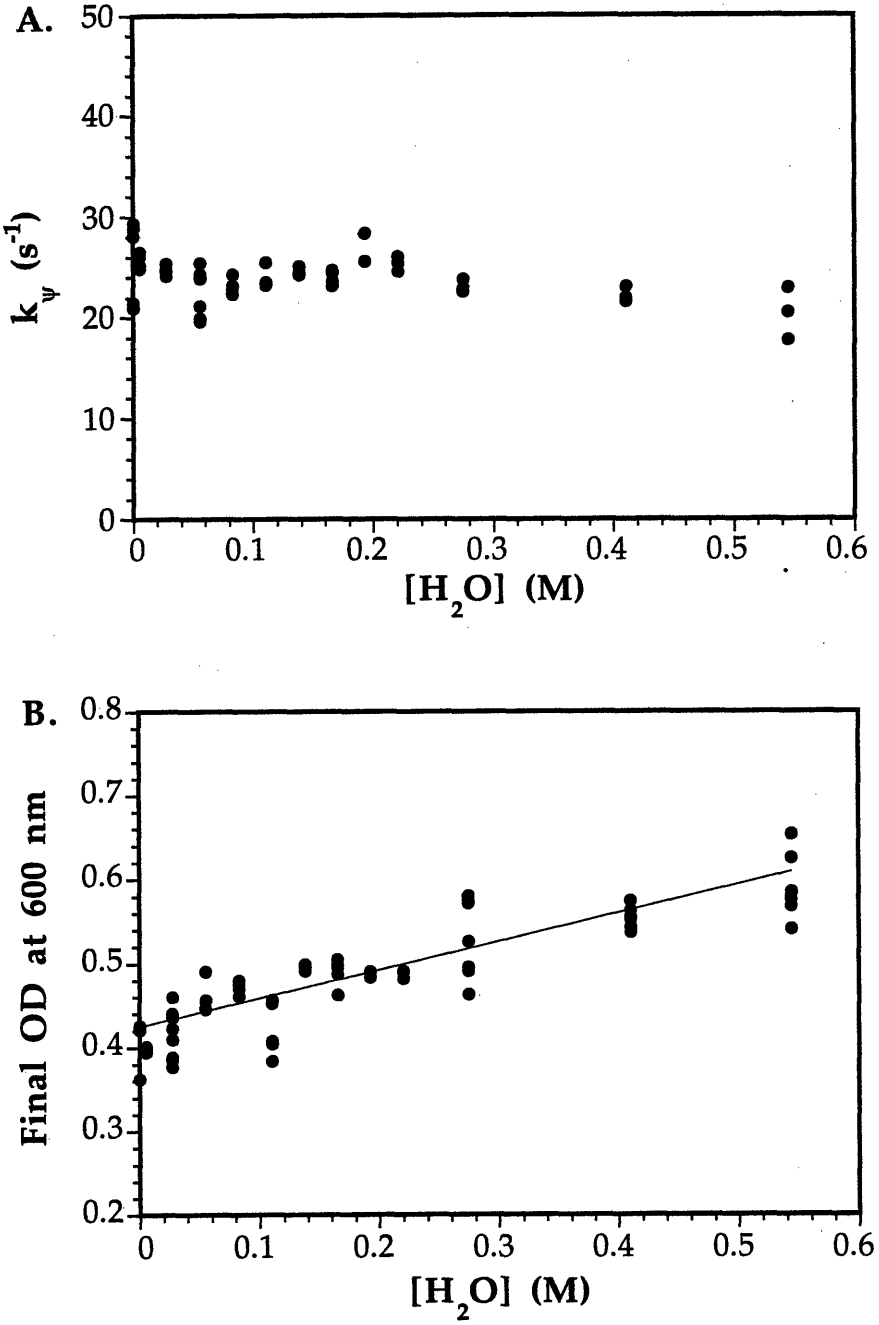

Figure 3.8. (A) A plot showing the effect of added water (0.0 - 0.54 M) on the reaction rate of 0.20 mM **3a** with 4.4 mM O_2 in propionitrile at 20 °C. (B) The effect of added water on the extinction coefficient of **3b** in propionitrile at 20°C. Similar effects were observed at low temperature (-40 °C) over a more limited range of water concentrations. Raw data are provided in Tables 3.S11 and 3.S12.

Decomposition of the Diferric Peroxide Species 1b - 3b. The complexes formed initially from the reaction of dioxygen and compounds **1a - 3a** are all metastable. When kept sufficiently cold, they survive indefinitely. The three compounds have quite different decomposition rates and temperature sensitivities, however.[29,31] The most stable adduct is **3b**, surviving for minutes to hours at room temperature depending on the concentration. This species is indefinitely stable below -35 °C. The least stable is **2b**. An initial report indicated that this peroxide adduct was not formed at room temperature.[31] The statement is incorrect, but the adduct decomposes so rapidly at this temperature that it cannot be observed visually. At -77 °C **2b** is quite stable. Compound **1b** was reported correctly to have stability properties between these two extremes.[29] Addition of polar aprotic co-solvents such as DMSO significantly stabilize acetonitrile solutions of **2b** and **3b**,[31] but an investigation of these solvent effects is beyond the scope of the present work.

We first consider the stoichiometry of the decomposition reaction. As noted above, the diiron(II) compounds react in a 1:1 ratio with dioxygen to form the peroxo intermediate. The original reports on compounds **2b** and **3b** noted that iron(III) decomposition products formed upon warming and that, at best, substoichiometric oxygen atom transfer occurred when good O-atom acceptors such as triphenylphosphine were present.[31] By carrying out more detailed manometric studies, we were able to establish the stoichiometry shown in Scheme 3.1. Dioxygen uptake was first monitored at low temperature, after which the reaction vessel was allowed to warm to room temperature. The net number of moles of dioxygen consumed by all three compounds after completion of the decomposition reaction was half the amount taken up during the low temperature reaction step (Table 3.1). In other words, half of the dioxygen taken up to form the peroxide adduct was

released following decomposition. We therefore write the decay reaction as a disproportionation yielding one equivalent of dioxygen and either two equivalents of a dinuclear ferric complex or one equivalent of a tetranuclear species (Scheme 3.1). Mixed isotope studies using $^{16}O_2$ and $^{18}O_2$ showed that no ^{16}O-^{18}O formed during the decomposition step.

Rate Law for the Decay of the Peroxide Intermediates 1b - 3b. A series of experiments systematically varying the concentrations of dioxygen and diiron(II) complexes was undertaken in a manner analogous to that described above for the formation of the intermediates, except that the temperatures used for these studies were higher to promote faster decomposition. The traces for this phase of the reaction were fit to second-order decay equations, providing the first indication that the process was bimolecular. As shown in Figure 3.9, the reactions all have a second-order dependence on the concentration of the peroxide intermediate.

The reaction order with respect to dioxygen was a little more difficult to extract from the data. The effect of varying the dioxygen concentration is shown in Figure 3.10. The simplest case is the decomposition of **3b** in which the reaction is clearly independent of the amount of dioxygen added. This result derives from the large difference between the rates of formation of **3b**, which is O_2 dependent, and decay. By the time the decay begins, the reaction of **3a** with O_2 to form **3b** is complete. Therefore, the formation of the peroxide adduct has no observable effect on the kinetics of the decay phase. For **1b** and **2b**, the separation of the two phases is less distinct. Since the kinetics are followed by using the optical band of the intermediate, no suitable absorptions being present in the spectra of the reaction products, a partial negative reaction order with respect to dioxygen is measured. This result derives from the formation of the peroxide discussed above and does not

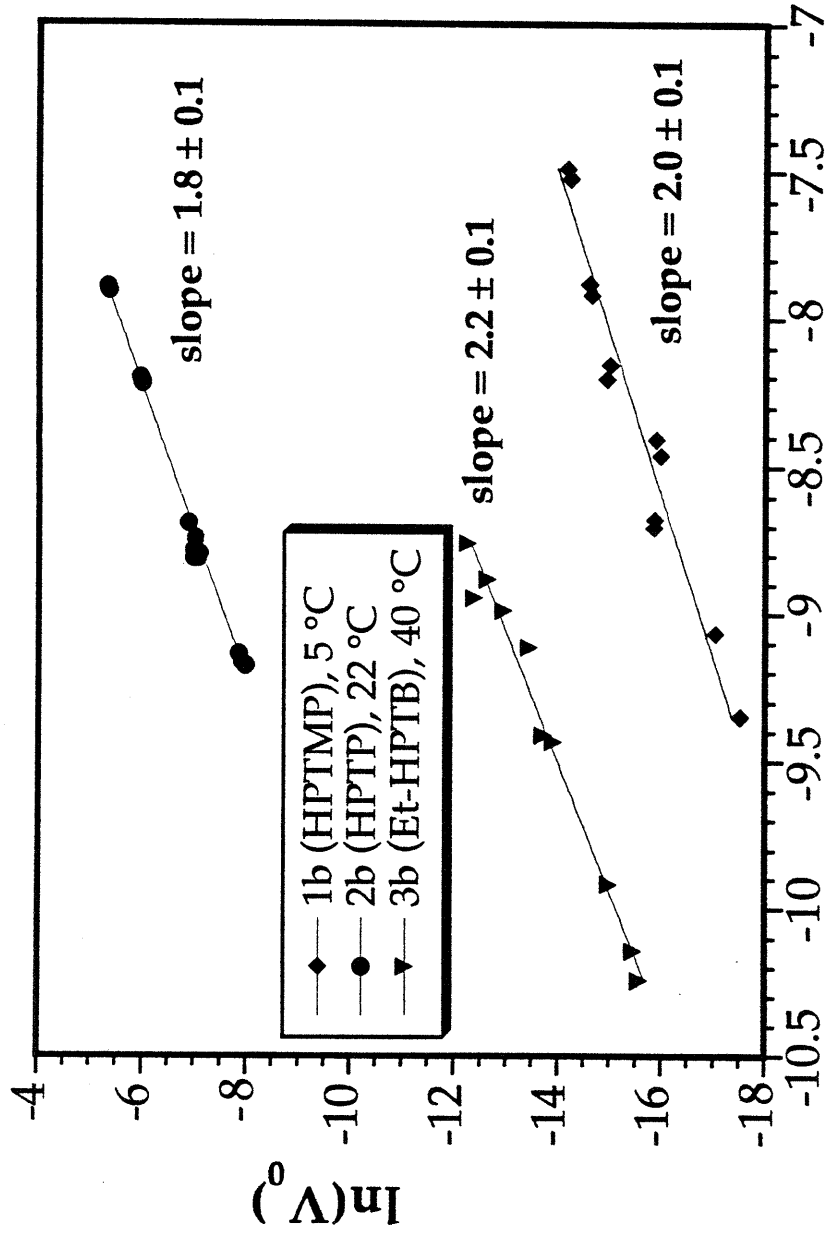

Figure 3.9. Reaction order plot showing the $\ln(V_0)$ for peroxide intermediate decomposition versus the $\ln([\mathbf{1b},\mathbf{2b},\mathbf{3b}])$, the concentration at which second-order decomposition is observed to begin. Raw data are provided in Tables 3.S12 - 3.S14.

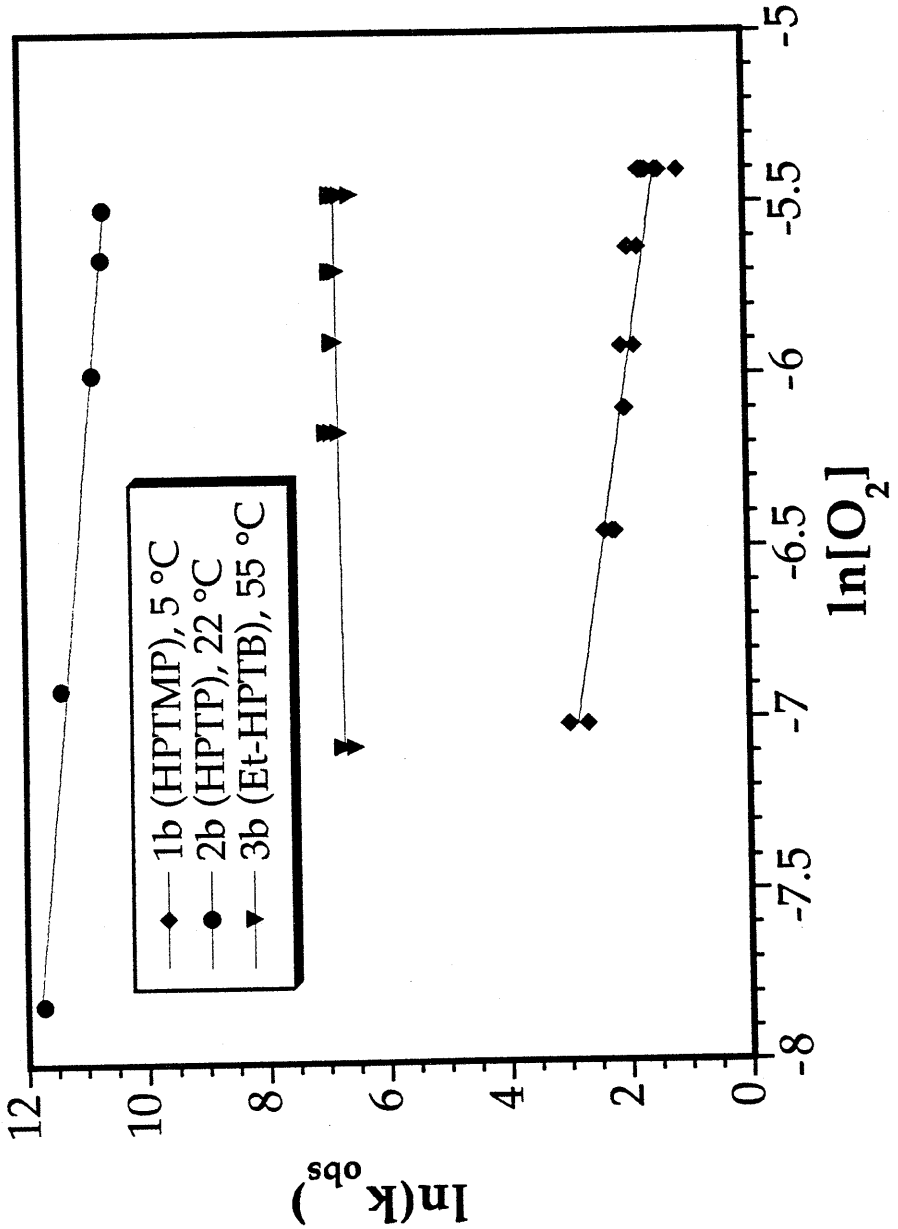

Figure 3.10. Reaction order plot showing the effect of $[O_2]$ (0.2 - 4.4 mM) on the observed second-order rate constant for the decay of the peroxide intermediates **1b** - **3b** (0.15 - 0.75 mM). Raw data are provided in Tables 3.S15 -3.S17.

relate to the actual decomposition step. A minimal rate law that describing this decay reaction is given by eq 3.15. By combining the two phases of the reaction the rate law in eq 3.16 can be written, the integrated form of which is shown in eq 3.6 above. One could add an additional term $-k_{-1}[\mathbf{B}]$, assuming a back reaction to reform the diiorn(II) starting material. In these intermediate regimes, however, satisfactory fits were obtained without such a term, showing that, from a kinetic standpoint, it was insignificant under the conditions studied.

$$-\frac{d[\mathbf{B}]}{dt} = k_2[\mathbf{B}] \tag{3.15}$$

$$\frac{d[\mathbf{B}]}{dt} = k_1[\mathbf{B}][O_2] - k_2[\mathbf{B}]^2 \tag{3.16}$$

Activation Parameters for the Decomposition of 1b - 3b. The temperature dependence of the decomposition reaction was studied in propionitrile over a wide range, 80 °C for **2b**, and because of the slower decomposition rates, 50 °C for **1b** and **3b** (Figure 3.11). The activation enthalpies vary from 52 kJ mol^{-1} for **2b** to 113 kJ mol^{-1} for **1b**, a more significant deviation than was observed for the oxygenation phase. A surprising feature is the dramatic change in activation entropy for the three reactions of 250 J mol^{-1} K^{-1}! Although the enthalpic variation is large, the massive entropy changes clearly determine the relative stabilities of these intermediates. This feature will be discussed in detail below.

The final kinetic experiment investigated whether a minimal mechanism analogous to that outlined in eq 3.15 applies to all three compounds. To obtain this information, the complex concentration was varied at different temperatures. For the simple case, a single elementary

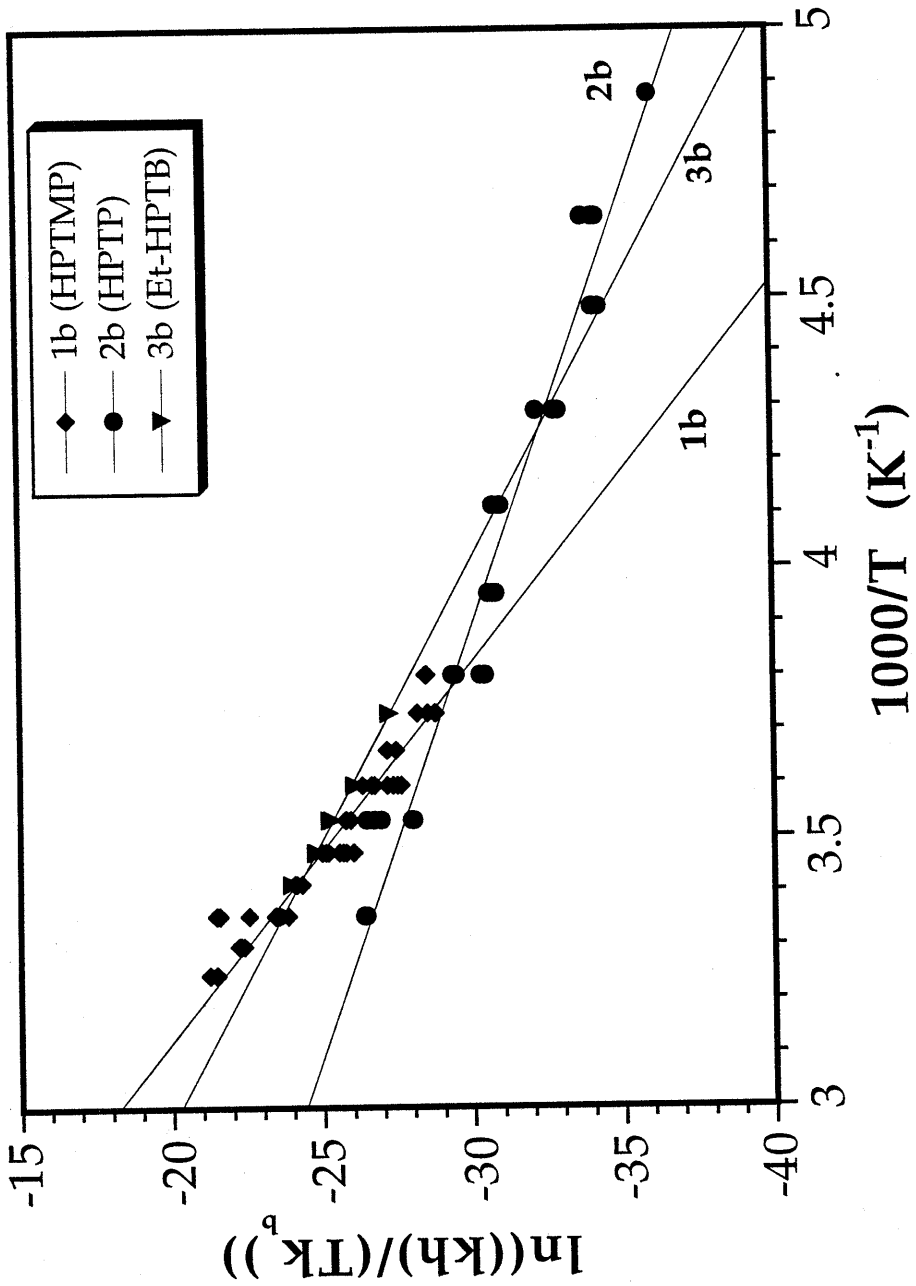

Figure 3.11. Eyring plot based on the observed second-order rate constants for the decay reaction of **1b - 3b** (≈ 0.74 mM) in EtCN at temperatures between 40 and -70 °C. Raw data are proved in Tables 3.S18 - 3.S20.

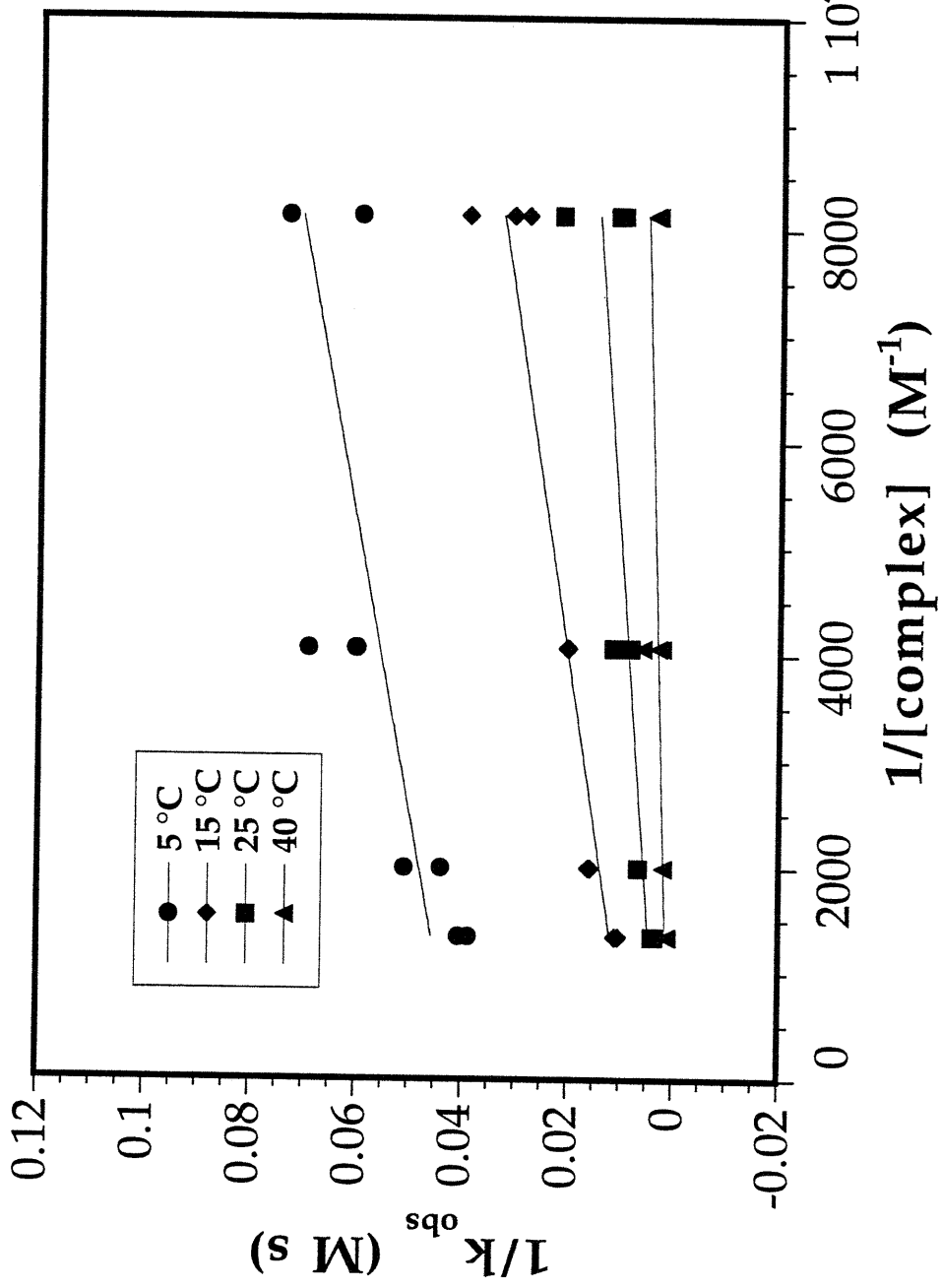

Figure 3.12. Double reciprocal analysis for the decay of **3b** based on eq 3.18. Data were collected between 5 and 40 °C and at **3b** concentrations between 1.0 - 0.125 mM. Data at each temperature were fit to a linear least-squares regression (solid lines). Raw data are provided in Table 3.S21.

reaction applies and the activation parameters are invariant. More complex behavior is indicated by changes in either $\Delta H^{\ddagger}$ or $\Delta S^{\ddagger}$, in which case a double reciprocal analysis analogous to eq 3.13 must be used. The activation parameters for the decomposition of **1b** and **2b** were invariant over a concentration range of 0.12 - 1.00 mM. The same could not be said for **3b**, however. Assuming that a pre-equilibrium step was involved, similar to the behavior of the oxygenation of **1a**, $1/k_{obs}$ was plotted against $1/[\mathbf{3b}]$ and a linear correlation was found at each temperature (Figure 3.12). This more complex system can therefore be described by the reaction scheme and rate laws given in eqs 3.17 - 3.20.

$$\mathrm{B} \underset{k_{-3}}{\overset{k_3}{\rightleftharpoons}} \mathrm{B'} \tag{3.17}$$

$$2\mathrm{B'} \xrightarrow{k_{2'}} \mathrm{C} \tag{3.18}$$

$$-\frac{d[\mathbf{B}]}{dt} = \frac{k_3 k_{2'}[\mathbf{3b}]^2}{k_{-3} + k_{2'}[\mathbf{3b}]} \tag{3.19}$$

$$\frac{1}{k_{obs}} = \frac{1}{k_3} + \frac{k_{-3}}{k_3 k_{2'}[\mathbf{3b}]} \tag{3.20}$$

Oxygen-Atom Transfer Chemistry. Previous workers have attempted to use the reactions of **1a - 3a** with dioxygen to perform oxygen-atom transfer.[31] These studies met with only limited success. A small amount of triphenylphosphine oxide was produced when this reaction was carried out in the presence of triphenylphosphine, but the kinetics of the peroxide decomposition were not significantly altered. The resulting oxidation herefore did not pertain to the major decomposition route.

Triphenylphosphine is a single oxygen atom acceptor, however. Interesting behavior was observed when a substrate capable of simultaneously accepting two oxygen atoms, such as thiophenol, was used. In this case, we observed immediate bleaching of the peroxide adduct and two products were observed, phenyl disulfide and diphenylsulfonatethioester (eq 3.21). The resulting reaction continued until dioxygen was depleted from solution affording an anaerobic solution of **3a**. This solution may be reoxygenated without significant loss in intensity of **3b**. PhSSPh does not react with **3b** even at room temperature. Since no $RS(O)_2SR$ is observed during this reaction, oxygen atom transfer must occur prior to disulfide bond formation.

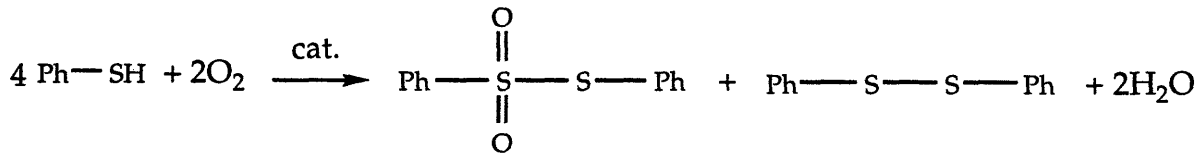

(3.21)

Discussion

The Role of Steric Factors in the Oxygenation Reaction. The three model compounds studied here are structurally quite similar (Scheme 3.1). The dinucleating ligand donor atoms are identical and each complex has an additional μ-benzoate bridge. Each is five-coordinate with an open binding site for dioxygen. The four pendant donor nitrogen atoms derive from slightly different residues, pyridyl, 6-methyl pyridyl, or N-ethyl-benzimidazolyl, but all of comparable basicity. Despite these similarities, the kinetic behavior of these three compounds in their reactions with dioxygen is dramatically different.

Three parameters can be used to define the dioxygen binding sites in **1a** - **3a**, pocket diameter, pocket depth and pocket capping. The diameter of the pocket is determined by the $[Fe_2(RO)(O_2CHPh)]^{2+}$ core and is identical for the three complexes. The depth of the pocket relates to the nature of the four pendant bases, in this case the aromatic rings which create it. Here, **3a** differs from **1a** and **2a** in the extra depth provided by the fused rings of the benzimidazole moieties. Ligands having quinoline rings have been employed to provide extra depth to pyridine-like bases in copper(I)-dioxygen reacion chemistry.[43] Finally, partial capping of the pocket is affected by the methyl groups of the HPTMP ligand (Figure 3.13).

These structural features are most likely the primary influence on the kinetic behavior rather than minor electronic differences. The vacant sites on the diiron center lie within the pockets just described. Pocket depth in **3a** provides little to no obstruction for a small ligand like O_2 approaching the dimetallic center since it is smaller than the diameter of the well. The effect of capping by HPTMP is far more obstructive, however. There is a void space below these convergent groups and a bridging peroxide ligand can be accommodated in this space, once it is there (Figure 3.13). It is the process of getting it into and out of this compartment that differentiates the oxygenation of these three systems. The decay of the peroxide intermediates is affected by a different parameter. **3b** decays much more slowly than the other two compounds and the temperature dependence of the reaction indicates that a dissociative step is important at lower temperatures. In this reaction, the relevant structural feature is the depth of the binding pocket (Figure 3.13). The fused rings of the benzimidazole groups of **3b** are substantially larger than the pyridyl arms of **1b** and **2b**, resulting in a deeper well and greater protection of the bound peroxide from bimolecular decomposition.

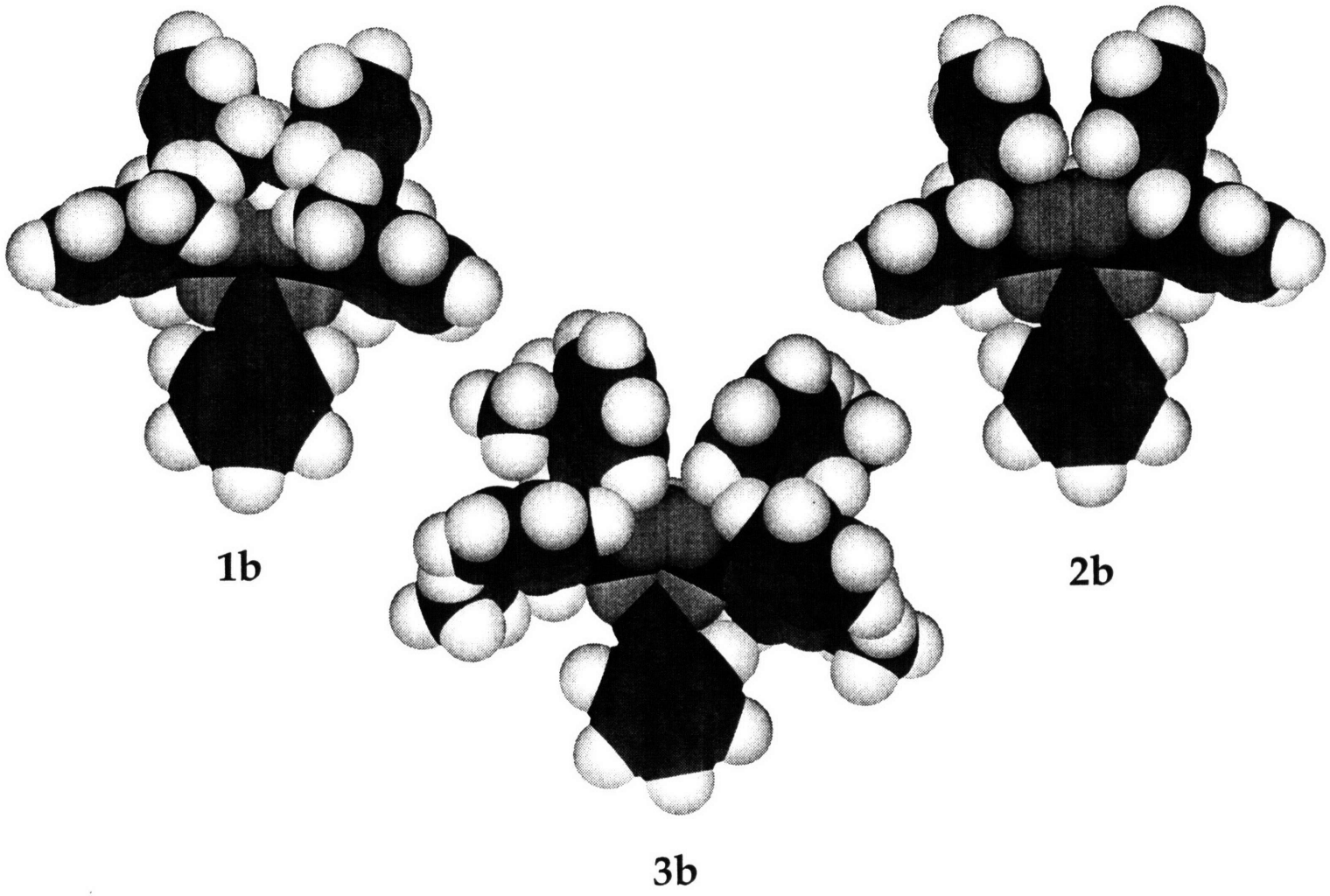

Figure 3.13. Space filling models of **1b - 3b** showing the dioxygen binding site from two angles.

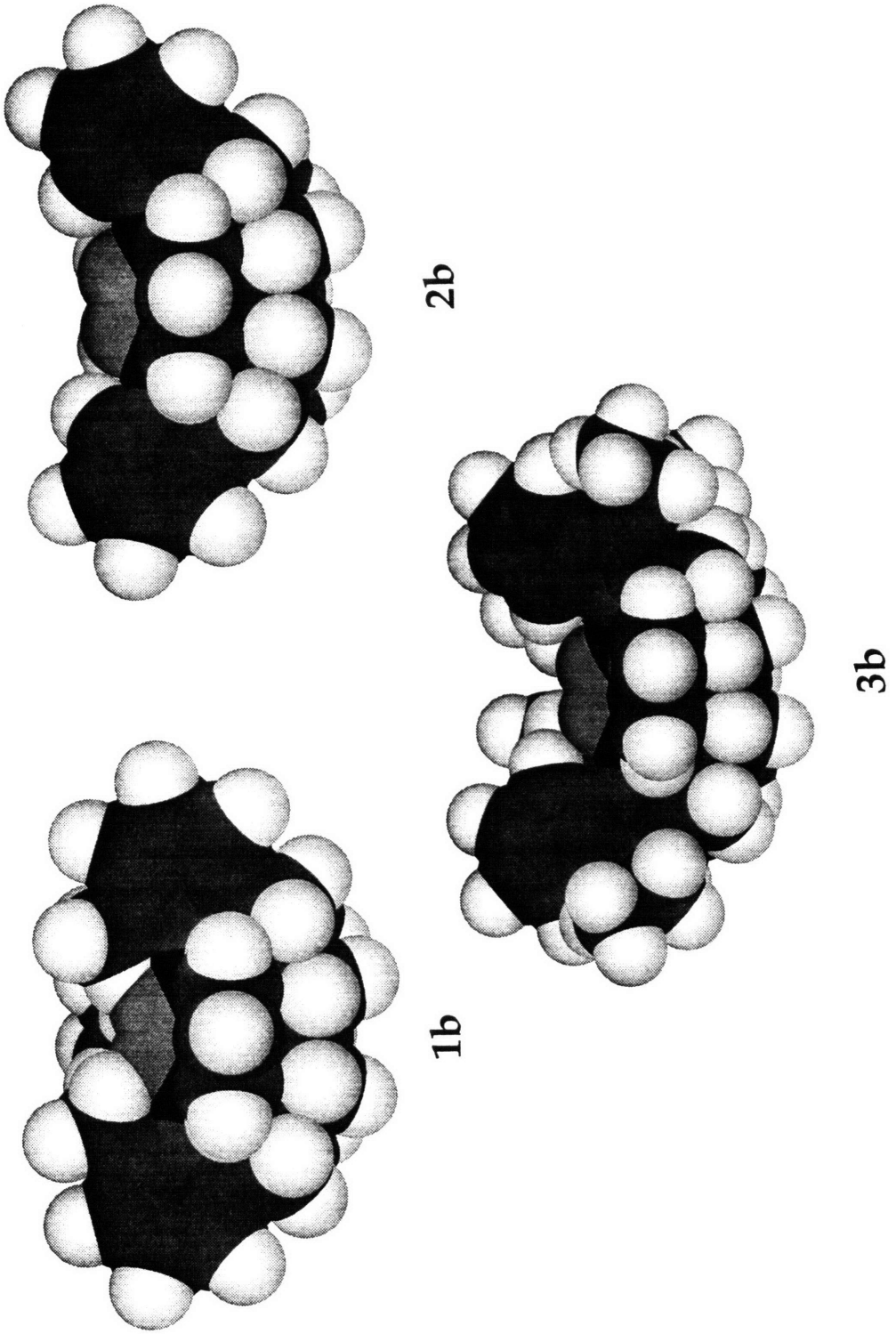
2b
3b
1b

Comparison of the Mechanism of Formation of 1b to that of 2b and 3b. The temperature-dependent results most clearly illustrate the contrast in mechanism for the reactions of dioxygen with **1a** compared either to **2a** or **3a**. Both the diminished order in dioxygen and the behavior of **1a** shown in Figure 3.5 can be explained by the pre-equilibrium step proposed in eq 3.9. The nature of **1a'** must be such that it accounts for the activation enthalpy of 39.6 kJ mol^{-1} measured for k_0. This value suggests a step that entails either partial or complete dissociation of a ligand to form a sufficiently stable intermediate having a defined life-time and not merely a ligand stretching mode. The entropic contribution for **1a'** formation is unfavorable, however, which argues against complete dissociation of any ligand component. It could reflect the need for a solvation change around the +2 cation resulting from equilibrium 3.9.

Two chemically reasonable possibilities for the **1a** $\rightleftharpoons$ **1a'** equilibrium exist. One is a carboxylate shift.[47] Carboxylate shifts have been implicated in the oxidation chemistry of coordinately saturated diiron(II) complexes[40,41] and are known to accompany redox state changes of both the sMMO hydroxylase and RNR diiron centers.[10,48,49] The steric difference between **1a** and the other two compounds is that the putative dioxygen binding site is blocked by the partial capping of the methyl groups. The shift from bridging to terminal coordination does not explain the kinetic results unless in the process a passageway for dioxygen is created. This motion contrasts with the role of carboxylate shift reactions in the oxidation of $[Fe_2(OH)(Me_3TACN)_2(OAc)_2](ClO_4)_2$, where the shift provides a dioxygen binding site.[40,41] Dissociation of a pyridyl arm is the other alternative. The four methyl groups provide a steric barrier to dioxygen approach to the metal

center which would be relieved by partial or complete dissociation of one of these arms. Iron(II) is a rather labile metal and the dissociation rates for any single arm are likely to be quite rapid.[50] The complex as a whole is stabilized by the chelate effect, which implies that statistically it is unlikely for more than one arm to dissociate at a given time.

If either of the foregoing proposals is correct, the same type of behavior should be occurring for **2a** and **3a**. The difference is that, for these compounds, the dioxygen binding step is not affected and the kinetics of adduct formation do not reflect the process. This point is important for it implies inner-sphere coordination prior to, or concomitant with, the rate-determining step in the oxidation to form peroxide adducts. For a series of capped cyclidene iron(II) complexes, complicated kinetic changes accompanied the O_2 binding process when the cavity was constricted to a size which prevented O_2 access.[51,52] Under such conditions, it was proposed that autoxidation proceeded by an outer-sphere electron transfer mechanism. Compound **1a** is unreactive with dioxygen over a period of hours below -77 °C in propionitrile. Brief exposure to higher temperatures followed by cooling results in the formation of stable **1b**. An outer-sphere mechanism for autoxidation is therefore not accessible in the present systems, or if it is, it must occur on a time scale beyond that which was investigated.

Interpretation of the Activation Parameters for Adduct Formation and Comparisons to Other Systems. The activation parameters of a reaction reflect the transition state, allowing deductions about the reaction coordinate and comparisons to other known reactions to be made. Theoretically, the Eyring equation is valid only for elementary reactions. When more complicated reactions are subjugated to such an analysis, negative curvature of the plot can be encountered, indicating that two separate steps can be rate-

limiting at the temperature extremes. In practice, however, it is often possible to study complex rate equations by this methodology so long as curvature is absent over a given temperature range. The values then correspond to the energy barrier for the rate determining elementary step in that range. The Eyring plot shown in Figure 3.6 exemplifies such behavior for the reaction of **1a** with dioxygen. Over the temperature range studied, a single step dominates the activation barrier and a linear plot results. The reactions of **2a** and **3a** are simple second-order reactions, studied under pseudo first-order conditions, and linearity is predicted.

The activation enthalpy for the reactions of **2a** and **3a** with dioxygen is remarkably similar to that of oxyHr formation. It is possible that this agreement is merely a coincidence, but more likely it represents the energy barrier to reach the transition state in the interaction of dioxygen with a reduced diiron(II) center having an accessible binding site to form a peroxydiiron(III) species. In Hr, one iron atom has such a vacant site. Since the structures of the peroxide adducts differ for Hr and the model compounds, the implication is that the binding of dioxygen and the associated two-electron oxidation of the iron center comprise the rate-determining step. Structural rearrangements to form a (μ-1,2-peroxo)diiron(III) intermeidate in the case of the models, or the terminal hydroperoxide with a hydrogen-bond to the oxo-bridge in Hr, are subsequent, kinetically silent, steps.

The volume of activation of the reaction provides an additional measure that can be used to compare the present kinetic study with those of the proteins and similar model compounds (Table 3.1). The measured value of -12.7 cm^3 mol^{-1} for **3b** formation is quite similar to that for oxygenation of dicopper(I) model systems.[53] In the case of $\Delta V^{\ddagger}$, proteins like Hr and Mb are at variance with the model systems. The pressure dependencies for the

proteins may reflect factors other than just dioxygen binding to the metal center, however.[54] The high pressure may cause shifts in the peptide fold such that the access of O_2 to the active site is altered.

Solvent Effects. Since water binds to **1a**,[29] its could potentially effect the kinetics of the oxygenation reaction by blocking a binding site. Extensive studies with added water, however, showed no significant effect on the kinetic parameters for oxidation of **3a** in the 2.0 mM to 0.5 M range. Exploratory work in MeCN and $CHCl_3$ similarly failed to reveal any dramatic changes. The absolute rates were slightly slower (a factor of 2-3) in $CHCl_3$, consistent with a passive role for the solvent in these reactions.

A significant effect on the extinction coefficient of **3b** was observed as a function of water concentration. The linear dependence of this effect indicated that it did not arise from coordination of water, which would have a 1/(1+x) dependence similar to that for the classical example of an acid-base titration. This finding implies that the changes in the optical density do not relate to a binding process. Instead, the observed changes must arise either from changes in ion pairing or the polarity of the solvent cage.

Nature of the Final Oxidation Products. Studies of the dinuclear ferric species $[Fe_2(O)(HPTB)(OBz)](NO_3)_2$, where HPTB is identical to Et-HPTB but lacks the N-ethyl groups, revealed aggregation of two dinuclear units to form a tetranuclear species.[55] This finding implies that the identification of products for the decomposition reaction of **1b** to **3b** by isolation and crystallization might not accurately reveal the nature of the product initially formed. The studies reported here used for kinetic analysis the decay of the optical absorption signal belonging to the peroxo intermediate for kinetic analysis. They therefore will not reflect subsequent reactions. In Scheme 3.1, we depict the products **1c** - **3c** as tetranuclear species. The complex **3c** was

reported as the product of the oxidation of **3a**.[13] The optical spectrum of **3c** and its extinction coefficients match that of the tetranuclear species previously cited as the product. Whether such a species results directly from the decomposition or is a manifestation of further equilibria is not addressed by the kinetic studies presented here.

Two Possible Peroxo Intermediate Decay Mechanisms. The results for decay of the peroxide intermediates provide some interesting clues about the behavior of these metastable species. This reaction is of primary interest to the chemist seeking to understand oxo-transfer chemistry or to carry out such a reaction. It is this step in the overall transformation which diverts small molecule models from mimicking the chemistry of the protein active sites. As already discussed, the model compounds form peroxide intermediates similar to those found in the native protein systems, and they do so with analogous activation parameters provided the diiron center is sterically accessible. Yet these same models cannot mimic substrate activation or catalysis. The reason for this deviant behavior is apparent from the kinetics of the decay reactions, which are second-order with respect to complex. In order for a catalyst to generate a highly energetic intermediate with enough oxidizing potential, for example, to break a C-H bond, all lower energy pathways leading to autoxidation must be avoided. The bimolecular reaction uncovered here is one such pathway, knowledge of which will allow a greater chance of overcoming the difficulty in future work.

We now consider the nature of the peroxide decomposition step. In work with two other model compounds, $[Fe_2(OH)(Me_3TACN)_2(OAc)_2](ClO_4)$ and $[Fe_2(BIPhMe)_2(O_2CH)_4]$, we proposed a ($\mu^4$-peroxo)diiron(II)diiron(III) species.[41] Such an activated complex would not be possible for **2b** and **3b** for two reasons. The first relates to the irreversibility of the formation of these

peroxide intermediates. Once dioxygen reacts with the diiron(II) compounds, it is impossible to reverse this process, even by using vacuum down to 10^{-3} torr. The second is based on the relative rates of the formation and decay of the peroxo intermediates, specially **3b**. The half-lives of the two phases of the reaction differ by 4-5 orders of magnitude depending on complex concentration. By the time **3b** begins to decompose, no **3a** is available. For **1a**, however, the reaction with dioxygen is reversible, a $P_{1/2}$ of 6 torr at -35 °C in CH_2Cl_2 having been measured.[29] Although this binding is reasonably strong, it is possible that the second-order decomposition results from reversal of the oxygenation step followed by reaction with another equivalent of the peroxo intermediate. Given the similarity of the three compounds, however, it is likely that the decomposition reactions follow similar pathways, with the only perturbations arising from for the different steric constraints.

Having discounted a mechanism in which an equivalent of the peroxide adduct reacts with the diiron(II) starting material, two possible mechanisms for the decomposition reaction. Both fit the kinetic data, resulting in second-order decay reactions with the loss of an equivalent of dioxygen. These possibilities are presented in Scheme 3.2. The first pathway (A) is based on an analogy to the decay of secondary and tertiary alkyl peroxide radicals, which proceed through a tetroxide species.[56-58] Following decomposition, these molecules yield an equivalent of alcohol, an equivalent of ketone, and a molecule of dioxygen. The other mechanism (B) involves more conventional nucleophilic attack and disproportionation. Mechanism A was differentiated from B by the $^{16}O_2/^{18}O_2$ labeling experiments discussed above. In mechanism B, the dioxygen molecule released following decomposition is one taken up during the first phase of the reaction. No O-O bonds are made during the reaction. In contrast, the tetroxide mechanism (A)

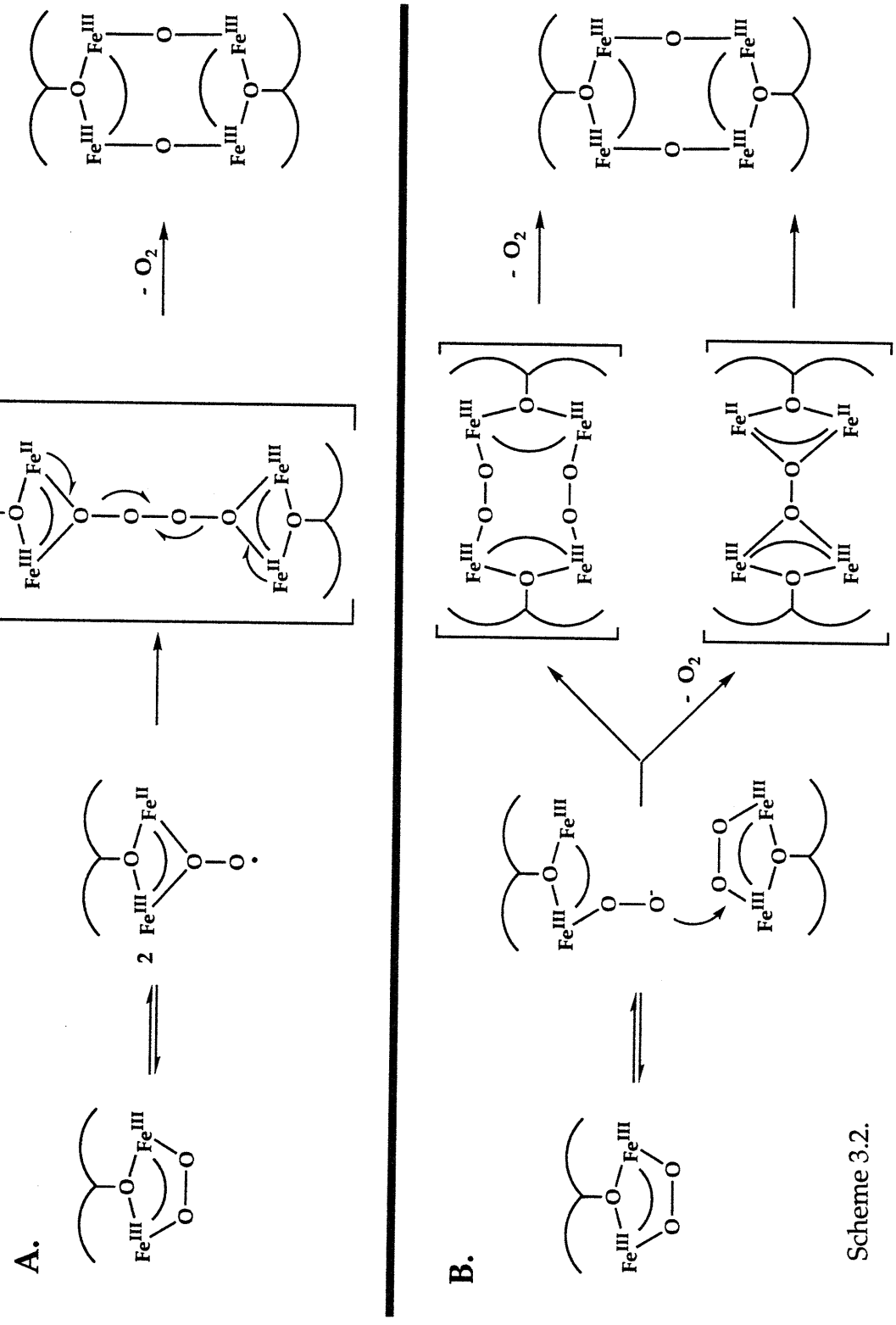

Scheme 3.2.

forms a new O-O bond in the decomposition step, the central two oxygen atoms of the tetroxide depart as O_2. In the O_2 labeling experiment where **3b** and **3b*** were mixed, degassed, and allowed to decompose under vacuum, no ^{16}O-^{18}O was recovered. Mechanism A can therefore be ruled out. Because dioxygen is released after a rate-determining, second-order step in mechanism B, it is impossible to determine whether this process occurs immediately or in a subsequent step. Both possiblilities are depicted in Scheme 3.2B.

The bottom pathway in Scheme 3.2B would provide a common intermediate in this decay pathway and the one proposed in previous studies.[40,41] A similar μ^4-peroxo adduct has been crystallographically characterized[59] although this molecule contains four ferric ions instead of the diiron(II)diiron(III) formulation of the transition state. As mentioned above, the loss of dioxygen from **2b** and **3b** is not observed even under vacuum. The energy barrier for the back reaction appears to be greater than the decomposition. The bimolecular collision might be a source of sufficient energy to free the dioxygen molecule. Once released, the diiron(II) material would be in position to react rapidly with the molecule of peroxo intermediate with which it collided.

Relation of the Kinetic Parameters to the Chemical Properties of the Compounds. The stability of the peroxide adducts **1b - 3b** is a property of considerable interest, since these species are analogues of the biological precursors to high-energy intermediates believed to carry out oxygenation chemistry at the active sites in the dinuclear non-heme iron enzymes. We have observed bimolecular decay. This pathway is prevented in the protein systems because the (peroxo)diiron(III) species is secluded deep within the protein fold. The measured activation parameters for the bimolecular reaction provide a measure of the instability of the protein intermediates

even though the decay mechanisms differ, however. The model compound will decompose by the lowest energy pathway, regardless of whether it is a unimolecular or bimolecular event. If the transition states for the two pathways are of comparable energy, then both reactions will occur parallel to one another. The kinetic traces in such cases would appear biphasic, the sum of a first-order and a second-order decay. Presumably a unimolecular pathway for the decay of **1b** - **3b**, such as the one the protein systems must employ, exists. Since clean second-order behavior was observed, this unimolecular reaction must occur with a higher energy barrier than that for the bimolecular pathway. Therefore, the activation energies presented here for the bimolecular reaction provide a lower limit for a comparable unimolecular mechanism.

A reaction coordinate diagram reflecting the experimentally determined activation parameters is presented in Figure 3.14. Not all of the information necessary for a complete reaction coordinate diagram was available, so approximations were made in preparing this figure. For **1a**, the value of $P_{1/2}$ for dioxygen binding is known (6 Torr at -35°C),[29] and corresponds to a ΔG value of -9.6 kJ mol^{-1}. Although the temperature dependence of the binding has not been reported, a crude approximation of 80 J mol^{-1} K^{-1} can be made based on the measured values reported for Hr.[60] The ΔG values for the decomposition of the peroxide intermediates were chosen arbitrarily, but since the reactions are irreversible, the importance of the **c** $\rightarrow$ **b** activation barriers is minimal. The reactions of **2a** and **3a** with dioxygen cannot be reversed by the application of vacuum. One may therefore conservatively set an upper limit on dioxygen binding at $P_{1/2} \leq 0.05$ Torr. This inequality leads to an upper bound of $\Delta G < -19$ kJ mol^{-1} for **2a** and **3a**, the value used in drawing Figure 3.14. It should be noted that the depth of the

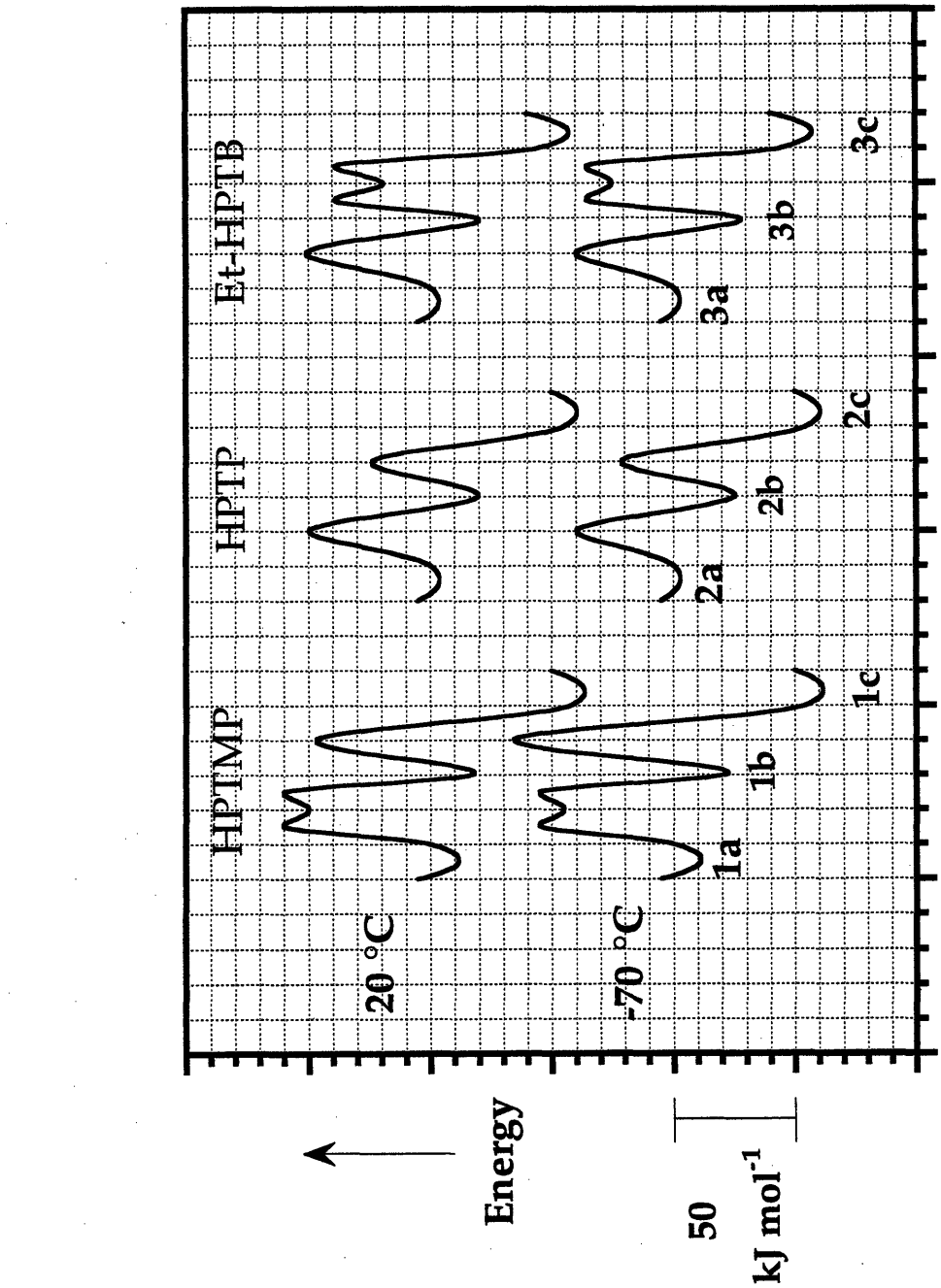

Figure 3.14. Reaction coordinate diagram showing $\Delta G^{\ddagger}$ for the reactions of **1a - 3a** with dioxygen at 20 and -70 °C.

wells containing **2b** and **3b** could be substantially deeper than actually shown. Microcalorimetry experiments would be required to determine these energies. Even by using the maximum values for ΔG it can be seen that **2b** is unlikely to be reversible at accessible temperatures. The potential for observing reversibility with **3b** is somewhat greater, but once again, the ΔG for the formation of **3b** could be substantially more favorable than actually depicted.

The formation of **1b** and the decay of **3b** are not elementary steps although linear behavior in an Eyring analysis is observed. The shallow wells shown as part of the transition from **1a** to **1b** and **3b** to **3c** (Figure 3.14) represent the structural rearrangement steps discussed above. The height of the net barrier for the reactions have been measured, but two component steps contribute to the overall transformation.

The variation in the activation parameters among the three peroxide intermediates reveals the primary difference in their stability to be entropic. For **1b** and **3b** formation, $\Delta S^{\ddagger}$ is large and favorable. Such a finding is unusual for a bimolecular event since the transition state is usually more ordered than the reactants. There are two potential explanations for this behavior. One is that $\Delta S^{\ddagger}$ reflects solvent reorganization. The reactants are +2 cations and will be highly solvated. On approaching the transition state, charge increases to +4. This process changes the surface to volume ratio of the charged species and could release many solvent molecules and lend to a large positive increase in the entropy of activation. Furthermore, ion pairing is more likely to occur to the +4 cation, further complicating the solvent contribution, but still providing a favorable solvent component to $\Delta S^{\ddagger}$. Addition of DMSO has been reported to stabilize peroxo adducts, especially **2b**.[31] By altering the nature of this solvation, very significant effects might be exerted on the entropic term. The second, more likely possibility is that the transition state

involves release of one equivalent of dioxygen (Scheme 3.2B, bottom pathway). Such a mechanism would offset the effect of a bimolecular collision and there would be no change in the net number of species.

In all three cases, the activation enthalpy for the decomposition of the peroxide adduct is a factor of 3-5 greater than that for its formation. The relative values of the activation entropy for the forward (k_3) and reverse (k_{-1}) reactions therefore dictates the relative decomposition rates. In addition, an important thermodynamic factor which plays a key role in the determining of the reversibility of the reaction is the ΔG for the conversion of the ferrous material to the peroxide adduct. This value effects the depth of the well in which the intermediate resides (Figure 3.13) and determines the chemical reversibility. The relative high energy of **1b** most likely reflects steric interactions between dioxygen and the methyl groups in the pocket it occupies (Figure 3.13).

This property of destabilizing the peroxide intermediate leads to an interesting possibility which contradicts the popular dogma of reversible dioxygen binding. In the case of Hr, it has often been proposed that the peroxide adduct is stabilized by hydrogen bonding and this interaction somehow prevents its decomposition via the pathways normally observed for sMMO and RNR. In these model systems however, the ground state of the reversible binder is higher than that of the molecules known to undergo only irreversible decomposition. By forming a dioxygen adduct which is too stable, the barrier to reversibilty cannot be overcome. Other systems such as the cyclidenes and capped porphyrins also bind dioxygen reversibly. It is possible that this ground state effect is in play in these cases too. The diiron centers in RNR and sMMO have vacant coordination sites on both iron atoms. The formation of a 1,2-bridging peroxide has been proposed in both

cases. The ground state of this peroxide intermediate may be too low in energy to undergo reversible binding and therefore is trapped into a decay pathway leading to dioxygen activation.

Summary and Conclusions

The dioxygen uptake and subsequent decomposition reactions for three diiron(II) model compounds have been studied by stopped-flow spectroscopy. The mechanistic results show that two of the model compounds very accurately mimic the oxygenation chemistry of Hr. When sufficient ligand steric constraints prevent efficient access to the diiron(II) center by the incoming dioxygen molecule, a dissociative reorganization step is required prior to the binding of dioxygen. The key steric factor was identified as the capping of the binding site (compound **1a**).

Thermal decomposition of the peroxide intermediates occurs in all three cases by a non-biomimetic second-order rate-determining step. In this reaction, an equivalent of dioxygen is evolved such that the stoichiometry of the overall transformation is 0.5 equiv O_2 per dinuclear center, similar to that observed for reactions of other non-heme diiron model compounds with dioxygen.[41] In order for efficient biomimetic oxygenation of substrates to occur, this second-order decay reaction must be eliminated. The trends observed for these three compounds reveal that, whereas capping is important for the O_2 binding step, the depth of the coordination pocket plays a larger role for the decomposition reactions.

A final finding from this study is that, whereas oxo transfer to Ph_3P did not occur, dioxygenase activity with thiophenol as the substrate was promoted by these compounds. This behavior may be inherent to diferric peroxide species but may not be observed in the protein active sites owing to the lack of a suitable acceptor. The stability of the μ-1,2-peroxide

intermediates studied here indicates that it is not likely to be the species directly responsible for oxygen transfer in the enzymes. This statement implies either that O-O bond cleavage occurs prior to C-H activation or that the dioxygen adduct isomerizes to a more activated form prior to its interaction with a substrate in monooxygenase reactions.

Acknowledgments; This work was funded by grants from the NIGMS and AKZO Corporation. A.L.F. also wishes to thank V. Pecoraro and A. Bakac for interesting discussions on tetroxides.

References

(1) A portion of this work has been previously communicated in Ref. 2.

(2) Feig, A.; Lippard, S. J. *J. Am. Chem. Soc.* **1994**, *116*, 8410-8411.

(3) Kurtz, D. M., Jr.; Shriver, D. F.; Klotz, I. M. *Coord. Chem. Rev.* **1977**, *24*, 145-178.

(4) Sanders-Loehr, J. In *Iron Carriers and Iron Proteins*; Loehr, T. M., Eds.; VCH: New York, 1989; Vol. 5; pp 373-466.

(5) Stenkamp, R. E. *Chem. Rev.* **1994**, *94*, 714-726.

(6) Nordlund, P.; Sjöberg, B.-M.; Eklund, H. *Nature* **1990**, *345*, 593-598.

(7) Stubbe, J. In *Advances in Enzymology and Related Areas of Molecular Biology*; Meister, A., Eds.; John Wiley and Sons: New York, 1990; Vol. 62; pp 349-420.

(8) Fontecave, M.; Nordlund, P.; Eklund, H.; Reichard, P. In *Advances in Enzymology and Related Areas of Molecular Biology*; Meister, A., Eds.; Wiley and Sons: New York, 1992; Vol. 65; pp 147-183.

(9) Nordlund, P.; Eklund, H. *J. Mol. Biol.* **1993**, *232*, 123-164.

(10) Rosenzweig, A. C.; Frederick, C. A.; Lippard, S. J.; Nordlund, P. *Nature* **1993**, *366*, 537-543.

(11) Lipscomb, J. D. *Annu. Rev. Microbiol.* **1994**, *48*, 371-399.

(12) Liu, K. E.; Lippard, S. J. *Adv. Inorg. Chem.* **1995**, in press.

(13) Que, L., Jr. In *Bioinorganic Catalysis*; Reedijk, J., Eds.; Marcel Dekker: New York, 1993; pp 347-393.

(14) Feig, A. L.; Lippard, S. J. *Chem. Rev.* **1994**, *94*, 759-805.

(15) Åberg, A.; Ormö, M.; Nordlund, P.; Sjöberg, B.-M. *Biochem.* **1993**, *32*, 9845-9850.

(16) Bollinger, J. M., Jr.; Edmondson, D. E.; Huynh, B. H.; Filley, J.; Norton, J. R.; Stubbe, J. *Science* **1991**, *253*, 292-298.

(17) Lee, S.-K.; Nesheim, J. C.; Lipscomb, J. D. *J. Biol. Chem.* **1993**, *268*, 21569-21577.

(18) Lee, S.-K.; Fox, B. G.; Froland, W. A.; Lipscomb, J. D.; Münck, E. *J. Am. Chem. Soc.* **1993**, *115*, 6450-6451.

(19) Bollinger, J. M., Jr.; Tong, W. H.; Ravi, N.; Huynh, B. H.; Edmondson, D. E.; Stubbe, J. *J. Am. Chem. Soc.* **1994**, *116*, 8015-8023.

(20) Bollinger, J. M., Jr.; Tong, W. H.; Ravi, N.; Huynh, B. H.; Edmondson, D. E.; Stubbe, J. *J. Am. Chem. Soc.* **1994**, *116*, 8024-8032.

(21) Ravi, N.; Bollinger, J. M., Jr.; Huynh, B. H.; Edmondson, D. E.; Stubbe, J. *J. Am. Chem. Soc.* **1994**, *116*, 8007-8014.

(22) Liu, K. E.; Valentine, A. M.; Wang, D.; Huynh, B. H.; Edmondson, D. E.; Salifoglou, A.; Lippard, S. J. *J. Am. Chem. Soc.* **1995**, in press.

(23) Stenkamp, R. E.; Sieker, L. C.; Jensen, L. H.; McCallum, J. D.; Sanders-Loehr, J. *Proc. Natl. Acad. Sci., USA* **1985**, *82*, 713-716.

(24) Shiemke, A. K.; Loehr, T. M.; Sanders-Loehr, J. *J. Am. Chem. Soc.* **1986**, *108*, 2437-2443.

(25) Hartman, J. R.; Rardin, R. L.; Chaudhuri, P.; Pohl, K.; Wieghardt, K.; Nuber, B.; Weiss, J.; Papaefthymiou, G. C.; Frankel, R. B.; Lippard, S. J. *J. Am. Chem. Soc.* **1987**, *109*, 7387-7396.

(26) Borovik, A. S.; Que, L., Jr. *J. Am. Chem. Soc.* **1988**, *110*, 2345-2347.

(27) Kitajima, N.; Fukui, H.; Moro-oka, Y. *J. Am. Chem. Soc.* **1990**, *112*, 6402-6403.

(28) Tolman, W. B.; Liu, S.; Bentsen, J. G.; Lippard, S. J. *J. Am. Chem. Soc.* **1991**, *113*, 152-164.

(29) Hayashi, Y.; Suzuki, M.; Uehara, A.; Mizutani, Y.; Kitagawa, T. *Chem. Lett.* **1992**, 91-94.

(30) Stassinopoulos, A.; Schulte, G.; Papaefthymiou, G. C.; Caradonna, J. P. *J. Am. Chem. Soc.* **1991**, *113*, 8686-8697.

(31) Dong, Y.; Menage, S.; Brennan, B. A.; Elgren, T. E.; Jang, H. G.; Pearce, L. L.; Que, L., Jr. *J. Am. Chem. Soc.* **1993**, *115*, 1851-1859.

(32) Hagen, K. S.; Lachicotte, R.; Kitaygorodskiy, A.; Elbouadili, A. *Angew. Chem. Int. Ed. Engl.* **1993**, *105*, 1404-1406.

(33) Zang, Y.; Elgren, T. E.; Dong, Y.; Que, L., Jr. *J. Am. Chem. Soc.* **1993**, *115*, 811-813.

(34) Kitajima, N.; Tamura, N.; Amagai, H.; Fukui, H.; Moro-Oka, Y.; Mizutani, Y.; Kitagawa, T.; Methur, R.; Heerwegh, K.; Reed, C. A.; Randall, C. R.; Que, L., Jr.; Tatsumi, K. *J. Am. Chem. Soc.* **1994**, *116*, 9071-9085.

(35) Herold, S.; Pence, L. E.; Lippard, S. J. *J. Am. Chem. Soc.* **1995**, *117*, 6135.

(36) Coucouvanis, D.; Reynolds, R. A., III; Dunham, W. R. *J. Am. Chem. Soc.* **1995**, *117*, 7570-7571.

(37) Menage, S.; Brennan, B. A.; Juarez-Garcia, C.; Münck, E.; Que, L., Jr. *J. Am. Chem. Soc.* **1990**, *112*, 6423-6425.

(38) Brennan, B. A.; Chen, Q.; Juarez-Garcia, C.; True, A. E.; O'Connor, C. J.; Que, L., Jr. *Inorg. Chem.* **1991**, *30*, 1937-1943.

(39) Perrin, D. D.; Armarego, W. L. F. *Purification of Laboratory Chemicals;* 3rd ed.; Butterworth-Heinemann: Oxford, 1988.

(40) See also Chapter II.

(41) Feig, A. L.; Masschelein, A.; Bakac, A.; Lippard, S. J. *J. Am. Chem. Soc.* **1995**, manuscript in preparation.

(42) van Eldik, R.; Gaede, W.; Wieland, S.; Kraft, J.; Spitzer, M.; Palmer, D. A. *Rev. Sci. Instrum.* **1993**, *64*, 1355-1357.

(43) Karlin, K. D.; Wei, N.; Jung, B.; Kaderli, S.; Niklaus, P.; Zuberbühler, A. D. *J. Am. Chem. Soc.* **1993**, *115*, 9506-9514.

(44) *Oxygen and Ozone*; Battino, R., Ed.; Pergamon Press: Oxford, 1981; Vol. 7.

(45) Petrou, A. L.; Armstrong, F. A.; Sykes, A. G.; Harrington, P. C.; Wilkins, R. G. *Biochim. Biophys. Acta* **1981**, *670*, 377-384.

(46) van Eldik, R. In *High Pressure Chemistry, Biochemistry and Material Science*; Winter, R. and Jonas, J., Eds.; Kluwer Academic: Dordrecht, 1993; pp 309-328.

(47) Rardin, R. L.; Tolman, W. B.; Lippard, S. J. *New J. Chem.* **1991**, *15*, 417-430.

(48) Rosenzweig, A.; Frederick, C. A.; Lippard, S. J. *Biology and Chemistry* **1995**, *2*, 409-418.

(49) Åberg, A. Thesis, Stockholm University, 1993.

(50) Porterfield, W. W. *Inorganic Chemistry - A Unified Approach*; Academic: New York, 1993.

(51) Sauer-Masarwa, A.; Dickerson, L. D.; Herron, N.; Busch, D. H. *Coord. Chem. Rev.* **1993**, *128*, 117-137.

(52) Busch, D. H.; Alcock, N. W. *Chem. Rev.* **1994**, *94*, 585-623.

(53) Becker, M.; Schindler, S.; van Eldik, R. *Inorg. Chem.* **1994**, *33*, 5370-5371.

(54) Projahn, H.-D.; Schindler, S.; van Eldik, R.; Fortier, D. G.; Andrew, C. R.; Sykes, A. G. *Inorg. Chem.* **1995**, in press.

(55) Chen, Q.; Lynch, J. B.; Gomez-Romero, P.; Ben-Hussein, A.; Jameson, G. B.; O'Connor, C. J.; Que, L., Jr. *Inorg. Chem.* **1988**, *27*, 2673-2681.

(56) Bartlett, P. D.; Guadaldi, G. *J. Am. Chem. Soc.* **1967**, *89*, 4799-7801.

(57) Bartlett, P. D.; Günther, P. *J. Am. Chem. Soc.* **1966**, *88*, 3288-3294.

(58) Traylor, T. G.; Bartlett, P. D. *Tet. Let.* **1960**, 30-36.

(59) Micklitz, W.; Bott, S. G.; Bentsen, J. G.; Lippard, S. J. *J. Am. Chem. Soc.* **1989**, *111*, 372-374.

(60) De Waal, D. J. A.; Wilkins, R. G. *J. Biol. Chem.* **1976**, *251*, 2339-2343.

Supplementary Materials for

CHAPTER III.

Mechanistic Studies of the Formation and Decay of Diiron(III) Peroxo Complexes in the Reaction of Diiron(II) Precursors with Dioxygen

Table 3.S1. Data for the Determination of the Reaction Order with Respect to Complex for **3a.**

[O2] (mM)	$[\mathbf{3a}]_0$ (mM)	Temp (°C)	k_ψ (s^{-1})	$t_{1/2}$ (ms)	V_0*10^3 (M s^{-1})[a]
4.4	0.40	20	28.7 ± 0.2	24.1 ± 0.2	7.03 ± 0.24
4.4	0.25	20	26.8 ± 2.3	26.0 ± 2.2	4.30 ± 0.62
4.4	0.20	20	28.1 ± 0.6	24.6 ± 0.5	3.85 ± 0.14
4.4	0.10	20	27.4 ± 1.1	25.3 ± 1.0	2.31 ± 0.13
4.4	0.060	20	23.1 ± 1.7	30.1 ± 2.3	1.22 ± 0.10

[a] $V_0 = \frac{m_2 m_3}{\varepsilon 2 \ln 2}$ where ε is the extincition coefficient of **3b** and m_2 and m_3 are defined by eq 3.4.

Table 3.S2. Data for the Determination of the Reaction Order with Respect to O_2 for **1a**.

[O2] (mM)	$[\mathbf{1a}]_0$ (mM)	Temp (°C)	$k_\psi * 10^3$ (s^{-1})	$t_{1/2}$ (s)
4.82	0.206	-50	3.99 ± 0.05	174 ± 3
3.62	0.206	-50	3.50 ± 0.26	199 ± 15
2.41	0.206	-50	2.94 ± 0.35	238 ± 27
1.69	0.206	-50	1.88 ± 0.20	369 ± 37
1.21	0.206	-50	1.56 ± 0.07	445 ± 22

Table 3.S3. Data for the Determination of the Reaction Order with Respect to O_2 for **2a**.

[O2] (mM)	$[\mathbf{2a}]_0$ (mM)	Temp (°C)	$k_\psi * 10^3$ (s^{-1})	$t_{1/2}$ (s)
4.94	0.272	-70	248.7 ± 1.2	2.79 ± 0.10
3.70	0.272	-70	218.6 ± 5.3	3.17 ± 0.08
2.47	0.272	-70	153.6 ± 2.6	4.62 ± 0.79
1.97	0.272	-70	123.6 ± 5.7	5.62 ± 0.26
1.48	0.272	-70	83.8 ± 1.3	8.27 ± 0.13
0.99	0.272	-70	63.1 ± 2.4	11.0 ± 0.4

Table 3.S4. Data for the Determination of the Reaction Order with Respect to O_2 for **3a**.

[O2] (mM)	$[\mathbf{3a}]_0$ (mM)	Temp (°C)	k_ψ (s^{-1})	$t_{1/2}$ (s)
4.77	0.25	-40	4.40 ± 0.02	0.414 ± 0.021
2.86	0.25	-40	2.74 ± 0.06	0.306 ± 0.006
2.38	0.25	-40	2.59 ± 0.07	0.322 ± 0.065
1.91	0.25	-40	1.88 ± 0.02	0.398 ± 0.006
0.95	0.25	-40	1.12 ± 0.01	0.259 ± 0.012

Table 3.S5. Data for the Double Reciprocal Analaysis in Figure 3.5A.

[O2] (mM)	$[\mathbf{1a}]_0$ (mM)	Temp (°C)	k_{obs} (s^{-1}) $*10^3$
4.52	0.205	5	153 ± 4
3.39	0.205	5	132.4 ± 2.6
1.36	0.205	5	82.6 ± 2.1
0.904	0.205	5	60.0 ± 1.4
4.60	0.205	-10	54.8 ± 1.7
3.45	0.205	-10	48.6 ± 1.6
2.30	0.205	-10	36.8 ± 0.1
1.38	0.205	-10	28.0 ± 0.7
4.66	0.205	-20	24.3 ± 2.1
2.33	0.205	-20	14.5 ± 0.5
1.40	0.205	-20	13.9 ± 0.28
4.71	0.205	-30	5.32 ± 0.69
3.53	0.205	-30	4.80 ± 0.22
2.36	0.205	-30	4.19 ± .09
1.41	0.205	-30	3.95 ± 0.22

Table 3.S6. Data for Double Reciprocal Analaysis in Figure 3.5B.

[O2] (mM)	$[\mathbf{2a}]_0$ (mM)	Temp (°C)	k_{obs} (s^{-1})
4.66	0.164	-20	10.5 ± 0.6
3.49	0.164	-20	7.14 ± 0.67
2.33	0.164	-20	6.01 ± 1.34
1.86	0.164	-20	4.59 ± 0.54
1.16	0.164	-20	5.04 ± 0.74
4.71	0.164	-30	6.06 ± 0.23
3.53	0.164	-30	4.10 ± 0.19
2.36	0.164	-30	4.05 ± 0.23
1.41	0.164	-30	2.84 ± 0.14
1.18	0.164	-30	1.60 ± 0.03
4.77	0.164	-40	4.22 ± 0.13
3.58	0.164	-40	3.72 ± 0.120
2.38	0.164	-40	2.83 ± 0.042
1.43	0.164	-40	2.07 ± 0.12
1.19	0.164	-40	2.04 ± 0.06
4.88	0.164	-60	2.18 ± 0.05
3.66	0.164	-60	1.59 ± 0.03
2.44	0.164	-60	1.14 ± 0.02
1.46	0.164	-60	0.769 ± 0.005
4.94	0.164	-70	1.15 ± 0.022
3.70	0.164	-70	0.899 ± 0.014
2.47	0.164	-70	0.731 ± 0.015
1.48	0.164	-70	0.411 ± 0.003

Table 3.S7. Temperature Dependence Data for the Oxidation of **1a**.

[O2] (mM)	$[\mathbf{1a}]_0$ (mM)	Temp (°C)	$k_\psi*10^3$ (s^{-1})	k_{obs} (M^{-1} s^{-1})[a]	$\ln((k_{obs}h)/Tk_b))$[b]
4.41	0.205	20	414 ± 17	93.8 ± 3.9	-24.8 ± 0.04
4.49	0.205	5	153 ± 4	34.0 ± 0.8	-25.8 ± 0.02
4.58	0.205	-10	53.6 ± 1.5	11.7 ± 0.3	-26.8 ± 0.03
4.63	0.205	-20	24.3 ± 2.1	5.23 ± 0.46	-27.6 ± 0.1
4.69	0.205	-30	5.32 ± 0.69	1.13 ± 0.15	-29.1 ± 0.1
4.77	0.205	-45	3.13 ± 0.40	0.656 ± 0.083	-29.5 ± 0.1

[a] $k_{obs} = k_\psi/[O_2]$

[b] h is Plank's constant, k_b is Boltzman's constant and T is the temperature in Kelvin.

Table 3.S8. Temperature Dependence Data for the Oxidation of **2a**.

[O2] (mM)	$[\mathbf{2a}]_0$ (mM)	Temp (°C)	k_ψ (s^{-1})	k_{obs} (M^{-1} s^{-1})[a]	$\ln((k_{obs}h)/Tk_b))$[b]
4.63	0.17	-20	10.49 ± 0.64	2384 ± 146	-21.50 ± 0.06
4.69	0.17	-30	6.06 ± 0.23	1378 ± 52	-22.01 ± 0.04
4.74	0.17	-40	4.22 ± 0.13	960 ± 30	-22.35 ± 0.03
4.85	0.17	-60	2.19 ± 0.05	497 ± 11	-22.94 ± 0.02
4.91	0.17	-70	1.15 ± 0.02	261.2 ± 5.0	-23.54 ± 0.02

[a] $k_{obs} = k\psi/[O_2]$

[b] h is Plank's constant, k_b is Boltzman's constant and T is the temperature in Kelvin.

Table 3.S9. Temperature Dependence Data for the Oxidation of **3a**.

$[O_2]$ (mM)	$[\mathbf{3a}]_0$ (mM)	Temp (°C)	k_ψ (s^{-1})	k_{obs} (M^{-1} s^{-1})[a]	$\ln((k_{obs}h)/Tk_b))$[b]
4.61	0.27	-15	7.79 ± 1.29	1690 ± 280	-21.82 ± 0.16
4.66	0.27	-25	7.23 ± 0.12	1550 ± 25	-21.85 ± 0.02
4.69	0.27	-30	5.19 ± 0.12	1107 ± 26	-22.17 ± 0.02
4.72	0.27	-35	5.54 ± 0.07	1174 ± 15	-22.09 ± 0.01
4.77	0.27	-44	4.00 ± 0.05	839 ± 9.5	-22.39 ± 0.01
4.77	0.27	-45	3.31 ± 0.01	692.7 ± 0.9	-22.57 ± 0.01
4.83	0.27	-55	2.39 ± 0.04	495.9 ± 7.9	-22.86 ± 0.02
4.85	0.27	-60	1.89 ± 0.02	389.8 ± 4.6	-23.08 ± 0.01
4.94	0.27	-75	0.669 ± 0.006	135.4 ± 1.1	-24.07 ± 0.01

[a] $k_{obs} = k_\psi/[O_2]$

[b] h is Plank's constant, k_b is Boltzman's constant and T is the temperature in Kelvin.

Table 3.S10. Effect of Pressure on the Oxidation of **3a**.

Pressure (MPa)	Temp (°C)	[**3a**] (mM)	$[O_2]$ (mM)	k_{obs} (s^{-1})	$\ln(k_{obs})$
10	20	0.20	4.4	19.4	2.97
20	20	0.20	4.4	19.5	2.97
25	20	0.20	4.4	20.3	3.01
40	20	0.20	4.4	24.3	3.19
50	20	0.20	4.4	25.5	3.24
60	20	0.20	4.4	25.3	3.23
80	20	0.20	4.4	25.3	3.23
75	20	0.20	4.4	27.4	3.31
100	20	0.20	4.4	30.7	3.42
120	20	0.20	4.4	34.1	3.53
140	20	0.20	4.4	39.3	3.67

Table 3.S11. The Effect of Added Water on the Oxidation of **3a**.

$[O_2]$ (mM)	$[\mathbf{3a}]_0$ (mM)	$[H_2O]$ (M)	Temp (°C)	k_ψ (s^{-1})	final O.D at 600 nm
4.4	0.20	<0.00189	20	25.0 ± 4.12	0.424 ± 0.002
4.4	0.20	0.00555	20	25.6 ± 0.773	0.398 ± 0.003
4.4	0.20	0.0278	20	24.6 ± 0.497	0.433 ± 0.019
4.4	0.20	0.0554	20	22.8 ± 2.23	0.459 ± 0.018
4.4	0.20	0.0831	20	23.2 ± 0.800	0.471 ± 0.008
4.4	0.20	0.111	20	24.1 ± 1.23	0.454 ± 0.002
4.4	0.20	0.138	20	24.6 ± 0.422	0.495 ± 0.004
4.4	0.20	0.166	20	24.2 ± 0.643	0.499 ± 0.005
4.4	0.20	0.193	20	27.5 ± 1.61	0.488 ± 0.004
4.4	0.20	0.220	20	25.4 ± 0.603	0.488 ± 0.004
4.4	0.20	0.275	20	23.1 ± 0.628	0.484 ± 0.018
4.4	0.20	0.411	20	22.2 ± 0.752	0.558 ± 0.016
4.4	0.20	0.545	20	20.4 ± 2.59	0.621 ± 0.034

Table 3.S12. Data for the Determination of the Reaction Order with Respect to Complex for the Decay of **1b**.

[O2] (mM)	$[\mathbf{1a}]_0$ (mM)	$[\mathbf{1b}]_0$ (mM)[a]	Temp (°C)	k_{obs} (M^{-1} s^{-1})	V_0*10^9 (M s^{-1})[b]	$t_{1/2}$ (s)
4.40	1.01	0.550 ± 0.013	5	3.47 ± 0.04	684 ± 33	649 ± 12
4.40	0.610	0.372 ± 0.010	5	4.22 ± 0.22	447 ± 15	729 ± 31
4.40	0.400	0.280 ± 0.009	5	5.09 ± 1.01	314 ± 13	798 ± 96
4.40	0.200	0.218 ± 0.008	5	2.78 ± 0.09	121 ± 8	1730 ± 26
4.40	0.177	0.168 ± 0.003	5	4.55 ± 0.76	129 ± 1	1310 ± 115
4.40	0.100	0.102 ± 0.020	5	1.94 ± 0.08	32.2 ± 10.7	4100 ± 769

[a] $[\mathbf{1b}]_0$ based on $m_1 + 1/m_2$ from curve fitting parameters.

[b] $V_0 = \frac{m_3}{m_2^2}$ where m_2 and m_3 are defined by eq 3.5.

Table 3.S13. Data for the Determination of the Reaction Order with Respect to Complex for the Decay of **2b.**

[O2] (mM)	$[\mathbf{2a}]_0$ (mM)	$[\mathbf{2b}]_0$ (mM)[a]	Temp (°C)	$k_{obs}*10^{-3}$ (M^{-1} s^{-1})	V_0*10^3 (M s^{-1})[b]	$t_{1/2}$ (ms)
4.05	0.49	0.372 ± 0.002	22	43.1 ± 0.2	4.74 ± 0.06	70.0 ± 0.4
4.05	0.34	0.272 ± 0.002	22	43.7 ± 0.3	2.51 ± 0.04	95.4 ± 0.6
4.05	0.25	0.160 ± 0.007	22	48.3 ± 1.0	0.902 ± 0.081	152 ± 6
4.05	0.20	0.105 ± 0.002	22	57.8 ± 1.0	0.357 ± 0.025	220 ± 9
4.05	0.15	0.151 ± 0.002	22	55.7 ± 2.1	0.899 ± 0.037	141 ± 5
4.05	0.098	0.105 ± 0.002	22	57.9 ± 0.9	0.356 ± 0.025	220 ± 8
4.05	0.049	0.0580 ± 0.0007	22	27.9 ± 2.3	0.0418 ± 0.0042	932 ± 82

[a] $[\mathbf{2b}]_0$ based on $m_1 + 1/m_2$ from curve fitting parameters.

[b] $V_0 = \frac{m_3}{m_2^2}$ where m_2 and m_3 are defined by eq 3.5.

Table 3.S14. Data for the Determination of the Reaction Order with Respect to Complex for the Decay of **3b**.

[O2] (mM)	$[\mathbf{3a}]_0$ (mM)	$[\mathbf{3b}]_0$ (mM)[a]	Temp (°C)	k_{obs} (M^{-1} s^{-1})	V_0*10^6 (M s^{-1})[b]	$t_{1/2}$ (s)
4.30	0.742	0.125 ± 0.014	40	887 ± 113	2.38 ± 0.90	31.3 ± 4.6
4.30	0.500	0.144 ± 0.019	40	529 ± 13	4.51 ± 0.42	28.6 ± 1.0
4.30	0.246	0.078 ± 0.0054	40	389 ± 78	1.09 ± 0.18	81.6 ± 28.3
4.30	0.123	0.0451 ± 0.0094	40	263 ± 21	0.226 ± 0.060	213 ± 60

[a] $[\mathbf{3b}]_0$ based on $m_1 + 1/m_2$ from curve fitting parameters.

[b] $V_0 = \frac{m_3}{m_2^2}$ where m_2 and m_3 are defined by eq 3.5.

Table 3.S15. Data for the Determination of the Reaction Order with Respect to O_2 for the Decay of **1b**.

$[O_2]$ (mM)	$[\mathbf{1b}]_0$ (mM)[a]	Temp (°C)	k_{obs} (M^{-1} s^{-1})	$t_{1/2}$ (s)
4.49	0.700 ± 0.048	5.0	4.33 ± 0.94	470 ± 137
3.59	0.460 ± 0.025	5.0	6.38 ± 0.64	513 ± 9
2.69	0.454 ± 0.019	5.0	7.03 ± 0.87	484 ± 18
2.24	0.479 ± 0.023	5.0	7.44 ± 0.14	468 ± 9
1.57	0.453 ± 0.096	5.0	9.60 ± 0.86	385 ± 14
0.898	0.325 ± 0.028	5.0	18.0 ± 2.6	328 ± 34

[a] $[\mathbf{1a}]_0$ = 0.99 mM, $[\mathbf{1b}]_0$ based on $m_1 + 1/m_2$ from curve fitting parameters.

Table 3.S16. Data for the Determination of the Reaction Order with Respect to O_2 for the Decay of **2b**.

$[O_2]$ (mM)	$[\mathbf{2b}]_0$ (mM)[a]	Temp (°C)	k_{obs} *10^{-3} (M^{-1} s^{-1})	$t_{1/2}$ (ms)
4.05	0.105 ± 0.002	22	58.0 ± 1.0	220 ± 9
3.50	0.184 ± 0.014	22	60.2 ± 2.1	109 ± 15
2.50	0.174 ± 0.004	22	71.1 ± 2.0	95 ± 4
1.00	0.151 ± 0.007	22	129.5 ± 5.1	61 ± 5
0.40	0.092 ± 0.005	22	180.3 ± 7.5	79 ± 8

[a] $[\mathbf{2a}]_0$ = 0.197 mM, $[\mathbf{2b}]_0$ based on $m_1 + 1/m_2$ from curve fitting parameters.

Table 3.S17. Data for the Determination of the Reaction Order with Respect to O_2 for the Decay of **3b**.

$[O_2]$ (mM)	$[\mathbf{3b}]_0$ (mM)[a]	Temp (°C)	k_{obs} (M^{-1} s^{-1})	$t_{1/2}$ (s)
4.22	0.128 ± 0.009	55	843 ± 113	10.0 ± 1.0
3.37	0.106 ± 0.011	55	914 ± 51	11.5 ± 1.3
2.74	0.0935 ± 0.0071	55	921 ± 25	13.7 ± 0.9
2.11	0.127 ± 0.009	55	946 ± 100	11.1 ± 1.8
0.84	0.0716 ± 0.0016	55	786 ± 88	25.0 ± 4.7

[a] $[\mathbf{3a}]_0$ = 0.150 mM, $[\mathbf{3b}]_0$ based on $m_1 + 1/m_2$ from curve fitting parameters.

Table 3.S18. Temperature Dependence Data for the Decay of **1b**.

[O2] (mM)	Temp (°C)	k_{obs} (M^{-1} s^{-1})	$\ln((k_{obs}h)/Tk_b))^a$
4.33	35	3040 ± 425	-21.4 ± 0.1
4.36	30	1210 ± 100	-22.3 ± 0.1
4.38	25	1180 ± 110	-22.7 ± 1.0
4.41	20	180 ± 23	-24.2 ± 0.1
4.44	15	45.4 ± 2.0	-25.6 ± 0.4
4.47	10	33.0 ± 2.8	-25.8 ± 0.1
4.49	5	10.5 ± 5.2	-27.1 ± 0.5
4.52	0	7.30 ± 1.52	-27.3 ± 0.2
4.55	-5	2.09 ± 0.62	-28.6 ± 0.3

[a] h is Plank's constant, k_b is Boltzman's constant and T is the temperature in Kelvin.

Table 3.S19. Temperature Dependence Data for the Decay of **2b**.

[O2] (mM)	Temp (°C)	$k_{obs} * 10^3$ (M^{-1} s^{-1})	$\ln((k_{obs}h)/Tk_b))^a$
4.38	25	85.3 ± 2.1	-26.4 ± 0.1
4.47	10	39.3 ± 26.4	-27.4 ± 0.7
4.58	-10	2.68 ± 1.31	-29.9 ± 0.5
4.63	-20	1.03 ± 0.10	-30.7 ± 0.1
4.69	-30	0.837 ± 0.110	-30.9 ± 0.1
4.74	-40	0.141 ± 0.052	-32.7 ± 0.3
4.80	-50	0.0289 ± 0.0029	-34.2 ± 0.1
4.84	-58	0.0330 ± 0.0085	-34.1 ± 0.2
4.90	-68	0.00424 ± 0.00010	-36.1 ± 0.10

[a] h is Plank's constant, k_b is Boltzman's constant and T is the temperature in Kelvin.

Table 3.S20. Temperature Dependence Data for the Decay of **3b**.

[O2] (mM)	Temp (°C)	k_{obs} (M^{-1} s^{-1})	$\ln((k_{obs}h)/Tk_b))^a$
4.38	25	277 ± 19	-23.76 ± 0.07
4.41	20	217 ± 1	-23.98 ± 0.03
4.44	15	92.8 ± 3.0	-24.82 ± 0.03
4.47	10	56.8 ± 3.3	-25.29 ± 0.06
4.49	5	25.2 ± 0.8	-26.08 ± 0.03
4.55	-5	7.62 ± 0.13	-27.25 ± 0.02

[a]h is Plank's constant, k_b is Boltzman's constant and T is the temperature in Kelvin.

Table 3.S21. Data for Double Reciprocal Analaysis in Figure 3.12.

[O2] (mM)	$[\mathbf{3a}]_0$ (mM)	Temp (°C)	k_{obs} (M^{-1} s^{-1})
4.30	0.742	40	886 ± 113
4.30	0.500	40	529 ± 13
4.30	0.246	40	315 ± 140
4.30	0.123	40	222± 83
4.38	0.742	25	277 ± 19
4.38	0.500	25	151 ± 3
4.38	0.246	25	104 ± 25
4.38	0.123	25	77 ± 27
4.44	0.742	15	93 ± 3
4.44	0.500	15	62.8 ± 1.1
4.44	0.246	15	49.6 ± 0.4
4.44	0.123	15	31.1 ± 5.2
4.49	0.742	5	25.2 ± 0.8
4.49	0.500	5	21.2 ± 2.2
4.49	0.246	5	15.9 ± 1.3
4.49	0.123	5	15.2 ± 2.2

CHAPTER IV.

Reactions of Nitric Oxide with Non-Heme Iron Centers in Biology and Chemistry

Introduction

The past few years have witnessed a renaissance in the chemistry of nitric oxide. This extremely poisonous gas, when present in minute quantities, carries out critical regulatory functions in mammalian cells where it serves as a rapid response vasodilator, regulates macrophage-based immune function, and acts as a neurotransmitter.[1,2] The recognition of these varied roles in biology and the emerging clinical relevance of these functions led to nitric oxide being named the 1992 Science Magazine Molecule of the Year.[3]

NO is a newcomer to neither inorganic nor bioinorganic chemistry, however.[4-6] The similarities and differences between NO, CO and O_2 as ligands have played an important role in the understanding of bonding and electron localization in transition metal complexes. The bonding in metal nitrosyls is difficult to describe.[4,7-10] Valence bond pictures are easily understood, but for nitrosyls, they are rarely accurate. This property contrasts with the transition metal chemistry of O_2, which can usually be classified by its spectroscopic properties as a ligand having dioxygen, superoxide or peroxide character.[11,12] In CO chemistry, the concept of backbonding quite often adequately accounts for the physical and chemical properties of the system.[13]

NO generally coordinates to metal centers capable of interacting with dioxygen. The asymmetry and odd electron count of the NO molecule often convey additional reactivity, however. Coordination through the nitrogen atom occurs for monodentate nitrosyls and O-atom bonding only arises in cluster compounds.[6] The π^* orbital is energetically suited to accept electron density from metal ions, but the oxygen sp^2 orbitals are not nucleophilic. This behavior contrasts with that of dioxygen. In a coordinated peroxide, for

example, high energy filled sp^2 orbitals can react with other metal centers. Therefore, even though NO is thermodynamically unstable, a kinetic pathway for N-O bond cleavage is often unavailable. Since, coordinated NO is usually stable toward further reduction, it can therefore mimic the unstable species O_2^- present on the pathway of dioxygen activation.

In this chapter, a brief introduction into the chemistry of nitric oxide with a particular focus on its relevance in the study of non-heme iron proteins is presented. The discussion is divided into four parts. First, an overview of the physical and chemical properties of NO and FeNO adducts is introduced as a framework for the later discussion. The use of NO as a dioxygen mimic is discussed next, the focus being primarily on spectroscopic studies of the enzyme nitrosyls. Since stable NO adducts provide the iron center of the protein with a rich set of observable spectroscopic transitions, nitric oxide allows EPR, MCD and optical techniques to be employed to study the metal center in its "activated" state. NO binds in the same site as dioxygen but without undergoing catalytic turnover, so properties of the reaction mechanism can be investigated. Probably the most important features discovered through the use of NO relate to the nature of substrate interactions with the metal center. The third section deals with what are believed to be deleterious side reactions of NO with iron enzymes in vivo and in vitro. These studies have predicted that ribonucleotide reductase (RNR), and possibly all iron enzymes, are a major biological target for NO. Finally, catalytic oxo-transfer chemistry has been observed with certain iron nitrosyl compounds and is presented as an example of the interesting small molecule activation chemistry involving the FeNO unit. This discussion is not intended to be comprehensive as in Chapter I, but illustrative, so that the

research in Chapters V and VI can be viewed in the context of the chemistry of iron with NO.

Physical and Chemical Properties of Nitric Oxide.

Nitric oxide is a poisonous, colorless gas, formed as a byproduct in many combustion processes.[14,15] As shown in eqs 4.1 and 4.2, NO is thermodynamically unstable toward decomposition.[16] It is, however, kinetically inert and a catalyst or thermal activation is required

$$3NO \longrightarrow N_2O + NO_2 \qquad \Delta H = -37.2 \text{ kcal mol}^{-1} \qquad (4.1)$$

$$NO \longrightarrow 1/2N_2 + 1/2O_2 \qquad \Delta H = -21.6 \text{ kcal mol}^{-1} \qquad (4.2)$$

for this reactivity to be observed. Because of its instability, reactions employing NO cannot be effectively induced by heat or pressure the way CO or O_2 reactions can be. Under harsh conditions, the decomposition of nitric oxide to more stable products ensues.

The electronic structure of nitric oxide is also quite interesting. Having 11 electrons, NO has a single unpaired electron in a $2\pi^*$ orbital, localized primarily on the nitrogen atom (Figure 4.1). The molecule can undergo one-electron oxidation or reduction, but most commonly acts as an oxidizing agent.[16] Based on this duality, nitric oxide is more like superoxide than dioxygen. The molecular orbital diagram in Figure 4.1 shows qualitatively the effect of metal coordination on the molecular orbitals for a hypothetical linear mononuclear iron nitrosyl of C_{4v} symmetry with the nitrosyl oriented along the z-axis. The frontier orbitals have 2e, $1b_2$ and 3e symmetry. The 2e orbitals are bonding with respect to the M-N bond but anti-bonding across the N-O fragment. The 3e orbitals are anti-bonding for all three atoms and the $1b_2$ orbital is metal centered and essentially non-bonding. Six-coordinate

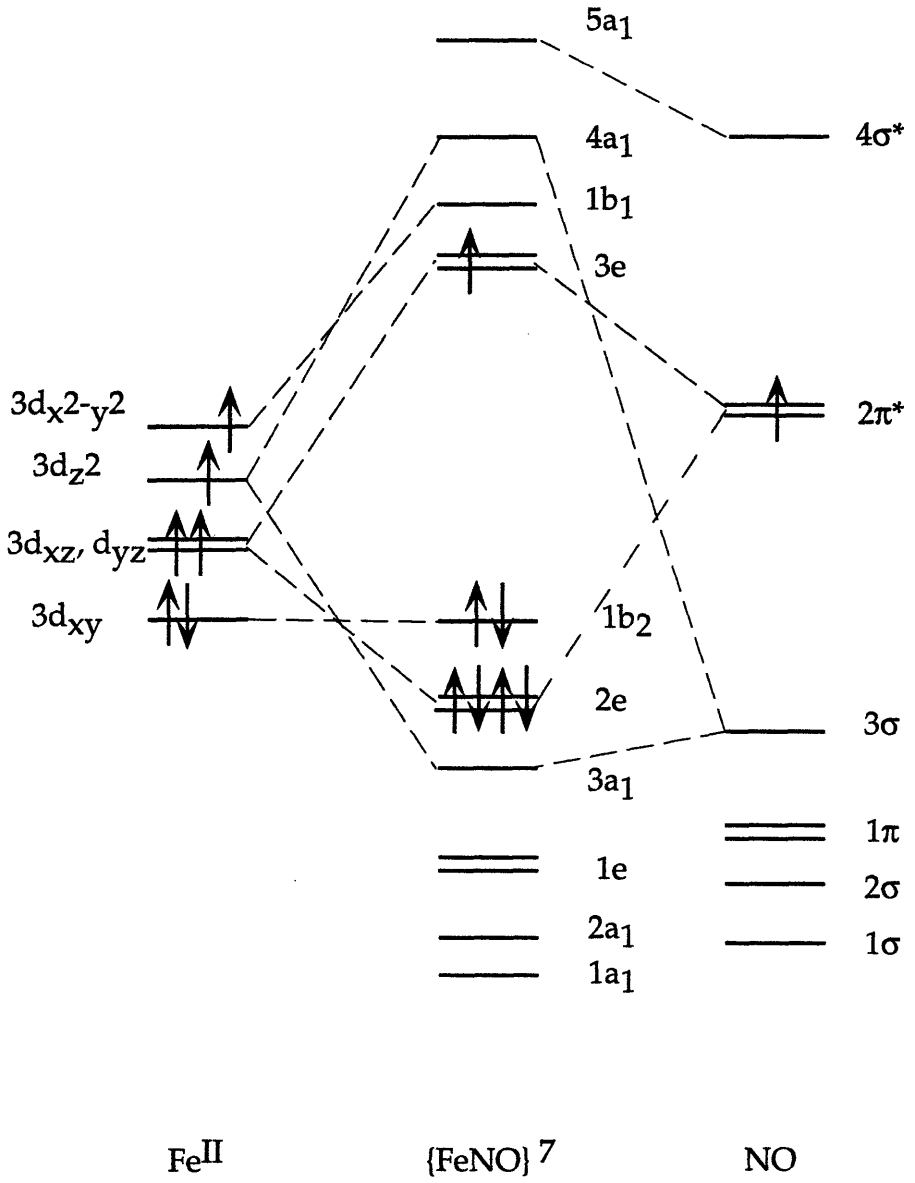

Figure 4.1. Qualitative molecular orbital scheme for the bonding of a linear iron nitrosyl fragment with C_{4v} symmetry. Only the frontier electrons are shown explicitly. The orbitals with energies below that of 2e are filled. Upon distortion from C_{4v} symmetry, the degenerate components of the 3e and 2e orbitals separate. (Adapted from ref. 8.)

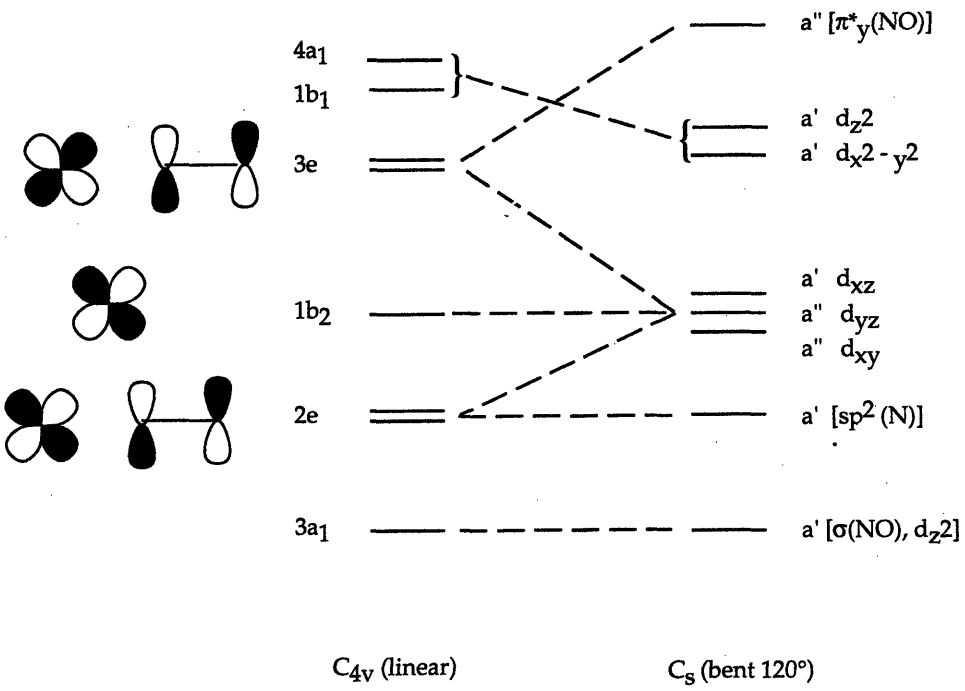

Figure 4.2. Correlation diagram relating one-electron molecular orbitals of linear and bent six-coordinate MNO complexes. The bend angle at which the orbital energies ($1b_2$ and formerly 3e and 2e orbitals) cross over will vary depending on the complex. (Adapted from ref. 4.)

metal nitrosyls with $\{MNO\}^n$, where $n \leq 6$ electrons, are invariably linear since the 3e orbitals are unfilled. Systems with more than 6 electrons in the {MNO} fragment are generally bent. This distortion results in separation of the formerly degenerate 3e orbitals into a′ and a″ orbitals and a net lowering of the total energy (Figure 4.2).[4]

The degree of bending in metal nitrosyls is difficult both to predict and to measure. In carbonyl chemistry, the C-O stretching frequency is a good indicator of π-back-bonding strength.[17] In nitrosyls, however, significant overlap in the stretching frequencies of linear and bent species renders problematic the use of IR spectra as a diagnostic tool.[6] The measurement of MNO bend angles (∠MNO) from X-ray crystal structures is sometimes hampered by disorder. Partial occupancy of the oxygen atom in two or four sites is common.[6] The result is that exact bend angles are sometimes obscured, being the average of multiple conformations. In the case of iron porphyrin nitrosyls, significant effort has been expended correlating the δ(Fe-N-O), ν(Fe-NO) and ν(Fe-L) vibration modes with the bend and tilt angles.[18,19] These correlations explain the properties of heme-containing systems, but seem less satisfactory for non-heme systems which can undergo a wider variety of geometric distortions.

Several mononuclear $\{FeNO\}^7$ systems have been reported, many of them structurally characterized. Geometric parameters for these complexes are listed in Table 4.1. Most of them have S = 3/2 ground states arising from strong antiferromagnetic coupling of a high spin (S = 5/2) Fe^{III} ion and the NO^- (S = 1) ligand.[7,10] From the molecular orbital diagram (Figure 4.1), it can be seen that this situation occurs when the pairing energy is greater than the $3e/1b_2$ energy gap. Two complexes in this table, [Fe(NO(salen)] and [Fe(NO(TMC)](BF$_4$), undergo a temperature-dependent S = 3/2 $\rightleftharpoons$ S = 1/2

Table 4.1. Structural Parameters of Spectroscopically Characterized {FeNO}^{7} Complexes.

Complex	Fe-NO (Å)	N-O (Å)	∠Fe-N-O (deg)	ν(NO) (cm^{-1})	approx. geometry	ref
$[Fe_2(NO)_2(EtHPTB)(OBz)](BF_4)_2$	1.749(8)	1.151(8)	166.6(7)	1785	O_h-6	20
	1.750(7)	1.156(8)	168.3(7)			
$[Fe(NO)TPA)(BF)](CLO_4)$[a]	1.72(2)	1.15(2)	159(2)	1794	O_h-6	21
$[Fe(NO)(Me_3TACN)(N_3)_2]$	1.738(5)	1.142(7)	155.5(10)	1690	O_h-6	22
$[Fe(NO)TMPzA)Cl](BPh_4)$	1.725(7)	1.15(1)	157.1(8)	1796	O_h-6	23
[Fe(NO)(EDTA)]	1.78[b]	1.10[b]	156(5)[b]	1776	nd	24
[Fe(NO)(salen)][c]	1.783(16)	1.10(3)	147(4)	1710	TBP-5	25
$[Fe(NO)TMC)](BF_4)_2$[c]	1.737(6)	1.137(6)	177.5(5)	1840	TBP-5	26

[a]Bond lengths and bond angles are the average of two conformers. [b]Determine by using GNXAS EXAFS. [c]23°C data. Both complexes undergo S = 3/2 $\rightleftharpoons$ S = 1/2 spin equilibrium. They exhibit S = 3/2 behavior at this temperature.

spin equilibrium.[25,26] Below ca -95 °C, S = 1/2 is the ground state. In the salen complex, a 20° change in Fe-N-O bend angle (147° at 25°C versus 127° at -80 °C) accompanies the change in spin state. This difference was described as only marginally significant, however, because of crystallographic disorder in the FeNO unit and the difficulty in getting an accurate measurement of the angle from the model.[25]

Nitric oxide reacts rapidly with dioxygen to form N_2O_4 and with superoxide to form peroxynitrite, as shown in eqs 4.3 and 4.4. Under acidic conditions, $ONOO^-$ rapidly rearranges to nitrate ion, but is reasonably stable

$$O_2 + 2NO \longrightarrow N_2O_4 \rightleftharpoons 2NO_2 \qquad (4.3)$$

$$O_2^- + NO \longrightarrow ONOO^- \xrightarrow{H^+} NO_3^- \qquad (4.4)$$

as an anion form. This species is a potent oxidant, capable of diffusing among cells and causing oxidative tissue damage.[1,27,28] In the presence of metal ions, the chemistry of peroxynitrite resembles that of peracids, persulfates and peroxides. The probability of metal catalyzed oxidations is therefore high. Since many non-heme iron enzymes are involved in dioxygen-dependent processes, the presence of nitric oxide could significantly alter the reactivity through peroxynitrite formation and its subsequent reaction with residues in the active site.

Nitric Oxide as a Dioxygen Mimic and Spectroscopic Probe.

NO Adduct of Hemerythrin. Extensive spectroscopic studies have been carried out on the nitric oxide adduct of Hr.[29,30] EPR, Mössbauer and optical spectroscopic parameters for deoxyHrNO and several other non-heme iron proteins are provided in Table 4.2. A single NO molecule coordinates the dioxygen binding site of deoxyHr resulting in a bent geometry ($\angle$FeNO $\approx$

111°). Analysis of the EPR spectra revealed the species to have an effective S = 1/2 ground state due to antiferromagnetic coupling between the S = 3/2 $\{FeNO\}^7$ unit and the adjacent high spin Fe(II) site (S = 2), with J = -23 cm^{-1}. Since the Fe-N-O bending vibration was sensitive to H_2O/D_2O substitution, it was proposed that a hydrogen bond occurs to the bridging hydroxo group. NO adduct formation was reversible, addition of O_2 to deoxyHrNO resulting in formation of oxyHr. Addition of anions such as azide or isocyanate also dissociated NO. Fluoride ion behaved differently, however, the simultaneous binding of F^- and NO being observed. It was hypothesized that, under these conditions, a fluoride ion replaced the hydroxo bridge.

The FeNO bond angle of deoxyHrNO is much more acute than generally observed in six-coordinate $\{FeNO\}^7$ model compounds (Table 4.1). It is also significantly more bent than any of the iron porphyrin nitrosyl adducts.[31-35] A rationale for the highly bent structure is based on a comparison with the observed ∠FeNN of metazidoHr and a very unusual isotopic perturbation of the δ(Fe-N-O) and ν(Fe-N) modes. Normally, the δ(Fe-N-O) mode is more strongly influenced by ^{15}NO substitution than the ν(Fe-N) vibration, whereas the reverse effect is observed for $N^{18}O$. For deoxyHrNO, however, equivalent shifts occurred upon substitution with either ^{15}NO or $N^{18}O$. A more strongly bent FeNO unit in deoxyHrNO than in the model compounds would explain this behavior. With such a small angle, the overlap between the nitrogen sp^2 orbital and the metal d_{xz} and d_{yz} orbitals is minimal, so the extreme valence bond Fe(III)-NO^- should hold. A reinvestigation of deoxyHrNO might be in order, however, using a technique such as EXAFS with the GNXAS analysis.[24] In this way, the bend angle of the FeNO unit might be directly determined.

Table 4.2. Spectroscopic Properties of the Nitrosyl Adducts of Non-heme Iron Enzymes.

	Parameter	deoxyHr NO	deoxyHrF NO	PMO + NO, no substrate	PMO + (4-NH_2)-OBz + NO[a]	PMO + (4-OMe)-OBz + NO[b]	IPNS +NO	IPNS + NO + ACV	4,5-PCD + NO + substrate
Mössbauer	D, cm^{-1}					12			12
	E/D					0.01			0.02
	ΔE_Q, mm s^{-1}	0.61 2.65	1.02 3.09			-1.4			-1.67
	η					0.2			0.07
	$A_0/g_N\beta_N$, T[c]					-23.5			-32
	Γ, mm s^{-1}					0.30			
	δ, mm s^{-1}	0.68 1.21	0.75 1.22			0.68			0.66
	T, K	100	100						4.2
EPR	g_1[d]			4.162	4.170	-			
	g_1[e]			4.093	4.08	4.101			
	g_2[e]			3.975	3.99	3.960			
	g_2[d]			3.892	3.882	-			
	g_3[d], g_3[e]			2.0	2.0	2.0			
	g	2.77 ± 0.02 1.84 ± 0.02	2.58 ± 0.01 1.80 ± 0.02				4.09 3.95 2.0	4.22 3.81 1.99	4.21 3.77 1.99
Optical	λ, nm (ε, M^{-1} cm^{-1})	408 (1200) 500 sh (700) 600 (500)	340 sh (2700) 450 (1200)				340 (1800) 430 (800) 600 (200)	508 (1600) 720 (350)	
RR	ν(Fe-N), cm^{-1}	433	420						
	δ (Fe-N-O), cm^{-1}	421							
ref.		30	30	38	38	38	36	36	40

[a]Uncoupling substrate. [b]Tight coupling substrate. [c] The parameter $A_0/g_N\beta_N$ is in units of internal field per spin 1, where $A_0 = A_x = A_y = A_z$, g_N is the nuclear g-factor, and β_N is the nuclear magneton. [d]Indicates spectral species with large tetragonal distortion. [e]Indicates spectral species with small tetragonal distortion.

Reactions of NO with Mononuclear Non-Heme Iron Enzymes.

Nitric oxide has been used to probe the non-heme iron centers in four enzymes: isopenicillin N synthase (IPNS),[36,37] 4-methyoxybenzoate monooxygenase (PMO),[38] protocatechuate 4,5-dioxygenase (4,5-PCD)[39-41] and soybean lipoxygenase (SBL).[7,42] The reactions that these enzymes catalyze were discussed in detail in Chapter 1.[43] Experiments involving 4,5-PCD are not explicitly discussed below, although the spectroscopic parameters are listed in Table 4.1, since the substrate coordination properties were not significantly different from those of the PMO system. The premise of all of these studies is that NO binds at the site normally occupied by dioxygen. In so doing, it provides the metal center with a spectroscopic probe of substrate or substrate analog addition.

Isopenicillin N Synthase. Addition of NO to the EPR silent IPNS enzyme resulted in the appearance of an S = 3/2 spectrum with features near g = 4 and 2.[36] Upon addition of ACV, the natural substrate, a new spectrum with features at g = 4.22, 3.81 and 1.99 appeared. The change in the EPR spectrum indicated that both NO and substrate coordinate to the iron center simultaneously. The order of addition did not matter and the binding was non-competitive, so the presence of substrate in the active site is not likely to prevent coordination of dioxygen during enzyme turnover.

The ability to observe the EPR spectrum of the nitrosyl adduct of IPNS led to several other insights regarding the active site and the enzyme mechanism. Hyperfine broadening was observed when ^{17}O-enriched water (I = 5/2) was used as the solvent for the IPNS-NO-ACV complex.[37] This experiment indicated that an additional vacant coordination site is available, even when substrate is bound. Therefore, a minimum of three labile coordination sites are present at the metal center. The coordination mode of

the substrate was also investigated by use of substrate analogs. When the cysteine thiol of the substrate was changed to either an alcohol or a sulfate functional group, both the EPR and optical properties of the nitrosyl adduct changed significantly, whereas other mutations in the substrate had no effect.[37] These data were used as evidence that the thiol group is coordinated to the iron center.

Studies using NO as a spectroscopic probe for the iron center in IPNS provided a great deal of understanding of the metal center. One note of caution is in order, however. Nitric oxide often weakens the coordination of ligands trans to it owing to the strong donation into the d_z2 orbital.[19] This property could result in opening of a site which might not be available during dioxygen binding. The most important result from these studies, was the increased understanding of substrate binding. In many iron enzymes, direct coordination of substrate to the metal center is unnecessary. It is sufficient for the enzyme to hold the substrate in the active site, available for attack by an activated oxygen species. The binding of the substrate indicates that, besides dioxygen, the enzyme probably also utilizes substrate activation to carry out a highly specific cyclization and prevent side reactions.

4-Methoxybenzoate monooxygenase. The role of nitric oxide in the study of 4-methoxybenzoate monooxygenase, also called putidamonooxin or PMO, is similar to that in IPNS. Addition of NO to the iron center made the enzyme EPR active. An important property investigated through the use of the nitrosyl adduct was substrate coupling. This enzyme exhibits two types of behavior, coupled and uncoupled turnover, depending on the substrate used. In the absence of a substrate, the enzyme does not react with dioxygen. When a coupling substrate is added, such as 4-methoxybenzoate, the enzyme consumes dioxygen and reductant and oxidizes the substrate to product. In

the presence of an uncoupled substrate, however, enzyme turnover consumes dioxygen and NADH, but the substrate remains unaltered. EPR studies carried out in the presence of nitric oxide were instrumental in determining the chemical difference between coupled and uncoupled substrates.[38] Addition of uncoupled substrates had no effect on the EPR spectrum of the enzyme-NO adduct whereas, in the presence of coupled substrates, there were significant changes in the rhombic portions of the signal. The studies also revealed that addition of NO to the reduced protein led to an increased binding affinity for the iron cofactor.[38]

In the case of PMO, it is unlikely that coordination of the substrate to iron results in the spectroscopic changes observed in the EPR spectra. Coordination of the substrate carboxylate group would be the most likely binding mode. This geometry would be unlikely to allow activity at the 4-position of the molecule, however. Instead, the carboxylate probably interacts with side chain residues, altering the geometry around the active site. This change could be the result of water displacement, a carboxylate shift or variation in a hydrogen bonding network involving a coordinated side chain. The example of the decoupling substrate used in the study was 4-amino benzoate. In this case, the presence of the positively charged amino group pointing towards the metal center may destabilize the normal position of the coupled substrates.

Soybean Lipoxygenase. The studies of the NO complex of soybean lipoxygenase (SBL) are quite interesting. Substrate interactions were probed by using linoleic acid and the findings were very different from those of the other mononuclear iron enzymes discussed above. In the case of SBL, NO and substrate bind competitively.[42] Linoleic acid is not believed to coordinate to the metal center, so this result was interpreted to mean that the NO and

substrate binding sites overlap in space. The competition was found to be pH dependent with a 10-fold lower substrate binding affinity observed at pH 7 than pH 9. This pH effect is accompanied by a dramatic loss of activity, but it should be noted that only the ferric enzyme is active whereas the binding affinity was measured for the Fe^{II}-NO adduct. There was no evidence for water coordination to the Fe-NO site based on $^{17}OH_2$ broadening experiments, indicating that the iron site is coordinately saturated in the presence of NO.

Recently, another group reinvestigated the SBL-NO complex with a rather different objective.[7,10] Whereas the previous experiments probed the nature of the enzyme active site and the enzyme-substrate complex, these later studies focused primarily on the Fe-NO bond itself. By using model systems ($[Fe(Me_3TACN)(NO)(N_3)_2]$ and $[Fe(EDTA)(NO)]^{2-}$) and the enzyme adduct in RR, MCD and XAS experiments, it was found that the iron atom in the $\{FeNO\}^7$ system more closely approximated the properties of Fe^{III} than Fe^{II}.[7,10] From this starting point, SCF-X_α calculations were used to show that the spectral features of the SBL-nitrosyl could be explained by high spin Fe^{III} ($S = 5/2$) antiferromagnetically coupled to NO^- ($S = 1$) resulting in the observed $S = 3/2$ ground state.

Theoretical studies on the NO adduct of SBL and these model compounds were extended to dioxygen in an attempt to use the NO bonding to understand O_2 activation.[10] A formalism involving an $\{FeOO\}^8$ unit was introduced based on that used for the nitrosyl. The results from these calculations were then used to predict spectral features of iron(III)superoxide units. It was found that the coordination of superoxide to an iron center would stabilize the O-O bond by removing electron density from the π^* orbital via a strong metal-ligand σ bond. With this theoretical basis in place, more detailed studies on the enzyme and model system will certainly follow.

Inactivation of Ribonucleotide Reductase by NO.

One of the biological functions of nitric oxide is to act as an antiproliferative agent in response to the stimulation of NO synthase activity.[44] The mechanism for this cytostatic behavior is not well understood, but several years ago, it was proposed that RNR was a potential mediator in this pathway.[45] RNR catalyzes a key step in the synthesis of DNA, so its inhibition would lead to a halt in the replication cycle,[46,47] Since this first report, significant data have supported the idea that NO reacts with RNR, as well as with other iron enzymes, in vivo. The studies probing this process have been carried out both in whole cells and with isolated RNR.[44,48-51] The results are comparable in both cases. Upon exposure of RNR to NO, the enzyme was inactivated. The EPR signal due to the stable tyrosyl radical disappeared and the incorporation of [6-^{3}H]thymidine into DNA ceased.

The RNR mechanism involves two processes, either of which could be the target of NO inhibition. The first phase of the reaction is activation, where O_2 reacts with the reduced diiron center to generate a tyrosyl radical.[46,52] The second phase involves transfer of the radical to a cysteine at the active site on the R1 protein. At the end of the catalytic cycle, the tyrosyl radical is regenerated. Although the diiron center is not used during turnover, it must remain viable to reactivate the system because quenching of the tyrosyl radical occurs at a slow but significant rate. Clearly, NO could react with the tyrosyl radical to form NO^+ and tyrosinate which would rapidly protonate. This reaction would not lead to inactivation since the iron center could reactivate the tyrosine.

Two possible mechanisms for the activity have been presented.[44,51] The first is that the iron center is modified. The iron could be mobilized entirely, leaving apo enzyme, or NO could inactivate the metal center by

coordinating to it. Either way, RNR would rapidly lose activity. The second explanation was that NO acted directly on the tyrosyl radical. As mentioned above, simple electron transfer is insufficient to explain the results. Therefore some form of covalent modification is required, such as nitration of the tyrosine residue. A hypothesis was recently put forth involving formation of a reversible coupling product between NO and the tyrosyl radical to explain the slow reactivation of RNR under vacuum following exposure to NO.[53] The proposal is intriguing but precedents for this type of behavior are scarce and peptide model studies with tyrosyl radicals are necessary to validate the theory.

The investigators studying the effect of NO on RNR have focused on EPR experiments to unravel the chemistry at the metal center. An EPR signal at g = 2.041 appears upon exposure to NO and the tyrosyl radical signal vanishes. This signal derives from the nitrosylation of an Fe-S cluster.[53] Unfortunately, these interpretations ignore the diiron center since no features in the EPR spectrum could be assigned to it.

Chapter V presents a complex synthesized to model the interaction between NO and RNR. Although many mononuclear FeNO complexes have been synthesized, dinuclear nitrosyls with oxygen and nitrogen donor ligands are rare. Complexes of this type will almost certainly be required to unravel the chemistry of RNR inactivation by NO. The data presented in Chapter V indicates that a diiron dinitrosyl species can be EPR silent due to antiferromagnetic coupling between the two $\{FeNO\}^7$ units. Both the mononuclear and dinuclear systems have strong optical transitions, however, so the presence of such a species might be detectable by visible spectroscopy of the R2 protein following exposure to NO.

Catalytic Oxo-transfer Chemistry Involving the Nitrate-Nitrosyl Couple.

Many nitrosyl compounds react with dioxygen. In general, such reactions form nitrato species[54-56] although nitrito products are occasionally observed.[57,58] The predominant behavior results from attack of dioxygen on the electrophilic nitrosyl to form an intermediate peroxynitrite anion which rapidly rearranges to nitrate (Figure 4.3).[6] The nitrito species is believed to result from a bimolecular event between the peroxynitrite intermediate and another equivalent of the nitrosyl starting material. Somewhere along this reaction coordinate lies a very active oxidant, for in a few rare cases, oxo-transfer reactions are observed.[6,59-62] Most of the substrate oxidation reactions catalyze oxo-transfer to coordinated ligands such as CO or PPh_3. A reaction, called the nitrate/nitrosyl couple, however, can oxidize olefins with the assistance of an iron(II) phosphine pre-catalyst.[61-66]

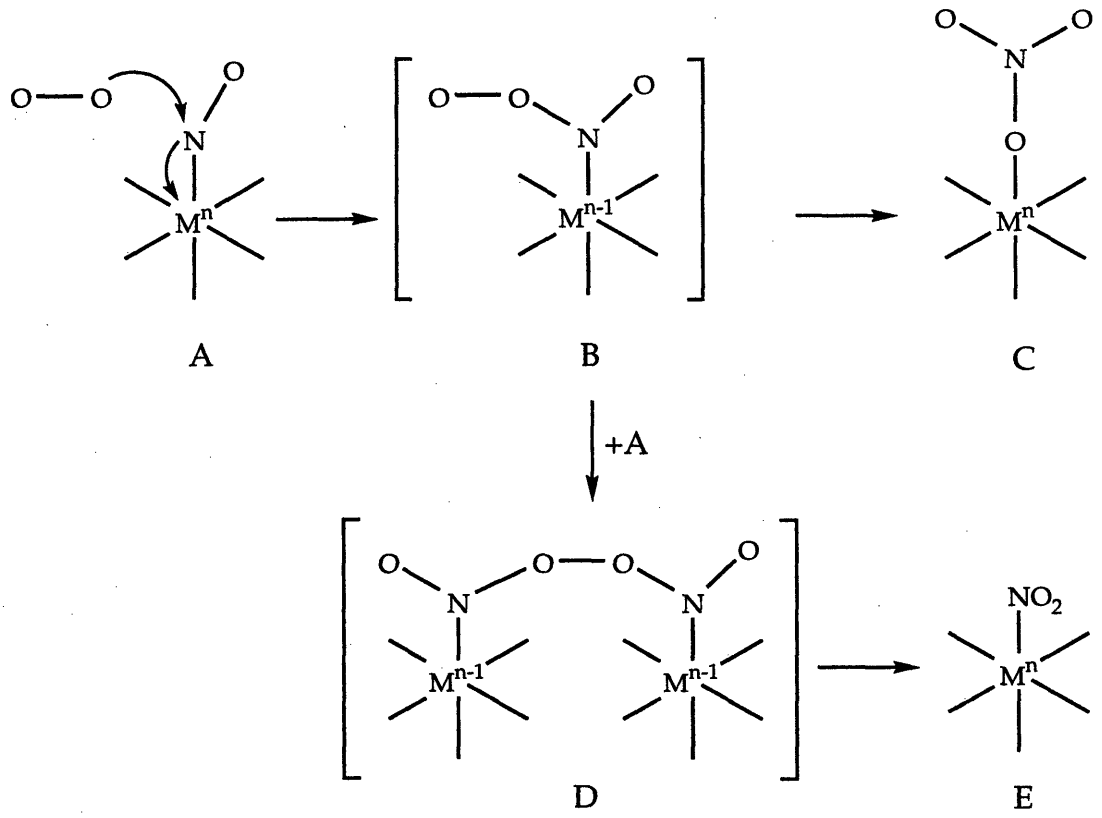

Figure 4.3. Mechanisms of Metal Nitrosyl Oxidation. (Adapted from Ref. 6.)

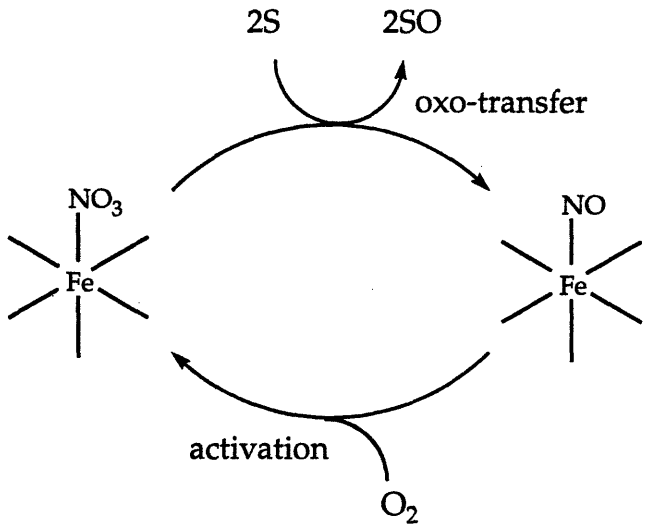

Scheme 4.1. (Adapted from Ref. 62)

The core of the nitrate/nitrosyl reaction is shown in Scheme 4.1. The iron nitrato species is highly activated, and even in the absence of dioxygen can oxidize phosphines to phosphine oxides, reforming the nitrosyl compound. Dioxygen is then required to cycle the system back to its oxidized, nitrato state. The iron pre-catalysts for this reaction are formulated as $Fe(NO)_2XL$ or $Fe(NO)X_2L$ (X = Cl, I, and L = HMPA, dppe or PPh_3) although the choice of ligands is somewhat flexible.[63] The phosphine ligand apparently plays a key role in this chemistry. When L = PPh_3, PPh_3O forms and olefin epoxidation is the primary oxo-transfer product.[63] When chelating phosphines such as dppe are used, however, the ligand is oxidized to O_2dppe and α,β-unsaturated ketones and enols are observed in a ratio of approximately 2:1.[64] The mechanism for this reaction is not well understood. For allylic oxidation, a radical mechanism was suggested but much work

remains to verify such a proposal. A satisfactory rationale for the role of the phosphine ligand in the substrate oxidation reaction is also not available.

Reactions similar to the NO_3^-/NO couple are involved in the global nitrogen cycle. Denitrifying bacteria contain metalloenzymes which consume NO_3^- according to eq 4.5, where NiR is nitrite reductase and NoR is nitric oxide reductase.[67,68] In these systems the oxygen atom of the nitrite ion is converted to water rather than being incorporated into a substrate. The proposed Cu^+-NO^+ intermediate would be highly electrophilic however, and in the presence of an olefin might be capable of oxo-transfer.

$$NO_3^- \longrightarrow NO_2^- \xrightarrow{NiR} NO \xrightarrow{NoR} N_2O \longrightarrow N_2 \qquad (4.5)$$

Chapter VI presents chemistry discovered while screening the (dinitrosyl)diiron complex described in Chapter V for olefin epoxidation behavior like that of the nitrate/nitrosyl couple. To our surprise, nitroolefins instead of oxiranes were observed in the reaction mixture after addition of dioxygen. Based on this observation, the reaction conditions were altered to those described below, and the catalytic nitration ensued.

References

(1) Schmidt, H. H. H.; Walter, U. *Cell* **1994**, *78*, 919-925.

(2) McCall, T.; Vallance, P. In *Second International Meeting on the Biology of NO*; Elsevier: London, UK, 1992; pp 1-6.

(3) *Science* **1992**, *258*, 1862-1863.

(4) Enemark, J. H.; Feltham, R. D. *Coord. Chem. Rev.* **1974**, *13*, 339-406.

(5) Feltham, R. D.; Enemark, J. H. *Topics in Stereochemistry* **1981**, *12*, 155-215.

(6) Mingos, D. M. P.; Sherman, D. J. *Adv. Inorg. Chem.* **1989**, *34*, 293-377.

(7) Zhang, Y.; Pavlosky, M. A.; Brown, C. A.; Westre, T. E.; Hedman, B.; Hodgson, K. O.; Solomon, E. I. *J. Am. Chem. Soc.* **1992**, *114*, 9189-9191.

(8) Farrar, J. A.; Grinter, R.; Pountney, D. L.; Thomson, A. J. *J. Chem. Soc. Dalton Trans.* **1993**, 2703-2709.

(9) Ruggiero, C. E.; Carrier, S. M.; Antholine, W. E.; Whittaker, J. W.; Cramer, C. J.; Tolman, W. B. *J. Am. Chem. Soc.* **1993**, *115*, 11285-11298.

(10) Brown, C. A.; Pavlosky, M. A.; Westre, T. E.; Zhang, Y.; Hedman, B.; Hodgson, K. O.; Solomon, E. I. *J. Am. Chem. Soc.* **1995**, *117*, 715-732.

(11) Sawyer, D. T. In *Oxygen Complexes and Oxygen Activation by Transition Metals*; Martell, A. E. and Sawyer, D. T., Eds.; Plenum: New York, 1988; pp 131-148.

(12) Vaska, L. *Acc. Chem. Res.* **1976**, *9*, 175-183.

(13) Collman, J. P.; Hegedus, L. S.; Norton, J. R.; Finke, R. G. *Principles and Applications of Organotransition Metal Chemistry*; University Science Books: Mill Valley, CA, 1987.

(14) National Research Council. *Nitrogen Oxides*; National Academy of Sciences: Washington, D.C., 1977.

(15) Correa, S. M. *Combust. Sci. and Tech.* **1992**, *87*, 329-362.

(16) Caulton, K. G. *Coord. Chem. Rev.* **1975**, *14*, 317-355.

(17) Cotton, F. A.; Wilkinson, G. *Advanced Inorganic Chemistry*; Wiley Interscience: New York, .

(18) Hu, S.; Kincaid, J. R. *J. Am. Chem. Soc.* **1991**, *113*, 2843-2850.

(19) Stong, J. D.; Burke, J. M.; Daly, P.; Wright, P.; Spiro, T. G. *J. Am. Chem. Soc.* **1980**, *102*, 5815-5819.

(20) See also Chapter V.

(21) Chiou, Y.-M.; Que, L., Jr. *Inorg. Chem.* **1995**, *34*, 3270-3278.

(22) Pohl, L.; Wieghardt, K.; Nuber, B.; Weiss, J. *J. Chem. Soc. Dalton Trans.* **1987**, 187-192.

(23) Randall, C. R.; Zang, Y.; True, A. E.; Que, L., Jr.; Charnock, J. M.; Garner, C. D.; Fujishima, Y.; Schofield, C. J.; Baldwin, J. E. *Biochem.* **1993**, *32*, 6664-6673.

(24) Westre, T. E.; Di Cicco, A.; Filipponi, A.; Natoli, C.; Hedman, B.; Solomon, E. I.; Hodgson, K. O. *J. Am. Chem. Soc.* **1994**, *116*, 6757-6768.

(25) Haller, K. J.; Johnson, P. L.; Feltham, R. D.; Enemark, J. H.; Ferraro, J. R.; Basile, L. J. *Inorg. Chim. Acta* **1979**, *33*, 119-130.

(26) Hodges, K. D.; Wollmann, R. G.; Kessel, S. L.; Hendrickson, D. N.; Van Derveer, D. G.; Barefield, E. K. *J. Am. Chem. Soc.* **1979**, *101*, 906-917.

(27) Koppenol, W. H.; Moreno, J. J.; Pryor, W. A.; Ischiropoulos, H.; Beckman, J. S. *Chem. Res. Toxicol.* **1992**, *5*, 834-842.

(28) Beckman, J. S.; Jun, C.; Ischiropoulos, H.; Crow, J. P. *Methods in Enzymology* **1993**, *233*, 229-240.

(29) Nocek, J. M.; Kurtz, D. M., Jr.; Sage, J. T.; Debrunner, P. G.; Maroney, M. J.; Que, L., Jr. *J. Am. Chem. Soc.* **1985**, *107*, 3382-3384.

(30) Nocek, J. M.; Kurtz, D. M., Jr.; Sage, J. T.; Xia, Y.-M.; Debrunner, P.; Shiemke, A. K.; Sanders-Loehr, J.; Loehr, T. M. *Biochem.* **1988**, *27*, 1014-1024.

(31) Deatherage, J. F.; Moffat, K. *J. Mol. Biol.* **1979**, *134*, 401-417.

(32) Piciulo, P. L.; Rupprecht, G.; Scheidt, W. R. *J. Am. Chem. Soc.* **1974**, *96*, 5293-5295.

(33) Scheidt, W. R.; Frisse, M. E. *J. Am. Chem. Soc.* **1975**, *97*, 17-21.

(34) Scheidt, W. R.; Piciulo, P. L. *J. Am. Chem. Soc.* **1976**, *98*, 1913-1919.

(35) Scheidt, W. R.; Brinegar, A. C.; Ferro, E. B.; Kirner, J. F. *J. Am. Chem. Soc.* **1977**, *99*, 7315-7322.

(36) Chen, V. J.; Orville, A. M.; Harpel, M. R.; Frolik, C. A.; Surerus, K. K.; Münck, E.; Lipscomb, J. D. *J. Biol. Chem.* **1989**, *264*, 21677-21681.

(37) Orville, A. M.; Chen, V. J.; Kriauciunas, A.; Harpel, M. R.; Fox, B. G.; Münck, E.; Lipscomb, J. D. *Biochem.* **1992**, *31*, 4602-4612.

(38) Twilfer, H.; Bernhardt, F.-H.; Gersonde, K. *Eur. J. Biochem.* **1985**, *147*, 171-176.

(39) Arciero, D. M.; Lipscomb, J. D.; Huynh, B. H.; Kent, T. A.; Münck, E. *J. Biol. Chem.* **1983**, *258*, 14981-14991.

(40) Arciero, D. M.; Orville, A. M.; Lipscomb, J. D. *J. Biol. Chem.* **1985**, *260*, 14035-14044.

(41) Arciero, D. M.; Lipscomb, J. D. *J. Biol. Chem.* **1986**, *261*, 2170-2178.

(42) Nelson, M. J. *J. Biol. Chem.* **1987**, *262*, 12137-12142.

(43) Feig, A. L.; Lippard, S. J. *Chem. Rev.* **1994**, *94*, 759-805.

(44) Lepoivre, M.; Raddassi, K.; Oswald, I.; Tenu, J. P.; Lemaire, G. In *39th Forum in Immunology*; 1992; pp 580-583.

(45) Hibbs, J. B., Jr.; Taintor, R. R.; Vavrin, Z.; Rachlin, E. M. *Biochem. Biophys. Res. Commun.* **1988**, *157*, 87-94.

(46) Stubbe, J. In *Advances in Enzymology and Related Areas of Molecular Biology*; Meister, A., Eds.; John Wiley and Sons: New York, 1990; Vol. 62; pp 349-420.

(47) Stubbe, J. *J. Biol. Chem.* **1990**, *265*, 5329-5332.

(48) Lepoivre, M.; Chenais, B.; Yapo, A.; Lemaire, G.; Thelander, L.; Tenu, J.-P. *J. Biol. Chem.* **1990**, *265*, 14143-14149.

(49) Lepoivre, M.; Fieschi, F.; Coves, J.; Thelander, L.; Fontecave, M. *Biochem. Biophys. Res. Commun.* **1991**, *179*, 442-448.

(50) Lepoivre, M.; Flaman, J.-M.; Henry, Y. *J. Biol. Chem.* **1992**, *267*, 22994-23000.

(51) Lepoivre, M.; Flaman, J.-M.; Bobe, P.; Lemaire, G.; Henry, Y. *J. Biol. Chem.* **1994**, *269*, 21891-21897.

(52) Fontecave, M.; Nordlund, P.; Eklund, H.; Reichard, P. In *Advances in Enzymology and Related Areas of Molecular Biology*; Meister, A., Eds.; Wiley and Sons: New York, 1992; Vol. 65; pp 147-183.

(53) Roy, B.; Lepoivre, M.; Henry, Y.; Fontecave, M. *Biochem.* **1995**, *34*, 5411-5418.

(54) Clarkson, S. G.; Basolo, F. *Inorg. Chem.* **1973**, *12*, 1528-1534.

(55) Kubota, M.; Phillips, D. A. *J. Am. Chem. Soc.* **1975**, *97*, 5637-5638.

(56) Trogler, W. C.; Marzilli, L. G. *Inorg. Chem.* **1974**, *13*, 1008-1010.

(57) Hubbard, J. L.; Zoch, C. R.; Elcesser, W. L. *Inorg. Chem.* **1993**, *32*, 3333-3338.

(58) Bhaduri, S. A.; Bratt, I.; Johnson, B. F. G.; Khair, A.; Segal, J. A.; Walters, R.; Zuccaro, C. *J. Chem. Soc., Dalton Trans.* **1981**, 234-239.

(59) Grundy, K. R.; Laing, K. R.; Roper, W. R. *Chem. Commun.* **1970**, 1500-1501.

(60) Graham, B. W.; Laing, K. R.; O'Connor, C. J.; Roper, W. R. *J. Chem. Soc. Dalton Trans.* **1972**, 1237-1243.

(61) Wah, H. L. K.; Postel, M.; Tomi, F. *Inorg. Chem.* **1989**, *28*, 233-238.

(62) Tomi, F.; Wah, H. L. K.; Postel, M. *New J. Chem.* **1988**, *12*, 289-292.

(63) Postel, M.; Tomi, F.; Li Kam Wah, H.; Mordenti, L.; Guillaume, P. *Phosphorus, Sulfur and Silicon* **1990**, *49/50*, 453-457.

(64) Munyejabo, V.; Guillaume, P.; Postel, M. *Inorg. Chim. Acta* **1994**, *221*, 133-139.

(65) Guillaume, P.; Postel, M. *Inorg. Chim. Acta* **1995**, *233*, 109-112.

(66) Guillaume, P.; Wah, H. L. K.; Postel, M. *Inorg. Chem.* **1991**, *30*, 1828-1831.

(67) Jackson, M. A.; Tiedje, J. M.; Averill, B. A. *FEBS Lett.* **1991**, *291*, 41-44.

(68) Ye, R. W.; Toro-Suarez, I.; Tiedje, J. M.; Averill, B. A. *J. Biol. Chem.* **1991**, *266*, 12848-12851.

CHAPTER V.

Studies on the Nitrosyl Adduct of a Dinuclear Non-heme Iron(II) Compound

Introduction

The biological roles of nitric oxide (NO) have received much attention in recent years. It carries out many critical functions and is one of the most versatile messenger molecules in biochemistry. Some of the biological activities of NO, such as its reaction with superoxide to form peroxynitrite ($ONOO^-$), require no catalyst, but metal ions are an important component of many NO-mediated processes within the global nitrogen cycle. Metalloenzymes containing copper and iron control the production and consumption of NO, and metal nitrosyls are believed to be key intermediates in the reaction mechanisms of these enzymes.[1,2] It is also well known that nitric oxide coordinates to and can be activated by transition metal ions in small molecule systems.[3,4]

One target of NO that is of particular relevance to this work is *E. coli.* ribonucleotide reductase (RNR).[5,6] It is not yet clear whether NO regulates RNR or if RNR is simply an adventitious target of the highly reactive NO molecule. Either way, RNR is inactivated by exposure to NO and, since RNR is a critical protein required for DNA biosynthesis, the inhibition of this enzyme has the potential to affect cell growth and proliferation.

The compound discussed in this chapter is a putative model for the dinuclear bis-nitrosyl species that might form as part of the inactivation of RNR by NO. Formed by the addition of NO to a diiron(II) precursor, this adduct represents one of the first models to address the issue of nitric oxide interaction with non-heme diiron proteins. Other dinuclear iron nitrosyl complexes have been synthesized, but they contain phosphine,[7] thiolate[8,9] or sulfide[10,11] ligands and do not model the protein systems. The reactions of several mononuclear non-heme iron(II) models with NO have been studied previously.[12-15]

Experimental

General Considerations. Anaerobic work was carried out in a nitrogen filled glove box or by using standard Schlenk techniques. Solvents were dried and purified by distillation from over CaH_2 (MeCN and EtCN), $Mg(OMe)_2$ (MeOH), or P_2O_5 ($CHCl_3$ and CH_2Cl_2). Nitric oxide was purchased from Matheson and extensively purified as described by Ruggiero et al.[16,17] Reduced stability of the nitrosyl adduct was observed if the NO purification was omitted. The ferrous precursor $[Fe_2(Et\text{-}HPTB)(OBz)](BF_4)_2$ (**1**) was prepared as previously described[18] and recrystallized from $MeCN/Et_2O$ prior to use. Optical spectra were recorded on a HP 8452 diode array spectrophotometer under an atmosphere of NO. A Bio-Rad FTS7 FTIR spectrometer was used to measure vibrational spectra of KBr pellets.

Synthesis of $[Fe_2(Et\text{-}HPTB)(OBz)(NO)_2](BF_4)_2$ (2). Two routes were used to prepare **2**. The primary method was to allow NO gas to react with **1** in acetonitrile, propionitrile or chloroform. By using a vacuum line, the solution was immediately transferred from a Schlenk flask to an appropriate sample cell via cannula. Excess NO gas could be removed by brief vacuum/argon cycles. To grow X-ray diffraction quality crystals outside of the glove box, septum-sealed crystallization vials containing MeCN solutions of **1** in a central container surrounded by diethyl ether were removed from the glove box. The N_2 atmosphere within the vial was replaced with NO by rapid sparging. Upon standing overnight, dark green crystals of **2** formed. In an alternative synthesis, NO gas was generated in a sealed vessel within the glove box from the decomposition of $NOBF_4$ (Ozark-Mahoning). A vial containing a stirred, saturated solution of **1** was placed within a larger vial containing solid $NOBF_4$ ($\approx$ 50 mg). Ether was then added to the outer vial and the sample was sealed. The $NOBF_4$ suspension slowly decomposed and the

reaction mixture turned the characteristic green color of the dinitrosyl adduct. Dark green crystals of **2** could be grown by vapor diffusion of Et_2O into the MeCN solutions under a nitrogen atmosphere by this procedure, but the samples were always contaminated with the yellow starting material due to slow reversibility of the NO addition reaction. The combination of the reversibility of adduct formation and extreme dioxygen sensitivity has made it impossible to obtain satisfactory elemental analysis data on this compound.

Reaction of 2 with O_2. Upon exposure of **2** to air, green solutions rapidly and irreversibly turn orange. The product of this reaction $[Fe_2(Et\text{-}HPTB)(NO_3)_2(OH)](NO_3)_2$ (**3**) can be obtained in crystalline form by vapor diffusion of Et_2O into MeCN solutions of the complex. This compound is identical to one previously reported based on the HPTB ligand, an analog of Et-HPTB which lacks the 4 N-ethyl groups.[19]

Manometry. Gas uptake experiments were performed as previously described.[20] In a typical experiment, an acetonitrile solution of **1** (91.1 mg in 11 mL, 81.3 μmol) was loaded into the sample cell and degassed by 3 freeze-pump-thaw cycles. The manometer was purged three times with nitric oxide and then the gas inlet was sealed and the initial pressure was noted. The sample cell was maintained at a constant temperature in a water bath. The valve connecting the sample cell to the manometer was opened and the cell was allowed to equilibrate until the pressure remained constant. Excess nitric oxide was removed from the sample cell by 3 freeze-pump-thaw cycles and the manometer was refilled with dioxygen. The uptake measurement was then repeated for the conversion of **2** to **3**. Background measurements for the gas solubilities were measured with 11 mL samples of pure MeCN and the amount of gas taken up was quantitated based on the ideal gas law and a calibration constant for the system.

X-ray Crystallography. A single crystal of **2**•3MeCN suitable for X-ray diffraction study was grown from an acetonitrile solution of **2** by vapor diffusion of Et_2O under an atmosphere of NO. The dark green rhombohedral crystal (0.30 x 0.30 x 0.15 mm) was coated in Paratone N (Exxon) and mounted on the tip of a quartz fiber. Rapid surface oxidation leading to loss of morphology and crystal integrity was observed upon exposure of the crystals to O_2. Once mounted on the diffractometer, the crystal was kept at -80 °C in a cold stream of nitrogen gas (Siemens LT2A). X-ray diffraction data were collected on a Siemens 3-circle diffractometer system fitted with a CCD by using the SMART[21] and SAINT[22] software packages. Data collection parameters are listed in Table 5.1. The unit cell was derived from the least-squares fitting of the entire data set. The structure was solved by direct methods (SIR92)[23] with the TEXSAN software.[24] An analytical absorption correction was applied based upon the measured intensities of equivalent reflections. All non-hydrogen atoms were refined anisotropically by least squares fitting. Hydrogen atoms were placed in their calculated positions 0.95 Å from their respective carbon atoms except for the hydrogens bound to the lattice solvent which were omitted from the model. The largest residual peak in the final difference Fourier map was 0.9 $e^-/Å^3$.

Electrochemistry. The electrochemical behavior of **1 - 3** was studied in solution by cyclic voltammetry by using a Princeton Applied Research 263 universal power supply interfaced with an IBM compatible computer running M270 software.[25] The electrochemical cell consisted of a platinum disk working electrode, a platinum wire counter electrode and a silver/silver chloride reference electrode. The potential of the cell was calibrated against ferrocene and data are reported relative to the Fc/Fc^+ potential. A saturated

Table 5.1. X-ray Crystallographic Information for $[Fe_2(Et\text{-}HPTB)(OBz)(NO)_2](BF_4)_2 \cdot 3MeCN$ (**2**).

	2•3MeCN
formula	$Fe_2C_{56}H_{63}B_2F_8O_5N_{15}$
mol wt (g/mol)	1311.57
a (Å)	13.5765(8)
b (Å)	15.4088(10)
c (Å)	16.2145(10)
α (deg)	73.656(1)
β (deg)	73.546(1)
γ (deg)	73.499(1)
V ($Å^3$)	3043.8
T (°C)	-80
Z	2
Radiation	Mo K_α
ρ_{calc} (g/cm^3)	1.30
space group	$P\bar{1}$
2θ limits (deg)	46
μ (cm^{-1})	5.52
total data	8052
unique data[a]	5644
no. of parameters	749
R^b =	0.085
R_w =	0.082

[a]Observation criterion $I > 3\sigma_I$. [b]$R = \Sigma||F_o| - |F_c||/\Sigma|F_o|$, $R_w = [\Sigma w(|F_o| - |F_c|)^2/\Sigma w|F_o|]^{1/2}$, where $w = 1/\sigma(F_o)$.[26]

solution of **1** (≈25 mg/10 mL) in MeCN containing 0.2 M $[Bu_4N][PF_6]$ was removed from the glove box and an aliquot was transferred by cannula to the N_2 purged electrochemical cell (working volume approximately 3 mL). Voltammagrams were collected at scan rates between 50 and 1000 mV/s. The potentials of the noted features did not vary significantly (<10 mV) as a function of scan rate and plots of the peak current versus the square root of the scan speed were linear. Another aliquot of the solution was treated with NO to form **2** before being transferred to the electrochemical cell. A blanket of N_2 was used to prevent oxidation of the sample. During the course of these experiments, the green color of **2** slowly bleached. Therefore, at regular intervals (approximately every 30 min) NO was briefly passed through the sample cell. The green color returned and excess NO was removed with N_2 before continuing with the experiment. After data collection, the sample was exposed to O_2, allowing the formation of **3**. Excess O_2 was removed before data were collected on this sample.

Magnetics. The magnetic moment of a crystalline sample of **2** (10.1 mg) was measured as a function of temperature between 4 and 300 K by using a Quantum Design SQUID susceptometer. The sample was loaded anaerobically into a gel capsule and suspended in a plastic straw. A background correction for the empty capsule and straw was applied to the data as was a correction for the diamagnetic contribution of the sample. Satisfactory fits to the data were not obtained, however.

EPR. EPR spectra were measured on a Bruker ESP-300 at approximately 8 K using a liquid helium cryostat. The dinitrosyl compound **2** was synthesized in situ by reaction of **1** with nitric oxide in 2:1 (v/v) propionitrile:toluene. Excess NO was removed by flushing the samples with

dry nitrogen prior to glassing in liquid nitrogen. Sample concentrations were approximately 3 mM.

Results

Manometry. The gas uptake experiments were the first indication that the isolated material was a dinitrosyl adduct. Upon exposure of **1** to NO in the manometer, 1.7 ± 0.1 equiv of NO were taken up. This value provides an 85% site occupancy at 1 atm and 22 °C. Upon exposure of O_2 to the resulting solution of **2**, 2.1 ± 0.1 equiv were consumed. Based on the observed products, it would be expected that the NO and O_2 uptake quantities would be comparable. The oxo bridge in the product may derive from residual water in the solvent.

Description of the Structure. The dinitrosyl adduct **2** crystallized in the triclinic space group $P\bar{1}$. An ORTEP drawing of the cation is shown in Figure 5.1. The geometry of the core iron atoms is best described as distorted octahedral. Selected interatomic angles and distances are provided in Tables 5.2 and 5.3. A complete table of positional parameters is provided as Supplementary Material (Table 5.S1). The coordination mode of the Et-HPTB ligand follows one of two general motifs observed for this class of tetra-substituted 1,3-diamino-2-propanol derived species, that involving a *syn* geometry of the adjacent benzimidazole arms. This mode was observed previously in a tetranuclear Fe^{III} complex of the Et-HPTB ligand.[27] The alternative *anti* geometry, which typically has an almost linear N-Fe-N angle, was observed in the diferric bis-nitrato species of the related HPTB and HPTP ligands.[19,28] The factors which dictate the coordination mode are not clear at present. The other minor difference is the Fe-O-Fe angle, which is 117° in this complex, 5-15° more acute than other diiron or dimanganese complexes of these ligands in the presence of μ-alkoxo, μ-carboxylato coordination.[19,27-31]

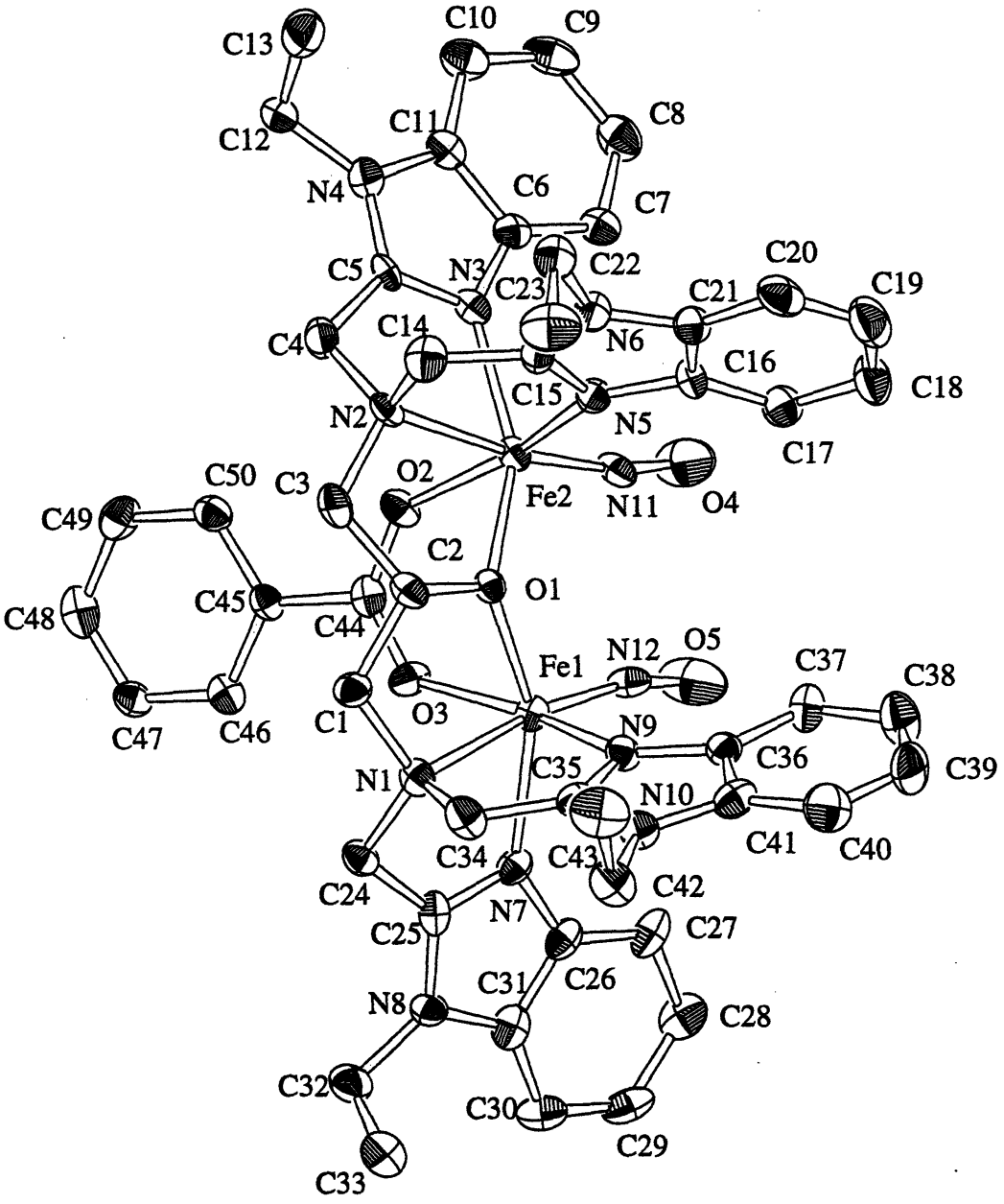

Figure 5.1. ORTEP representation of the cation of **2** (40% probability ellipsoids) with the hydrogen atoms removed for clarity.

Table 5.2. Selected Bond Lengths (Å) for **2**•3MeCN.[a]

atom	atom	distance	atom	atom	distance
Fe(1)	O(1)	2.017(5)	Fe(2)	O(1)	2.006(5)
Fe(1)	O(3)	2.117(5)	Fe(2)	O(2)	2.134(6)
Fe(1)	N(1)	2.290(6)	Fe(2)	N(2)	2.282(7)
Fe(1)	N(7)	2.119(7)	Fe(2)	N(3)	2.114(7)
Fe(1)	N(9)	2.117(7)	Fe(2)	N(5)	2.135(7)
Fe(1)	N(12)	1.749(8)	Fe(2)	N(11)	1.750(7)
O(5)	N(12)	1.151(8)	O(4)	N(11)	1.156(8)

[a]Numbers in parentheses after distances are estimated standard deviations for the last significant digit. See Figure 5.1 for atom labeling scheme.

The nitrosyl ligands on the two metal centers are equivalent. Each metal center can be described by the $\{FeNO\}^7$ formalism introduced by Feltham and Enemark.[32] This electron count results from either a formal Fe(III)-NO^- complex (5 d electrons plus a 2-electron anionic ligand) or Fe(II)-NO (6 d electrons and a neutral 1-electron donor) Both nitrosyl units display the short Fe-N ($\bar{x}$ = 1.75 Å) and N-O bond lengths ($\bar{x}$ = 1.15 Å) typical of metal nitrosyl adducts and slight bend angles of 166.6(7) and 168.3(7)°. Although the nitrosyls do bend away from one another, no close steric contacts exist in their vicinity, so the adopted geometry must be dictated by electronic considerations. The bend angles of the nitrosyl ligands are intermediate between the rigidly linear and 120° extremes.[32] A similar case has recently been observed in the chemistry of a copper compound in which a bend angle of 163.4° was observed.[16] It was postulated that the extreme steric

Table 5.3. Selected Bond Angles (deg) for **2**•3MeCN.[a]

atom	atom	atom	angle	atom	atom	atom	angle
Fe(1)	N(12)	O(5)	166.6(7)	Fe(2)	N(11)	O(4)	168.3(7)
O(1)	Fe(1)	O(3)	83.6(2)	O(1)	Fe(2)	O(2)	82.7(2)
O(1)	Fe(1)	N(1)	79.5(2)	O(1)	Fe(2)	N(2)	79.3(2)
O(1)	Fe(1)	N(7)	153.6(2)	O(1)	Fe(2)	N(3)	153.4(2)
O(1)	Fe(1)	N(9)	89.8(2)	O(1)	Fe(2)	N(5)	91.8(2)
O(1)	Fe(1)	N(12)	107.8(3)	O(1)	Fe(2)	N(11)	108.0(3)
O(3)	Fe(1)	N(1)	87.0(2)	O(2)	Fe(2)	N(2)	86.6(2)
O(3)	Fe(1)	N(7)	87.4(2)	O(2)	Fe(2)	N(3)	86.7(2)
O(3)	Fe(1)	N(9)	164.1(2)	O(2)	Fe(2)	N(5)	164.0(2)
O(3)	Fe(1)	N(12)	98.0(3)	O(2)	Fe(2)	N(11)	97.7(3)
N(1)	Fe(1)	N(7)	75.2(2)	N(2)	Fe(2)	N(3)	75.7(2)
N(1)	Fe(1)	N(9)	77.6(3)	N(2)	Fe(2)	N(5)	77.6(2)
N(1)	Fe(1)	N(12)	171.5(3)	N(2)	Fe(2)	N(11)	171.9(3)
N(7)	Fe(1)	N(9)	92.3(2)	N(3)	Fe(2)	N(5)	91.7(2)
N(7)	Fe(1)	N(12)	98.0(3)	N(3)	Fe(2)	N(11)	97.6(3)
N(9)	Fe(1)	N(12)	97.7(3)	N(5)	Fe(2)	N(11)	98.2(3)
Fe(1)	O(1)	Fe(2)	117.7(2)				

[a]Numbers in parentheses after angles are estimated standard deviations for the last significant digit. See Figure 5.1 for atom labeling scheme.

bulk of the substituted tris(pyrazolyl)borate ligand used led to the deformation. The structure presented here indicates that, at least for iron, these partially bent species are stable even in the absence of steric pressure.

Nitrosyl ligands usually exert a large trans influence due to strong sigma donation into the d_z2 orbital.[32] This property generally leads to lengthening of the metal ligand bonds opposite the nitrosyl. In **2**, the aliphatic amine coordinates in this position. Generally, this bond is longer than the Fe-N_{arom} ligand bonds and the same is true for **2** as well. The bonds are not inordinately long, however, and there does not appear to be significant weakening relative to that found in similar Fe^{III} complexes.[18,29] The most substantial distortion from octahedral geometry lies along the O1-Fe2-N3 and O1-Fe1-N7 vectors. These angles are bent 26.5° from the ideal 180° value, and remove O1 from the plane defined by the two {FeNO} units.

Optical and Vibrational Spectroscopy. The NO stretching frequency of **2** is 1785 cm^{-1}. This value is high for 6-coordinate bent $\{MNO\}^7$ complexes and in the range generally observed for linear MNO units.[3] Use of the stretching frequency alone as a geometric indicator is inadvisable, however, since the ranges for linear and bent complexes have significant overlap. The optical spectra of **1** - **3** are shown in Figure 5.2. For **1**, the visible region is featureless and consists just of the tailing from the strong UV band. A broad feature centered at 620 nm ($\varepsilon = 579 \pm 7$) is present for **2** and a second band appears as a shoulder at 520 nm ($\varepsilon = 395 \pm 6$). The other common visible feature of Fe-NO adducts at 420 nm does not appear to be present for this complex, but it is difficult to be certain due to tailing of the UV band into the visible region. The UV band has its λ_{max} at 330 nm ($\varepsilon \approx 26{,}000$). The optical spectrum of **3** matches that reported for the complex $[Fe_2(HPTB)(OH)(NO_3)_2](NO_3)_2$.[19]

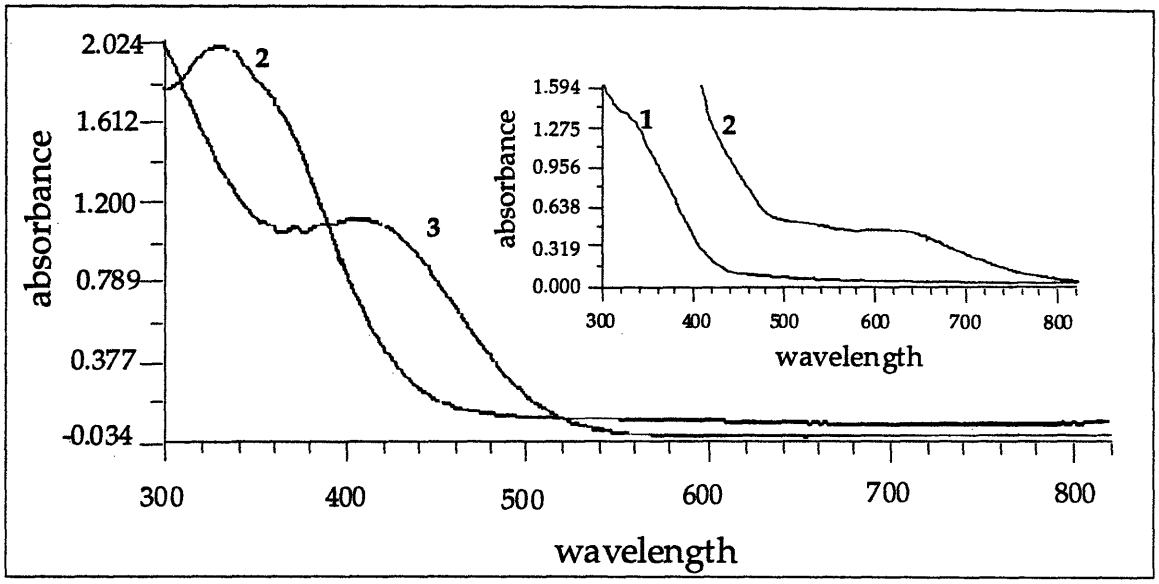

Figure 5.2. Optical spectrum of **1 - 3** in MeCN. The spectrum of **2** was collected under an 1 atm NO. The inset shows the spectra of **1** and **2** at lower concentration so that the absorption bands in the visible region can be observed.

Electrochemistry. Two reversible oxidations are observed for **1** at -44 and +425 mV vs Fc/Fc^+ (Figure 5.3). These features can be assigned to the II,II/II,III and II,III/III,III redox couples, respectively since the electrochemical behavior changes upon addition of NO and/or O_2. Were this oxidation Et-HPTB centered, **1 - 3** would be expected to exhibit similar voltammagrams. The behavior of the nitrosyl adduct **2** is a bit more complicated (Figure 5.3). Two reversible oxidation waves are present as well as three irreversible to quasi-reversible reduction features. The potentials of these waves are listed in Table 5.3. A plot of the peak current versus the square root of the scan speed for the reversible waves is provided as Figure 5.S1. The linearity of this plot was used to define reversible behavior in this system. During the electrochemistry experiment, bleaching of the dark green color was observed over time. This process resulted from the slow dissociation of NO from **2**

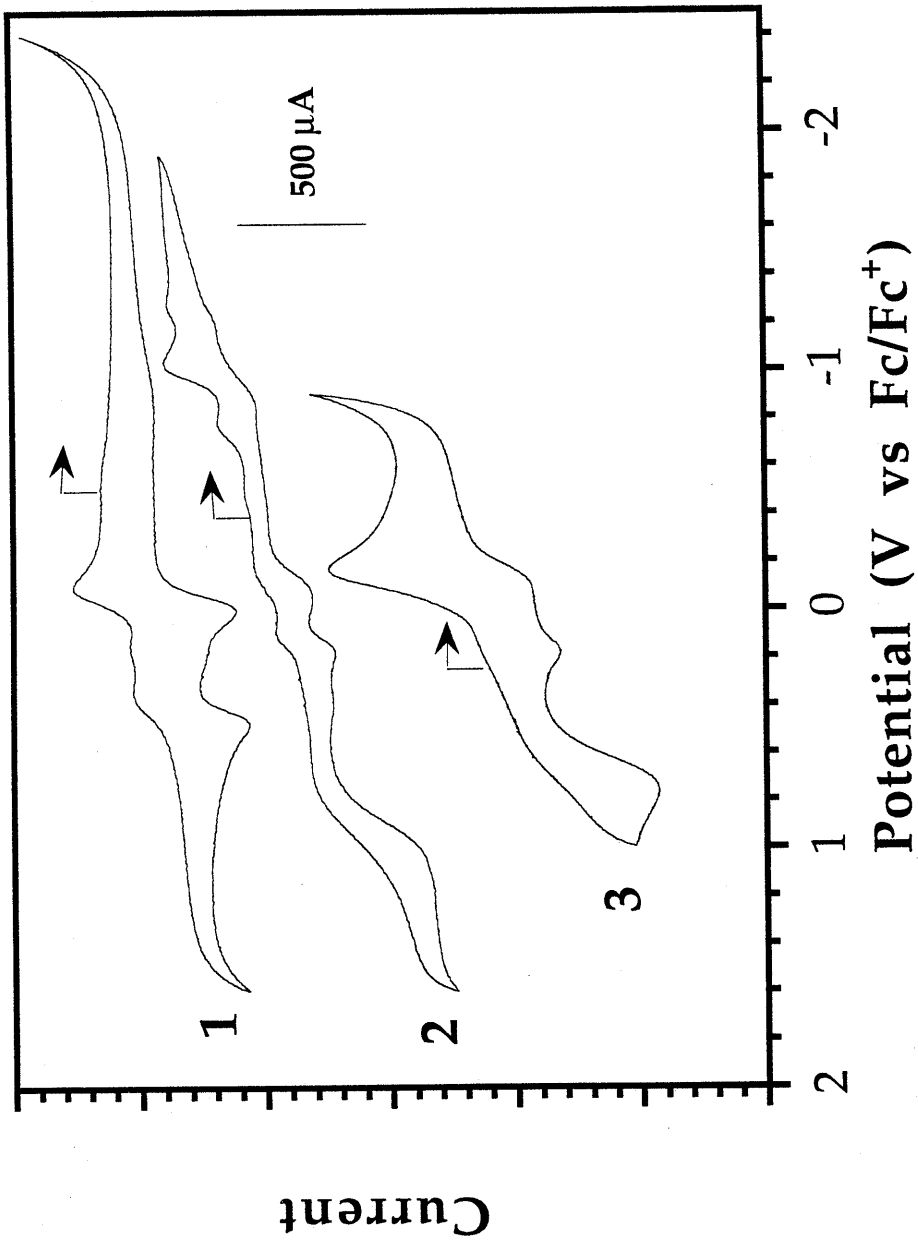

Figure 5.3. Cyclic voltamagrams of **1**, **2**, and **3**. Conditions: 22 °C, 0.2 M $[Bu_4N][PF_6]$ supporting electrolyte in MeCN, scan rate = 250 mV/s. The initial voltages and the scan directions are indicated by the arrows.

Table 5.3. Electrochemical Potentials of **1 - 3** in mV versus Fc/Fc^+.[a]

	1	**2**	**3**
Reductions			
E_{pa-1}		-778	-167
E_{pc-1}			-105
E_{pa-2}		-1036	
E_{pc-2}		-872	+178
E_{pa-3}		-1272	
E_{pc-3}		-1206	
Zero current potential	-402	-260	+443
Oxidations			
$E_{1/2}$ (ΔE)	-44 (87)	-118 (124)	
$E_{1/2}$ (ΔE)	+425 (104)	+138 (83)	
E_{pc-1}		≈1100	≈+750
E_{pa-1}		+668	

[a]Data were collected in anaerobic MeCN solutions under the following conditions: 0.2 M $[Bu_4N](PF_6)$ supporting electrolyte, scan speed = 250 mV/s, Temp = 22 °C. The electrochemical cell consisted of a platinum disk working electrode, a coiled platinum wire as counter electrode and an aq Ag/AgCl reference electrode the potential of which was calibrated against ferrocene.

with concomitant regeneration of **1**. The adduct reformed upon addition of fresh NO as indicated by the return of the green color.

The bis-(nitrato)diiron(III) species **3** resulting from the oxidation of **2** was also studied. The behavior of this species differed significantly from that of **1** and **2**. This compound exhibits a 2-electron reduction wave rather than two one-electron features. Therefore, the mixed valence complex is only accessible from the reduced state. The return wave consists of two 1-electron events. Furthermore, the potential at which no current passed through the system was very different for **3** relative to **1** and **2**. The addition of O_2 to **2**

resulted in a +0.70 V shift in this potential compared to the +0.14 V shift upon addition of NO to **1**.

Magnetic Susceptibility of 2. Measurements of the magnetic moment of **2** as a function of temperature allow us to state qualitatively that the core is antiferromagnetically coupled. Plots of χ_{para} and μ_{eff} versus temperature are provided in Figure 5.4. At high temperature, the species approaches an S = 2 state, but beyond that, little of quantitative value can be determined from the data. There is a small paramagnetic impurity in the sample as indicated by the sharp rise in magnetic moment at very low temperature. As stated above, this feature probably arises from the difficulty in obtaining a pure crystalline sample without partial loss of NO or oxidation to **3**.

EPR Spectrum. The EPR spectrum of **2** is shown in Figure 5.5. Three signals are visible in the spectrum. The high field feature around g = 1.9 can be attributed to dissolved NO. This signal is always present, but its intensity varies depending on how well the sample is sparged with N_2 prior to glassing. Some dinuclear iron nitrosyl compounds exhibit EPR signals around g = 2.[7] Unfortunately, this signal will be obscured in our case due to the presence of free NO. This problem of overlapping signals from free and bound NO has been noted previously in studies of the Soybean Lipoxygenase-NO complex.[33] The feature at g = 4 is typical of mononuclear $\{FeNO\}^7$ systems and is most likely the paramagnetic impurity observed in the magnetic data.[12] Upon exposure to O_2, the g = 4 signal converts to one at g = 4.3, as can be seen in Figure 5.5B.

Chemical Reactivity of 2. Some metal nitrosyls carry-out oxo-transfer chemistry based on the nitrate/nitrosyl couple.[34,35] Such behavior was not observed for **2**, but another interesting reaction was discovered in the process

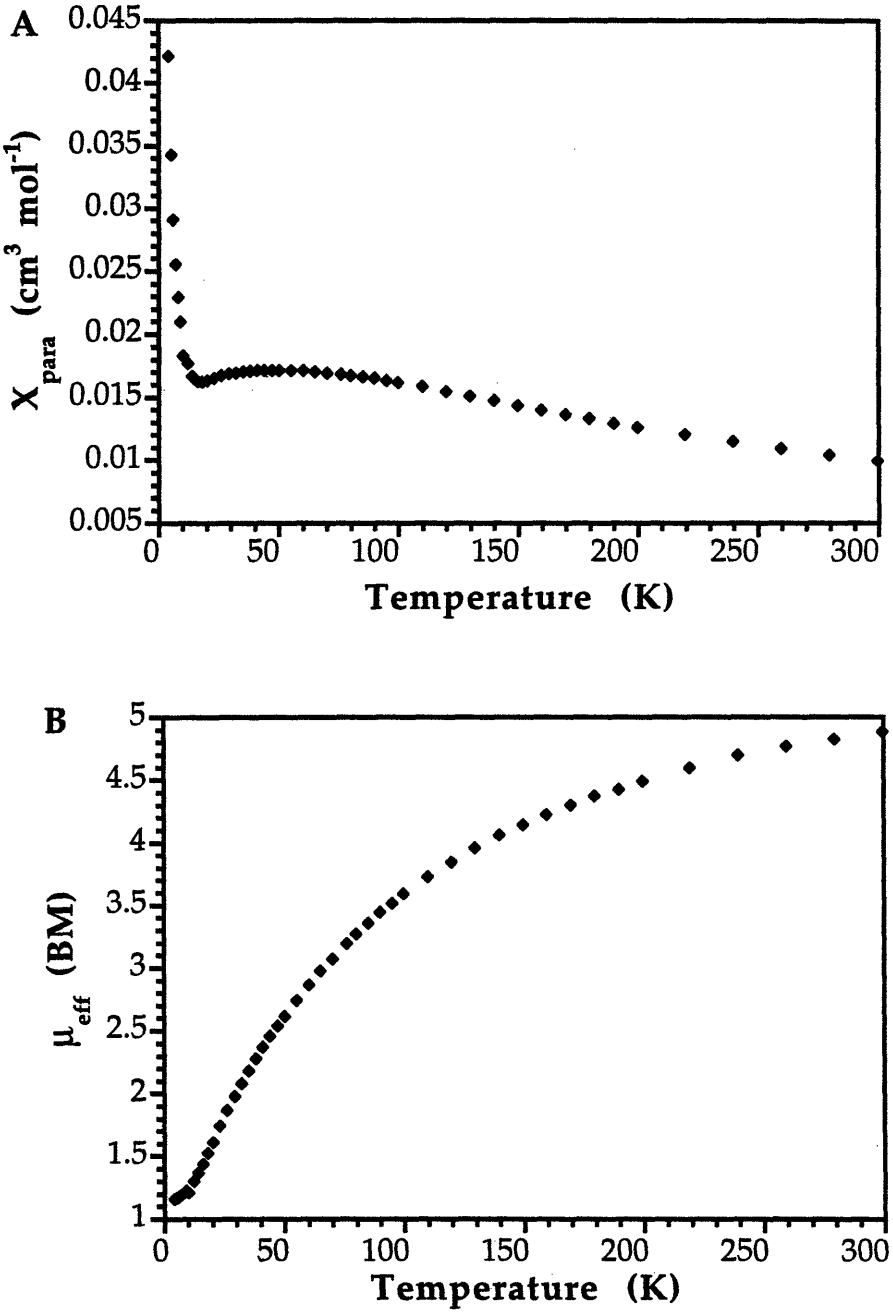

Figure 5.4. Magnetic susceptibility studies on **2**. A. Plot of χ_m versus Temperature between 4 and 300 K. Data were corrected for the diamagnetic contributions of the complex and the sample container. B. Plot of μ_{eff} versus Temperature over the same temperature range.

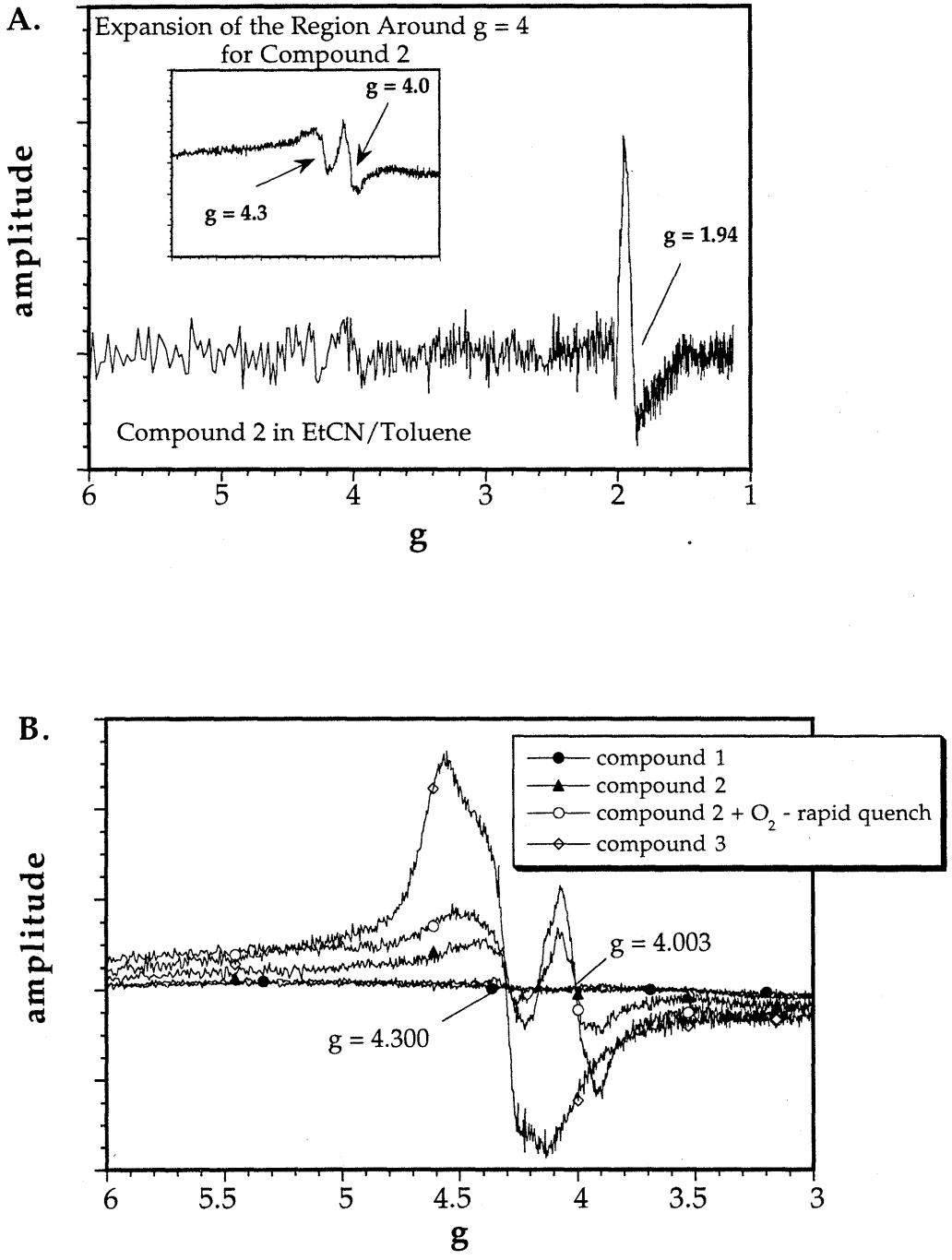

Figure 5.5. EPR Spectrum of **2**A. EPR spectrum at 8 K of **2** as a frozen glass in 2:1 propionitrile:toluene. B. EPR spectra of **2** showing the changes which occur in the g = 4 region upon reaction with O_2.

of surveying its activity. In the absence of substrate, the reaction of **2** with O_2 leads to the formation of a previously identified bis-nitrate compound **3**. If olefins such as cyclohexene were added during the oxidation, however, a complex reaction mixture was observed by GC/MS analysis (Figure 5.S2). The main product in this reaction was the nitroolefin which was obtained in substoichiometric yield. Since the product of the reaction involved nitration, and the only source of this group was the coordinated nitric oxide, reactions were run by first adding dioxygen and then nitric oxide. The results of such experiments are discussed in Chapter VI.

Discussion

Nature of the Bonding in the {FeNO}^{7} unit of 2. The nature of the bonding in metal nitrosyl complexes has been debated. Feltham and Enemark circumvented many of the complicated issues by developing the {MNO}^{n} nomenclature, where n is the total number of electrons in the frontein orbitals. This formalism assigns electrons to the molecular fragment instead of to discrete orbitals. Whereas this nomenclature is useful for general discussions of these complexes and allows comparisons to be made between different complex types, it does not allow for the description of variations observed within one class. For mononuclear {FeNO}^{7} units, two theories of the bonding have been presented to explain the observed S = 3/2 ground state, a molecular orbital approach based on extended Hückel calculations of $[Fe(H_2O)_5(NO)]^{2+}$,[13] and SCF-Xα calculations, which separate the metal and ligand orbital fragments. In the latter, high-spin Fe^{III} (S = 5/2) and NO^- (S = 1) are antiferromagnetically coupled to yield the S = 3/2 system.[14,15] Both of these approaches satisfactorily explain the optical absorption, EPR and MCD properties of the mononuclear species studied. The edge energy measured by XAS, a form of spectroscopy used to probe the

oxidation state of metal centers, is more indicative of the Fe^{III}-NO^- assignment, however.[14,15]

In the most simple case, one might predict that a dinitrosyl system, such as **2**, could be treated as two independent mononuclear FeNO units. These two centers would presumably be magnetically coupled in some manner, probably antiferromagnetically. Such an extrapolation of the theories discussed above, however, fails to explain the properties of **2**. The structural and electrochemical data for **2** can best be interpreted by using an Fe^{II}-NO valence bond model as opposed to the Fe^{III}-NO^- model accepted in the mononuclear systems.

The first reason for proposing this model derives from structural evidence. Based on the molecular orbital diagrams derived for the mononuclear systems, one electron at each iron center would populate the 3e anti-bonding orbital (see Figures 4.1 and 4.2). The FeNO unit bends to lower the energy of this unfavorable electron configuration, and with sufficient distortion, the electron ultimately populates a state which is primarily a nitrogen-based sp^2 orbital. Therefore, increased FeNO bending correlates with formal electron transfer from Fe^{II} to NO. The modest 167° mean bend angle of **2** clearly shows that it is energetically favorable not to maintain a perfectly linear geometry. This angle is 10° larger than most 6-coordinate $\{MNO\}^7$ species, however.[32] Table 5.4 compares the structural parameters of **2** to those of other $\{FeNO\}^7$ systems. The greatest distortions from the octahedral geometry of **2** occur in the O1-Fe1-N7 and O1-Fe2-N3 angles which would be linear in perfect octahedra. Bending these two units out of the xy plane (where the Fe-NO bond defines the z-axis) reduces the potential overlap of iron d_{xz} and d_{yz} orbitals into the NO π system. This distortion therefore

Table 5.4. Structural Parameters of Spectroscopically Characterized $\{FeNO\}^7$ Complexes.

Complex	Fe-NO (Å)	N-O (Å)	∠Fe-N-O (deg)	ν(NO) (cm^{-1})	approx. geometry	ref
$[Fe_2(NO)_2(EtHPTB)(OBz)](BF_4)_2$	1.749(8)	1.151(8)	166.6(7)	1785	O_h-6	this
	1.750(7)	1.156(8)	168.3(7)			work
$[Fe(NO)(TPA)(BF)](CLO_4)$[a]	1.72(2)	1.15(2)	159(2)	1794	O_h-6	34
$[Fe(NO)(Me_3TACN)(N_3)_2]$	1.738(5)	1.142(7)	155.5(10)	1690	O_h-6	35
[Fe(NO)TMPzA)Cl](BPh_4)	1.725(7)	1.15(1)	157.1(8)	1796	O_h-6	34, 36
[Fe(NO)(EDTA)]	1.78[b]	1.10[b]	156(5)[b]	1776	nd	37
[Fe(NO)(salen)][c]	1.783(16)	1.10(3)	147(4)	1710	TBP-5	38
$[Fe(NO)TMC)](BF_4)_2$[c]	1.737(6)	1.137(6)	177.5(5)	1840	TBP-5	39

[a]Bond lengths and bond angles are the average of two conformers. [b]Determine by using GNAXS EXAFS. [c]23 °C data. Both complexes undergo S = 3/2 $\rightleftharpoons$ S = 1/2 spin equilibrium. They exhibit S = 3/2 behavior at this temperature.

minimizes the back-bonding interaction between the iron and the nitrosyl ligand. The result is that the electron remains in an iron-centered orbital.

The second reason for proposing an Fe^{II}-NO complex is based on the electrochemistry of **2**. Figure 5.3 compares the behavior of compounds **1** - **3**. The most striking feature is the common reversible wave at approximately -100 mV versus Fc/Fc^+. For compounds **1** and **2**, this wave is the first of two observed oxidations, whereas for **3** this feature is a 2-electron reduction. The similarity between **1** and **2** argues for a common electronic structure at the diiron center. The extra irreversible and quasi-reversible reduction features can be ascribed to the addition of an electron to the neutral nitrosyl ligand to form NO^-. Since an equilibrium exists between bound and free NO, one might expect reduction features for both species to be present. Formally, the one-electron reduction of **2** would generate a $\{MNO\}^8$ at one iron atom. Such complexes generally display even greater bend angles than species with the n = 7 configuration due to the extra electron in the anti-bonding orbital.[36] $\{MNO\}^8$ systems are also more likely to be 5-coordinate because the trigonal bipyramidal geometry results in a lower energy for the filled anti-bonding orbital.[36] The irreversibility of the reduction behavior might therefore reflect ligand dissociation.

With minimal donation into the NO π^* orbital, one would expect the FeNO unit to have several properties. First of all, one would expect a strong N-O bond and relatively weak Fe-N bond. Whereas the N-O and Fe-NO bond distances are in the normal range for six coordinate $\{MNO\}^7$ complexes,[32] the strength of these bonds can also be judged by the NO stretching frequency. The ν(NO) vibration was observed at 1785 cm^{-1} compared to the free NO frequency of 1860 cm^{-1}.[3] This value is in the range of linear Fe-NO units and high in energy for a bent complex. A strong N-O

bond is therefore present. A major factor in the observed ν(NO) may be the charge of the metal center, however. The three charged 6-coordinate species listed in Table 5.4 all show vibrations at the high energy extreme of the region. This result compares to that for the one neutral compound which shows a more normal value for a bent $\{MNO\}^7$ unit. The number of cases to support this hypothesis is still too small for a conclusive argument to be made.

EPR and Magnetic Coupling. The observed EPR and magnetic susceptibility data are consistent with one another, but both are difficult to explain. Neither valence bond formalism for $\{FeNO\}^7$ systems can explain the data. The most problematic feature is the high temperature limit of μ_{eff}, which approaches 4.9 BM, the spin only value for an S = 2 system. The coupling of two S = 3/2 $\{FeNO\}^7$ moieties would be expected to yield a S = 3 limit at high temperature, however. Without a suitable model for the electronic structure, fitting of the susceptibility data to extract coupling constants is impossible.

At a qualitative level, the SQUID data show that the diiron core of **2** is antiferromagnetically coupled. The plot of χ_{para} versus temperature passes through a maximum with a T_N of 44 ± 1 K. At very low temperature, the value for μ_{eff} falls below that expected for an S = 1/2 state before the presence of a paramagnetic impurity in the sample begins to dominate the signal. A perfectly clean sample might therefore be expected to be diamagnetic at 8 K, the temperature at which the EPR spectra were acquired.

In agreement with the SQUID data, the main signal in the 8 K EPR spectrum of **2** arises from free NO. Since the EPR data were collected on a glassed solution rather than a solid, the presence of a small amount of free NO is unavoidable. A separate, weak feature is observed at g = 4.0 and is

typical of mononuclear iron nitrosyl signals.[12] The species giving rise to this resonance might also be the paramagnetic impurity contaminating the SQUID samples. A further indication that the g = 4.0 signal reflects a mononuclear impurity is that upon exposure to air, a g = 4.3 signal replaces the one at 4.0.

Summary and Conclusions

A dinitrosyl diiron complex **2** was isolated from the reaction of NO with the diiron(II) compound **1**. An X-ray crystallographic study revealed that the MNO units are equivalent with distorted octahedral geometry at both iron centers and display only moderate bend angles for the nitrosyl ligands. The two iron centers are antiferromagnetically coupled, but even at room temperature the complex does not have the S = 3 ground state expected by analogy to the mononuclear $\{FeNO\}^7$ systems. Based on structural and electrochemical studies, we postulate that the electronic structure of **2** approximates the Fe^{II}-NO valence bond scheme in contrast to the Fe^{III}-NO^- structure found in the mononuclear systems. Upon exposure to dioxygen, the complex oxidizes to a bis-nitrato species with consumption of two equivalents of dioxygen.

References

(1) Ye, R. W.; Toro-Suarez, I.; Tiedje, J. M.; Averill, B. A. *J. Biol. Chem.* **1991**, *266*, 12848-12851.

(2) Jackson, M. A.; Tiedje, J. M.; Averill, B. A. *FEBS Lett.* **1991**, *291*, 41-44.

(3) Mingos, D. M. P.; Sherman, D. J. *Adv. Inorg. Chem.* **1989**, *34*, 293-377.

(4) Fanning, J. C. *Coord. Chem. Rev.* **1991**, *110*, 253-273.

(5) Lepoivre, M.; Fieschi, F.; Coves, J.; Thelander, L.; Fontecave, M. *Biochem. Biophys. Res. Commun.* **1991**, *179*, 442-448.

(6) Lepoivre, M.; Flaman, J.-M.; Bobe, P.; Lemaire, G.; Henry, Y. *J. Biol. Chem.* **1994**, *269*, 21891-21897.

(7) Guillaume, P.; Wah, H. L. K.; Postel, M. *Inorg. Chem.* **1991**, *30*, 1828-1831.

(8) Butler, A. R.; Glidewell, C.; Hydr, A. R.; McGinnis, J.; Seymour, J. E. *Polyhedron* **1983**, *2*, 1045-1052.

(9) Glidewell, C.; Harman, M. E.; Hursthouse, M. B.; Johnson, I. L.; Motevalli, M. *J. Chem. Res. Synop.* **1988**, *7*, 212-213.

(10) Rauchfuss, T. B.; Weatherill, T. D. *Inorg. Chem.* **1982**, *21*, 827-830.

(11) Glidewell, C.; Hyde, A. R.; McKechnie, J. S.; Pogorzelec, P. J. *J. Chem. Ed.* **1985**, *62*, 534-536.

(12) Rich, P. R.; Salerno, J. C.; Leigh, J. S.; Bonner, W. D., Jr. *FEBS Lett.* **1978**, *93*, 323-326.

(13) Farrar, J. A.; Grinter, R.; Pountney, D. L.; Thomson, A. J. *J. Chem. Soc. Dalton Trans.* **1993**, 2703-2709.

(14) Zhang, Y.; Pavlosky, M. A.; Brown, C. A.; Westre, T. E.; Hedman, B.; Hodgson, K. O.; Solomon, E. I. *J. Am. Chem. Soc.* **1992**, *114*, 9189-9191.

(15) Brown, C. A.; Pavlosky, M. A.; Westre, T. E.; Zhang, Y.; Hedman, B.; Hodgson, K. O.; Solomon, E. I. *J. Am. Chem. Soc.* **1995**, *117*, 715-732.

(16) Ruggiero, C. E.; Carrier, S. M.; Antholine, W. E.; Whittaker, J. W.; Cramer, C. J.; Tolman, W. B. *J. Am. Chem. Soc.* **1993**, *115*, 11285-11298.

(17) See also Chapter VI.

(18) Dong, Y.; Menage, S.; Brennan, B. A.; Elgren, T. E.; Jang, H. G.; Pearce, L. L.; Que, L., Jr. *J. Am. Chem. Soc.* **1993**, *115*, 1851-1859.

(19) Brennan, B. A.; Chen, Q.; Juarez-Garcia, C.; True, A. E.; O'Connor, C. J.; Que, L., Jr. *Inorg. Chem.* **1991**, *30*, 1937-1943.

(20) Tolman, W. B.; Liu, S.; Bentsen, J. G.; Lippard, S. J. *J. Am. Chem. Soc.* **1991**, *113*, 152-164.

(21) SMART, V. 4.0; Siements Industrial Automation, Inc.; Madison, WI, 1994.

(22) SAINT, V. 4.0; Siemens Industrial Auotmation, Inc.; Madison, WI, 1995.

(23) Burla, M. C.; Camalli, M.; Cascarano, G.; Giacovazzo, C.; Polidori, G.; Spagna, R.; Viterbo, D. *J. Appl. Cryst.* **1989**, *22*, 389-393.

(24) TEXSAN; *Single Crystal Structure Analysis Software*, V. 1.6; Molecular Structure Corporation; The Woodlands, TX, 1992.

(25) M270, V. 2.0; Princeton Applied Research, Corp.; Princeton, NJ, 1990.

(26) Carnahan, E. M.; Rardin, R. L.; Bott, S. G.; Lippard, S. J. *Inorg. Chem.* **1992**, *31*, 5193-5201.

(27) Chen, Q.; Lynch, J. B.; Gomez-Romero, P.; Ben-Hussein, A.; Jameson, G. B.; O'Connor, C. J.; Que, L., Jr. *Inorg. Chem.* **1988**, *27*, 2673-2681.

(28) Weiss, A.; Dick, S. Z. *Naturforsch.* **1994**, *49b*, 1051-1058.

(29) Hayashi, Y.; Suzuki, M.; Uehara, A.; Mizutani, Y.; Kitagawa, T. *Chem. Lett.* **1992**, 91-94.

(30) Upadhyay, M.; Trivedi, B. M.; Bhattacharya, P. K.; Ganeshpure, P. A.; Satish, S. *J. Mol. Cat.* **1992**, *73*, 287-295.

(31) Shank, M.; Barynin, V.; Dismukes, G. C. *Biochem.* **1994**, *33*, 15433-15436.

(32) Feltham, R. D.; Enemark, J. H. *Topics in Stereochemistry* **1981**, *12*, 155-215.

(33) Nelson, M. J. *J. Biol. Chem.* **1987**, *262*, 12137-12142.

(34) Tomi, F.; Wah, H. L. K.; Postel, M. *New J. Chem.* **1988**, *12*, 289-292.

(35) Wah, H. L. K.; Postel, M.; Tomi, F. *Inorg. Chem.* **1989**, *28*, 233-238.

(36) Enemark, J. H.; Feltham, R. D. *Coord. Chem. Rev.* **1974**, *13*, 339-406.

(37) Chiou, Y.-M.; Que, L., Jr. *Inorg. Chem.* **1995**, *34*, 3270-3278.

(38) Pohl, L.; Wieghardt, K.; Nuber, B.; Weiss, J. *J. Chem. Soc. Dalton Trans.* **1987**, 187-192.

(39) Randall, C. R.; Zang, Y.; True, A. E.; Que, L., Jr.; Charnock, J. M.; Garner, C. D.; Fujishima, Y.; Schofield, C. J.; Baldwin, J. E. *Biochem.* **1993**, *32*, 6664-6673.

(40) Westre, T. E.; Di Cicco, A.; Filipponi, A.; Natoli, C.; Hedman, B.; Solomon, E. I.; Hodgson, K. O. *J. Am. Chem. Soc.* **1994**, *116*, 6757-6768.

(41) Haller, K. J.; Johnson, P. L.; Feltham, R. D.; Enemark, J. H.; Ferraro, J. R.; Basile, L. J. *Inorg. Chim. Acta* **1979**, *33*, 119-130.

(42) Hodges, K. D.; Wollmann, R. G.; Kessel, S. L.; Hendrickson, D. N.; Van Derveer, D. G.; Barefield, E. K. *J. Am. Chem. Soc.* **1979**, *101*, 906-917.

Supplementary Materials for

CHAPTER V.

Studies on the Nitrosyl Adduct of a Dinuclear Non-heme Iron(II) Compound

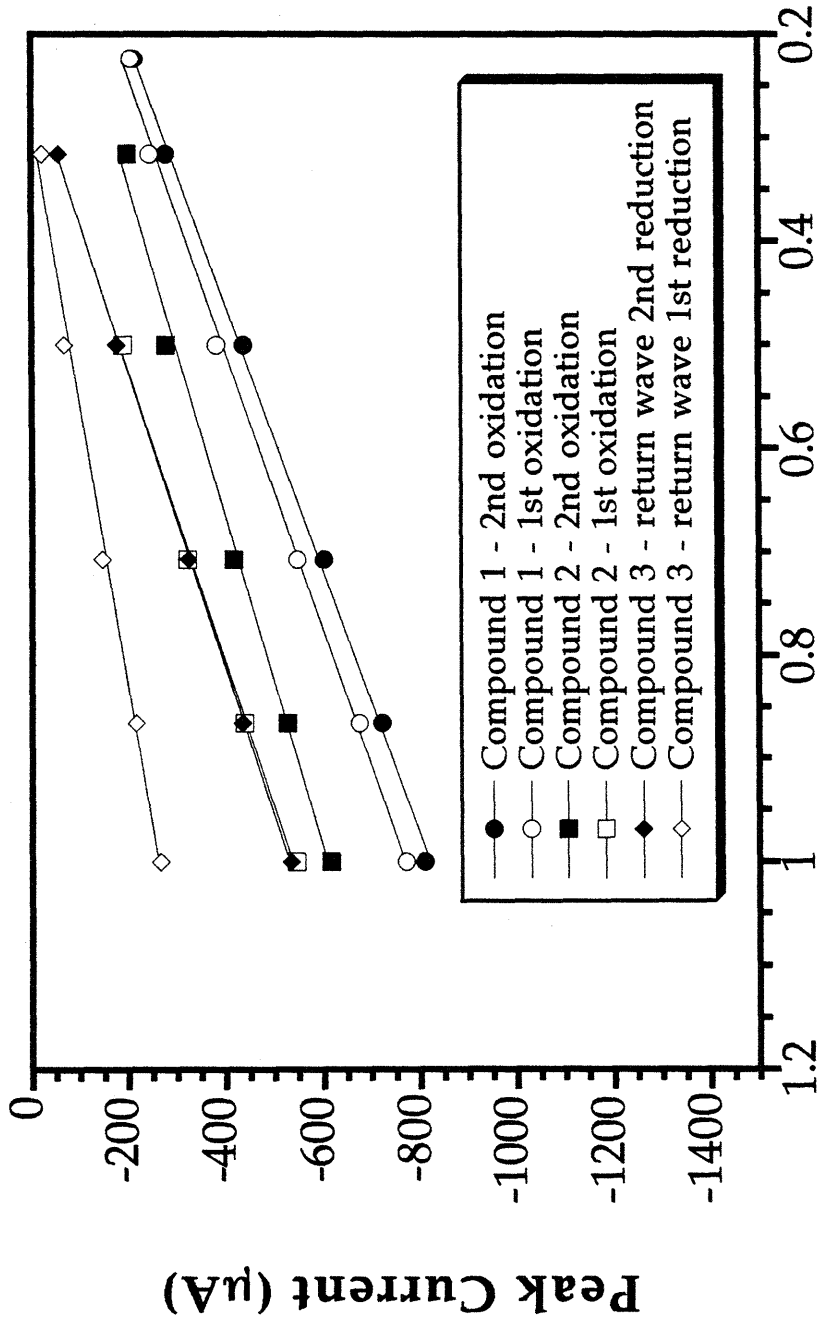

Figure 5.S1. Plot of the peak current versus the square root of the scan speed for the reversible features in the electrochemistry of **1 - 3**. Redox potentials for these features are listed in Table 5.4.

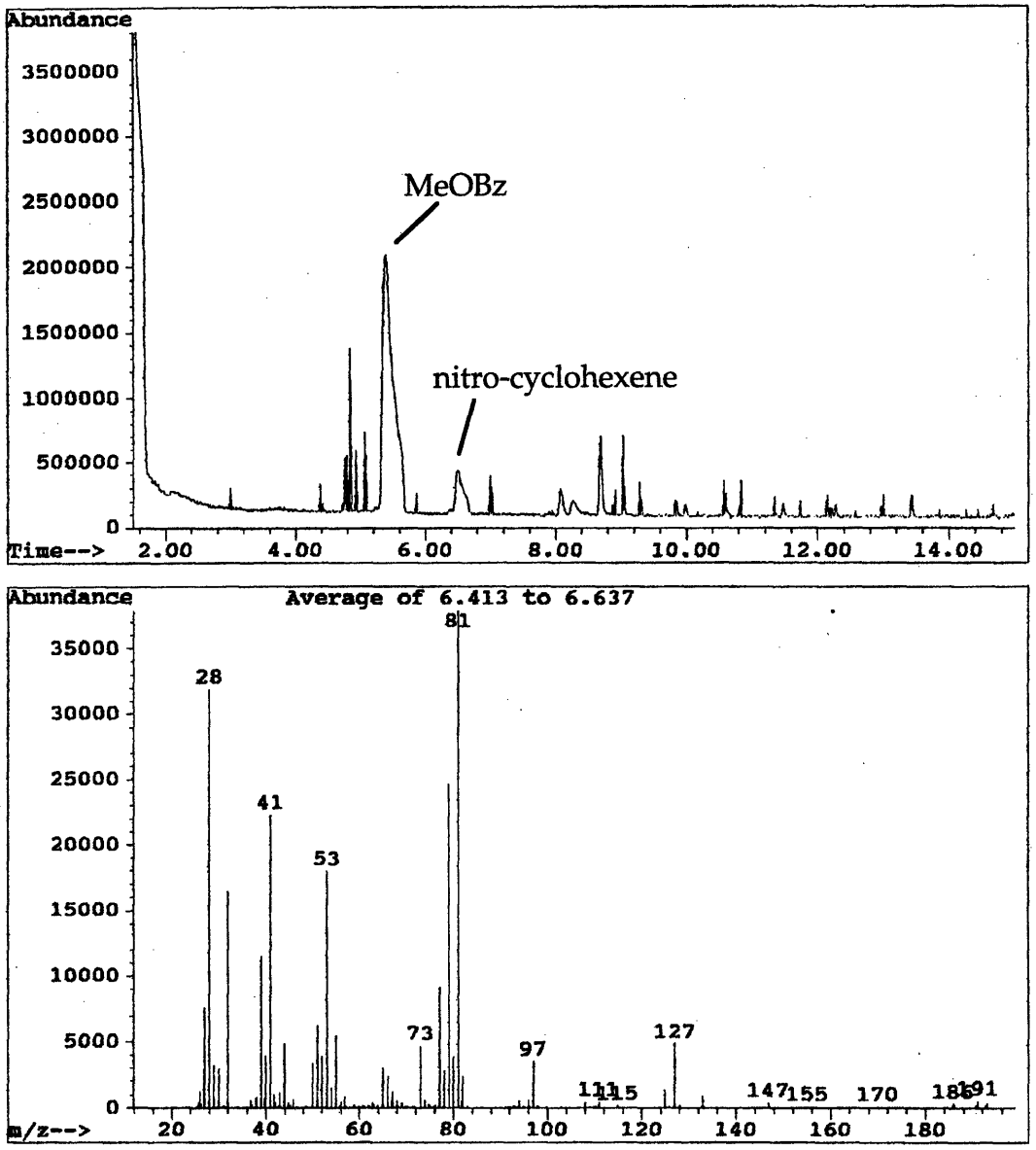

Figure 5.S2. GC/MS trace of the reaction mixture following addition of O_2 to an MeCN solution of **2** containing 1.23 M cyclohexene.

Table 5.S1. Final Positional Parameters of $[Fe_2(Et\text{-}HPTB)(OBz)(NO)_2](BF_4)_2 \cdot 3MeCN$ **(2)**.[a]

atom	x	y	z	B_{eq} Å^{2b}
Fe(1)	0.31162(10)	0.08822(8)	0.78190(8)	2.11(3)
Fe(2)	0.30769(9)	0.27057(8)	0.60111(8)	2.08(3)
F(1)	0.3357(4)	-0.2531(4)	0.6797(3)	4.6(2)
F(2)	0.1602(4)	-0.2413(4)	0.7255(3)	4.2(1)
F(3)	0.2650(5)	-0.3055(4)	0.8216(3)	5.0(2)
F(4)	0.2702(5)	-0.3823(4)	0.7194(4)	5.8(2)
F(5)	0.8309(5)	-0.2348(4)	0.7433(4)	5.8(2)
F(6)	0.7232(6)	-0.2228(7)	0.8690(5)	11.5(3)
F(7)	0.6554(5)	-0.2159(5)	0.7584(4)	7.8(2)
F(8)	0.7507(6)	-0.3447(5)	0.8209(8)	14.1(4)
O(1)	0.2846(4)	0.1424(3)	0.6596(3)	1.9(1)
O(2)	0.4688(4)	0.2027(4)	0.5985(4)	2.5(1)
O(3)	0.4713(4)	0.0805(4)	0.7154(4)	2.5(1)
O(4)	0.2748(7)	0.3826(5)	0.7268(5)	6.6(2)
O(5)	0.2895(7)	0.2272(5)	0.8772(5)	6.7(3)
N(1)	0.3237(5)	-0.0442(5)	0.7384(4)	2.3(2)
N(2)	0.3256(5)	0.2133(4)	0.4810(4)	2.0(2)
N(3)	0.3639(5)	0.3715(4)	0.4927(4)	2.2(2)
N(4)	0.4351(5)	0.4153(5)	0.3503(5)	2.7(2)
N(5)	0.1526(5)	0.3171(5)	0.5767(4)	2.2(2)

[a]Numbers in parentheses are errors in the last significant figure. See Figure 5.1 for atom labeling scheme. [b]$B_{eq} = (4/3)^*[a^2\beta_{11} + b^2\beta_{22} + c^2\beta_{33} + 2ab^*\cos(c)\beta_{12} + 2ac^*\cos(\beta)\beta_{13} + 2bc^*\cos(\alpha)\beta_{23}]$

Table 5.S1. cont.

atom	x	y	z	B_{eq} Å^{2b}
N(6)	0.0448(5)	0.3397(5)	0.4887(4)	2.5(2)
N(7)	0.3658(5)	-0.0215(5)	0.8827(4)	2.2(2)
N(8)	0.4344(5)	-0.1705(5)	0.9305(4)	2.4(2)
N(9)	0.1555(5)	0.0686(5)	0.8284(4)	2.2(2)
N(10)	0.0408(6)	-0.0208(5)	0.8545(4)	2.5(2)
N(11)	0.2888(5)	0.3300(5)	0.6838(5)	2.5(2)
N(12)	0.2957(5)	0.1803(5)	0.8310(4)	2.5(2)
N(13)	0.0202(8)	0.1289(7)	0.6400(6)	5.9(2)
N(14)	0.0115(10)	-0.5628(10)	0.9041(8)	10.4(4)
N(15)	0.4191(8)	-0.6047(7)	0.8760(6)	6.4(2)
C(1)	0.3501(7)	-0.0168(6)	0.6414(5)	2.5(2)
C(2)	0.2966(7)	0.0819(6)	0.6045(6)	2.6(2)
C(3)	0.3549(7)	0.1116(6)	0.5118(6)	3.0(2)
C(4)	0.4098(7)	0.2495(6)	0.4112(6)	2.8(2)
C(5)	0.4023(6)	0.3465(5)	0.4163(6)	2.0(2)
C(6)	0.3717(6)	0.4631(6)	0.4771(6)	2.3(2)
C(7)	0.3454(7)	0.5241(6)	0.5329(5)	2.6(2)
C(8)	0.3615(8)	0.6128(7)	0.4957(7)	3.5(3)
C(9)	0.4059(8)	0.6394(6)	0.4048(7)	3.7(3)
C(10)	0.4337(7)	0.5807(7)	0.3496(6)	3.4(3)
C(11)	0.4158(6)	0.4912(6)	0.3874(6)	2.4(2)
C(12)	0.4799(7)	0.4137(6)	0.2573(6)	3.0(2)
C(13)	0.4038(8)	0.4647(7)	0.1999(6)	4.1(3)

Table 5.S1. cont.

atom	x	y	z	B_{eq} Å^{2b}
C(14)	0.2256(7)	0.2442(6)	0.4475(6)	3.2(2)
C(15)	0.1410(7)	0.3016(6)	0.5037(6)	2.5(2)
C(16)	0.0564(7)	0.3691(6)	0.6107(6)	2.5(2)
C(17)	0.0203(7)	0.4039(6)	0.6863(6)	2.9(2)
C(18)	-0.0821(7)	0.4545(7)	0.7058(6)	3.8(3)
C(19)	-0.1481(8)	0.4712(7)	0.6465(7)	4.4(3)
C(20)	-0.1151(7)	0.4358(7)	0.5726(7)	3.6(3)
C(21)	-0.0119(6)	0.3844(6)	0.5560(6)	2.5(2)
C(22)	0.0061(7)	0.3376(6)	0.4132(6)	3.2(2)
C(23)	-0.0515(8)	0.2592(7)	0.4371(6)	4.7(3)
C(24)	0.4098(6)	-0.1161(6)	0.7731(5)	2.3(2)
C(25)	0.4025(6)	-0.1044(6)	0.8628(6)	2.5(2)
C(26)	0.3746(6)	-0.0354(6)	0.9698(6)	2.5(2)
C(27)	0.3494(7)	0.0261(7)	1.0246(6)	3.2(2)
C(28)	0.3665(8)	-0.0067(7)	1.1080(6)	3.5(3)
C(29)	0.4097(8)	-0.1008(7)	1.1364(6)	3.7(3)
C(30)	0.4360(7)	-0.1626(6)	1.0835(6)	3.4(3)
C(31)	0.4172(7)	-0.1277(7)	0.9991(6)	2.8(2)
C(32)	0.4816(7)	-0.2694(6)	0.9327(6)	3.3(2)
C(33)	0.4021(8)	-0.3284(7)	0.9786(6)	4.4(3)
C(34)	0.2245(7)	-0.0751(6)	0.7708(6)	3.0(2)
C(35)	0.1402(7)	-0.0082(6)	0.8182(5)	2.5(2)
C(36)	0.0584(7)	0.1124(6)	0.8726(5)	2.5(2)
C(37)	0.0266(7)	0.1951(7)	0.8997(6)	3.1(2)
C(38)	-0.0775(8)	0.2183(7)	0.9452(7)	4.2(3)

Table 5.S1. cont.

atom	x	y	z	B_{eq} Å^{2b}
C(39)	-0.1468(8)	0.1621(8)	0.9624(7)	4.3(3)
C(40)	-0.1167(8)	0.0806(7)	0.9347(7)	4.2(3)
C(41)	-0.0135(7)	0.0558(7)	0.8905(6)	2.9(2)
C(42)	-0.0019(7)	-0.0976(6)	0.8549(6)	3.6(3)
C(43)	-0.0593(8)	-0.0755(7)	0.7822(7)	4.7(3)
C(44)	0.5116(7)	0.1271(6)	0.6436(6)	2.3(2)
C(45)	0.6286(6)	0.0888(5)	0.6057(5)	2.0(2)
C(46)	0.6837(7)	0.0088(6)	0.6508(5)	2.5(2)
C(47)	0.7883(7)	-0.0268(6)	0.6147(6)	2.7(2)
C(48)	0.8371(7)	0.0178(7)	0.5338(7)	3.3(3)
C(49)	0.7819(7)	0.0984(7)	0.4868(6)	3.1(2)
C(50)	0.6776(7)	0.1338(6)	0.5230(6)	2.5(2)
C(51)	-0.166(1)	0.2138(10)	0.7160(9)	8.2(4)
C(52)	-0.059(1)	0.1645(8)	0.6739(8)	5.7(3)
C(53)	0.007(1)	-0.380(1)	0.8561(9)	8.2(4)
C(54)	0.011(1)	-0.483(1)	0.8775(9)	8.2(4)
C(55)	0.243(1)	-0.5260(10)	0.9631(9)	8.3(4)
C(56)	0.3428(10)	-0.5709(8)	0.9139(7)	5.3(3)
B(1)	0.2588(9)	-0.2967(8)	0.7353(8)	3.2(3)
B(2)	0.739(1)	-0.2547(9)	0.7976(8)	3.8(3)
H(1)	0.42418(10)	-0.02252(8)	0.62257(8)	2
H(2)	0.32970(9)	-0.05772(8)	0.61855(8)	2
H(3)	0.2279(4)	0.0807(3)	0.6020(3)	3
H(4)	0.3381(4)	0.0827(4)	0.4746(4)	3
H(5)	0.4284(4)	0.0932(4)	0.5095(4)	3

Table 5.S1. cont.

atom	x	y	z	B_{eq} Å^{2b}
H(6)	0.4766(7)	0.2121(5)	0.4197(5)	3
H(7)	0.4012(7)	0.2492(5)	0.3552(5)	3
H(8)	0.3174(5)	0.5056(5)	0.5942(4)	3
H(9)	0.3424(5)	0.6566(4)	0.5318(4)	4
H(10)	0.4166(5)	0.7008(4)	0.3817(4)	4
H(11)	0.4638(5)	0.5991(5)	0.2887(5)	4
H(12)	0.5391(5)	0.4414(5)	0.2380(4)	3
H(13)	0.5019(5)	0.3510(5)	0.2516(4)	3
H(14)	0.3814(5)	0.5278(5)	0.2047(4)	4
H(15)	0.4369(5)	0.4616(5)	0.1404(4)	4
H(16)	0.3444(5)	0.4373(5)	0.2181(4)	4
H(17)	0.2391(6)	0.2799(5)	0.3889(4)	3
H(18)	0.2029(5)	0.1912(5)	0.4479(5)	3
H(19)	0.0658(5)	0.3931(5)	0.7249(4)	3
H(20)	-0.1078(7)	0.4778(6)	0.7582(5)	4
H(21)	-0.2174(7)	0.5081(6)	0.6587(6)	5
H(22)	-0.1605(7)	0.4457(6)	0.5342(6)	4
H(23)	-0.0409(7)	0.3950(6)	0.3970(6)	3
H(24)	0.0641(6)	0.3284(5)	0.3650(6)	3
H(25)	-0.1099(6)	0.2684(6)	0.4850(6)	5
H(26)	-0.0757(7)	0.2588(6)	0.3877(5)	5
H(27)	-0.0048(8)	0.2016(7)	0.4533(7)	5
H(28)	0.4013(8)	-0.1762(6)	0.7763(7)	2
H(29)	0.4761(7)	-0.1079(7)	0.7361(6)	2
H(30)	0.3207(6)	0.0901(6)	1.0044(6)	3

Table 5.S1. cont.

atom	x	y	z	B_{eq} Å^{2b}
H(31)	0.3490(7)	0.0344(6)	1.1466(6)	4
H(32)	0.4212(8)	-0.1225(7)	1.1946(6)	4
H(33)	0.4656(7)	-0.2264(6)	1.1034(6)	4
H(34)	0.5090(7)	-0.2777(6)	0.8740(6)	3
H(35)	0.5372(7)	-0.2886(6)	0.9631(6)	3
H(36)	0.3748(7)	-0.3209(6)	1.0376(6)	5
H(37)	0.3463(7)	-0.3098(7)	0.9484(6)	5
H(38)	0.4350(8)	-0.3916(7)	0.9786(7)	5
H(39)	0.2023(7)	-0.0803(7)	0.7222(7)	3
H(40)	0.2355(6)	-0.1339(6)	0.8101(6)	3
H(41)	0.0737(7)	0.2346(6)	0.8879(6)	3
H(42)	-0.1014(8)	0.2747(7)	0.9650(6)	5
H(43)	-0.2169(6)	0.1802(6)	0.9942(5)	5
H(44)	-0.1651(6)	0.0425(6)	0.9453(6)	4
H(45)	0.0544(6)	-0.1501(6)	0.8480(6)	4
H(46)	-0.0495(7)	-0.1117(7)	0.9099(6)	4
H(47)	-0.1163(8)	-0.0235(7)	0.7888(6)	5
H(48)	-0.0122(8)	-0.0617(7)	0.7269(6)	5
H(49)	-0.0855(7)	-0.1274(6)	0.7849(6)	5
H(50)	0.6502(7)	-0.0221(7)	0.7067(6)	3
H(51)	0.8262(7)	-0.0820(6)	0.6459(6)	3
H(52)	0.9089(8)	-0.0065(7)	0.5097(6)	3
H(53)	0.8155(7)	0.1286(6)	0.4306(6)	3
H(54)	0.6394(7)	0.1887(6)	0.4916(5)	3

CHAPTER VI.

Nitration of Olefins Using Iron Catalysts and Nitric Oxide

Introduction

Nitroolefins are an important class of organic molecules. Recent articles and books have reviewed their use as synthetic intermediates.[1-4] In brief, these molecules can be used as precursors to aldehydes and ketones as well as to chiral amines and alcohols. In addition, nitroolefins are employed as starting materials for several annulation reactions and often serve as dienophiles in Diels Alder reactions. A number of synthetic approaches to these compounds are already available.[4-10] The development of new and varied synthetic routes to these intermediates adds versatility to the methodologies that employ nitroolefins.

In this chapter, a new synthetic route to nitroolefins is presented. The discovery was serendipitous, and occurred during an investigation on the reactivity of a bis-nitrosyl diiron(II) complex (see Chapter V) with dioxygen. GC/MS analysis of the solution after the reaction revealed the presence of nitroolefin. This behavior was unanticipated and separate from the goal of the initial study, but due to the extensive utility of nitroolefins in organic synthesis, we began an investigation of the reaction. We found that by changing the order of addition such that nitric oxide was added to the (μ-peroxo)diiron(III) complex, the reaction became catalytic with respect to the diiron species. The work presented here outlines the utility of this reaction, the extent to which it is general and the limitations encountered with respect to substrate reactivity.

Nitric oxide (NO) is known to react with reduced iron containing proteins in vivo, sometimes, as in the case of ribonucleotide reductase (RNR), resulting in enzyme inactivation.[11-13] We have been studying the reactions of NO with diiron(II) model compounds in an attempt to understand how

NO regulates the chemistry at diiron centers.[14] Since many of the reduced non-heme diiron proteins are involved in reactions with dioxygen, the materials for this catalytic reaction, NO, O_2 and a catalyst, might be present in the enzyme active sites. Covalent modification of the enzyme by a reaction of this type, therefore might be responsible for the observed inhibition of RNR by NO.

Experimental

General Considerations. The ferrous precursors to the catalysts ([Fe_2(Et-HPTB)(OBz)]$(BF_4)_2$ (**1a**), [Fe_2(HPTMP)(OBz)]$(BPh_4)_2$ (**2a**), [Fe_2(HPTP)(OBz)]$(BPh_4)_2$ (**3a**), were prepared as previously described.[15-17] Manipulations of **1 - 3** were carried out in a Vacuum Atmospheres glove box under a nitrogen atmosphere. Solvents used in the catalytic reactions were dried and distilled by standard procedures.[18] Solvents for the purification of products by column chromatography were of HPLC grade and used without further purification. Nitric oxide, 99+% (Matheson) must be purified prior to use to obtain reproducible results.[19] The gas was passed through successive bubblers of 1) 12 M NaOH, 2) 12 M NaOH, 3) 6 M H_2SO_4 and then solid beds of 4) Drierite ($CaSO_4$), 5) KOH pellets, and 6) P_2O_5 dispersed in $CaSO_4$ or $MgSO_4$. The final step in the purification was a bed of glass beads in a -77 °C trap. The purification system was purged with Ar prior to beginning experiments to ensure the removal of any O_2 that might have diffused through the tubing and could contaminate the purified gas.

Instrumentation. GC and GC/MS analysis were run by using a HP-5970 gas chromatograph connected to a HP-5971 mass analyzer. A HP-101 (12 m x 0.2 mm x 0.2 μm) capillary column was used to effect separation with a temperature ramp of 50 - 200 °C at 10 deg/min. Identity of products was determined by GC/MS. Integrations were obtained by FID detection run

parallel to mass spectrometry by using an HP-3393A integrator. FID response calibration constants of 0.88 and 0.89 were measured by using isolated pure material for the integration against methyl benzoate of nitrostilbene and nitrostyrene respectively.

Nitration Reaction Protocol. Standard procedures for the nitration reaction were used to compare substrates. Stock solutions of **1** (1.11 mM in MeCN) and methyl benzoate (diluted $1:10^3$ in MeCN, 8.0 mM) were prepared in the glove box. The reaction mixture consisted of 1.0 mL of catalyst solution, 1.0 mL of methyl benzoate solution and 1.5 mmole of substrate. MeCN was added to a total volume of 10 mL. These solutions were then transferred to 50 mL Schlenk flasks containing magnetic stir bars. The flasks were sealed and removed from the glove box. The reaction mixture was cooled to approximately -20 °C (dry ice/ethylene glycol) and the atmosphere was replaced with dioxygen. The peroxo adduct **1b** formed immediately judging from the formation of a distinct blue color. After 5 minutes, excess dioxygen was removed by freeze/pump/thaw or, for non-volatile substrates, vacuum/argon cycles. The reaction was initiated by addition of 1 atm of nitric oxide and the flask was immediately transferred to 22 °C water bath. Reactions were terminated after 30 minutes by removal of excess NO by freeze/pump/thaw cycles. **NOTE: freezing in these cycles must be done at -77 °C and not 77 K to avoid condensation of NO!** Aliquots of the reaction mixture were diluted 1:10 with MeCN and analyzed by GC. Time course experiments were run by using multiple flasks containing identical reaction mixtures or by withdrawing aliquots of the reaction mixture via cannula. Repeated piercing of septum seals must be avoided, however, since this process can lead to contamination by O_2. Nitric oxide reacts rapidly with O_2 leading to the formation of NO_2 which reacts with olefins by a well known

radical pathway.[4] For experiments in which yields were calculated, larger volumes of nitric oxide were required than would conveniently fit in a Schlenk flask. Therefore, a slow constant purge through an oil bubbler was employed (flow rate approximately 1 bubble/5 seconds). Reactions were run until gas consumption ceased as judged by a constant pressure reading after closing the gas inlet.

Products from the nitration of stilbene and styrene were isolated by silica gel column chromatography using 2% ethyl acetate in hexane. Yields were based on the amount of substrate in solution and do not account for the unreacted starting material recovered after the reaction. Nitrostilbene and nitrostyrene (100 mg) were reduced to 1,2-diphenylethylamine and 1-phenyl-2-ethylamine, respectively, by reaction with $LiAlH_4$ (10 equiv) in dry THF (50 mL). Excess $LiAlH_4$ was removed by filtration through a plug of glass wool and the reaction was quenched by addition of a few drops of ethanol. The reaction mixture was then diluted with 25 mL of 1 M HCl and extracted three times with Et_2O. The aqueous phase was made basic (pH 14) by addition of aq KOH. The amines were extracted three times into the Et_2O and were isolated pure after drying with $MgSO_4$ and removing the Et_2O under reduced pressure. The products were compared by GC/MS to authentic standards obtained from Aldrich. The isolated yield for a typical reduction of nitrostilbene was 69%.

Analysis of Gaseous Products. The atmosphere above the reaction was analyzed by use of a modified 500 mL Toepler pump (Pope Scientific, Figure 3.1). Modifications consisted of a valve connecting the pump inlet and outlet and an attachment for a collection tube. These alterations allowed pre-evacuation of the pump, collection tube, and connection between the reaction flask and the pump. The gas above the reaction mixture was transferred via

the pump to a collection tube suitable for pressurization and injection into the GC/MS. Comparisons were made, with identical manipulations, for parallel reactions in the presence and absence of catalyst.

Results and Discussion

Catalytic Nitration of *trans*-Stilbene. Figure 6.1 shows the results over an extended time period of the nitration reaction in the presence and absence of catalyst **1**. Several key features of the chemistry can be discerned from this plot. As described in the Experimental Section, time zero is defined as the point when the reaction solution reached room temperature. Samples taken at earlier time points revealed that no nitration occurred at -20 °C. In the absence of catalyst, there was no reaction. Nitric oxide was the limiting reagent under the conditions employed since recharging the vessel with a fresh atmosphere of NO reinitiated the reaction.

Benzaldehyde is a common side-product in both the oxidation and nitration reactions of aryl olefins.[4,20-22] Benzaldehyde formation is probably responsible for poor yields reported for the nitration of stilbene by other methodologies. The sharp rise in the benzaldehyde concentration observed late in the time course (> 6 h, Figure 6.1) probably results from the presence of a punctured septum. In the presence of dioxygen, NO reacts to form NO_2 (eq 6.1) which can then attack the olefin in the absence of catalysts. This reaction is not particularly specific for nitration[4] and affords a ratio of roughly 1:1 in benzaldehyde to nitroolefin. The present 10:1 to 20:1 ratios observed from the catalytic reaction are notably more specific.

$$2NO + O_2 \rightarrow 2NO_2 \qquad (6.1)$$

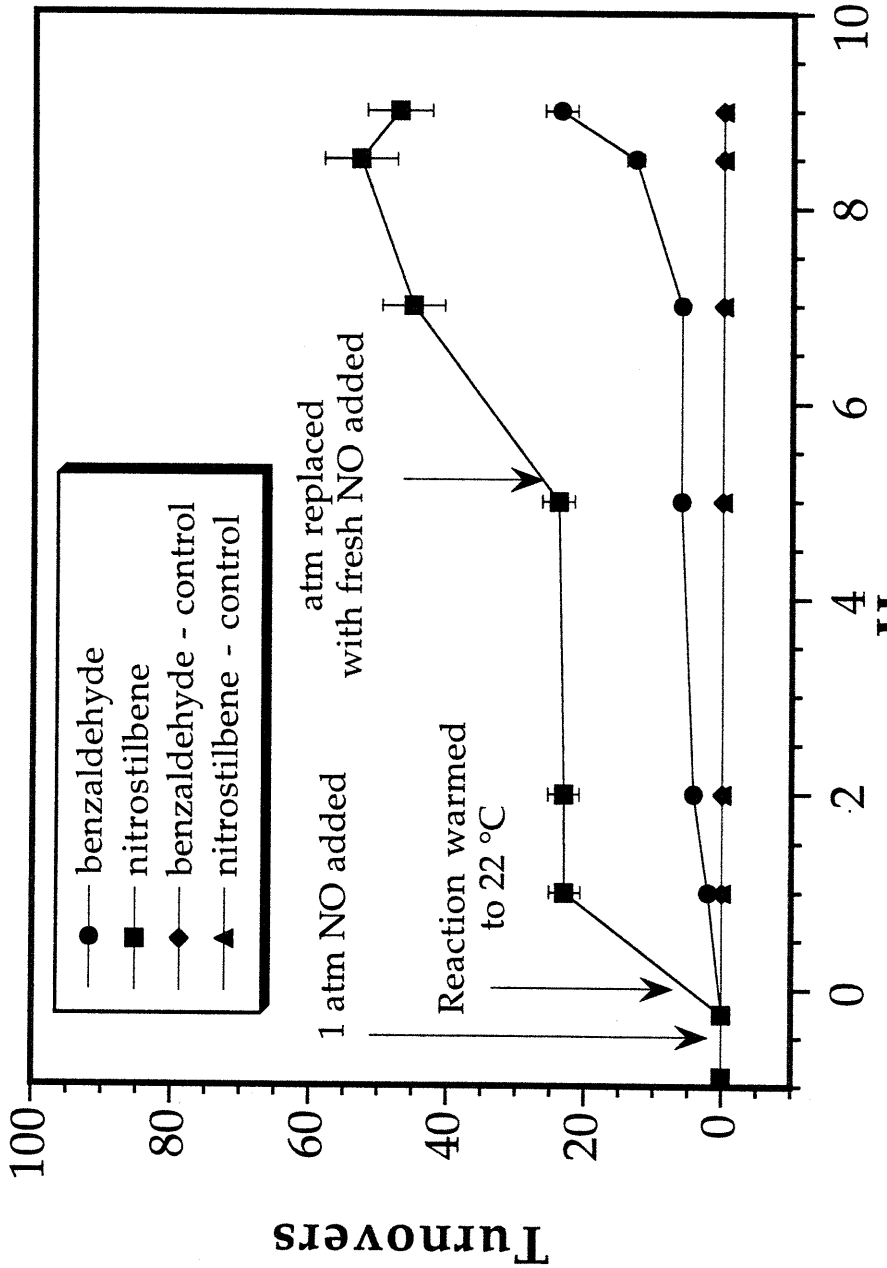

Figure 6.1. Extended time course for the nitration of *trans*-stilbene by **1a** in acetonitrile as observed by gas chromatography. Dioxygen was added to the cold reaction mixture at t = -1 h. At t = -0.5 h, nitric oxide was added to the cold reaction mixture. At t = 0, the reaction flask was warmed to 22°C. Aliquots were removed at various time intervals thereafter. Additional NO was added after taking the aliquot at t = 5 h. Control reactions contained no catalyst.

The reaction rate depends on catalyst concentration between 0 and 0.2 mM (Figure 6.2). Above this concentration, the rate becomes independent of catalyst concentration. This type of saturation behavior is expected for solution reactions involving a gaseous substrate. The available NO in solution is rapidly consumed upon initiation of the reaction when a high concentration of catalyst is present. The rate-limiting step then becomes the dissolution of NO. When less catalyst is present, the difference in rate between NO consumption and dissolution is smaller and the amount of dissolved NO reaches a steady state level. A further complication in a reaction of this type results from the composition of the gas phase. As discussed below, the make-up of the atmosphere in the vessel changes during the reaction as NO is consumed. As the mole fraction of NO above the reaction drops, so too will the concentration of NO in solution. Consequently, the reaction rate is expected to taper off as a function of time. For this reason, comparative studies employed a constant and relatively short reaction time of 30 minutes. Studies on the overall yield required longer reaction times as well as periodic replacement of NO in the head space or the use of a constant slow stream of NO into reaction flasks connected to bubblers to allow excess gas to escape. The greatest reaction rates and highest specificity for nitrostilbene production were observed at very high substrate concentrations. The general conditions for stilbene employed 0.06 mole percent catalyst.

Scope of the Nitration Reaction. The above discussion focused on the use of *trans*-stilbene as a substrate for several reasons. Low volatility is an important parameter in this reaction because of the extensive gas manipulations involved in initiating the reaction. Furthermore, the stability of the α-nitrostilbene product, its ease of isolation and rapid reaction rate

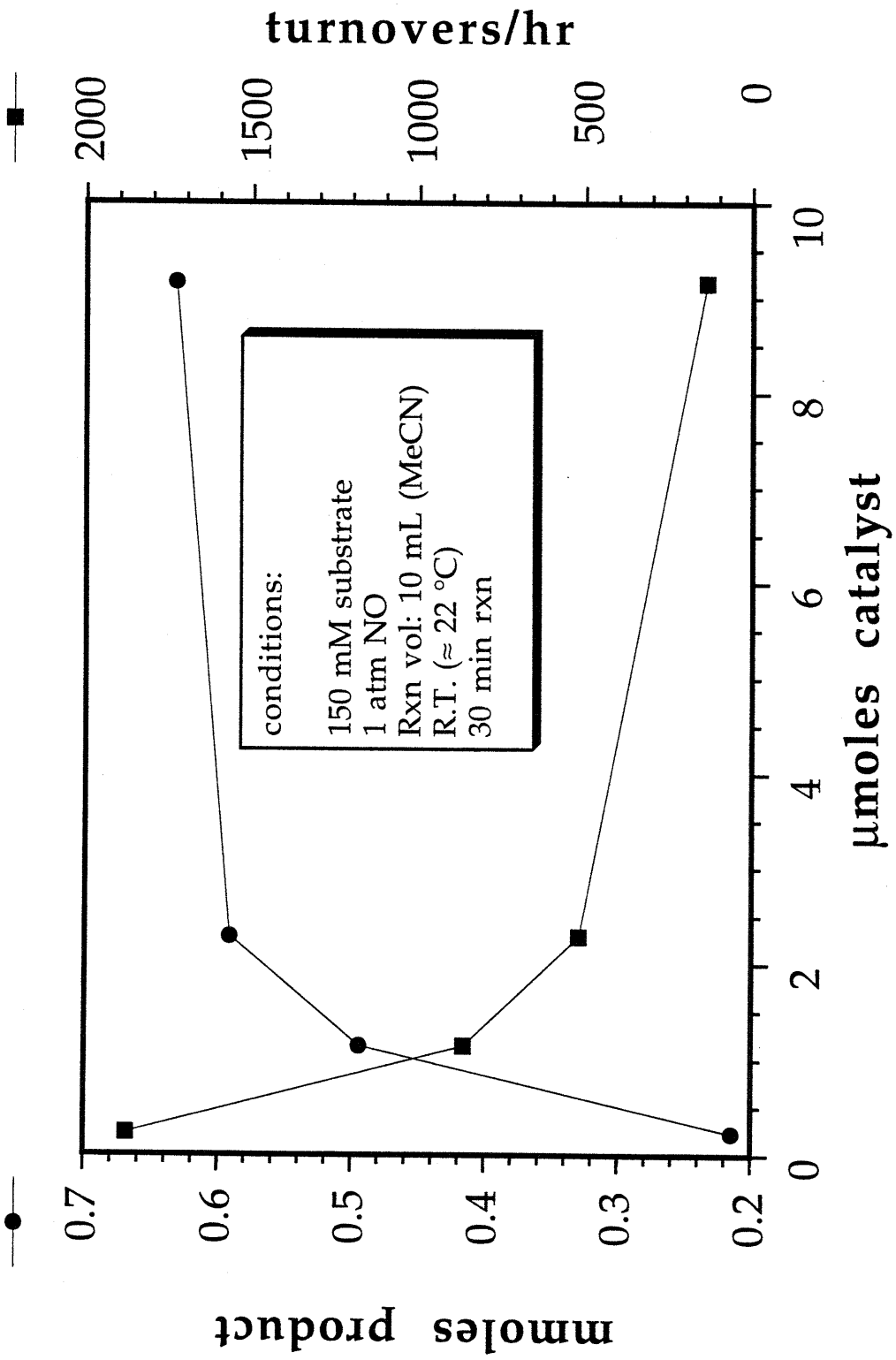

Figure 6.2. The effect of catalyst concentration on the reaction rate for the nitration of *trans*-stilbene.

made it attractive to study. The nitration of olefins by NO with the present catalysts is much more general, however. Table 6.1 lists a series of substrates that have been examined under identical conditions. The nitration activities for these substrates were compared by measuring their reaction rates in a standardized 30 min trial using the conditions optimized for stilbene. The aryl olefins were the most reactive substrates under these conditions and a wide variety of substitution patterns could be tolerated. The difference in the reaction rates for *trans*-stilbene, styrene and substituted styrenes is not significant. An exception is *cis*-stilbene, for which in a 30 minute time course, no nitration was observed. Over longer periods (2-5 h), some *trans*-nitrostilbene was observed, however, this reactivity was due to the prior isomerization of *cis* to *trans*-stilbene (observed by GC). The nitration reaction proceeds at slower rates with both linear and cyclic aliphatic olefins. Chlorinated olefins, tetrasubstituted olefins, olefins conjugated to carbonyl functionalities (ketones, acids and esters) and alkynes were all unreactive. Compounds with extensive functionality not electronically coupled to the olefin, such as the keto-olefin 6-methyl-hept-5-ene-2-one, were reactive.

The substrate specificity provides several insights regarding the reaction mechanism and raises some questions. One key property of the reaction was discerned from the reactivity of styrene. If the mechanism of the reaction involved radical coupling of nitric oxide with the substrate, one would expect to observe only β-nitrostyrene. Attack of a NO_2• radical on the β carbon allows the formation of a stable benzyl radical intermediate. An example of this behavior is observed in the CAN/ultrasound nitration of styrene, in which NO_2 generated in-situ is the reactive intermediate.[5] Both the α– and the β-isomers were observed in the present iron-catalyzed nitration reaction, however, indicating that the mechanism is not simply a

Table 6.1. Survey of Substrates.[a,b]

substrate	major product(s)	nitration rate [c] (turnovers/hr)	isolated yield[d]
trans-stilbene	*trans*-nitrostilbene[e]	538	48 %
cis-stilbene	isomerization to *trans*-stilbene followed by rxn as above[e]	no rxn	
styrene	α-nitrostyrene[e]	490[f]	20 %
	β-nitrostyrene		21 %
α-methyl styrene	*trans*-α-methyl nitrostyrene[e]	275	
	cis-α-methyl nitrostyrene	532	
trans-β-methyl styrene	α-nitro-β-methyl styrene[e]	370[e]	
	β-nitro-β-methyl styrene		
cyclohexene	1-nitro-1-cyclohexene	79	
6-methyl-hept-5-ene-2-one	5-nitro-6-methyl-hept-5-ene-2-one[g]	131	
2,4,4-trimethyl-2-pentene	3-nitro-2,2,4-trimethyl-2-pentene	20	

[a] Reaction conditions: 1.5 mmole substrate, 1.1 μmole **1**, 80 μmole methyl benzoate (internal standard) in a total volume of 10 mL MeCN.

[b] The following substrates were studied and found to be unreactive: 3-methyl-2-cyclohexene-1-one, 2-cyclohexene-1-one, dimethylmaleate, diphenylacetylene, methyl crotonate, allyl benzene, 3-chloropropene, hexachloropropene.

[c] Nitration rates were determined by GC analysis of the reaction mixture after a 30 minute reaction.

[d] Isolated yield based on scaled up reaction using 1.0 - 2.5 g of substrate. Products isolated by column chromatography (stilbene) or vacuum distillation (styrene).

[e] Benzaldehyde was observed as a side-product.

[f] These isomers were not sufficiently resolved by the GC analysis to assign independent rates of formation.

[g] 4-Oxovaleraldehyde was observed as a side-product.

new route to NO_2 formation. The results for *cis*-stilbene are similarly revealing. *Cis*-stilbene reacts faster in porphyrin catalyzed epoxidation reactions,[23-25] a result attributed to unfavorable steric interactions of the trans isomer with the putative oxo-intermediate.[24] Since non-heme systems have more flexibility in their coordination properties, the steric effects of the substrate may be less important. Some epoxidation studies employing metal triflate salts and iodosylbenzene, found that the *trans* substrates were more reactive than their *cis* isomers.[21] No suitable mechanism was provided to explain this behavior.

Composition of the Atmosphere After Nitration. In an effort to understand the chemistry involved in the nitration reaction, the atmosphere

Table 6.2. Composition of the Atmosphere in the Reaction Flask After the Catalytic Nitration of *trans*-Stilbene.[a]

	% composition		Δ
	catalytic reaction	control reaction	
N_2	29.6	12.4	+ 17.2
NO	39.9	69.3	-29.4
O_2	1.1	1.9	-0.8
Ar	27.1	7.5	+ 19.6
N_2O	1.4	4.6	-3.2
NO_2	0.9	4.3	-3.4

[a]Conditions: 1 mg (0.89 μmoles) catalyst **1**, 180 mg (1 mmole) *trans*-stilbene in 10 mL total volume MeCN. Atmosphere collected by Toepler pump after a 30 min reaction at 22 °C.

in the flask was analyzed by mass spectrometry at the end of the time course. This sample was compared to that of a control reaction in which no catalyst was present. The results of this analysis are shown in Table 6.2. The important feature to note is the very slight changes in NO_2 and N_2O levels. The major difference after catalysis is an increased level of N_2. A similar observation of N_2 formation was reported for the oxidation of coordinated phosphines by NO.[26] The only dinitrogen source for the system is NO, and significant leakage of air into the system would have resulted in NO_2 contamination based on the chemistry shown in eq 6.1. The change in the argon level is a consequence of its use in vacuum/Ar cycling to remove excess O_2 after generating the precatalyst. The amount of residual argon in the system when NO was added should be approximately constant between the catalytic and control flasks, but reduced total pressure following the catalytic reaction leads to an increase in its percent composition.

The Nature of the Catalyst. The reactions discussed were initiated by addition of NO to the diiron peroxide(III) species **1b**. It was shown in Figure 6.1 that product was not observed until the reaction solution warmed to room temperature. Since a blue to orange color change occurs upon addition of NO to **1b** at low temperature, this complex is therefore not the true catalyst, but a pre-catalyst. Several potential pre-catalysts were screened. Compounds **1a - 3a** are similar species with minor variations in the steric properties of the metal center. The peroxide adducts of these three compounds catalyzed the nitration of *trans*-stilbene at approximately equal rates. This comparison was carried out in propionitrile solution, using a -77 °C bath in the oxygenation step rather than the normal one held at -20 °C. This modification was required because of the instability of the **2b** and **3b** peroxo species at the higher temperature. When oxygenation of the precatalyst was omitted, no nitration

reaction was observed for any of the compounds. $FeCl_2$ and $Fe(NO_3)_3$ were also examined as control reactions. No reaction was observed for $FeCl_2$, whereas in the presence of $Fe(NO_3)_3$ both nitrostilbene and benzaldehyde formed in approximately a 1:1 ratio. This result differs from the 10:1 - 20:1 ratios of nitration product to benzaldehyde observed for reactions of **1** - **3**. Further work is required to determine the exact nature of the catalyst, but $LFe^{III}\text{-}NO_3$ or $LFe^{III}\text{-}NO_2$ species are the most likely candidates.

Mechanism. The mechanism for the nitration is unknown, but eqs 6.2 - 6.6 describe reactions which together might explain the observed results. NO_2 is capable of nitrating olefins in the absence of catalysts. The results

$$3\,NO \xrightarrow{\text{catalyst}} N_2O + NO_2 \tag{6.2}$$

$$N_2O + NO \xrightarrow{\text{catalyst}} N_2 + NO_2 \tag{6.3}$$

$$2\,NO_2 \rightleftharpoons N_2O_4 \tag{6.4}$$

$$N_2O_4 + \begin{matrix} R_2 & & R_3 \\ & \diagdown\!=\!\diagup & \\ R_1 & & H \end{matrix} \xrightarrow{\text{catalyst (?)}} HNO_2 + \begin{matrix} R_2 & & R_3 \\ & \diagdown\!=\!\diagup & \\ R_1 & & NO_2 \end{matrix} \tag{6.5}$$

$$4\,NO + \begin{matrix} R_2 & & R_3 \\ & \diagdown\!=\!\diagup & \\ R_1 & & H \end{matrix} \xrightarrow{\text{catalyst}} N_2 + HNO_2 + \begin{matrix} R_2 & & R_3 \\ & \diagdown\!=\!\diagup & \\ R_1 & & NO_2 \end{matrix} \tag{6.6}$$

cannot be explained solely by the presence of free NO_2 since it forms a much greater amount of benzaldehyde than we observed. The reaction of NO to form N_2O and NO_2 requires either a catalyst or photochemical or thermal activation, and is similar to known reaction modes for nitric oxide with CO.[27,28] Since N_2O is not observed after the reaction and is incapable of initiating nitration on its own, eq 6.3 must be invoked to consume any N_2O formed in eq 6.2.

Many synthetic routes to nitroolefins are based on the generation of NO_2 radicals in solution.[4,5] Such reactions are useful, but their regioselectivity is linked to the stability of the radical intermediates. The primary difference between free NO_2 and the proposed reactions in eq 6.2 - 6.6 is that NO_2/N_2O_4 is formed on the catalyst. The iron center will therefore effect the selectivity of the chemistry and allows for tuning of the reaction based on ligand modification. Such modification could prove fruitful since the three related species all effectively catalyze the nitration of *trans*-stilbene. Equation 6.6 sums the component steps and predicts a 4:1 stoichiometry for the consumption of nitric oxide and formation of nitroolefin product.

Conclusions

In summary, a new route to the synthesis of nitroolefins has been developed which is capable of converting a variety of olefin substrates. The reaction consumes NO and gives off N_2. As a catalytic method for the nitration of olefins, the potential for designed regiospecificity based on ligand modification is high. The properties and the selectivity against benzaldehyde formation differentiate the new reaction from the many other routes to these important synthetic intermediates.

Acknowledgments

This work was supported by NIGMS and AKZO Corporation. We thank J. Groves for helpful discussions about the mechanism.

References

(1) Corey, E. J.; Estreicher, H. *J. Am. Chem. Soc.* **1978**, *100*, 6294-6295.

(2) Corey, E. J.; Estreicher, H. *Tetrahedron Lett.* **1980**, *21*, 1113-116.

(3) Barrett, A. G. M.; Graboski, G. G. *Chem. Rev.* **1986**, *86*, 751-762.

(4) Perekalin, V. V.; Lipina, E. S.; Berestovitskaya, V. M.; Efremov, D. A. *Nitroalkenes: Conjugated Nitrocompounds*; John Wiley & Sons: West Sussex, 1994.

(5) Hwu, J. R.; Chen, K.-L.; Ananthan, S. *J. Chem. Soc. Chem. Commun.* **1994**, 1425-1426.

(6) Jew, S.-S.; Kim, H.-D.; Cho, Y.-S.; Cook, C.-H. *Chem. Lett.* **1986**, 1747-1748.

(7) Ono, N.; Kamimura, A.; Kawai, T.; Kaji, A. *J. Chem. Soc. Chem. Commun.* **1987**, 1550-1551.

(8) Node, M.; Itoh, A.; Nishide, K.; Abe, H.; Kawababta, T.; Masaki, Y.; Fuji, K. *Synthesis* **1992**, 1119-1124.

(9) Ballini, R.; Castagnani, R.; Petrini, M. *J. Org. Chem.* **1992**, *57*, 2160-2162.

(10) Denmark, S. E.; Marcin, L. R. *J. Org. Chem.* **1993**, *58*, 3850-3856.

(11) Lepoivre, M.; Fieschi, F.; Coves, J.; Thelander, L.; Fontecave, M. *Biochem. Biophys. Res. Commun.* **1991**, *179*, 442-448.

(12) Lepoivre, M.; Chenais, B.; Yapo, A.; Lemaire, G.; Thelander, L.; Tenu, J.-P. *J. Biol. Chem.* **1990**, *265*, 14143-14149.

(13) Lepoivre, M.; Flaman, J.-M.; Bobe, P.; Lemaire, G.; Henry, Y. *J. Biol. Chem.* **1994**, *269*, 21891-21897.

(14) See also Chapter V.

(15) Dong, Y.; Menage, S.; Brennan, B. A.; Elgren, T. E.; Jang, H. G.; Pearce, L. L.; Que, L., Jr. *J. Am. Chem. Soc.* **1993**, *115*, 1851-1859.

(16) Hayashi, Y.; Suzuki, M.; Uehara, A.; Mizutani, Y.; Kitagawa, T. *Chem. Lett.* **1992**, 91-94.

(17) Feig, A.; Lippard, S. J. *J. Am. Chem. Soc.* **1994**, *116*, 8410-8411.

(18) Perrin, D. D.; Armarego, W. L. F. *Purification of Laboratory Chemicals;* 3rd ed.; Butterworth-Heinemann: Oxford, 1988.

(19) Ruggiero, C. E.; Carrier, S. M.; Antholine, W. E.; Whittaker, J. W.; Cramer, C. J.; Tolman, W. B. *J. Am. Chem. Soc.* **1993**, *115*, 11285-11298.

(20) Bryant, D. K.; Challis, B. C.; Iley, J. *J. Chem. Soc. Chem. Commun.* **1989**, 1027-1028.

(21) Van Atta, R. B.; Franklin, C. C.; Valentine, J. S. *Inorg. Chem.* **1984**, *23*, 4121-4123.

(22) Upadhyay, M.; Trivedi, B. M.; Bhattacharya, P. K.; Ganeshpure, P. A.; Satish, S. *J. Mol. Cat.* **1992**, *73*, 287-295.

(23) Groves, J. T.; Nemo, T. E.; Myers, R. S. *J. Am. Chem. Soc.* **1979**, *101*, 1032-1033.

(24) Groves, J. T.; Nemo, T. E. *J. Am. Chem. Soc.* **1983**, *105*, 5786-5791.

(25) Nee, M. W.; Bruice, T. C. *J. Am. Chem. Soc.* **1982**, *104*, 6123-6125.

(26) Guillaume, P.; Wah, H. L. K.; Postel, M. *Inorg. Chem.* **1991**, *30*, 1828-1831.

(27) Mingos, D. M. P.; Sherman, D. J. *Adv. Inorg. Chem.* **1989**, *34*, 293-377.

(28) Fanning, J. C. *Coord. Chem. Rev.* **1991**, *110*, 253-273.

About the Author

I grew up in Los Angeles, the youngest of three children, where my father is a professor of pediatrics at UCLA and my mother a teacher of learning handicapped children. Although we were encouraged to be interested in a wide variety of areas, science always captured my attention. At the age of 14, I took what my parents like to call a sabbatical from them. That year, 9th grade, I spent living on an island south of Stockholm, Sweden, an experience I will remember all of my life. The Bondes, Carl and Caroline, and their kids, Elisabeth, Charlotte, Gustaf and Fredric, are amazing people, and truly made me a part of their family. The experience added perspective to my life growing up in Los Angeles.

I began to work in research laboratories at UCLA every afternoon shortly after returning from my year abroad. I really have never looked back. I realized that in the classroom I was learning about discoveries made by scientists years ago, but in the laboratory, I was uncovering facts that no one has ever known before. After this revelation, textbooks, although necessary, were unsatisfying. I started in the laboratory of Robert Seeger, and was the recipient of a Westinghouse Science Talent Search Scholarship based on this work. Then, after starting college at Yale, I spent two summers in the lab of Dave Sigman at UCLA. It was under Dave's tutelage that I became interested in the field of bioinorganic chemistry and began my shift from studying biochemistry toward inorganic chemistry. Throughout all of my research projects, however, my roots in the area of biochemistry have shown themselves.

I did my senior thesis at Yale in the laboratory of Robert Crabtree before coming to MIT to begin my graduate work with Stephen Lippard. The preceding pages attest to Steve's commitment to science and the training of young chemists. His approach of answering the fundamental questions by whatever means are necessary is inspiring and lets those of us who work with him extend ourselves into a wide variety of experimental areas. He taught me that there is no experiment that is technically too difficult, although imaginative solutions are sometimes in order.

Now that I am finishing my Ph.D., I am making another change. I am moving to Boulder, CO where I will be working as a NSF Postdoctoral Fellow in the laboratory of Olke Uhlenbeck. There, I will apply my training in inorganic chemistry to the biological problem of RNA catalysis. I will give up small molecules for a while and study something a little larger. At the core, however, lies a metal ion, the ligand is just a little more elegant than those to which I am accustomed.

Andrew L. Feig

August, 15, 1995